INFORMATION TO USERS

This manuscript has been reproduced from the microfilm master. UMi films the text directly from the original or copy submitted. Thus, some thesis and dissertation copies are in typewriter face, while others may be from any type of computer printer.

The quality of this reproduction is dependent upon the quality of the copy submitted. Broken or indistinct print, colored or poor quality illustrations and photographs, print bleedthrough, substandard margins, and improper alignment can adversely affect reproduction.

In the unlikely event that the author did not send UMI a complete manuscript and there are missing pages, these will be noted. Also, if unauthorized copyright material had to be removed, a note will indicate the deletion.

Oversize materials (e.g., maps, drawings, charts) are reproduced by sectioning the original, beginning at the upper left-hand corner and continuing from left to right in equal sections with small overlaps.

Photographs included in the original manuscript have been reproduced xerographically in this copy. Higher quality 6" x 9" black and white photographic prints are available for any photographs or illustrations appearing in this copy for an additional charge. Contact UMI directly to order.

University of Alberta

Ground Penetrating Radar for Detection of Rock Structure

by

Lori-Ann Wilchek ©

A thesis submitted to the Faculty of Graduate Studies and Research in partial fulfillment of the

requirements for the degree of Master of Science

in

Geotechnical Engineering

Department of Civil and Environmental Engineering

Edmonton, Alberta

Fall, 2000

Your file Votre référence

Our file Notre référence

0-612-59900-0

Canada

<center>

University of Alberta

Library Release Form

</center>

Name of Author: Lori-Ann Wilchek

Title of Thesis: Ground Penetrating Radar for Detection of Rock Structure

Degree: Master of Science

Year this Degree Granted: 2000

Permission is hereby granted to the University of Alberta Library to reproduce single copies of this thesis and to lend or sell such copies for private, scholarly or scientific purposes only.

The author reserves all other publication and other rights in association with the copyright in the thesis, and except as herein before provided, neither the thesis nor any substantial portion thereof may be printed or otherwise reproduced in any material form whatever without the author's prior written permission.

<div align="right">

Lori-Ann Wilchek
#7 - 11606, 132 Street
Edmonton, Alberta
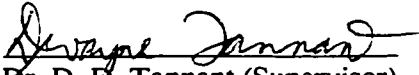T5M 1G4

</div>

Date: June 1, 2000

ABSTRACT

Based on a review of the literature and reflection surveys conducted at various field sites, ground penetrating radar (GPR) was found to be an effective tool for detecting rock structure under appropriate site conditions: sites where reflector geometries are simple, host rock conductivity is low, and there is a sharp contrast in dielectric constant between the host rock and the target. Most importantly, the smallest target dimension must be sufficiently large to be detected.

The results of this thesis show that a dry fracture, such as joint, with an aperture (or width) less than 10 mm may be detected using antenna frequencies greater than 300 MHz. But, the minimum detectable aperture is about 3 mm. Under saturated conditions, a joint aperture less than 10 mm may be detected using frequencies greater than 100 MHz, however the minimum detectable aperture is about 0.2 mm.
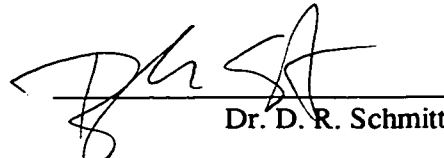
University of Alberta

Faculty of Graduate Studies and Research

The undersigned certify that they have read, and recommended to the Faculty of Graduate Studies and Research for acceptance, a thesis entitled Ground Penetrating Radar for Detection of Rock Structure submitted by Lori-Ann Wilchek in partial fulfillment of the requirements for the degree of Master of Science in Geotechnical Engineering.

Dr. D. D. Tannant (Supervisor)

Dr. D. M. Cruden

Dr. D. R. Schmitt

Date: _May 30, 2000_

ACKNOWLEDGEMENTS

TABLE OF CONTENTS

LIST OF TABLES

LIST OF FIGURES

LIST OF SYMBOLS

α	=	attenuation constant	dB/m
α_A	=	actual dip	degrees
α_R	=	radargram dip	degrees
A	=	pulse amplitude	-
$\overline{B}$	=	magnetic flux density vector	Wb/m^2
c	=	speed of light (3×10^8 m/s)	m/s
Δ_x	=	Nyquist sampling interval	m
D	=	dipole moment density	C/m^2
ε	=	dielectric permittivity	$C^2/(N.m^2)$
ε_o	=	permittivity through a vacuum (8.85×10^{-12} F/m)	$C^2/(N.m^2)$
ε_r	=	dielectric constant (or relative permittivity)	(dimensionless)
E	=	electric field	V/m
f_c	=	antenna centre frequency	Hz
f_N	=	Nyquist frequency	Hz
f_t	=	transition frequency	Hz
Δf	=	frequency bandwidth	Hz
H	=	magnetic field	A/m
φ_1, φ_2	=	incident and reflection angles	degrees
φ_c	=	critical incident angle	degrees
i	=	imaginary number ($=\sqrt{-1}$)	-
J_C	=	conduction current	A/m^2
$J_D = \left(\dfrac{\partial \overline{D}}{\partial t}\right)$	=	displacement current	-
λ	=	dominant wavelength	m
λ_V	=	vertical resolution	m
μ	=	magnetic permeability	H/m
v	=	signal propagation velocity	m/ns
Q	=	system performance	dB
ρ	=	electric resistivity	$\Omega.m$
r	=	radius of the Fresnel Zone	m
R	=	reflection coefficient	-
R_t	=	Fresnel reflection coefficient	-
σ	=	electric conductivity	mS/m
t	=	thickness of a thin layer	m
t	=	time	s
T	=	transmission coefficient	-
tan δ	=	loss tangent	-
w	=	width of Fresnel zone or horizontal resolution	m
ω	=	angular frequency ($= 2\pi f$)	rad/s
x	=	antenna separation distance	m
z	=	depth	m

CHAPTER 1: INTRODUCTION

For many rock engineering projects it is essential to detect structure such as joints and foliation within a rock mass because they represent planes of weakness across which the rock is structurally discontinuous. Once these structures are identified the engineer can then do a proper analysis and design to ensure these discontinuities will not have a detrimental effect on the project. Unfortunately, many structural features go undetected because of either overburden or weathering, because they do not daylight at the surface, or because they are simply missed by localized drilling and sampling. Because of these problems, the engineering community is looking at geophysical exploration techniques such as ground penetrating radar (GPR) for detecting rock structure.

At present, GPR is regarded as a fast, reliable, portable, and relatively inexpensive tool for high resolution, non-destructive mapping of the ground. This tool identifies subsurface interfaces that have a significant contrast in dielectric constant by emitting short, high frequency, electromagnetic pulses into the ground. Compared to other geophysical methods such as seismic or EM, it has superior resolution however at the expense of more limited depths of penetration (i.e. maximum penetration of 100 m in ideal ground conditions). GPR surveying and interpretation also requires experienced people who have an understanding of geophysical theory.

1.1   THESIS OBJECTIVES

The use of GPR for discontinuity detection in both soft and hard rock has been examined by a number of researchers in the last two decades. However the opinions regarding how well it works are somewhat conflicting. As well, these studies on discontinuity detection are buried amongst the geophysical literature and have not reached the engineering community. Because of these issues, the objectives of this thesis are:

1. to review the theory of this geophysical technique;
2. to evaluate whether ground penetrating radar can be used to detect rock structure with a focus on discontinuities with apertures less than 1 cm (i.e. small-scale structural features);
3. to determine the conditions required for successful detection of rock structure;
4. to determine the limitations of GPR for this application.

This thesis is written from the perspective of a geological engineer. As a result, it is likely that this thesis is written with quite a different view point from that of a geophysicist. This thesis has also been written at a level such that any person can begin to understand what ground penetrating radar is, how it works, and for what engineering applications it can be used.

This thesis presents an informed assessment of how successful GPR is in detecting rock structure. Structure or discontinuities are both collective terms used to encompass a variety of rock features (e.g. joints, faults, dykes, veins, bedding planes, etc.) and will be used synonymously throughout the thesis. As well, a distinction will be made between small-scale and large-scale structure. Small-scale refers to structural features with their smallest dimension less than 1 cm; for example, joints, foliation, and bedding planes all represent small-scale structure. In contrast, large-scale refers to structural features with their smallest dimension greater than 1 cm; for example, veins, dykes, faults, and fracture/fault zones are examples of large-scale structure. This distinction is important because small-scale features approach the limits of practical detection using commercially available GPR systems. It is also important to note that the research presented in

1

this thesis is concerned only with detection of rock structure, not characterization because it is nearly impossible to do so using radar.

Based on the discontinuity (or fracture) detection case studies from the literature and my own GPR reflection surveys conducted in Sudbury, Ontario the conditions required for successful fracture detection will be defined. In this context, both the site and survey conditions will be considered. In addition, because the Fresnel Reflection Coefficient (R_t) governs detection of small-scale and sometimes large-scale structural features, the threshold value (or range of values) that separates successful target detection from non-detection will be provided.

The last objective is to determine the limitations of GPR. Specifically what types of rock are best suited for radar and what antenna frequency should be used for a specific target? In addition, what is the minimum fracture thickness that can be detected using various antenna frequencies? And finally, are there any unique difficulties associated with using GPR for detection of rock structure?

1.2   SCOPE OF THESIS

To evaluate the suitability of GPR for this application, GPR theory will be complemented with an assessment its effectiveness in practice. The latter will be accomplished by performing a critical review of case studies on fracture detection from the literature and conducting field surveys at various sites around Sudbury, Ontario. The field component involves conducting GPR reflection surveys using 100 MHz and 1 GHz antennas on blocks of quarried rock, surface outcrops and within an underground hard-rock mining environment. Based on this literature review and the GPR survey results, I will determine how successful radar is for the detection of rock structure.

For this evaluation of rock structure detection, a commercially available impulse radar system was used. It is important to be aware that there are other types of radar systems available but these are not as common due to their higher costs and/or increased complexity (e.g. stepped-frequency radar system). As well, there are a number of manufacturers and suppliers of GPR equipment (GSSI, Sensors & Software, MALA GeoScience, Rockradar, etc.) of which there may be variations between the systems. Therefore problems may arise when comparing the various fracture detection case studies because different GPR systems were used. Unfortunately, this is a problem that cannot be avoided.

The importance of using the correct antenna centre frequency at a site will be stressed several times throughout this thesis. Frequency is critical because it controls the depth of penetration into the ground and target detection. Antenna frequencies that are presently available range between 10 MHz to 1000 MHz. For the field component of this thesis, only 100 MHz and 1000 MHz antennas were used to conduct the various reflection surveys. It would have been beneficial to test more antenna frequencies but both time and financial restrictions prevented this.

1.3 ORGANIZATION

The evaluation of GPR for rock structure detection begins with a chapter on the basic physics that governs ground penetrating radar – Chapter 2. Chapter 3 describes how to conduct GPR surveys. wherein the equipment and the various operational modes are described in detail. As well. data processing and general interpretation of GPR data is included in this chapter. Chapter 4 is a comprehensive literature review on how GPR has been used as a site investigation tool for various applications in geotechnical engineering. This chapter also includes a comparison of all case studies that investigated the use of GPR for fracture detection as well as a section on identification of rock structure in radar profiles.

The field component of this thesis is described in Chapters 5 and 6. Specifically. Chapter 5 describes each of the nine project sites within the Sudbury District and the surveys conducted at each individual site. Chapter 6 describes the results of all 32 surveys in terms of processing. interpretation and preliminary conclusions. The final chapter (Chapter 7) contains concluding remarks regarding the potential to use GPR for rock structure detection and recommendations for further research in this area.

The appendix follows the list of references and includes tables for all 32 reflection surveys. These tables contain specific details concerning the system parameters, survey details, and processing details that may not have been discussed in the main body of the report.

CHAPTER 2: GROUND PENETRATING RADAR REVIEW

2.1 INTRODUCTION

The geophysical technique which uses high frequency radio waves to penetrate the ground and detect buried dielectric interfaces called ground penetrating radar is described in this Chapter. Section 2.2 describes what radar is and the historical development of GPR. Section 2.3 then describes the concept of GPR. The basics of electromagnetic theory are presented in Section 2.4 for the purpose of understanding how GPR works in earth materials. Section 2.5 discusses the electrical properties of geological materials followed by radar propagation in Section 2.6. GPR performance is described in terms of penetration and resolution (Section 2.7) and a summary/conclusions is given in the final section (Section 2.8). Note that throughout this Chapter the focus will be on the use of GPR in rock because its importance to this thesis.

2.2 RADAR

Radar is an acronym for **RA**dio **D**etection **A**nd **R**anging. Radar is a means of detecting the location of a distant object through emission of a narrow beam of extremely high frequency radio waves which is then reflected by the object back to the source (Collins English Dictionary, 1994). The distance to the object is determined by measuring the time it takes the pulse to travel between the transmission and reception points.

Radar is often used on aircrafts and ships for the detection of large metallic objects, such as other ships, or landmasses. With this type of radar, electromagnetic signals primarily propagate through air, which is a low attenuation medium. During the earliest stages of radar research at the turn of the twentieth century, it was discovered that radar energy could be used to penetrate the ground for the purpose of detecting buried objects (Noon, 1996). Unfortunately the effective penetration range in geologic media is significantly smaller than in air due to larger attenuation.

The concept of ground penetrating radar (GPR) was attributed to Hulsmeyer in 1904 (Daniels, 1996). The first radar systems developed between 1904 and 1910 were known as continuous wave because the energy was confined about a specific frequency (White et al., 1996). However, despite the early recognition of GPR, the first portable GPR system was not developed until 1967. This system was developed for the detection of near surface tunnels in soil but through the 1970's and 1980's many applications for GPR were proposed (Noon, 1996). Considerable efforts were made to examine the use of GPR to measure coal thickness in underground mines, the thickness of glaciers, and to detect buried pipes and cables. Some of the earliest work used radar for exploration of rocks and minerals (Cook, 1975). Notwithstanding its successes, it took until the 1990's for GPR to develop into a well-established geophysical tool (Noon, 1996).

Today, ground penetrating radar is regarded as high-resolution radar, where the geological media attenuates and scatters the penetrating radio signals more than the free-space used in conventional radar systems (Noon, 1996). There are three different types of high-resolution radar: frequency-modulated continuous wave (FMCW), pulse-compression radar, and impulse radars. Most GPR systems are a type of impulse radar, where the transmitter emits a short energy pulse (Noon, 1996). Present GPR systems are different from the systems developed in the early 1900's because pulses are emitted across a broad band of frequencies. The bandwidth of most commercial GPR systems is 100% of the centre frequency. For example, if the centre antenna

frequency is 100 MHz, the bandwidth will range from 50 MHz to 150 MHz. The broad band nature of GPR is beneficial for improving resolution and penetration capabilities (Noon, 1996).

2.3   GENERAL OVERVIEW OF GPR

Ground penetrating radar is a geophysical survey tool that allows high-resolution imaging of the earth's shallow subsurface. The GPR system transmits short duration high frequency (10-1000 MHz) electromagnetic pulses from a transmitting antenna into the ground. As the radar energy propagates through the ground it reflects off subsurface features with contrasting dielectric properties. A receiving antenna picks up energy as the system measures the total travel time, the amplitude and polarity of the electromagnetic wave. The resulting plot of radar signal amplitude versus travel time is a pseudo cross-section of the subsurface where buried features are observed as reflection events (White et al., 1996). The distance to an object or interface is estimated based on the measured travel time and an assumed or measured signal propagation velocity.

GPR surveys are categorized as either low-resolution surveys, which have antenna frequencies in the range of 10 MHz to 200 MHz, or high-resolution surveys, which have antenna frequencies in the range of 250 MHz to 1200 MHz. Most commercial GPR systems have only surface antennas but borehole antennas are available. Borehole antennas are ideal in hard rock environments, but are also more intrusive and therefore more expensive. Borehole antennas are also available in a more limited frequency range of 50 MHz to 200 MHz. Frequency range is important because it has a major influence on the resolution and the depth range into the ground (Section 2.7).

Development of GPR as an investigation tool for geotechnical engineers in the last 10 years has been rapid. This is due to the constant demand for high-resolution near-surface mapping. Geophysical surveys are advantageous because they are non-intrusive, cost less in comparison to conventional drilling, and can be conducted both quickly and easily. GPR can also be carried out at sites where access is limited so drill rigs cannot be brought in. As well, new instrumentation and field procedures, improved data processing software for data interpretation, and decreasing equipment and rental costs are becoming more attractive to engineers.

There are also limitations to using ground penetrating radar. It does not work well in environments with highly conductive ground or in sites with lots of background noise. Interpretation of radar profiles is also difficult because like other geophysical techniques, radar suffers from nonuniqueness: there is no unique solution to the interpretation of any single data set. Lastly, GPR provides only information regarding location and possibly orientation of a subsurface target, not physical characteristics such as color or composition.

Despite these problems, there are a number of applications that use GPR as a profiling technique for high-resolution mapping and engineers are constantly looking for more. GPR is used in mining exploration, civil/geotechnical engineering, and environmental engineering. Some of the more common uses of GPR in these fields are:
- mapping of snow and ice thickness
- mapping mineral resources
- measuring depth to bedrock
- mapping fresh and contaminated groundwater
- detection of buried tunnels and mine shafts
- locating buried utilities
- locating faults, fractures, and voids

GPR applications and case studies are discussed further in Chapter 4.

2.4 Fundamental Electromagnetic Physics

The basic building blocks of electromagnetic theory provide the foundations of GPR. The electromagnetic signals that are transmitted into the subsurface by the transmitter antenna are described by two sets of equations: 1) Maxwell's equations, which describe electromagnetic physics and 2) constitutive equations, which describe the geological material properties (Annan, 1999).

Detailed descriptions of Maxwell's differential equations can be found in many physics textbooks, however Ampere's Law is one of the more important equations for understanding GPR.

Ampere's Law
$$\nabla \times \overline{H} = \overline{J}c + \frac{\partial \overline{D}}{\partial t}$$
(2-1)

Ampere's Law defines the relationship between the tangential component of the magnetic field ($\overline{H}$), the electric conduction current ($\overline{J}c$), and the electric displacement current ($\frac{\partial \overline{D}}{\partial t}$). As will be discussed in this section, it is the relative importance of these two currents which ultimately determines how electromagnetic waves propagate into the earth.

The electrical and magnetic properties are the two physical properties required to describe geological materials involved in GPR surveys. Specifically, the three important physical parameters are electric conductivity ($\tilde{\sigma}$), dielectric permittivity ($\tilde{\varepsilon}$), and magnetic permeability ($\tilde{\mu}$). The following three constitutive equations adequately describe how particles within a medium will respond to the application of electric and magnetic fields:

Constitutive Equation #1
$$\overline{J}c = \tilde{\sigma}\overline{E}$$
(2-2)

Constitutive Equation #2
$$\overline{D} = \tilde{\varepsilon}\overline{E}$$
(2-3)

Constitutive Equation #3
$$\overline{B} = \tilde{\mu}\overline{H}$$
(2-4)

In the above equations, $\overline{B}$ is the magnetic flux density vector, $\overline{E}$ is the electric field strength vector and $\overline{D}$ is the electric displacement vector. The three physical parameters $\tilde{\sigma}$, $\tilde{\varepsilon}$, and $\tilde{\mu}$ are third-order tensors but for the majority of GPR applications, and for the rest of this thesis, they are assumed to be scalars (Annan, 1999). In other words, geologic media is typically anisotropic and heterogeneous so these physical parameters vary spatially and in direction. However because it is difficult to model such complex conditions, it is assumed that geologic media is instead homogeneous and isotropic so the physical parameters are constant in both space and direction. In addition to this assumption, magnetic permeability (μ) is normally ignored for GPR because for most geological environments the magnetic variations are small compared to the electrical variations. As a result, electric conductivity (σ) and dielectric permittivity (ε) become the focus of GPR.

GPR involves time-varying electromagnetic fields that propagate through the earth. It is the interaction between these fields and the ground which controls how the electromagnetic waves spread and attenuate as they pass through the geological medium (Annan, 1999). The electric field applied to the ground causes movement of electric charge (or current flow). This total current is a mixture of conduction current (J_C) and displacement current $\left(J_D = \partial \overline{D}/\partial t \right)$.

Conduction Current $\boxed{J_C = \sigma E}$ (2-5)

Displacement Current $\boxed{J_D = i\omega\varepsilon E}$ (2-6)

In these two current equations, E is the electric field, ω is the angular frequency equal to $2\pi f$, and i is an imaginary number equal to $\sqrt{-1}$. Note also that Equations 2-2 and 2-5 are essentially the same.

Conduction current, J_C is free charge that moves with a constant velocity when an electric field is applied. Once the field is removed, the charge stops moving but remains in the newly acquired position. Similarly, the displacement current, J_D also moves with application of an electric field but with removal of the field the charges return to their original position. As such, these charges are referred to as constrained (or bound) charges because they are unable to permanently move to another location (Annan, 1999). The charge displacement that occurs with J_D creates an intrinsic dipole moment with charge separation described in terms of a dipole moment density, D (Annan, 1999). Dielectric permittivity, ε is described as the ratio between the dipole moment density and the electric field.

Generally, one of the two types of current will dominate when an electric field is applied to a medium. The ratio of these currents - referred to as the loss tangent - determines whether GPR can be used; in other words, these current determine whether the electromagnetic (EM) waves will propagate through the earth or diffuse and attenuate.

Loss Tangent $\boxed{\tan\delta = \dfrac{|J_C|}{|J_D|} = \dfrac{\sigma}{\omega\varepsilon}}$ (2-7)

The value of the loss tangent determines how GPR waves propagate into the ground. Figure 2-1 shows how total current, displacement current and conduction current vary as a function of frequency. The location where J_C equals J_D is referred to as the transition frequency, f_t and is important when considering whether EM waves will propagate or diffuse in the subsurface.

For a medium where $\tan\delta \gg 1$ (exist below the transition frequency), the conduction current will be significantly greater than the displacement current. EM waves will be diffusive in this regime and will quickly attenuate as they move through the medium. This situation arises when the medium's conductivity is large. However, if $\tan\delta \ll 1$ (exist above the transition frequency), the displacement current dominates and the EM waves will propagate through the medium as sinusoidal waves. This is the regime where GPR will be effective. Such geological environments are referred to as low loss.

In low loss, homogeneous, isotropic geological materials the relative propagation velocity (v) of the GPR waves can be described in terms of the speed of light, c (3×10^8 m/s) and the relative permittivity, ε_r.

Signal Propagation Velocity

$$v = \frac{c}{\sqrt{\varepsilon_r}}$$

(2-8)

Because all materials are conductive to some degree, the GPR waves will always be somewhat attenuated as they move through the ground. The attenuation constant, α (in dB/m) of a material is a function of the conductivity, σ (in mS/m) and the relative permittivity, ε_r (dimensionless).

Attenuation Constant

$$\alpha \approx \frac{1.69\sigma}{\sqrt{\varepsilon_r}}$$

(2-9)

2.5 IMPORTANT ELECTRICAL PROPERTIES OF GEOLOGICAL MATERIALS

In the previous section, it was explained that the electrical properties typically dominate the magnetic properties for ground penetrating radar. As a result, dielectric constant, ε_r and electrical conductivity, σ (or conversely resistivity ρ) are the two parameters used to describe the electrical properties of geological materials (Davis and Annan, 1989). For most geological materials, the electrical properties are primarily controlled by water content (Davis and Annan. 1989) as will be discussed in this section.

2.5.1 Dielectric Constant (ε_r)

Dielectric permittivity, ε is a measure of the electrical polarization or the ease with which constrained charges are displaced in a medium through application of an electric field. For GPR, it is more convenient to use relative permittivity or dielectric constant, ε_r, to describe a geological medium at higher frequencies, where the displacement properties dominate the conductive properties. Relative permittivity is the ratio between the permittivity of the medium, ε, and the permittivity through a vacuum, $\varepsilon_0 = 8.85*10^{-12}$ F/m.

Dielectric Constant

$$\varepsilon_r = \frac{\varepsilon}{\varepsilon_0}$$

(2-10)

For rock, the dielectric constant depends on the mineral assemblage and porosity. In more porous saturated rocks, such as sandstones, the bulk permittivity is dominated by the presence of water, which has a high dielectric constant of 80. However, hard unweathered rocks generally have a low porosity, so the dielectric constant is often more dependent on the mineral assemblage and discontinuities with the rock mass. Estimates of dielectric constant for various minerals and rock can be found in Keller (1989) and Telford et al. (1990).

2.5.2 Electrical Conductivity (σ)

Electrical conductivity describes the ease with which free charges form a current in the presence of an applied electric field (Annan, 1999). All geological media have some conductivity and if the value is too high, GPR will not be successful, as described in Section 2.4. For GPR, conductivity is assumed to be constant but in reality, conductivity is both non-linear and

frequency dependent, conductivity increases with frequency. There are also some geological materials that have conductive anisotropy due to the presence of structure. For example, sedimentary rock is likely to have maximum conductivity parallel to bedding and minimum conductivity perpendicular to bedding (Telford et al., 1990).

For any medium, electrical conductivity (σ) can also be described by its inverse value, electrical resistivity (ρ).

Electrical Resistivity $$\boxed{\rho = \frac{1}{\sigma}}$$ (2-11)

Resistivity, ρ has units of ohm.metre (Ω.m) and conductivity, σ has units of siemens per metre (S/m). For successful GPR work, the geological medium should have a conductivity less than 10 to 15 mS/m (Horvath, 1998) or a resistivity value greater than 67 to 100 Ω.m.

Most rocks and minerals are considered to be poor conductors, however electrical conductivity has enormous variations, especially in comparison to dielectric constant (Telford et al., 1990). This variability is primarily due to porosity— the ratio between the volume of void space (or pores) to the total volume in the rock. For the more porous rocks, electrical conductivity of the bulk rock (excluding fractures) is influenced by volume, shape, and arrangement of the pores. However, rock conductivity varies more importantly with the conductivity and amount of water contained within the pore space (Telford, et al., 1990). Variations in water conductivity are dependent on the amount and conductivity of dissolved ionic substances (Telford et al., 1990). Typical porosities for various sedimentary, igneous, and metamorphic rocks are shown in Table 2-1.

The highly variable porosity values for both sedimentary and volcanic rocks are a result of their genesis. Sedimentary rocks are formed from the accumulation of grains and rock fragments so their percent porosity can range from 0 to 90%. Volcanic rocks can also have high porosities when there is preservation of vesicles. In contrast, unweathered plutonic and metamorphic rocks typically have a low porosity (less than 1 to 2%) due to their interlocking crystal structure. With all rock types, porosity decreases with age and depth below the surface. In near surface rocks, exposure to weathering and fracturing increases the overall rock porosity by about 2 to 5 % (Fetter, 1988). In summary, porous sedimentary, volcanic, and highly weathered rocks that are saturated generally have high conductivities (or lower resistivities). Plutonic and metamorphic rocks have low porosities and low conductivities (or high resistivities) and thus are better for GPR surveys.

In addition to highly porous media, clay-rich ground and conductive ore bodies also have high conductivities. Figure 2-2 shows typical resistivity and conductivity values for various earth materials. In general, conductivity ranges between 10^{-2} mS/m to 10^5 mS/m. Shales, weathered rocks, massive sulphides and graphite have the highest conductivities. These rock types are considered poor media for GPR, in this thesis, because detection of rock structure within these rocks would be very difficult to impossible.

2.5.3 Typical Values of Electrical Constants of Geological Materials

Table 2-2 contains typical values of dielectric constant and conductivity for various geological materials at GPR frequencies. Signal propagation velocity and attenuation constant values have also been included because they can be calculated directly from ε_r and σ using Equations 2-8 and 2-9. Velocity and attenuation are discussed in detail in Section 2.6.

For some of the materials in Table 2-2 there is a range given for dielectric constant and conductivity, these ranges are due to the variation with water content. The influence of water on the electrical properties of geological materials has been mentioned previously, however reiteration of its importance is warranted.

In general, most dry geological materials have a dielectric constant between 4 to 8 but as the water content increases the bulk dielectric constant of the material increases. It is water's natural intrinsic dipole moment that results in a high dielectric constant of 80.

Conductivity also increases with increasing water content. Telford et al. (1990) noted that even small changes in the percentage of water has enormous affects on the overall conductivity. For example, a basalt under dry conditions was found to have a conductivity of 7.6×10^{-6} mS/m but with a 0.95% water content the conductivity increased to 0.025 mS/m (Telford et al., 1990). This corresponds to an increase in conductivity by a factor of 3,250.

Laboratory tests can be conducted on rocks and minerals to determine both the resistivity and dielectric constant. Further information on the exact testing procedures can be found in Telford et al. (1990).

2.6 GPR WAVE PROPAGATION

Ground penetrating radar utilizes time-varying electric fields typically within the 10 MHz to 1 GHz bandwidth. This frequency range is called the wave propagation regime because radar waves propagate through the earth instead of diffusing[1]. Within this regime, GPR systems have a maximum depth of investigation of several tens of metres in ideal conditions. As the antenna centre frequency increases, the resolution increases and the depth of penetration decreases.

Propagation of radio waves is influenced by two factors: propagation velocity and attenuation of the ground (Davis and Annan, 1989). Because both factors are dependent on the electric properties (discussed in Section 2.5), once ε_r and σ of the medium are known, the loss tangent, velocity and attenuation of the electromagnetic waves should be calculated according to Equations 2-7, 2-8, and 2-9.

Sections 2.6.1 and 2.6.2 focus on understanding how GPR waves propagate through the ground in terms of signal propagation velocity and attenuation. Section 2.6.3 examines the reflections produced by subsurface boundaries of contrasting dielectric properties in terms of the calculated reflection coefficient. Finally, Section 2.6.4 considers the reflectivity of 'thin layers' which are representative of most structural features in rock.

---

[1] Frequency divides the wave propagation regime – which occurs at frequencies above 1 MHz – from the diffusion regime – frequencies less than 100 kHz (Hyde and Dyke, 1999).

2.6.1 Signal Propagation Velocity

Energy from the GPR transmitter antenna propagates into the ground with a velocity controlled by the dielectric properties of the geological medium. In Section 2.4, the GPR signal propagation velocity for low loss (tan $\delta \ll 1$), non-magnetic, geological media was defined as being inversely proportional to the square root of the dielectric constant, ε_r (Equation 2-8). So, as the water content in the geological material increases, the dielectric constant increases and the signal propagation velocity decreases.

Excluding metallic material where the dielectric constant can be assumed to equal infinity, travel through water and air defines the velocity limits in a geologic medium. The radar velocity through air is about 0.3 m/ns whereas the velocity through fresh water is an order of magnitude smaller ($v \approx 0.034$ m/ns). The typical velocity through most dry rocks assuming a dielectric constant between 4-8 (Davis and Annan, 1989) ranges from 0.11 to 0.15 m/ns, which is approximately half the velocity through air. Table 2-2 contains velocities of typical soils and rocks.

Velocity through the ground does however vary with conductivity and frequency. Figure 2-3 (modified from Davis and Annan, 1989) shows that as either conductivity decreases or frequency increases, velocity increases; however, if ground conductivity is less than 10 mS/m the velocity remains essentially constant within the GPR frequency range of 10 to 1000 MHz. This figure also shows that at frequencies above 1 GHz, large velocity increases occur due to the relaxation effect of the water molecule (Davis and Annan, 1989). Fortunately this is not a big concern for GPR as there are not many commercial antennas available with frequencies above 1 GHz. Velocity variations will also not likely be a big concern on a project where more than one antenna frequency is used as long as the antennas are within the frequency range of 100 to 1000 MHz and the conductivity of the host medium is relatively low ($\sigma < 10$ mS/m).

Figure 2-4 shows a similar plot of velocity versus frequency for some common rock types in the GPR frequency range only. This plot shows that with frequencies above 200 MHz, it is an appropriate assumption that velocity is constant however, below 200 MHz, velocities may be either slightly lower or slightly higher depending on the type of host. This fact is important when conducting surveys using multiple low frequency (10-200 MHz) antennas.

Quite often a direct measurement of the signal propagation velocity through a geological medium is determined instead of the dielectric constant through field-testing. The two common field tests are referred to as common-midpoint survey (CMP) and the wide-angle reflection and refraction (WARR). Another less-common method of velocity estimation is tomographic imaging. These field methods are described further in Sections 3.4.2 and 3.4.3. Velocity can be also be calculated indirectly using the dielectric constant determined from laboratory tests. Telford et al. (1990) states that an ac bridge can be used to back-calculate the dielectric constant, which can then be used to estimate velocity.

2.6.2 Attenuation Constant

All geological materials have some conductivity - but it is often quite low - so there will always be some signal attenuation as the radar wave propagates through the earth. Attenuation is directly proportional to the conductivity of the material and inversely proportional to the square root of the dielectric constant (Section 2.4 - Equation 2-9). Attenuation decreases the amplitude of the radar energy making it more difficult to distinguish the desired reflections from the background

noise (Horvath, 1998). Signal attenuation also occurs by geometrical spreading losses and scattering (Horvath, 1998). Geometrical or spherical spreading losses causes a decrease in signal amplitude at a rate inversely proportional to the square of the distance from the signal source (Davis and Annan, 1989). Scattering is related to the target's geometry and roughness, contrasts in dielectric properties, signal frequency and wavelength (Davis and Annan, 1989).

Figure 2-5 shows that, similar to velocity, attenuation also increases with increasing conductivity and/or antenna frequency. As well, attenuation shows a substantial increase at frequencies above 1 GHz due to the water relaxation effect, however it is incorrect to assume a constant attenuation value within the GPR frequency range of 10-1000 MHz. In fact, attenuation of the radar signal will be non-linear within this range according to Figure 2-5. This fact becomes important when considering the use of a higher antenna frequency – the attenuation will be higher so the system will not be able to 'see' as far into the ground. Figure 2-5 also supports why conductive rock is poor medium for GPR – because these materials have high attenuation (Section 2.5.2).

Estimates of both attenuation and velocity can be determined using the antennas in transillumination mode. Transillumination mode is described in detail in Section 3.4.3.

2.6.3 Reflection and Transmission Coefficients

In a layered environment, radar energy emitted from the transmitter antenna propagates into the ground until it impinges upon a subsurface boundary with a sufficient contrast in dielectric constant from that of the overlying strata. Upon reaching this boundary part of the energy is reflected back towards the surface at an angle equal to the angle of incidence, while the remaining energy is transmitted through. Energy transmitted beyond the boundary will have a reduced amplitude however it has the opportunity to reflect at deeper subsequent interfaces.

The amount of energy reflected and transmitted at the interface can be described in terms of the reflection coefficient, R and transmission coefficient, T which solely depend on the dielectric constants of the two layers. The reflection coefficient is the ratio of the amplitude of the reflected pulse to the amplitude of the incident pulse, whereas the transmission coefficient is the ratio of the amplitude of the transmitted pulse to the amplitude of the incident pulse. These two coefficients are calculated using the dielectric constant of the ground above and below the interface.

If an electromagnetic wave passes from the upper Layer 1 with a dielectric constant, ε_{r1} to Layer 2 with material of dielectric constant, ε_{r2}, these two coefficients can be calculated for that particular interface using the following equations:

Reflection Coefficient
$$R = \frac{\left(\sqrt{\varepsilon_{r1}} - \sqrt{\varepsilon_{r2}}\right)}{\left(\sqrt{\varepsilon_{r1}} + \sqrt{\varepsilon_{r2}}\right)}$$
(2-12)

Transmission Coefficient
$$T = \frac{2\sqrt{\varepsilon_{r2}}}{\left(\sqrt{\varepsilon_{r1}} + \sqrt{\varepsilon_{r2}}\right)}$$
(2-13)

Summing the two coefficients together should equal unity (R+T = 1).

12

The key to successful target detection is to have a large contrast in dielectric constant, which will result in a high reflection coefficient (R) and large signal amplitude. It is recommended that the reflection coefficient, R should at least be greater than 0.01 for successful detection (Milsom, 1996).

The reflection coefficient has both a magnitude and a polarity determined by the sign. When radar energy propagates from ground with a high to low dielectric constant, the reflected signal will have the same polarity as the incident signal – Figure 2-6. Conversely, traveling into a medium of higher dielectric constant, the reflected signal will have an opposite polarity to the incident signal (or a 180° horizontal flip of the wavelet).

For example, if in karstic terrain, energy passes from carbonaceous rock with a ε_{r1} of 7 into a dry void space with a ε_{r2} of 1, both the reflection and transmission coefficients will yield positive values (i.e. R = 0.45 and T = 0.55). However, if the same void space is filled with water (ε_{r2} increases to 80) the reflection coefficient becomes a negative value indicating a phase shift of the energy that is reflected back to surface (i.e. R = -0.54 and T= 1.54). In the literature, the power reflection coefficient R^2 is sometimes mentioned but this parameter should be used with caution because this term does not reflect the phase change that occurs when energy passes from a low to high permittivity medium (Milsom, 1996).

The percentage of radar energy reflected from a subsurface reflector is a function of the target dimensions and type of surface as well as the amplitude reflection coefficient, R. For example, the larger the target is, the stronger the reflection will be. A rule of thumb for successful target detection is that the smallest lateral dimension of the target should be greater than $1/10^{th}$ the target's depth (Milsom, 1996). Using this criterion, a rock fracture located roughly 2 metres from the face should have an aperture greater than 20 cm for successful detection. As for the influence of a target's surface, smooth surfaces are preferred because rough surfaces tend to scatter energy which decreases reflected radar amplitudes (Milsom, 1996).

2.6.4   Thin Layer Reflectivity

Detection of rock structure, such as joints or bedding planes, are best represented in terms of a 'thin layer' concept. In GPR, a thin geologic layer is defined as a layer that has a thickness (t) less than the dominant radar wavelength (λ).

Thin Layer Criteria $\boxed{t \ll \lambda}$ where $\lambda = \dfrac{v}{f_c}$ (2-14)

In the above criteria, v is the velocity through the thin layer (in m/s) and f_c is the antenna centre frequency (in Hz). For the GPR frequency range of 10 MHz to 1000 MHz, a thin layer in a rock represents interfaces with a thickness less than 12 cm to 12 m assuming a typical signal propagation velocity of 0.120 m/ns. This indicates that all small-scale (< 1 cm) structural features fall under the definition of a thin layer, but so will some large-scale features whose thickness is less than 12 m but greater than 1 cm.

The thin layer concept is essentially defined as a layer with a finite thickness, t (in m), relative permittivity, ε_{r2} and velocity, v_2 (in m/ns) sandwiched between two infinite bodies of relative permittivity, ε_{r1} – Figure 2-7. The amplitude of a reflection from a thin layer is determined from the Fresnel Reflection Coefficient, R_t (Annan, 1999).

Fresnel Reflection Coefficient

$$R_t = \left(\frac{R}{1-R^2}\right)\left(\frac{4\pi t f_c}{v_2}\right) \text{ where } \frac{4\pi t f_c}{v_2} \ll 1 \quad (2\text{-}15)$$

In the above equation, R is the reflection coefficient calculated according to Equation 2-13 and f_c is the antenna centre frequency (Section 3.2). Equation 2-15 also shows that reflectivity of a thin layer is proportional to the thickness of the layer. A point to note is that if the thickness of the layer is approximately equal to ¼λ, a tuning effect occurs which gives rise to a strong reflection (Section 2.7.2.1).

Because this thesis focuses on detection of small-scale discontinuities, the reflection coefficient has been calculated for both water and air-filled joints of various thicknesses, and using antenna centre frequencies between 100 MHz and 1 GHz antenna - Figure 2-8. The curves for the various frequencies have been plotted assuming a ε_r of 6.25 for rock, ε_r of 1 for air, and ε_r of 80 for water. Be aware that for small-scale structural features such as joints, the thickness in the thin layer concept represents the aperture of open discontinuities or width of filled discontinuities. It does not represent joint spacing or distance between two adjacent discontinuity planes.

At present there is no criterion for what R_t threshold allows for successful detection of a 'thin layer'. This is why there is a questionable boundary line marked on both plots in Figure 2-8. With R_t being a measure of the reflection amplitude, the criterion that at least 1% of the incident energy to be reflected for successful detection (R > 0.01) may hold but there is no evidence to either confirm or deny this. With the literature review in Chapter 4 and the GPR field surveys described in Chapters 5 and 6, a better understanding of R_t threshold value (or range of values) is presented in this thesis (Section 6.5).

Despite the uncertainty of where this threshold lies, the reflectivity plots in Figure 2-8 show certain facts. First of all, by increasing the antenna centre frequency there is an increased chance of target detection. Secondly, water-filled fractures have a greater chance of being detected in comparison to air-filled fractures of the same aperture. This is because the higher contrast in dielectric constant yields a higher Fresnel Reflection Coefficient. Also, reflections caused by saturated fractures will experience a change in the polarity, which may be observed in the radargram. Lastly, water-filled fractures can be detected to smaller apertures than air-filled fractures using the same antenna centre frequency.

2.7 PERFORMANCE CHARACTERISTICS OF GPR

The above sections have examined the relationships between electromagnetic wave propagation and the ground material properties for GPR frequencies, so the performance of a GPR system can now be discussed. Performance of ground penetrating radar is defined in terms of two characteristics: depth of penetration and resolution. This section will describe the depth of penetration (Section 2.7.1) and resolution in terms of both lateral and vertical resolution (Section 2.7.2). Because the two performance characteristics are not independent of each other, Section 2.7.3 discusses the required trade-off between penetration and resolution.

2.7.1 Depth of Penetration

The depth of penetration (or radar signal range) is defined as the depth at which the amplitude is reduced such that it is indistinguishable from the background noise. Targets can only be distinguished if they are above the penetration depth. The depth of penetration is affected

14

primarily by the radar system performance (Q), ground attenuation (α) and reflection properties at the boundary where the dielectric properties vary (Davis and Annan, 1989).

System performance or dynamic range, Q represents the ratio between the largest and smallest amplitude that can be measured by the system. However, Q is more conveniently expressed in terms of system powers and therefore has units of decibels.

System Performance Factor
$$Q = 10\log_{10}\left[\frac{Source.power}{Re\,ceiver.noise.power}\right]dB \qquad (2-16)$$

Q is an important parameter because it influences both the radar range of the system and target size that can be detected (Annan, 1999). Q should therefore be designed with a high value since increasing system performance will increase the depth of penetration. As well, by increasing Q the system will more accurately measure amplitude variations (Kearey and Brooks, 1991). However, despite the fact that GPR system designers have a lot of control over the value of Q, most commercial GPR systems are designed to accurately measure travel time, not amplitude (Parry and Davis, 1992).

System performance is dependent on a defined integration time or amount of stacking (Noon, 1996). Davis and Annan (1989) stated that GPR systems generally have a Q ranging between 120 to 160 dB however there is no mention to the amount of stacking this range applies to. Noon (1996) more specifically stated that a typical Q value for impulse radar systems range between 100 to 130 dB with no stacking. The RAMAC/GPR system used in this study had a Q greater than 150 dB, however there is no mention of the degree of stacking.

The depth that electromagnetic signals will penetrate the ground depends on the attenuation of the ground, which is ultimately influenced by the electrical conductivity. As the attenuation of the signal increases, the depth of penetration decreases. Ground attenuation, α (dB/m) decreases the original signal amplitude, A_o with depth, z (m) according to the following equation:

Pulse Amplitude at Depth, z
$$A = A_o e^{-\alpha z} \qquad (2-17)$$

Materials with high conductivity (i.e. clays or metallic ore bodies) have high attenuation rates and corresponding shallow depths of penetration.

The radar range equation (RRE) introduced by Annan and Davis (1977) allows the depth of penetration to be estimated. The radar range calculation considers all events from signal generation in the transmitter antenna to the signal that is picked up at the receiver antenna. The equation is a function of the system performance, antenna efficiencies, antenna gains, distances from target to transmitter and receiver antennas, effective area of the receiver antenna, velocity through medium, frequency, backscatter gain of the target, scattering cross-sectional area of the target, and the attenuation constant of the medium. When using the equation to estimate the depth of penetration for a selected antenna frequency, it is recommended that the worst case conditions are assumed (Davis and Annan, 1989) and the calculations are done using a spreadsheet. Annan and Davis (1977) and Annan (1999) contain example calculations of RRE.

Unfortunately, the RRE cannot always be used because it requires many input parameters, some of which are unknown. In cases where there is limited information about the site, a trial run

should be conducted to determine the depth of penetration. If finances do not allow this, a rough estimate of the penetration depth can be made using the following equation:

Depth of Penetration (Rough Estimate) $$z = \frac{35}{\sigma}$$ (2-18)

where depth, z is in metres and conductivity, σ is in mS/m. Equation 2-17 is valid when ground attenuation is > 0.1 dB/m or conductivity is > 1 mS/m.

Once the depth of penetration is calculated by one of these means, the survey designer should ensure the radar target is above this depth. A conservative rule-of-thumb for successful detection is to ensure the target is located less than 50% of the penetration depth (Annan, 1999).

2.7.2 Resolution

Resolution is defined as the ability of a radar system to distinguish between two subsurface targets that are close to each other in time. GPR surveys are designed to provide a specific degree of resolution for the subsurface in both the vertical and horizontal directions. Not only is vertical and lateral resolution important to understand in regards to conducting the survey, but they should be examined separately because they are based on different criteria.

2.7.2.1 Vertical Resolution

Vertical resolution relates to how close two reflectors can be placed vertically and still be detected as distinct reflection events. In terms of rock structure (for features that are not thin layers) the vertical resolution will define the minimum thickness such that both the top and bottom contacts of the structural feature are individually identifiable – Figure 2-9.

Vertical resolution is primarily dependent on the dominant wavelength[2], λ of the recorded signals, regardless of target's depth (Pilon et al., 1996).

Dominant Wavelength $$\lambda = \frac{v}{f_c} = \frac{c}{f_c \sqrt{\varepsilon_r}}$$ (2-19)

Despite the fact most radar systems have a theoretical resolving capability of 1/100 th of the dominant wavelength (Pilon et al., 1996), the threshold for vertical resolution is generally one quarter of the dominant wavelength (Yilmaz, 1987).

Vertical Resolution $$\lambda_v = \frac{\lambda}{4}$$ (2-20)

This vertical resolution limit means it is nearly always possible to pick the onset of radar energy to 1/4 the wavelength (Pilon et al., 1996). Be aware that this limit is still subjective and should only be used as a guide because vertical resolution is ultimately dependent on the noise level in

---

[2] The term dominant wavelength is used when dealing with waves that contain a spectrum of frequencies (Sheriff, 1973).

16

the data (Yilmaz, 1987). For example, when the reflection coefficient is small (R < 0.01) this limit will likely be too generous (Yilmaz, 1987).

Table 2-3 provides estimates of the threshold vertical resolution through rock media (assuming a propagation velocity of 0.12 m/ns) using various GPR antenna frequencies. The values in this table show that resolution can be improved by increasing the frequency, however the disadvantage is that the depth of penetration decreases accordingly. Lastly, vertical resolution may be improved with advanced data processing by using a seismic technique called 'deconvolution'. Processing by deconvolution is briefly described in Section 3.7.2, however Yilmaz (1987) provides a more detailed discussion.

Unfortunately, resolution does not consider amplitude. Because signal amplitude decreases with depth, it is often detection and not resolution that is the main issue for many GPR problems (Yilmaz, 1987). Most rock structure fits the criteria of a thin layer so the higher frequency (> 200 MHz) antennas should be used to increase detection and resolution. If GPR is used in low conductivity, igneous or metamorphic shield rock, it should be possible to detect fracture apertures (or widths) in the millimetres range (Pilon et al., 1996). This is because the energy reflected from these thin targets should not be attenuated beyond the recording capability of the system (Pilon et al., 1996).

2.7.2.2   Lateral Resolution

Lateral resolution defines how close two targets can be situated horizontally in the subsurface and still be seen in the radargram as separate entities. For example, if GPR was being used to detect two buried pipes, lateral resolution would help to define how far apart the pipes have to be in order to show up as two reflections events in the radargram instead of one large event – Figure 2-10. Lateral resolution is more complicated to assess in comparison to vertical resolution because it is controlled by the Fresnel zone.

The Fresnel zone is best explained by considering a horizontal subsurface interface that is composed of an infinite number of point scatterers that produce an infinite number of backscattered rays. When GPR energy hits the interface, detectable reflected energy comes only from a portion of the interface called the Fresnel zone. In this zone, energy interferes constructively building up a reflected signal[3], whereas outside of this zone, energy interferes destructively and cancels out.

The Fresnel zone corresponds to a circular area on the reflector whose size is a function of the depth to the target, signal velocity and dominant frequency - Figure 2-11. The radius is defined as

Radius of Fresnel Zone $\boxed{r = \sqrt{z\lambda}}$ (2-21)

where λ is the dominant wavelength and z is the closest distance from the antenna midpoint to the target (Holloway and Mugford, 1990).

The limit of the horizontal resolution is defined by the width of the Fresnel zone. Hence, subsurface horizontal targets have to be separated by a distance larger than the width of the

---

[3] Within the Fresnel zone, energy is reflected within 1/2 a wavelength of the initial reflected arrival (Kearey and Brooks, 1991).

Fresnel zone in order to be individually distinguished (Kearey and Brooks, 1991). The Fresnel zone width, w is also function of dominant wavelength, λ and depth to the reflector, z.

Width of Fresnel Zone
(or Horizontal Resolution)

$$\boxed{w = \sqrt{2z\lambda}} \text{ where } z \gg \lambda \qquad (2\text{-}22)$$

Because the width of the Fresnel zone depends on the dominant wavelength which is inversely proportional to frequency (Equation 2-17), as the frequency increases the width of the Fresnel zone decreases. It is beneficial to have a narrow Fresnel zone because this increases the ability to differentiate between two horizontal reflectors (Yilmaz, 1987). However due to attenuation of the radar signal as it moves down through the subsurface, the dominant frequency decreases causing the Fresnel zone to increase with depth. As a direct result of this, horizontal resolution deteriorates with increasing reflector depth (Kearey and Brooks, 1991).

On reflectors at depth, a smearing or blurring effect is observed in the radargram - reflections widen and overlap each other. In this situation, lateral resolution can be improved by advanced data processing using a technique called 'migration'. Migration decreases the width of the Fresnel zone, allowing for separation of features that originally could not be seen. Lateral resolution can also be improved by decreasing the station spacing (Section 3.4.1.4).

2.7.3   Trade-off Between Depth of Penetration and Resolution

Both penetration and resolution are dependent on the radar operating frequency and therefore are parameters always in contention with each other. Generally, GPR is used for its superior resolution capability, however if higher frequency antennas are used to increase resolution the depth of penetration will decrease. Because of this effect, there will always be a trade-off between the depth of penetration and resolution.

To help with selection of a proper antenna frequency, most manufacturers have approximate values of penetration and resolution for their specific antennas - Table 2-4. The values in Table 2-4 are what can be achieved in a 'normal' geological environment. MALA GeoScience does no adequately define the term 'normal' but it likely represents an environment were the conductivity is less than 10 mS/m. As a result, the penetration and resolution values give in this and other similar tables should be used as a rough guide only.

For designers, low frequencies are easier to work with because it is easier to put more power into the transmitted pulse which in turn increases system performance, Q and ultimately increases the depth of penetration (Davis and Annan, 1989). Because of this, Davis and Annan (1989) recommend that it is better to accept a reduced resolution for a higher penetration (i.e. a lower frequency antenna over a higher frequency antenna). For this thesis however, one of the main objectives is to detect small-scale features such as joints therefore the use of higher frequency antennas is more applicable.

Another recommendation is to conduct a GPR survey using at least two or three different antenna frequencies. This is in response to the difficulty in selecting the proper antenna frequency. Quite often if frequencies are too high, unwanted reflectors will overwhelm the radargram obscuring the reflectors of interest. An initial estimate of suitable antenna frequency can be made if there is a desired spatial resolution, d:

Estimate of Suitable Frequency

$$f_c = \frac{150}{d\sqrt{\varepsilon_r}}$$

(2-23)

A more complete discussion of the importance of antenna frequency can be found in Section 3.4.1.1.

2.8   SUMMARY AND CONCLUSIONS

The concept of ground probing radar may have been around as early as 1904, but only in the last 20 years has this technique been regarded as a valuable means of examining near-surface ground variability. Clearly it is GPR's unique merits of high-resolution capability, non-destructive detection, portability and efficiency that have caused it to gain rapid recognition as a reliable tool for a diverse number of applications.

GPR operates in the wave propagation regime because it uses high frequencies – at these frequencies the displacement current is significantly larger than the conduction current. Operating in this regime equates to superior resolution capability, increased accuracy in depth and thickness estimation in comparison to other geophysical methods such as seismic and EM; however, this is at the expense of decreased depth of penetration. Typically radar has a depth of penetration between 1 to 100 m for antenna centre frequencies of 1000 to 10 MHz respectively.

For radar, it is the electrical properties - dielectric constant and conductivity - that are important when assessing how well GPR will propagate through geologic media. Typically, the ideal rock conditions for GPR are non-conductive, unweathered, homogeneous, shield rock. GPR has the capability to detect both lateral and vertical changes in dielectric constant in the ground. Since variations in dielectric constant often occur due to rock structure, it is anticipated that radar can be used to detect rock structure. For example, changes in dielectric constant may be associated with changes in rock type, small-fractures with various infillings, faults, or other rock inclusions such as dykes or sills.

Not only should there be a sufficient contrast in dielectric constant but the target has to be large enough such that it can be detected. For large-scale structures detection is generally not a problem and in some cases, the width can even be determined. For small-scale targets, detection is dependent on the thickness of the interface hence the thickness cannot be resolved. The 'thin-layer concept' and the Fresnel Reflection Coefficient are important concepts as they provide the theoretical basis behind detection of small-scale (and sometimes large-scale) rock structure. Using higher antenna frequencies detection of thin targets is possible, however there is presently no guidance as to what the minimum thickness (or aperture or width) can realistically be detected.

Table 2-1 Porosity values of typical rocks (Todd, 1964; Goodman, 1989; Brassington, 1998; Fetter, 1988; and Davis, 1969).

	Rock Type	Porosity (%)
Sedimentary Rocks	Dolomite	0.4 to 3
	Limestone	0.5 to 43
	Sandstone	1 to 37
	Shale	1 to 34
Volcanic Rocks	Basalt	1 to 17
	Pumice	87
	Tuff	14 to 40
	Volcanic Ash	50
Plutonic Rocks	Diabase	< 1
	Gabbro	< 1
	Granite	< 1
	Tonalite	7
	Weathered Granite	45
Metamorphic Rocks	Marble	< 1
	Schist	38

Table 2-2 Typical electrical properties of geologic materials (Davis and Annan, 1989).

Geological Medium	Dielectric Constant, ε_r	Conductivity, σ (mS/m)	Propagation Velocity, v (m/ns)	Attenuation Constant, α (dB/m)
Air	1	0	0.3	0
Ice	3 – 4	0.01	0.16	0.01
Water (fresh)	80	0.5	0.033	0.1
Water (salt)	80	3000	0.01	1000
Soils				
Clays	5 – 40	2 – 1000	0.06	1-300
Sand (dry)	3 – 5	0.01	0.15	0.01
Sand (saturated)	20 – 30	0.1 - 1.0	0.06	0.03-0.3
Silts	5 – 30	1 – 100	0.07	1-100
Minerals				
Calcite[1]	7.8 – 8.5	5×10^{-10}	0.11	3×10^{-10}
Quartz[1]	4.2 – 5	$3\times10^{-8} - 5\times10^{-12}$	0.13-0.15	$2\times10^{-8} - 4\times10^{-12}$
Sedimentary Rocks				
Limestone	4 – 8	0.5 – 2	0.12	0.4-1.0
Salt (dry)	5 – 6	0.01 – 1	0.13	0.01-1
Sandstone (dry to moist)[1]	4.7 - 12	$1\times10^{-5} - 0.7$	0.09-0.14	$5\times10^{-8} - 0.6$
Shales	5 – 15	1-100	0.09	1-100
Igneous Rocks				
Basalt[1]	12	$8\times10^{-6} - 0.025$	0.09	$4\times10^{-6} - 0.01$
Dacite[1]	6.8 – 8.2	0.05	0.12	0.03
Diabase[1]	10.5 - 34.5	$2\times10^{-5} - 50$	0.05-0.09	$1\times10^{-5} - 26$
Diorite[1]	6	0.0002-0.002	0.12	0.0001-0.001
Gabbro[1]	8.5 - 40	0.001-1	0.05-0.10	$3\times10^{-4} - 0.6$
Granite	4 – 6	0.01-1	0.13	0.01-1
Norite[1]	61	0.02-1	0.04	0.004 - 0.2
Obsidian[1]	5.8 - 10.4	n/a	0.11	n/a
Peridotite[1]	8.6	0.15-0.33	0.10	n/a
Metamorphic Rocks				
Gneiss[1]	8.5	0.0003-0.02	0.10	n/a
Argillite[1]	n/a	1-100	n/a	n/a
Quartzites[1]	n/a	$5*10^{-6}-100$	n/a	n/a

Notes
1. Values taken from Telford et al. (1990) where ε_r values are for frequencies 100 kHz and up.
2. n/a = not available

Table 2-3 Estimates of vertical resolution for various frequencies in rock.

Antenna Centre Frequency (MHz)	Vertical Resolution $\lambda/4$ (m)
25	1.2
50	0.6
100	0.3
200	0.15
400	0.075
1000	0.03

Table 2-4 Typical performance characteristics within GPR frequency range (modified from MALA GeoScience, 1997).

Antenna Centre Frequency (MHz)	Vertical Resolution (m)	Depth of Penetration (m)
25	≥ 1.0	5-30
50	≥ 0.5	5-20
100	0.1-1.0	2-15
200	0.05-0.50	1-10
400	≈ 0.05	1-5
1000	cm	0.05-2
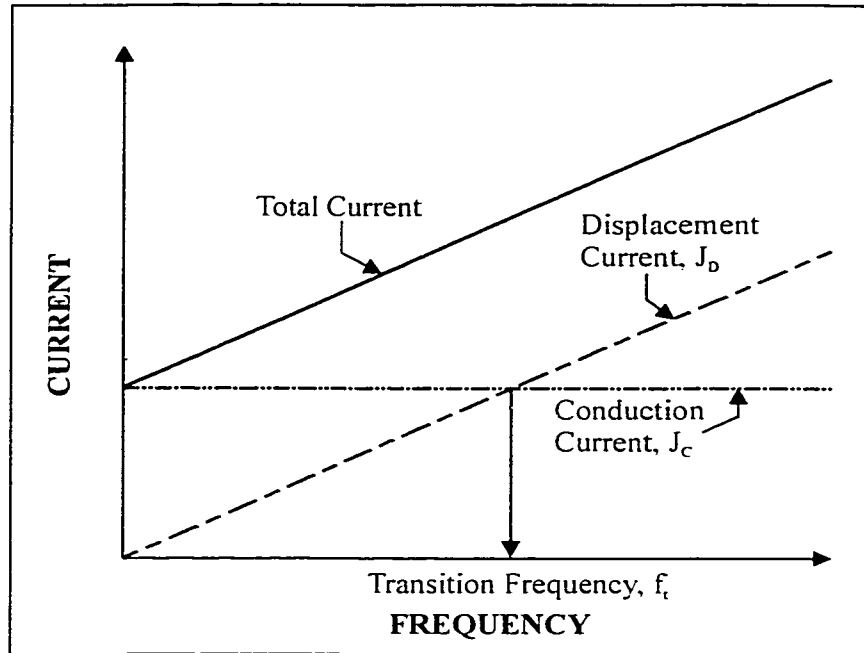
Figure 2-1 GPR current versus frequency.
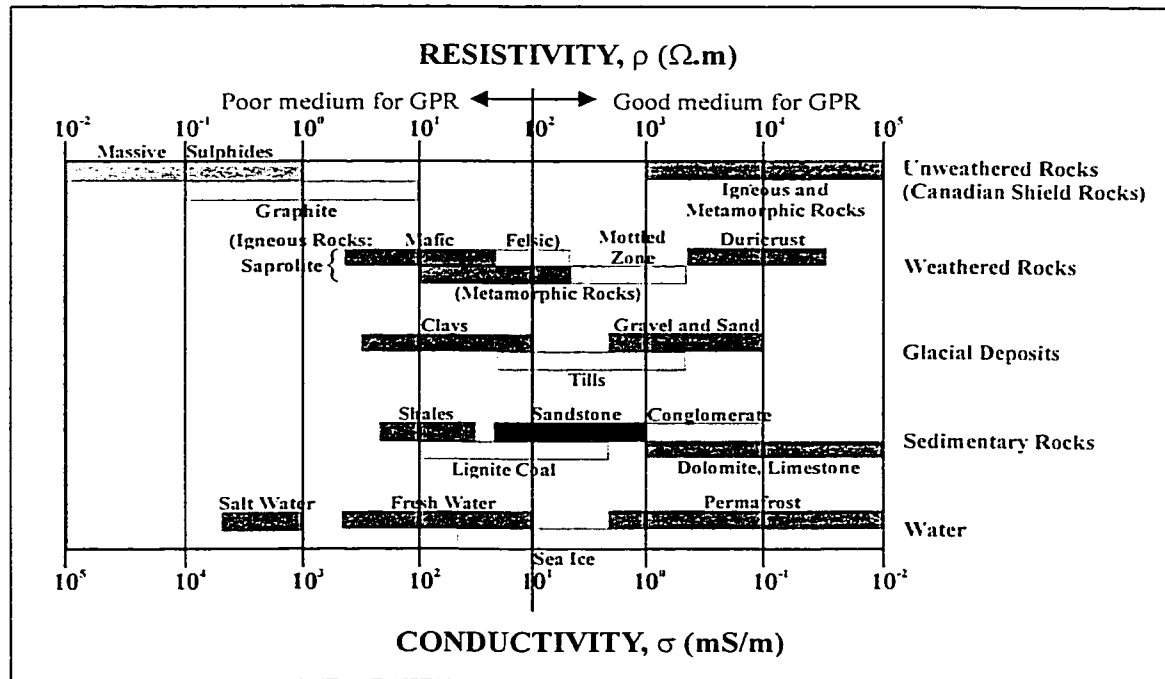
Figure 2-2 Typical conductivity and resistivity values for geological media
(modified from Palacky, 1988).
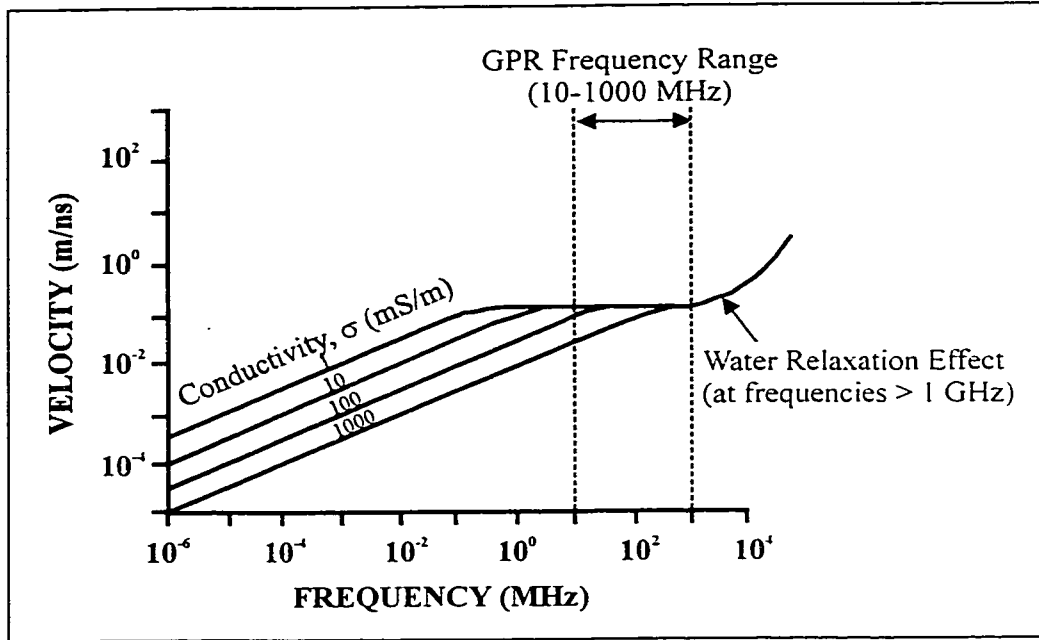
Figure 2-3 Signal velocity variations with frequency and conductivity
(modified from Davis and Annan, 1989).
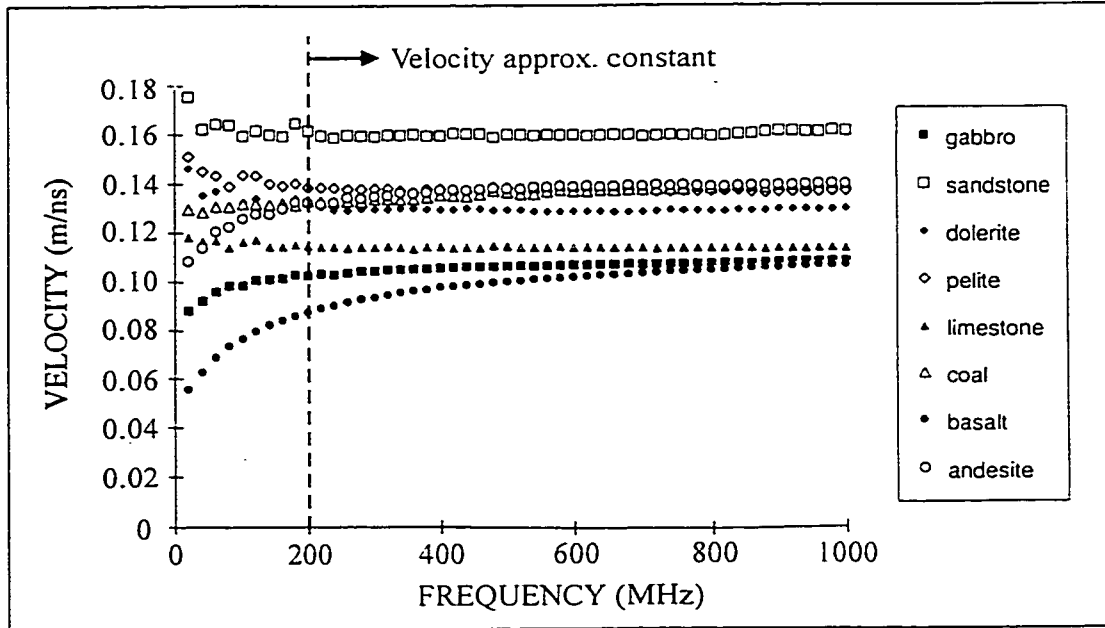
Figure 2-4 Signal velocity versus frequency for various types of rocks
(modified from Turner, 1992).
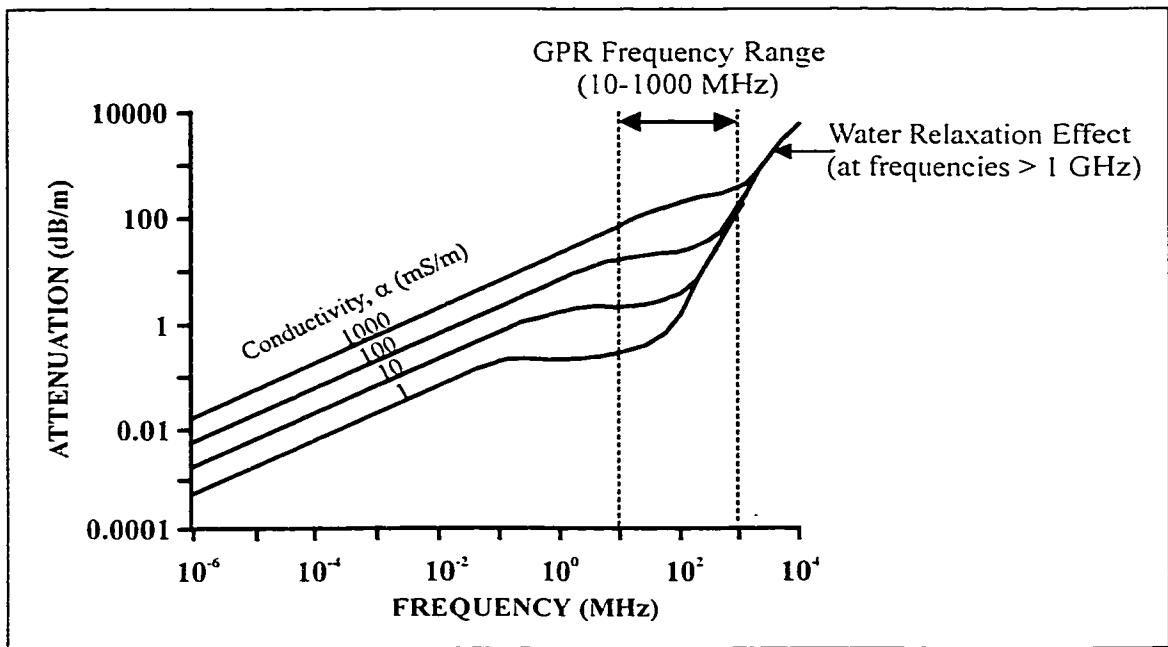
Figure 2-5 Attenuation variations with frequency and conductivity
(modified from Davis and Annan, 1989).
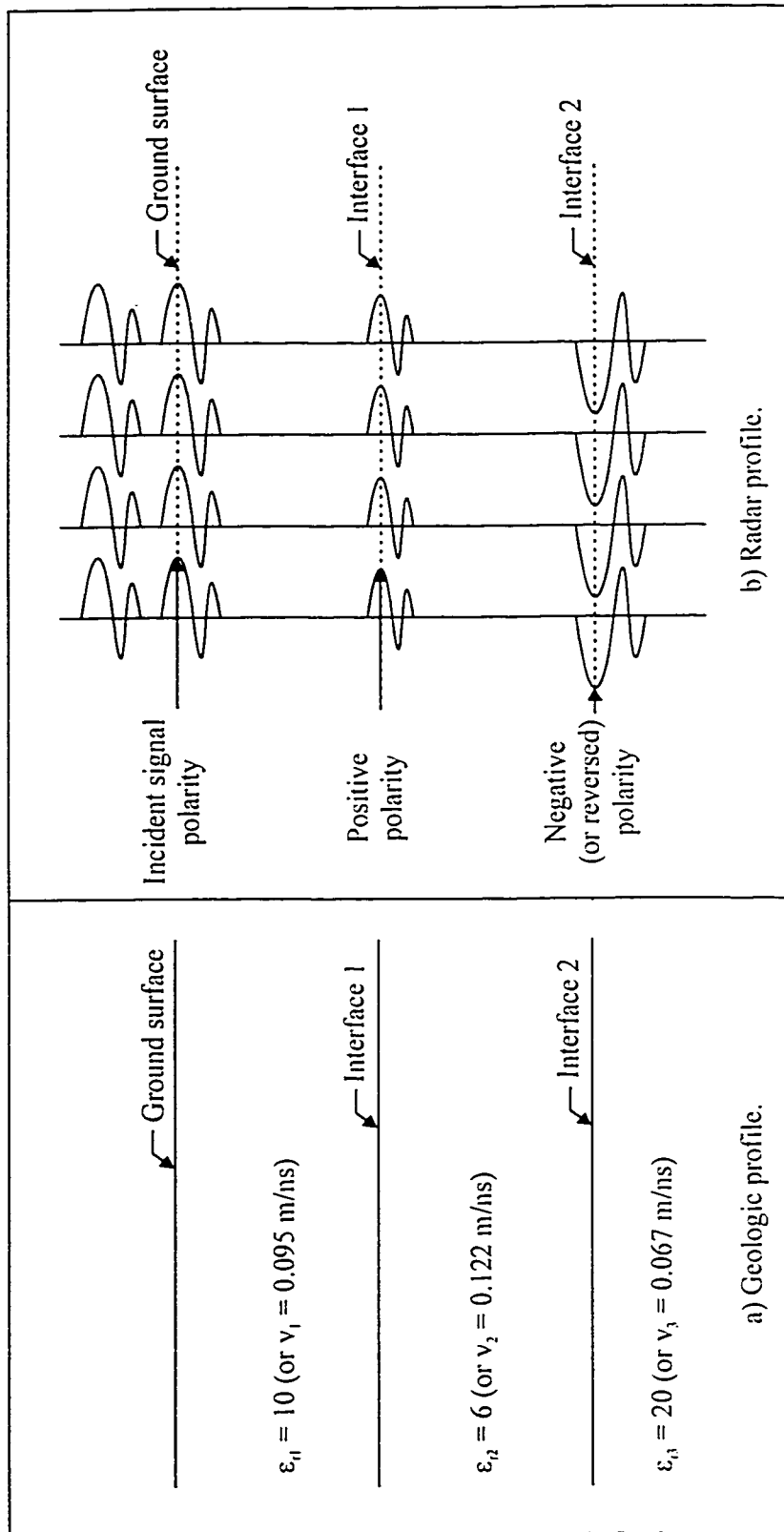
Figure 2-6 Example of radar polarity.

b) Radar profile.

Ground surface

Interface 1

Interface 2

Incident signal polarity

Positive polarity

Negative (or reversed) polarity

Ground surface

Interface 1

Interface 2

$\varepsilon_{r1} = 10$ (or $v_1 = 0.095$ m/ns)

$\varepsilon_{r2} = 6$ (or $v_2 = 0.122$ m/ns)

$\varepsilon_{r3} = 20$ (or $v_3 = 0.067$ m/ns)

a) Geologic profile.

26
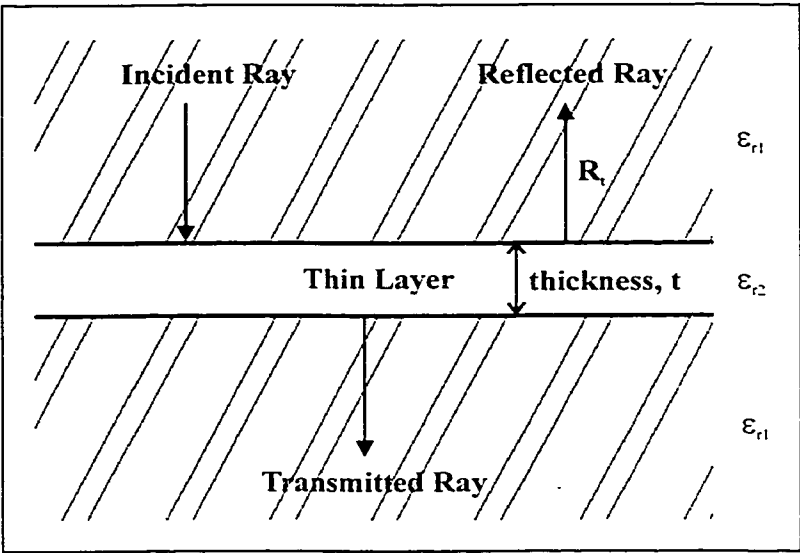
Figure 2-7 Thin layer concept - Fresnel reflection coefficient, R_t.
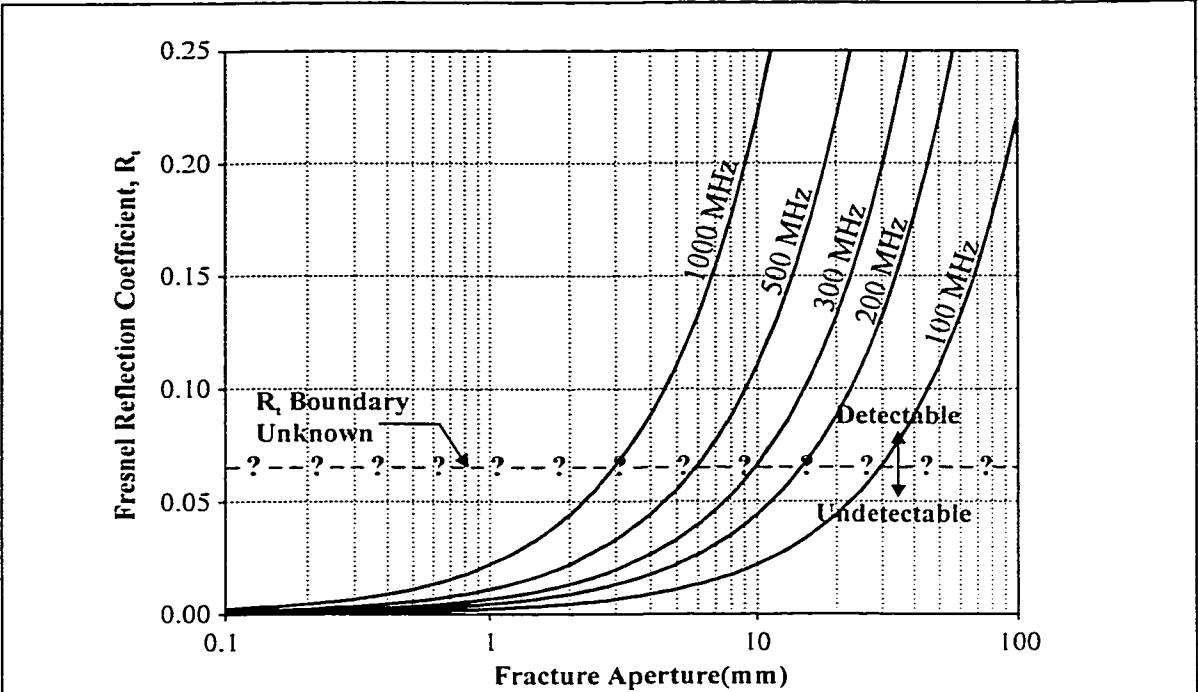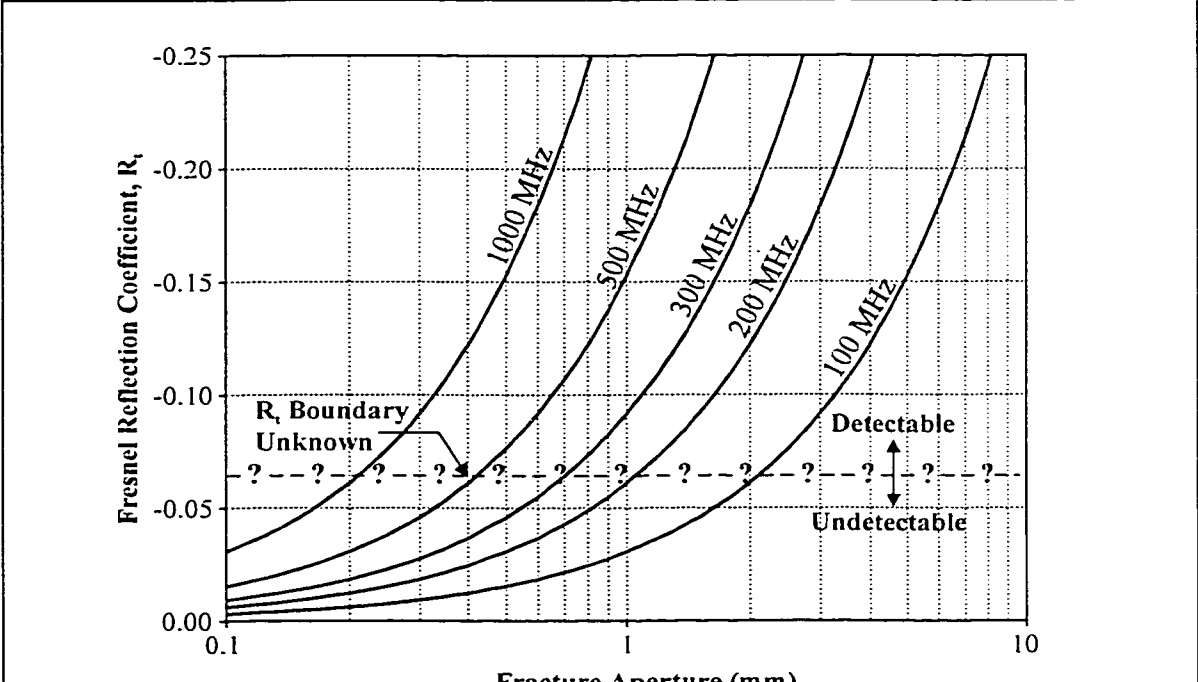
Figure 2-8 Reflectivity plots for small-scale (wet & dry) fractures using various GPR antenna frequencies. (Note: Assumed $\varepsilon_r = 6.25$ for rock, $\varepsilon_r = 1$ for air, & $\varepsilon_r = 80$ for water.)

28
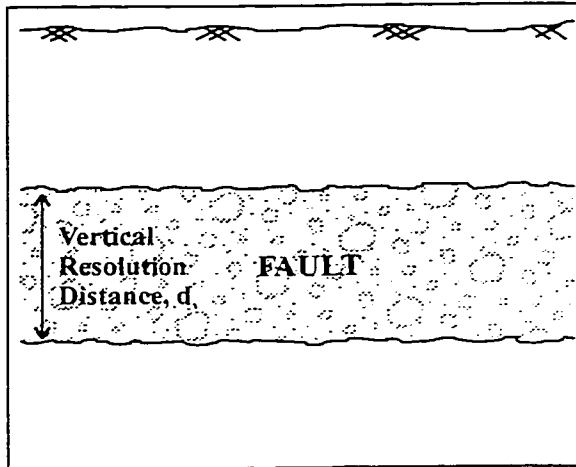
Figure 2-9 Example of vertical resolution.
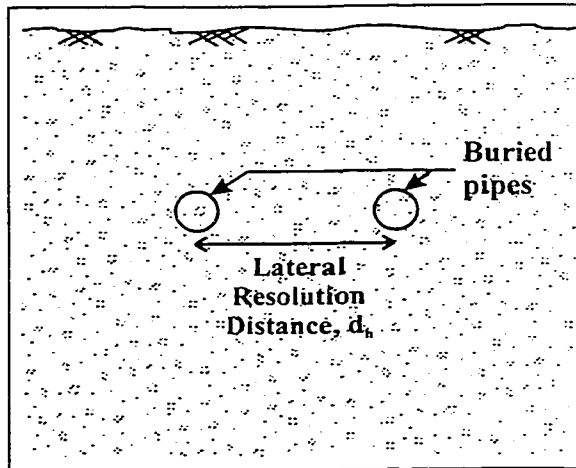
Figure 2-10 Example of lateral resolution.
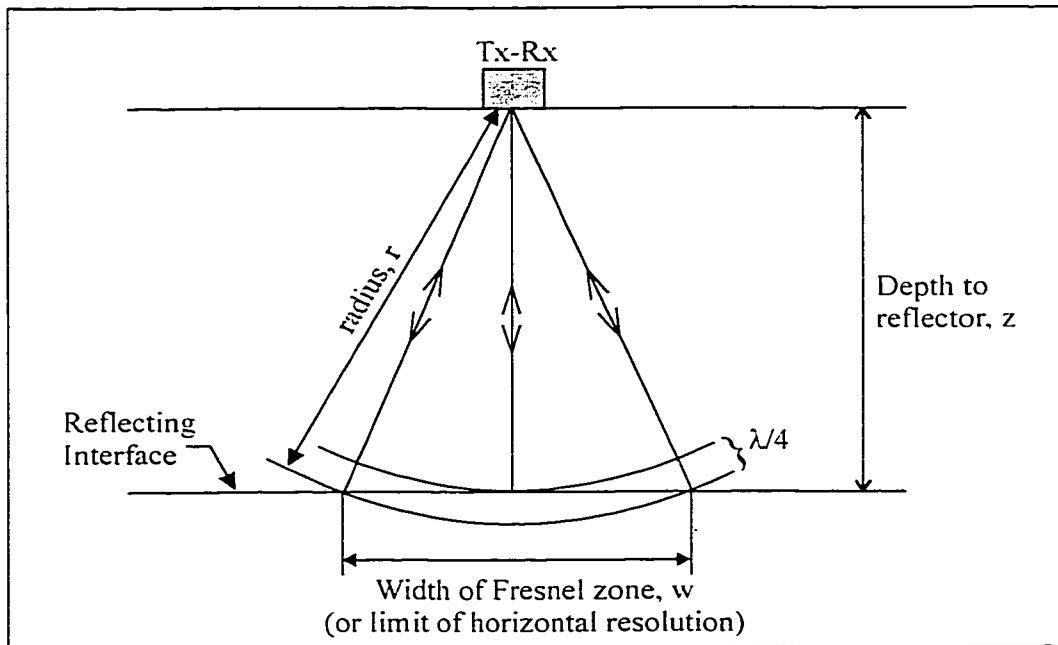
Figure 2-11 Fresnel zone.

CHAPTER 3: GPR SURVEYS

3.1 INTRODUCTION

Chapter 3 examines the steps involved in conducting a GPR survey with a focus on reflection surveying. Section 3.2 outlines the various components and the basic operation of the RAMAC/GPR system used in this project. Sections 3.3 and 3.4 describe the primary radar pulse pathways and the three basic survey modes. Since reflection surveying was used in the field component of this study, the seven most important factors and their corresponding geophysical criteria, which aid in the selection of the GPR input parameters, are given in Sections 3.4.1.1 to 3.4.1.7. For the site reconnaissance, Section 3.5 lists a number of site and ground conditions that need to be considered in order to gauge the success of GPR. Data collection and an introduction to processing are described in Sections 3.6 and 3.7 respectively. Finally, Section 3.8 discusses general interpretation of GPR radargrams and Section 3.9 contains summary remarks and conclusions for Chapter 3.

3.2 EQUIPMENT

There are four major components that make up a commercially-available digital GPR system such as the RAMAC/GPR system used in this project: control unit, transmitter (Tx) component, receiver (Rx) component, and personal computer - Figure 3-1. The basic operation of the GPR system involves the following steps: the control unit sends a control signal to the transmitter which then generates short radar pulses that propagate through the ground. If the energy contacts an interface or a buried object with a high contrast in dielectric constant, part of the energy is then reflected back towards the surface where it can be picked up by the receiver. The receiver amplifies and registers the pulses as a function in time and passes the collected information to the control unit. The control unit converts the signal and sends it to the computer for storage, display and later analysis.

The control unit is the heart of the system for it controls the timing, storage, and stacking of single radar measurements. Attached to both the Tx and Rx electronics via optical fibres, the control unit both commands the Tx to send out pulses and starts the Rx sampling process. The control unit is connected to the computer with a communications cable through the computer's parallel port. A trig box, measuring wheel or hip chain are optional devices that can be connected to the control unit, to help control data collection along a survey line.

The transmitter is composed of an electronic unit plus an antenna. In the RAMAC/GPR system the electronic parts are mounted directly on the antennas using metal clamps. The Tx electronic unit generates the electromagnetic energy in the form of a high amplitude pulse, which is then transmitted into the ground via the Tx antenna. A single pulse is generated every time a control signal is received from the control unit via the optical fibre.

The receiver is also composed of an electronic unit and an antenna. The Rx antenna picks up reflected signals which are then converted to a numerical integer value by the Rx electronic unit. Unlike the Tx, there are two leads from the Rx electronic unit to the control unit. One lead transfers information from the control unit regarding sampling timing and the other sends the collected information from the Rx electronics to the control unit.

The Tx antenna is designed to emit a single sinusoidal radar pulse of duration. Δt with a centre frequency, $f_c = 1/\Delta t$ and a frequency bandwidth, Δf - Figure 3-2. The RAMAC/GPR system antennas are bow-tie antennas. These antennas have a bandwidth of 100% and are preferred for impulse GPR systems (Noon, 1996). Figure 3-2 shows how bow-tie antennas with a centre frequency of 100 MHz has a bandwidth that ranges from 50 to 150 MHz. Bow-tie antennas are also non-dispersive, which means the antennas experience minimal broadening of the radar pulse during transmission and receiving (Noon, 1996).

All the major components are powered by battery packs, although most personal computers come with an AC adapter as well as a rechargeable battery. For the RAMAC/GPR system, the battery packs for the control unit and transmitter and receiver components are specially designed such that they are all identical. The battery packs come in either rechargeable or alkaline form.

Communication between the control unit and the Tx and Rx components is via optic fibre cables. These are advantageous to use because the signal will not deteriorate along the cable, however they are also easily damaged. It is therefore recommended that any person conducting a GPR survey ensures that the cables are never excessively bent and that no dirt enters the connectors.

3.3 TYPES OF ARRIVALS

When radar pulses are emitted from the Tx antenna into the subsurface. energy propagates radially away from the transmitter. In cross-section the radar energy can be represented by arcs and a straight ray path represents a route of one part of the wavefront (or the path of radar pulse between the antennas) - Figure 3-3. Radar pulses will then reflect at an angle (φ_2) equal to the angle of incidence (φ_1) at buried interfaces with a contrast in dielectric properties – Figure 3-3. The receiver picks up the reflected pulses and records the travel time between the antennas and the pulse amplitude. Aside from the basic reflected pulse, there are other pathways a pulse can take once it is emitted. The simplest paths are called first order ray paths of which there are four main types: direct air wave, direct ground wave, reflected wave, and critically refracted wave (Figure 3-4).

A direct air wave is generated when the radar pulse travels in a straight-line path from the Tx to Rx antenna through the air. The direct air wave is always the first to arrive since the maximum signal propagation velocity is through air ($v_{Air} = 0.3$ m/ns). The travel time formula for the direct air wave is

Direct Air Wave Travel Time
$$t = \frac{x}{v_{Air}}$$
(3-1)

where x is the antenna separation distance in metres.

The direct ground wave is similar to the direct air wave except the pulse moves in a straight-line path through the surface skin of the ground. The direct ground wave always arrives after the direct air wave because the velocity through geological media is on average half the velocity through air. The travel time formula for the direct ground wave is

Direct Ground Wave Travel Time

$$t = \frac{x}{v}$$

(3-2)

where x is still the distance between the antennas but v is the signal propagation velocity through the ground.

Of most importance are the pulses that reflect off interfaces with contrasting dielectric properties – i.e. reflection waves. The two-way travel time for the shortest path between the surface to the reflector (i.e. perpendicular path between two planar features) is

$$t_o = \frac{2z}{v}$$

(3-3)

where z is the depth to the reflector and v is the average velocity through the ground. However, since the antennas are separated by a distance, x the ray path is somewhat longer, so the two-way travel time for a reflection event becomes the equation for a hyperbola:

Reflected Wave Travel Time

$$t^2 = t_o^2 + \frac{x^2}{v^2} = \frac{\sqrt{4z^2 + x^2}}{v}$$

(3-4)

Critically refracted waves are governed by Snell's Law where φ_1 and φ_2 are the incident and refracted angles and the pulse travels from medium 1 (ε_{r1}) to medium 2 (ε_{r2}).

Snell's Law

$$\sin \varphi_2 = \sqrt{\frac{\varepsilon_{r1}}{\varepsilon_{r2}}} \ \sin \varphi_1$$

(3-5)

When a wave travels into a higher velocity (or lower dielectric constant) medium, a critically refracted wave that travels along the interface at the higher velocity is created. Critically refracted waves are only produced at a specific angle of incidence called the critical angle. φ_c for which the angle of refraction is 90° – Figure 3-5.

Critical Incident Angle

$$\varphi_c = \sin^{-1}\left(\sqrt{\frac{\varepsilon_{r2}}{\varepsilon_{r1}}}\right)$$

(3-6)

Following along a total path length of $2l_c$, the minimum distance the critically refracted air wave will appear is at a critical distance, x_c from the Tx antenna (Figure 3-5). However. it is more likely that once the wave reaches the surface it travels through the air some distance before it reaches the Rx antenna. Therefore, the two-way travel time for a critically refracted air wave is

Critically Refracted Air Wave Travel Time
$$t = \frac{(x - x_c) + 2l_c\sqrt{\varepsilon_{rl}}}{c}$$
(3-7)

where c is the speed of light.

All four of these primary ray paths have characteristic signatures in the radar profile. as will be described in the upcoming Section 3.8. Refer also to Figure 3-21 and Figure 3-22 for examples of how the direct waves and reflected waves typically appear in radargrams.

3.4 SURVEY MODES

There are three basic modes of operation for GPR surveys: reflection profiling mode. velocity sounding (CMP and WARR) mode, and transillumination mode. Focus will be placed on the most common mode of operation, reflection profiling. because it was the sole method for the Sudbury field surveys (Section 3.3.1). Common mid-point (CMP) and wide-angle reflection and refraction (WARR) measurements are similar so they will be discussed together in Section 3.4.2. Finally, a brief discussion on transillumination mode will be given in Section 3.4.3.

3.4.1 Reflection Profiling Mode

All GPR surveys conducted for this study were common-offset. single-fold reflection profiles. In this survey mode, the transmitter and receiver antennas are separated a fixed distance apart and both are moved along a survey line with constant station spacing – Figure 3-6. At each station. an average radar trace is recorded at the midpoint between the antennas. Each average trace is based on the collection of a number of single traces – this process is referred to as stacking. Stacking is a requirement of GPR since it helps to minimize the random noise and increases the depth of penetration (Robinson and Michaud, 1999).

As the antennas are moved along the survey lines, traces are compiled generating a profile (or radargram) of the subsurface showing survey position on the horizontal axis and two-way travel time on the vertical axis. Once the signal velocity is known, the time scale can then be converted to depth. Geologic structure and other buried subsurface targets will appear as coherent reflectors and/or diffraction hyperbolas.

Reflection survey design requires selection of the following seven important parameters (Annan. 1999) with the goals of the survey and the local sites conditions in mind:

  i. Antenna Operating Frequency
 ii. Temporal Sampling Interval/Sampling Frequency
iii. Time Window
 iv. Station Spacing
  v. Antenna Separation
 vi. Survey Grid and Coordinate System
vii. Antenna Orientation

34

These parameters relate to either instrumentation (antenna operating frequency), data acquisition (sampling frequency, time window, station spacing, antenna separation, and antenna orientation), or survey geometry (survey grid). Some of the parameters are crucial for success of a survey and others are important for viewing the results (i.e. time window) and performing adequate quality control (i.e. survey grid). All seven parameters will be discussed in the following sections with reference to the GPR field surveys conducted in Sudbury, Ontario.

3.4.1.1   Antenna Operating Frequency

The most important decision when selecting GPR instrumentation is the antenna centre frequency – recall that antennas are designed with a specific centre frequency and bandwidth (Section 3.2). Not only does frequency have a large influence on GPR performance, but selection of the correct antenna centre frequency for a particular project site can be difficult. For this project, a set of low frequency unshielded 100 MHz antennas and a set of high frequency shielded 1 GHz antennas were used. These antenna frequencies were selected for the purpose of identifying rock structure, but were not selected for a specific site, so target depth, required spatial resolution, and clutter[4] was unknown. This is not an ideal situation, as it is more beneficial to have some understanding of the electrical properties of the ground and a sense of the required penetration and resolution. If these conditions are known, Table 2-5 or Equation 2-23 can be used as an aid for selection of a suitable antenna centre frequency.

Fortunately, the two antenna frequencies that were selected did allow examination of a wide GPR frequency range (100 MHz –1000 MHz[5]). Using the antennas on rock, the low frequency (100 MHz) antennas were expected to give a maximum range of approximately 15 m with a vertical resolution of approximately 30 cm. The high frequency (1 GHz) antennas were expected to have a maximum range of approximately 2 m and a vertical resolution of approximately 3 cm in rock.

3.4.1.2   Temporal Sampling Interval/Sampling Frequency

The temporal sampling interval is the time interval between points on a recorded waveform and cannot be greater than half the period of the highest frequency signal in the record. If the highest frequency for a given antenna centre frequency is $1.5f_c$, assuming a bandwidth to centre frequency ratio of unity, the signal should be sampled at a rate of twice this frequency (Annan, 1999). Incorporating a safety factor, the recommended sampling rate[6] (or sampling frequency) is at least six times the centre frequency of the antenna.

The sampling frequency is a data acquisition parameter that is critical for GPR success. Table 3-1 shows that the actual sampling frequencies used for the Sudbury field surveys were above the recommended sampling frequencies.

---

[4] Background clutter are radar signals from heterogeneity within geological media. These are undesirable signals that may prevent signals from reflecting off the desired target(s).
[5] The 1 GHz antennas were the manufacturers' highest frequency antennas available at the time.
[6] The maximum sampling interval is the inverse of the sampling rate.

3.4.1.3 Time Window

The time window is a data acquisition parameter important for proper viewing of the recorded signal by governing how much of the recorded signal is viewed in the plot of two-way travel time versus position. By definition, time window is the length of time the Rx waits for received reflector pulses from the start of the transmitted pulse (Robinson and Michaud, 1999).

To estimate the required time window, the maximum depth and minimum velocity likely to be encountered at the site are input for the following equation (Annan, 1999):

Time Window
$$W = 1.3\left(\frac{2 \times \text{Maximum Depth}}{\text{Minimum Velocity}}\right)$$
(3-8)

If the signal velocity is unknown, the time window should be $\geq 50\%$ the anticipated depth of penetration as a rule-of-thumb (Robinson and Michaud, 1999).

Unfortunately, the software that comes with the RAMAC system does not allow the user to change the time window directly. Instead the user has to change the sampling frequency which automatically changes the time window accordingly. In general, as the sampling frequency increases the time window decreases. Based on the sampling frequencies recorded in Table 3-1, the time window generally ranged from 420-390 ns for the 100 MHz antennas and from 73-24 ns for the 1 GHz antennas.

3.4.1.4 Station Spacing

Station spacing is the distance between each collected trace. The station spacing is another important input parameter for data acquisition and is critical for survey resolution (Section 2.7.2.2). The spacing needs to be small enough such that the original signal is accurately represented. If the targets are narrow in length the lateral resolution becomes important and a small station spacing is required. The Nyquist sampling interval governs selection of station spacing:

Nyquist Sampling Interval
$$\Delta_x = \frac{c}{4 f_c \sqrt{\varepsilon_r}}$$
(3-9)

The inverse of the Nyquist sampling interval is the Nyquist frequency, f_N. The Nyquist frequency is the highest frequency that can be restored or the highest frequency sinusoid that can be recorded with fidelity. A station spacing smaller than the Nyquist Sampling Interval has to be chosen or a phenomenon called 'aliasing' will occur. Aliasing either causes the higher signal frequencies to be lost or they will fold back onto the spectrum and appear as spurious lower frequencies (Yilmaz, 1987). Hence, aliasing has disastrous consequences on interpretation and needs to be avoided.

Table 3-2 shows the calculated Nyquist sampling frequency (assuming a dielectric constant of 6.25 through rock) and the actual sampling frequencies used in this project. The Nyquist frequency was exceeded at three of the nine project sites for two different reasons. At the WGMC Outcrops, the surveyed surfaces were so irregular that a smaller spacing could not be

36

used. However, at Hwy 17 Bypass and Vermilion River the targets were relatively flat-lying features which allows the criteria for recommended station spacing to be relaxed.

3.4.1.5   Antenna Separation

Antennas where the transmitter and receiver components are separate units are called bistatic mode. For these antennas, it is important to determine the correct antenna separation distance prior to conducting the survey in order to achieve the best coupling between the antennas and the target (Annan, 1999). There is an optimum antenna separation that is calculated according to the following equation:

Optimum Antenna Separation
$$S_{opt} = \frac{2z}{\sqrt{\varepsilon_r - 1}}$$
(3-10)

where z is the depth of investigation and ε_r is the dielectric constant of the geologic material.

Aside from the optimum value, there is also a minimum antenna separation distance that should be adhered to.

Minimum Antenna Separation
$$S_{min} = 0.5\lambda = 0.5\left(\frac{v}{f_c}\right)$$
(3-11)

Selection of the most suitable antenna separation can still be difficult since there is often quite a range between the S_{opt} and S_{min}. A small antenna separation (i.e. approaching S_{min}) can be beneficial because it minimizes near-surface geometric distortion, however it can cause the production of large direct air or ground waves that may overload the electrical circuit. As well, a small separation will make it more difficult to detect targets that lie at a depth less than or equal to the antenna separation. On the other hand, a larger separation distance (i.e. approaching S_{opt}) is advantageous because it increases the reflectivity of flat lying reflectors (Annan, 1999). The disadvantage is that there may not be enough room at the site to use a large antenna separation distance.

For this project, the unshielded 100 MHz RAMAC antennas were in bistatic mode and the manufacturers' recommended antenna separation distance of 1 m was used for all the surveys. Unfortunately, the 1 GHz shielded antennas were housed in a single module where the antenna separation was fixed at 10 cm. Although the high frequency antennas were easier to handle in this form, velocity soundings could not be conducted.

Table 3-3 shows the calculated optimum separation, minimum separation and actual separation for the two antenna frequencies used in this project, assuming an estimated dielectric constant of 6.25 (or velocity = 0.120 m/ns) for the various rock environments. The tabulated results show that the actual antenna separations were much closer to S_{min} than S_{opt}. In fact, the separation for the 1 GHz is slightly lower than the minimum recommended separation but the survey operator was not able to adjust this separation.

3.4.1.6   Survey Grid and Coordinate System

Survey grids are useful when conducting GPR surveys because if common reflection events are viewed in more than one profile, there is increased confidence that the radar system is 'seeing' the target. Unfortunately for this project the majority of the sites were limited in size so no grid surveys were conducted. Because the length of the antennas and the separation distance both increase as the centre antenna frequency decreases, the 100 MHz antennas required a larger survey area compared to the 1GHz antennas. The following equation shows how antenna length is inversely proportional to the transmitter frequency:

Antenna Length
$$L \approx \frac{c}{(2 \times f_c)}$$
(3-12)

Survey line location and orientation are also important, especially when the target location and orientation are known. It is recommended that the survey line be oriented perpendicular to the strike of a planar feature (Annan, 1999). This assumes the survey is conducted along a horizontal plane so the GPR system will record the dip of the target along the line. However, if the survey is conducted along a near-vertical plane, the GPR will then record the target's strike relative to the survey line.

For the field studies conducted for this thesis, the topography of each site dictated the survey line location and orientation. As a result, not all surveys were conducted perpendicular to rock structure. For example, underground surveys were conducted along the sidewalls of specific drifts. These survey lines allowed detection of the strikes of the various rock joints; however, the location of the lines were restricted by the presence of the wire mesh support and other conductive objects attached to the sidewalls (e.g. metal bracket for holding the scaling bars).

Co-ordinate systems can also be important to use, especially when the results of the GPR surveys are to be correlated with site maps and/or drill holes. For this thesis, the four cardinal points of a compass (north, south, east & west) were used to define the trends of all survey lines. As well, the approximate locations of the project field sites were plotted on topographic maps.

3.4.1.7   Antenna Orientation

Lastly, the orientation of the transmitter and receiver antennas with respect to each other and to the survey line can be important because it affects the subsurface footprint size (Annan, 1999). With antennas that are dipolar and radiate energy with a preferred polarity (such as the RAMAC antennas) it is recommended they be oriented such that the electric field is polarized parallel to the strike of the fracture (Annan, 1999). If both the surveyed surface and target(s) are relatively planar and parallel to each other, there is no preferred antenna orientation.

For all of the GPR field surveys conducted in this thesis, the antennas were oriented in the most common orientation - perpendicular broadside (PR-BD) mode. In this mode the long axes of the transmitter and receiver antennas are parallel to each other but perpendicular to the survey line direction. This mode gives a broader subsurface footprint size, and minimizes side-swipe clutter from features offline (Annan, 1999).

3.4.2 Velocity Sounding (CMP/ WARR) Mode

Estimates of radar signal velocity can be determined from either a Common Mid-Point (CMP) or Wide Angle Reflection and Refraction (WARR) survey. These two survey modes are similar because they both involve moving the transmitter and receiver antennas apart from a fixed location and record the increase in travel time to a known reflector – Figure 3-7.

In a CMP survey, the antennas are moved incrementally apart about a single point midway between the antennas, collecting an average trace at each station – Figure 3-7 a). The final separation distance or the constant interval the antennas are moved depends on the size of the site. As a rule of thumb, the maximum distance between the antennas should be at least 1-2 times the depth to the known reflector and a minimum of 20 traces should be collected (Robinson and Michaud, 1999). The signal propagation velocity through geologic media that lies above the reflector is determined by measuring the difference in two-way travel time and comparing it to the difference in travel distance.

In a WARR survey, one antenna (normally the Tx antenna) is held stationary while the other antenna is move out incrementally – Figure 3-7 b). A CMP survey is however preferred to a WARR survey because reflections are more likely to come from a single fixed subsurface location (Annan, 1999). Fisher et al. (1992a) provides a complete description of the WARR survey mode.

Converting the time scale on the GPR radargram to depth can only be done if the signal propagation velocity is known. The resulting GPR plot for a CMP survey has antenna separation (in metres) is on the horizontal axis and the two-way travel time (in nanoseconds) is on the vertical axis. All reflection events for a CMP survey have a characteristic hyperbolic shape because as the antennas are moved outward, the travel time for the reflected pulses increases for a flat-lying or dipping subsurface interface - Figure 3-8 a).

Although the CMP radargram normally contains all the first order ray paths (discussed in Section 3.3), the reflected waves are most important for calculation of the signal propagation velocity. Assuming a flat-lying reflector, the best method for estimating the average velocity of the material above the reflector is from a plot of (reflection two-way travel time, t)^2 versus (antenna separation, x)^2 - Figure 3-8 b). Recalling that the two-way travel time of a reflected pulse is defined by the hyperbolic equation (Equation 3-4), the slope is equal to $1/v^2$. The depth to the reflector can be estimated using Equation 3-3 and the y-intercept (t_o value). The signal propagation velocity can also be estimated directly from the CMP radargram using the slope of the reflection event.

To conduct a CMP survey at a site, the presence of a known, well-defined, flat-lying reflector – such as a fault – is required. It is easiest to conduct velocity sounding surveys on horizontal ground with a horizontal reflector, but with additional field personnel these surveys can also be conducted on flat vertical faces with known vertical reflectors. Regardless of the orientation, a relatively planar survey surface is required in order to ensure close contact between the ground and the antennas. In addition, since clean radar signals are vital, a velocity survey should only be conducted at sites that are free of external sources of interference or background noise because the antennas are often separated far apart near the end of the survey. Lastly, it is highly recommended that more than one CMP be conducted at a site in order to determine a more accurate velocity (Robinson and Michaud, 1999).

Unfortunately, if the conditions described in the above paragraph cannot be met the CMP will be unsuccessful or in some cases cannot be conducted at all. This was the situation for the field surveys conducted within the Sudbury district. In these unfortunate cases, the velocity can be determined by either laboratory tests or estimated using typical values provided in the literature.

3.4.3   Transillumination Mode

Transillumination mode involves placing the transmitter and receiver antennas on opposite sides of a medium in order to look through it. This survey mode is commonly used for mining applications either on the surface of pillars or in boreholes using borehole antennas. In a pillar survey, the surface antennas are placed on opposite sides of the massive block of rock in order to map the thickness and possibly the geometry — Figure 3-9.

In a borehole survey, the GPR antennas are placed in two separate boreholes that exist in the same plane. The procedure for crosshole radar tomography is as follows: The Tx antenna is placed down the borehole and held stationary while the Rx antenna moves down the borehole past the Tx, collecting information at a constant interval (Figure 3-10). Once the Rx reaches the bottom of the hole, the Tx antenna is moved a set interval and held constant while the Rx again moves down the borehole collecting information. This is repeated until the Tx reaches the bottom of the borehole. A more complete description of transillumination surveying is beyond the scope of this report so refer to Annan and Davis (1978) for a more detailed discussion.

3.5   ASSESSING CONDITIONS PRIOR TO CONDUCTING A GPR SURVEY

Before a GPR survey is conducted a site reconnaissance needs to be made in order to assess both the site and ground conditions. The following is a list of items to be considered when conducting this site visit:

1. *What is the ground conductivity?* As a rule, materials that are highly conductive will cause large signal attenuation. This does not necessarily mean the radar system will not be able to detect subsurface targets, but it does severely limit the depth of penetration. In general, dry, unweathered, shield (igneous or metamorphic) rock is easier to probe in comparison to clay-rich, massive sulphide, or highly weathered rock.

2. *What are the external sources of interference?* The GPR surveyor needs to recognize and avoid sources of external interference that may totally preclude the use of GPR at the site. Unwanted noise can be generated by independent power sources such as power transmission lines or cultural interference by objects such as railway tracks that tend to swamp or interfere with the desired signal. Powerlines, buried metallic utilities, railroads, buildings, vehicles and other metallic objects are all sources of interference if located too close to the survey line. Radio transmitters should also be avoided as they may saturate the receiver (Robinson and Michaud, 1999).

3. *How will the survey lines be set out such that they are in the best position for target detection?* The preferred orientation of the survey line is perpendicular to the strike of a planar target. It site accessibility does not permit this recommended orientation, suitable alternative(s) has to be sought.

4. *What is the moisture content of the geologic medium?* Water has a large influence on the results of GPR due to its high dielectric constant (Section 2.5.3). The porosity and degree of

fracturing of the rock control the moisture content and therefore the dielectric constant. The advantage of a high moisture content is the increased resolution however the attenuation rate also increases. If there are dissolved minerals in the water, it can further increase attenuation.

5. *Are there any strong subsurface reflectors?* Strong reflectors such as the water table can cause a large amount of the energy to be reflected back to surface. This is often undesirable because there is little energy left to detect additional interfaces at depth. This is especially disadvantageous when the strong near-surface reflector is not the primary focus of the survey.

6. *What is the required penetration and resolution for the site?* There is always a trade-off between these two parameters (Section 2.7.3) however it is recommended that penetration be chosen over resolution when designing a GPR survey. Since it is often difficult to select a single antenna frequency, an alternative is to conduct a preliminary survey with two or three different centre frequency antennas. This allows determination of which antenna frequency will give the best compromise between range, resolution, and perhaps portability.

7. *How will the ground dielectric properties be determined?* The importance of determining the signal velocity (or dielectric constant) and attenuation (or conductivity) was described in Chapter 2. The designer of the GPR survey should try to identify where a proper velocity sounding could be conducted at the site during the site reconnaissance. Recall, that a CMP or WARR survey requires a well-defined, flat-lying reflector, and a relatively planar survey surface with background noise at a minimum. If site accessibility does not allow a velocity sounding survey to be conducted, the electrical properties should be determined from lab testing. Estimates of the electrical properties can also be obtained from the literature but should be used with caution due to the great variability in composition and porosity of most geological materials.

8. *Is there sufficient contrast in the dielectric properties between the target(s) and the host medium?* GPR works best when there is a large contrast in dielectric constant. The contrast should also be sharp and distinct since gradual changes in ε_r generally will not be detected. By estimating the dielectric properties of the target and host medium and calculating the reflection coefficient, the designer can then assess whether GPR will be successful at this site.

9. *Is there information currently available to help verify the subsurface reflections observed in the radargram?* Geophysics (i.e. GPR) is not a stand alone investigative tool but should be used in association with other more conventional exploration techniques such as drilling and sampling or test pits. With additional information regarding the subsurface, the radar data can then be properly correlated.

Even after considering the above questions, it can still be difficult to confidently state whether GPR will yield the desired results at a site for a particular application. The best way to determine the effectiveness of GPR is to conduct a preliminary on-site test survey using 2 or 3 various antenna frequencies. If this is not possible (e.g. due to financial restrictions) an alternate is to use the radar range equation discussed in Section 2.7.1. The radar range equation performs a balance of the power input into the ground to the power lost by various mechanisms (i.e. scattering and attenuation losses). The final result will be a yes/no answer to whether a specific target will be detected (Annan, 1999). In addition, the maximum range to the target, R_{max} can be estimated. The biggest disadvantage of the radar range equation is its complexity since it requires the input of many parameters, most of which are often unknown.

3.6 DATA COLLECTION

Once is it concluded that GPR is the appropriate geophysical technique, the next stage is to conduct the survey(s). The first step in conducting a survey is to lay out the survey line(s). The line(s) should be straight or reflector continuity may be affected (Robinson and Michaud, 1999). For a reflection survey, the antennas should be placed at a starting point and moved systematically along the survey line in the same direction, collecting a single average trace at every station spacing. Each trace corresponds to the midpoint between the antennas.

Most commercially available systems (including the RAMAC/GPR) are relatively portable since the systems are designed to be small and lightweight, with battery operated components. Systems such as the RAMAC/GPR are also promoted as 'one-man systems' that can be used in difficult to access areas. This is achieved by carrying both the control unit and laptop computer like a backpack. If the survey is relatively short the field person will merely move the antennas along the line pausing only to record each trace. For a large survey area with flat terrain, the antennas can be placed in a non-conductive skid box (or sled) and towed behind a vehicle. However, the surveyor should ensure the antennas are not moved too fast or the lateral resolution will be decreased as the system becomes unable to collect the information fast enough (Robinson and Michaud, 1999).

As the system is moved along the survey line the collection of traces produces a radar profile (or radargram) which is displayed on the computer. The operator should continuously check the profile to ensure the system is working correctly. Changes in topography and other important features along the survey line should be recorded, as they help with future data interpretation.

3.7 DATA PROCESSING

Once the field surveys have been collected, the next step is to process the raw data. GPR processing involves the manipulation and sometimes alteration of the original data for improved interpretation. This is especially important when the final radargrams are shown to non-geophysicists. The degree of data processing conducted on a section can vary from no processing to sophisticated processing.

Although GPR processing is considered to be in its infancy[7] the topic itself is large and at present is still growing (Annan,1999). Because of this, only data processing for reflection profiling will be discussed in this section. Data processing techniques will be described in terms of basic processing (Section 3.7.1), which normally requires a few hours, and advanced processing (Section 3.7.2), which can take days or weeks. All processing is subjective and ultimately depends on the experience of the processor, however for a novice the key is to understand what each technique does to the data set.

---

[7] GPR is still relatively young in comparison to other geophysical techniques such as seismic.

3.7.1 Basic Data Processing

Basic processing involves relatively straightforward techniques that even the novice should be able to carry out with minimal problems. The following is a list of the more common basic processing steps in the approximate order they should be carried out, if required:

1. removal of dead and/or erroneous traces
2. topographic corrections
3. signal saturation corrections
4. time gain
5. spatial and temporal filtering
6. stacking
7. CMP velocity estimate
8. dip correction

The first step in processing of raw GPR data is basic data editing. Data re-organization, file merging, eliminating bad data, and making topographic corrections all fall under the umbrella of data editing (Annan, 1999). Although it is normally one of the simplest steps. data editing can still be time consuming.

Removal of Dead/Erroneous Traces

Removal of bad GPR data is the elimination of dead and/or erroneous traces. Dead traces occur when there is a break in the fibre optic cable causing the radar pulses either to not be emitted by the Tx antenna or not being collected by the Rx antenna (Horvath, 1998). Erroneous traces occur when the surveyor takes more than one trace at a single station or when there is incorrect antenna placement due to difficult ground conditions (Horvath, 1998).

Topographic Corrections

All surveys are plotted assuming perfectly level ground, however in reality this is seldom the case. Surface topography can distort subsurface reflectors making interpretation more difficult. For example. assuming a hypothetical flat-lying subsurface reflector. positive topographic features will give an upwards concave radargram image because the travel time to the reflector will be increased – Figure 3-11. On the other hand, negative surface features will yield a convex image due to the reduction in travel time.

Topographic corrections are applied to the data to account for changes in elevation along the survey line. However, correcting for elevation is not always required because it depends on the required degree of accuracy of the final results, the antenna centre frequency, and the elevation changes along the survey line. If it is crucial to know the depth of the reflector at every point along the survey line, the topographic correction is probably important. If however the average maximum change in elevation along the survey is only 5 cm and the 100 MHz antennas are giving a maximum depth of penetration of 10 m into the ground, introducing a topographic correction is not warranted – it will have a negligible effect on the final results. For this thesis, crude topographic surveys where conducted along survey lines where there were large changes in elevation along the line in comparison to the depth of penetration.

Signal Saturation Corrections

Signal saturation corrections removes low frequency noise from the large energy produced by the direct air wave, direct ground wave and/or near surface reflectors. These large reflections can saturate the receiver electronics rendering the system unable to adjust to large variations between vertical stacks fast enough (Fisher et al., 1994). The low frequency noise produced by this phenomenon makes the desired reflection arrivals more difficult to distinguish. The signal saturation corrections are normally a DC offset correction plus a low-cut filter (Fisher et al., 1994).

Time Gain

Signal attenuation with depth causes later arrivals on a signal trace to have noticeably smaller amplitudes compared to the earlier arrivals. In fact, raw GPR data often shows few deep reflectors until some amplification has been applied to the later signals (Robinson and Michaud, 1999). A time-dependent gain function tries to compensate for the rapid attenuation of the signal by equalizing the amplitudes (Annan, 1999).

There are many different types of gains to choose from – i.e. automatic gain control (AGC), constant gain, and spherical and exponential compensation gain (SEC). These different gains emphasize various parts of the profile, so proper selection of the time gain can be greatly aided if the interpreter has some knowledge of the target's depth or the depth range of importance. Annan (1999) recommends that the effect of each gain be clearly understood, and both amplitude fidelity and the preliminary physical model be considered.

Automatic gain control (AGC) is a time variable gain that tries to equalize the reflector amplitudes down the entire trace. The first step in the process involves computation of the average signal over a time window down each trace. Then the data point at the centre of the time window is amplified by the ratio between the desired output value and the average signal amplitude. The advantage of the AGC, over the other type gains, is that it enhances weak, deep reflectors making it ideal for monitoring reflector continuity. However, although AGC is a commonly used gain function, many processors do not recommend it because it removes the original relative relationships between reflector amplitudes (Robinson and Michaud, 1999).

Because of the greater need to maintain relative reflector amplitudes, the more preferred gains include the constant gain (CONST) and the spherical and exponential compensation gain (SEC), which do not eliminate the relative reflector amplitudes. The constant gain multiplies all data by a constant value. The SEC gain attempts to compensate for spherical and spreading losses and exponential ohmic dissipation of energy. The SEC gain requires the input of attenuation and velocity of the medium.

Figure 3-12 contains images of a radar profile before and after a time gain has been applied. This figure also shows how different the profile appears using a constant gain versus an AGC gain or a SEC gain. The constant gain is generally better if the target(s) exist near the surface (i.e. reflections just below the direct air and ground wave events), but if the target(s) exist at depth, the AGC or SEC is the preferred time gain. Regardless of which type is applied, the importance of the time gain is clearly shown in this figure since no reflectors below 1.5 m depth can be seen without the gain.

Spatial and Temporal Filtering

Spatial and temporal filters are used to remove the unwanted frequency (noise) from the data. In general, filters are applied following a time gain however they can be applied prior to the gain. There are many different types of filters to choose from, but the majority will either enhance flat-lying reflectors by suppressing dipping reflectors or enhance dipping reflectors by suppressing flat-lying reflectors. As such, it is important for the interpreter to understand the orientation of the target relative to the survey line.

Spatial filters of importance for this thesis are the trace-to-trace average, trace difference, and the low and high-pass filters. The trace-to-trace average (or trace stacking) involves the averaging of two or more adjacent traces together resulting in a decrease in random signal noise. This filter will improve the continuity of flat-lying reflectors and therefore should not be used for dipping targets. Conversely, when enhancement of dipping reflections is required a trace difference filter may be beneficial. This filter works by subtracting each trace in a profile from the previous trace. Finally, the low and high pass spatial filters work by removing frequencies above or below a selected cutoff spatial frequency (in cycles per metre). Similar to trace differencing, a high pass filter is used to enhance dipping reflectors and suppress flat-lying events, whereas a low pass filter does the exact opposite. The high and low pass filters work best when the signal and noise have distinct frequency characteristics from which they can be separated (Kearey and Brooks, 1991).

In the time domain, there are filters that work by discriminating against chosen frequency components of the waveform – i.e. low-pass, high-pass, and bandpass filters. The high and low pass frequency filters are similar to the spatial filters described above. For example, a low-pass filter stops all high frequencies above a certain cut-off frequency thereby retaining only the lower frequencies.

Bandpass filters however use fast Fourier transforms (FFT) and various types of linear and non-linear time domain convolution filter operators. Generally this type of filter removes frequencies outside a certain bandwidth. In order select the appropriate bandwidth, the waveform should be expressed in terms of the frequency domain. This is accomplished by creating an amplitude spectrum - a plot of amplitude versus frequency - for the data set. The amplitude spectrum shows how the majority of radar energy is limited to a finite bandwidth and has a centre frequency somewhat lower than the manufacturers' rating due to ground attenuation.

Figure 3-13 a) shows the amplitude spectra for a 1000 MHz GPR data set before and after a bandpass filter has been applied. The manufacturers' antenna centre frequency rating was 1000 MHz however the spectrum reveals an actual centre frequency of $\approx$ 800 MHz through this geologic medium. The original spectrum was used to select the frequency bands 200-300 MHz and 1500-1800 MHz. The trapezoidal bandpass filter used for this data set is shown in Figure 3-13 b) and is defined by the four chosen corner frequencies f1 = 400, f2 = 600, f3 = 1000, & f4 = 1500.

Bandpass filters are advantageous to use as they improve the signal-to-noise ratio without appreciably altering the original data. They are also used more commonly than the low and high pass frequency filters because GPR data sets often contain both low and high frequency noise.

There are also simpler temporal filters such as the down-the-trace average filter which were used for much of the data processing in this thesis. The down-the-trace average (or point stacking) filter is based on a running average computed along the time axis of each individual trace. The processor need only input the number of points the average should be taken over. This filter is

45

most effective for enhancing dipping reflectors, however the processor should not to average too many points together or it will cause a decrease in resolution. This cautionary note is applicable to all filtering discussed above.

Stacking

Stacking is not the next step in processing but is often regarded as part of basic data processing. Recall from Section 3.4.1, that a stacking value – the number of traces that will be added together to produce an average trace – needs to be entered at the data collection stage. Stacking is important because it improves the signal-to-noise ratio, but if the stacking value is too low, it cannot be adjusted afterwards. A high stacking value is recommended since the final results improve as the stacking value increases, however higher stacking also increases the survey time and uses up more memory. Robinson and Michaud (1999) recommends a stacking value of 32 to 64 for most GPR surveys.

Velocity Estimate

Because most clients require quantitative data from the GPR survey (i.e. depth to the reflector), the y-axis time scale has to be converted to a depth scale. This can only be done if the subsurface velocities are known. If a CMP or WARR survey is conducted, the velocity can be estimated by plotting (travel time)^2 versus (antenna separation distance)^2 – Section 3.4.2. If these surveys cannot be conducted, the signal propagation velocity can be determined from laboratory testing, or published values can be used (Table 2-2).

Dip Correction

The dip correction is a geometrical correction that allows the correct orientation and distance of a dipping planar reflector to be determined. Assuming the transmitter and receiver separation is small in comparison to the depth to the dipping interface, only energy that impinges upon the reflector hits and reflects normal to the surface is picked up by the receiver antenna - Figure 3-14. All other rays are reflected and refracted away from the Rx antenna in accordance to Snell's Law (Equation 3-5).

The GPR system measures the travel time of the pulses between the antennas assuming the energy comes from vertically below the midpoint between the Tx and Rx antennas. This assumption however is not valid for dipping reflectors so a dip correction has to be made. Without the dip correction the actual distance to the reflector is underestimated. Figure 3-15 shows the dip correction procedure required to move the apparent point of reflection to its actual point of reflection, thereby creating the true reflector. The recorded surface and the actual surface are related by the following equation:

Dip Correction $$\boxed{\sin\alpha_A = \tan\alpha_R}$$ (3-13)

where α_A is the actual dip of the recorded surface and α_R is the radargram dip in the resulting profile.

This trigonometric correction is most conveniently expressed in graphical form – Figure 3-16. Because of the non-linear relationship between the actual and radargram dip, the correction is really only imperative when actual reflector dip is greater than 30° (assuming GPR survey is conducted over a horizontal surface). Also note that for a vertical reflector (i.e. α_R of 90°), the recorded dip is 45°, which is the maximum dip that can be observed in a radargram.

3.7.2 Advanced Data Processing

Advanced data processing involves more sophisticated analysis techniques that can make significant changes to the original data. Advanced processing can make weaker signals more discernible and improve specific data components for interpretation (Annan, 1999). However, advanced processing can also introduce artifacts[8] making interpretation more difficult. This type of processing requires an experienced processor since it involves more complex GPR operations such as background removal or the use of seismic processing techniques.

Seismic processing is now being applied to GPR data because of the similarities between GPR and reflection seismic[9] and the introduction of digitally recorded GPR data. There is a standard sequence of operations involved in seismic processing (Figure 3-17), however defining each processing step is beyond the scope of this thesis. Refer to Yilmaz (1987) or other sources for a more complete discussion on seismic data processing.

The following advanced GPR and seismic processing methods are discussed in this section:

- background removal
- f-k filtering
- deconvolution
- migration

Background Removal

Background removal involves the subtraction of a background trace from every trace in the profile. Background removal is normally either a high pass filter or an average trace removal filter (Annan, 1999). Average trace removal is a form of spatial filtering that allows weaker signals to become visible (Annan, 1999). Although background removal may be necessary, Annan (1999) warns that routine use is indicative of serious equipment problems during data acquisition.

F-k filtering

F-k filtering is a two-dimensional filtering technique that transforms time-distance data into frequency-wavenumber data using Fourier transform. Filtering is then conducted on the transformed data set. F-k filtering is typically used to remove noise that has a regular trace-to-trace expression along the profile. For example, Maijala (1992) used f-k filtering to remove inclined reflections produced by near-surface point reflectors and/or the equipment. Unfortunately, f-k filtering is not recommended for large data sets because of the long processing time and limited horizontal data length counted in scans (Maijala, 1992).

Deconvolution

When noise lies outside of the frequency spectrum of the reflected pulses, frequency filtering techniques discussed in Section 3.7.1 can be used to separate the noise from the true signal. However, noise that lies within the frequency spectrum may be removed by a seismic processing technique called deconvolution. Deconvolution is a type of inverse filter that discriminates

---

[8] An artifact is the name given to describe a false reflection caused by the GPR system or by processing – i.e. a type of noise.

[9] Both radar and seismic pulses propagate into the ground with velocities dependent on the earth's material properties and reflect where the properties change (Fisher et al., 1992b).

against noise and improves signal character using criteria other than frequency (Kearey and Brooks, 1991).

Deconvolution was mentioned in Section 2.7.2.1 as a technique used to improve vertical resolution. The increased resolution is most beneficial for closely spaced targets that occur in the near-surface (Todoeschuck et al., 1992). There are different types of deconvolution: spiking deconvolution, zero-phase deconvolution, and predictive deconvolution. Descriptions of each of deconvolution methods are beyond the scope of this these, so refer to Maijala (1992), LaFleche et al. (1991) and Todoeschuck et al. (1992) for detailed discussions of these methods.

Deconvolution is not straightforward and is not always beneficial (Annan, 1999). Maijala (1992) found that deconvolution could be successfully applied to parts of the profile but often the output was still too noisy to really improve interpretation. Annan (1999) also concludes that deconvolution is hard to apply systematically and often shows minimal increase in resolution. Deconvolution is more applicable when there are multiple reflections (Section 3.8) in the data set (Annan, 1999).

Migration
Migration is another powerful seismic processing technique which can help to place subsurface reflectors into their correct location and increases the signal-to-noise ratio that enhances target detection and location. Migration was developed in the 1940's by the oil industry to help identify potential oil-bearing structures and is used extensively for seismic data reduction (Hogan, 1988). This technique involves the use of a mathematical algorithm to focus dispersed energy along a hyperbolic (or diffraction) curve to the point where the energy originates - generally the apex of the curve (Hogan, 1988). This focusing of energy improves identification of multiple targets (i.e. improves lateral resolution – Section 2.7.2.2). Noise and ringing energy can also be distinguished because this energy will not focus (Hogan, 1988).

Migration helps to collapse hyperbolic events caused by point reflectors and vertical faces (Kearey and Brooks, 1991) – Figure 3-18. Migration also corrects for synform features along an irregular reflection surface. A sharp synform feature will appear as a convex 'bow-tie' shape in the non-migrated radargram (Figure 3-19), but migration will convert it back to its actual shape – Figure 3-20.

Although there is more than one algorithm for migration of GPR data, only a few have actually been used. Kirchoff diffraction migration and reverse-time migration are two algorithms that have been used successfully (Fisher et al., 1992b; Hogan, 1988). When selecting a type of migration, the specific advantages and disadvantages of each process needs to be understood by the processor. For example, Kirchoff-migration is directly applicable to data for all antenna separations but is difficult to implement when there are spatial velocity variations (Fisher et al., 1992b). On the other hand, reverse-time migration easily accommodates for velocity variations (Fisher et al., 1992b).

Although migration can produce an improved profile, there are a number of disadvantages to using it. First of all, migration is a subjective technique to apply and requires an understanding of the ground velocity with depth. It is also extremely computation intensive (MacArthur, 1988), expensive, and the potential benefits are data-dependent (Fisher et al., 1992b). The shape, position, and relative amplitude of the reflectors are reliable, however not the absolute amplitude. And since migration is only two-dimensional, reflections off the survey line will not be migrated correctly (Fisher et al., 1992b). Finally, multiple reflections and free-surface reflections are not handled correctly (Fisher et al., 1992b).

48

Because of these problems, migration should only be used by experienced processors who are aware of its ability and limitations (Annan, 1999). In general, migration is only applicable in environments with a conductivity < 10 mS/m and where frequencies between 0.1 to 1000 MHz are used (Fisher et al., 1992b). As well, migration will be more successful when used for more homogenous profiles (Maijala, 1992).

3.7.3 Processing Conclusions

Most GPR data needs some degree of data processing so the use of a computer and some type of commercial software are normally required. Most of the GPR software for data collection includes basic processing, however advanced processing is often not included – as was the case for the RAMAC/GPR system software. Advanced processing is generally only conducted when a strong increase in both accuracy and resolution to help interpretation is required (Fisher et al., 1992b). If advanced processing has to be conducted a processor can use seismic processing techniques. This is for two main reasons: 1) many researchers have had success using seismic data processing on GPR (Fisher et al., 1992a, b; Fisher et al., 1994; Hogan, 1988; LaFleche et al., 1991; and Maijala, 1992); and 2) GPR data processing does not have capability, flexibility and accessibility as seismic processing (Fisher et al., 1992a). Despite this, it should be remembered that GPR data is not identical to seismic data. GPR data requires scaling and some of the processing parameters will need adjusting in order to use seismic techniques (Fisher et al., 1992a).

Because GPR systems now record data digitally, personal computers are presently faster and more economical, and due to advances in software, there is the ability to do vast amounts and various types of processing. As such, the limitations for processing are not in the computing ability but are in the time and financial constraints. The desire is often to conduct more advanced processing in hopes that the final GPR profiles will improve, however the danger is that the results become more dependent on the experience of the processor and therefore more biased. As well, this processing will likely require the purchase of additional software, more time allocated to processing, more money, and experienced processors. The key to successful processing and interpretation of radar data is therefore to use experienced processors, conduct processing with an objective in mind, and always consider the benefit-to-cost ratio (Annan, 1999).

3.8 GENERAL INTERPRETATION OF RADAR DATA

Similar to data processing, interpretation is subjective and dependent on the experience of the interpreter, available ground truth information and quality of the raw data (Pilon et al., 1996). For interpretation, it is important to understand the geological setting and the survey objective or target(s) (Annan, 1999). It is also beneficial to make interpretations based on visual observations and ground samples. If ground-truthing information is not available, the interpreter should recommend that plans be made to collect such data.

As an aid for assessing the type of response to be expected and thus as an aid for interpreting radargrams, synthetic radargrams or synthetic reflection profiles can be generated. For simple layered ground, generation of a synthetic radargram is based on a plane-layered model with a plane wave incident and estimates of the ground's dielectric properties (i.e. dielectric constant and conductivity). A more detailed description of this process is given in Annan and Chua (1992).

For more complex ground, synthetic plots can be created by modeling wave propagation. This is accomplished with two and three-dimensional finite difference/finite element or ray tracing programs. The ray tracing method is described in McMechan (1981) and Annan and Chua (1992). Generation of synthetic responses by these methods requires an understanding of the ground conditions, however in reality the estimation of reliable dielectric properties is poor. As well, only a few of the simpler programs are commercially available.

As with all geophysical surveying, GPR suffers from inherent ambiguity or non-uniqueness which makes interpretation difficult. This means a reflection event from a rock contact cannot be distinguished from a joint or bedding plane or foliation plane. This inherent ambiguity cannot be avoided however the degree of uncertainty in GPR interpretation can be reduced to an acceptable level by taking additional measurements - i.e. more surveys lines with a high stacking ratio (Kearey and Brooks, 1991) and having an understanding of the target(s).

The non-uniqueness problem encourages the introduction of assumptions that restrict the number of solutions (Kearey and Brooks, 1991). The following paragraphs present the well-known GPR assumptions and criteria used to help interpret radar profiles.

Direct Air/Ground Waves
The direct air and ground waves always appear in the radargram as straight-line events (prior to topographic corrections). As stated previously in Section 3.3, the direct air wave is always the first event and the direct ground wave is always the second event. For a GPR reflection survey, the direct waves will appear as horizontal events in the resulting profile, but for a CMP survey these same waves will appear as dipping events – Figure 3-21 and Figure 3-22.

Reflected/Critically Refracted Waves
Reflected and critically refracted waves from subsurface targets appear after the direct waves. Assuming the target interface and surveyed surface are approximately planar and parallel to each other, the reflected wave on a reflection survey radargram will appear as a flat-lying (or horizontal) event, whereas on a CMP radargram it will appear as a hyperbolic event. If the reflector is dipping, it will appear as a dipping event on a reflection radargram with a dip that is shallower that in reality. In Figure 3-23 the dipping reflector has a dip of 30° in the radargram image but the actual dip is 35° using the dip correction described in Section 3.7.1.

Multiple Reflections
Aside from the primary reflections from the first order ray paths (Section 3.3), multiple reflections are commonly present in radargrams. These are waves that reflect off the same interface or other surface(s) more than once (Figure 3-24). Identifying multiples in a radargram is essential because failure to do so can lead to serious interpretation error. For flat-lying reflecting interfaces, multiples are predictable because the travel time is merely a multiple of the primary reflection travel time – Figure 3-25. Also multiples generally have lower amplitudes compared to primary reflections because of the loss of energy at each reflection. Multiples cannot be avoided during data collection but can sometimes be suppressed by data processing techniques such as deconvolution (Kearey and Brooks, 1991).

Buried Point Targets

Because of energy dispersion, a point target in the subsurface has a characteristic hyperbolic signature in a radar profile. An example of a point target is a buried metallic pipe – Figure 3-26. The hyperbolic curve is always greater than the actual size of the target; the exact shape of the curve is a function of the depth to the target and the signal propagation velocity with depth. Unfortunately detection of buried point targets can be masked due to the presence of noise, overlapping hyperbolas, geologic structure and ringing (Hogan, 1988).

Vertical Faces

Because radar energy not only travels downwards but a certain portion also travels sideways, reflections occur off vertical to sub-vertical free surfaces which exist close to the survey line (Grasmueck, 1996) – Figure 3-27. Reflections off these faces will appear as hyperbolic-shaped events which can clutter the radargram taking away from the expression of actual targets (Grasmueck, 1996) – Figure 3-28. These unwanted reflections can generally only be removed using advanced processing such as migration (Brewster and Annan, 1994).

Water Table

The water table will likely produce a continuous, high amplitude, negative polarity reflection and depending on the topography will be more or less horizontal. The high amplitude is due to the large contrast in dielectric constant between dry ground and saturated ground. The negative polarity results in a flipped wavelet that can sometimes be observed depending on the scale of the profile. As described in Section 2.6.3, negative polarity occurs when the energy passes from a medium with low dielectric constant to high dielectric constant (i.e. a significant reduction in signal velocity at the interface).

3.9   SUMMARY AND CONCLUSIONS

Chapter 3 describes the equipment used in typical GPR system as well as the various survey modes. With a focus on GPR reflections surveys, Sections 3.4.1.1 to 3.4.1.7 provide guidance on the selection of appropriate input survey parameters. The survey parameters chosen for the Sudbury field surveys were generally always within the geophysical guidelines; however, for some of the field surveys the station spacing and/or the antenna separation did not meet the guidelines. Generally, station spacing is not as crucial when the target is flat-lying and this was the case for these surveys. As for the antenna separation, the high frequency antennas were enclosed in a single housing unit and could not be adjusted.

Although Chapter 3 discusses some of the survey procedures, data processing, and interpretation of the final results, it is important to be aware that there are no clearly defined specifications or standards available for any of these steps. This is not because GPR is a relatively young geophysical technique in comparison to others (i.e. seismic) but is due to the variability in the site and ground conditions. All investigations are inherently unique and cannot be defined with a simple routine procedure (McCann, 1997). So aside from the guidance provided in this chapter, I recommend consulting additional references such as Annan (1999), Coffeen (1986), Robinson and Michaud (1999), and Yilmaz (1987). I also recommended that the engineer become familiar with all the geophysical methods and have an independent geophysical advisor who can give sound advice.

Table 3-1 Comparison of recommended to actual sampling frequencies.

Antenna Centre Frequency	Maximum Frequency[1]	Recommended Sampling Frequency	Actual Sampling Frequency (Range)
100 MHz	150 MHz	≥ 600 MHz	1100-1200 MHz
1 GHz	1.5 GHz	≥ 6 GHz	7-20 GHz

Note 1: Assumed a bandwidth to centre frequency ratio of unity.

Table 3-2 Nyquist sampling interval versus actual station spacing.

Antenna Centre Frequency	Nyquist Sampling Interval	Actual Station Spacing (Range)
100 MHz	0.30 m	0.10-0.20 m
1 GHz	0.03 m	0.01-0.05 m

Table 3-3 Calculated optimum and minimum antenna separation versus actual antenna separation.

Centre Antenna Frequency	Depth of Penetration	Optimum Antenna Separation	Minimum Antenna Separation	Actual Antenna Separation
100 MHz	10 m	8.7 m	0.6 m	1 m
1 GHz	1 m	0.88 m	0.12 m	0.10 m
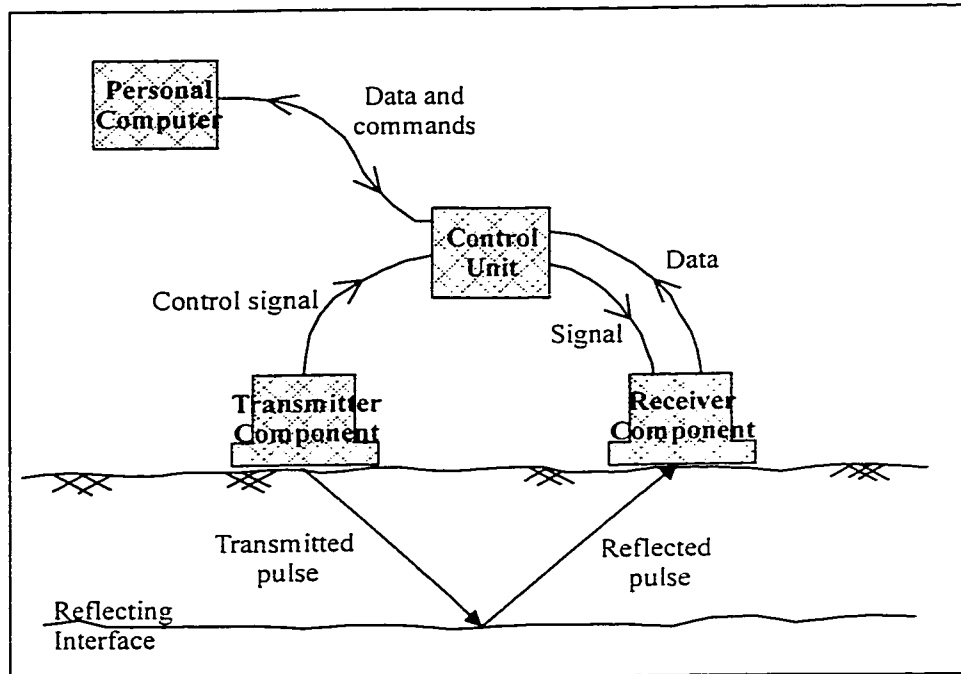
Figure 3-1 Schematic diagram of GPR system components.
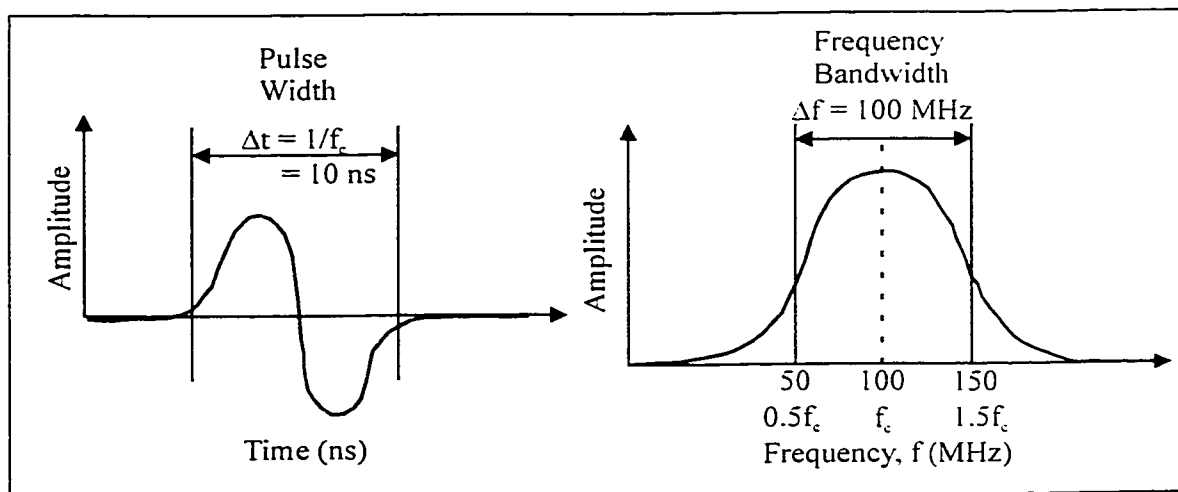
Figure 3-2 GPR signal pulse waveform in the time and frequency domain for 100 MHz
centre frequency antennas.
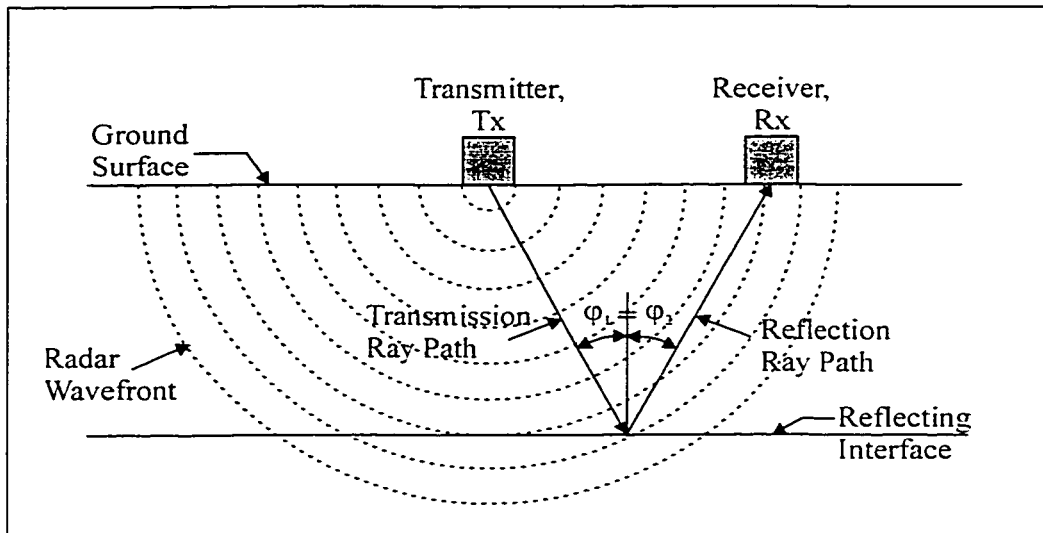
Figure 3-3 GPR signal path through geologic medium.
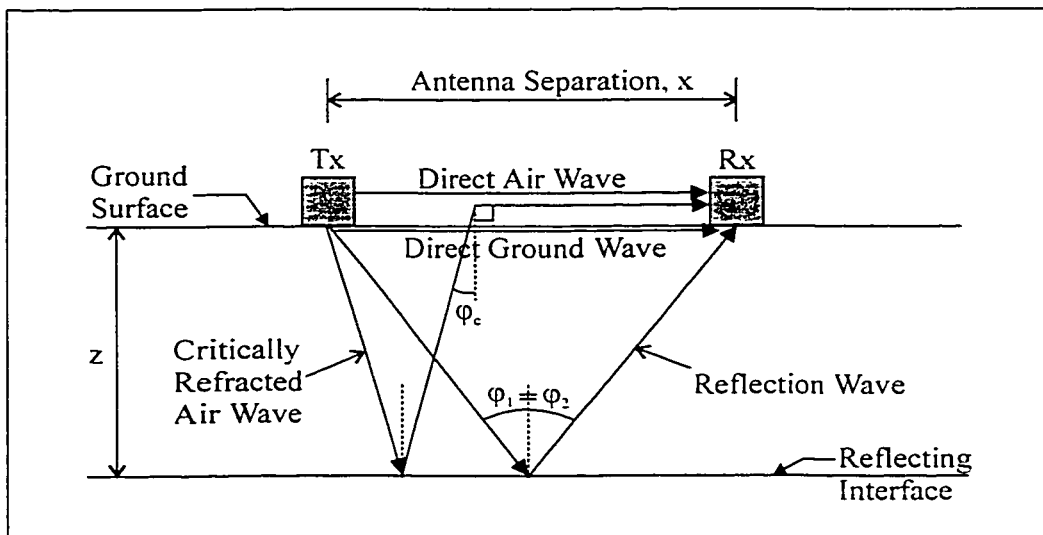
Figure 3-4 First order ray paths.
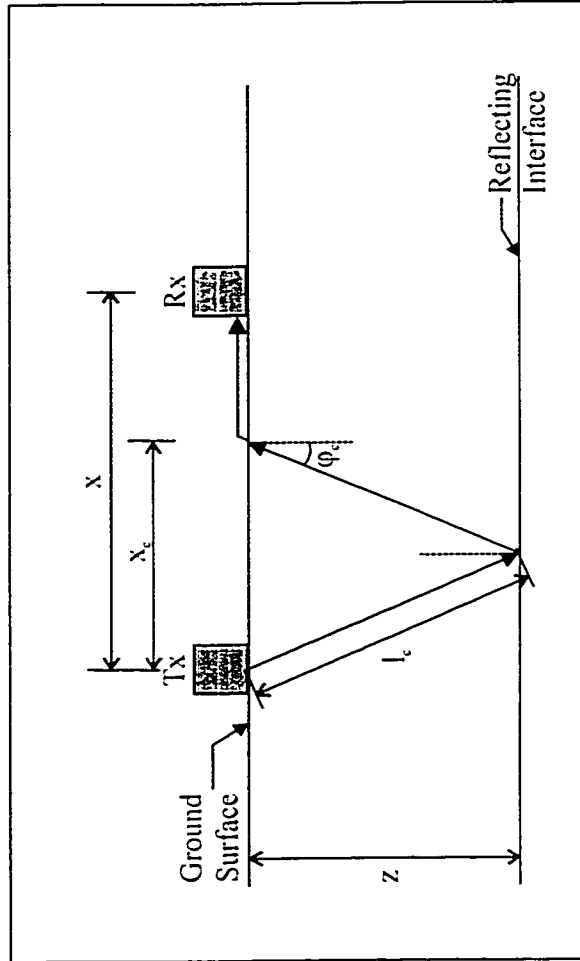
Figure 3-5 Critically refracted air wave.

55
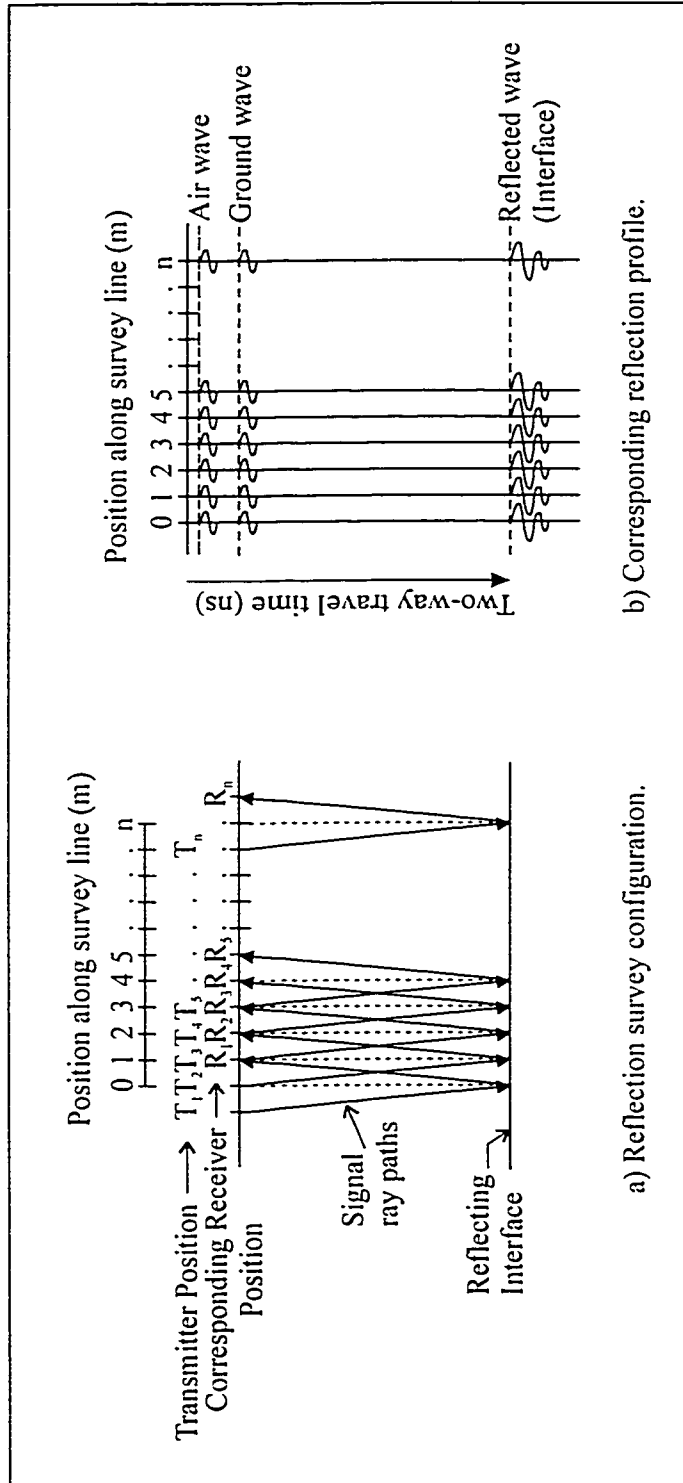
Figure 3-6 Reflection survey mode.

a) Reflection survey configuration.

b) Corresponding reflection profile.

56

CMP

← →

Transmitter Position | Corresponding Receiver Position

T₅ T₄ T₃ T₂ T₁ | R₁ R₂ R₃ R₄ R₅

Reflecting Interface

a) Common-Midpoint Survey Configuration.

Fixed Transmitter Position

Moving Receiver →

T R₁ R₂ R₃ R₄ R₅

Reflecting Interface

b) Wide Angle Reflection and Refraction Survey Configuration.

Figure 3-7 Velocity Sounding Mode Configurations.

57
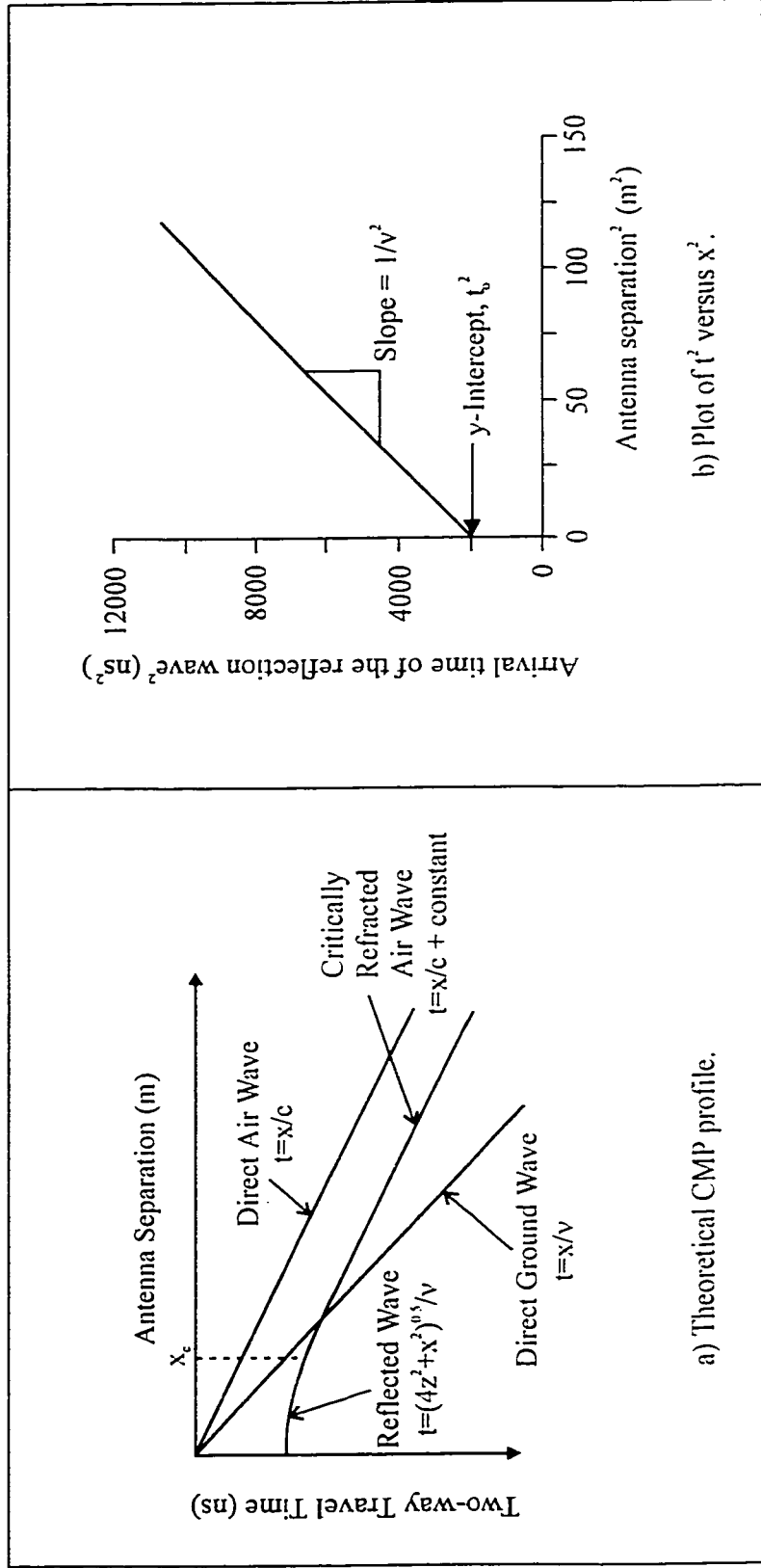
Figure 3-8 CMP velocity calculation.

b) Plot of t^2 versus x^2.

Slope = $1/v^2$

y-Intercept, t_0^2

Antenna separation^2 (m^2)

Arrival time of the reflection wave^2 (ns^2)

a) Theoretical CMP profile.

Direct Air Wave
t=x/c

Critically
Refracted
Air Wave
t=x/c + constant

Direct Ground Wave
t=x/v

Reflected Wave
t=$(4z^2+x^2)^{0.5}$/v

Antenna Separation (m)

x_c

Two-way Travel Time (ns)
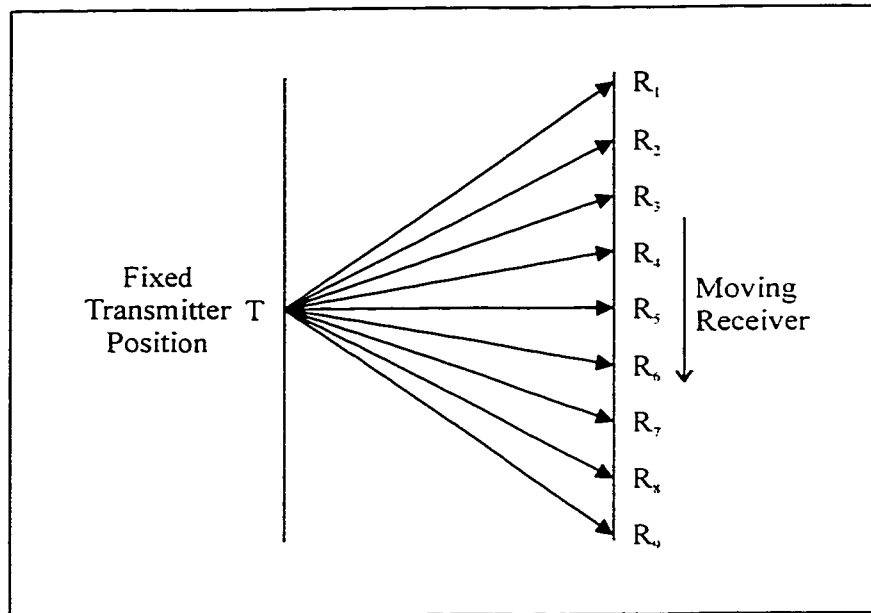
Figure 3-9 Transillumination configuration.
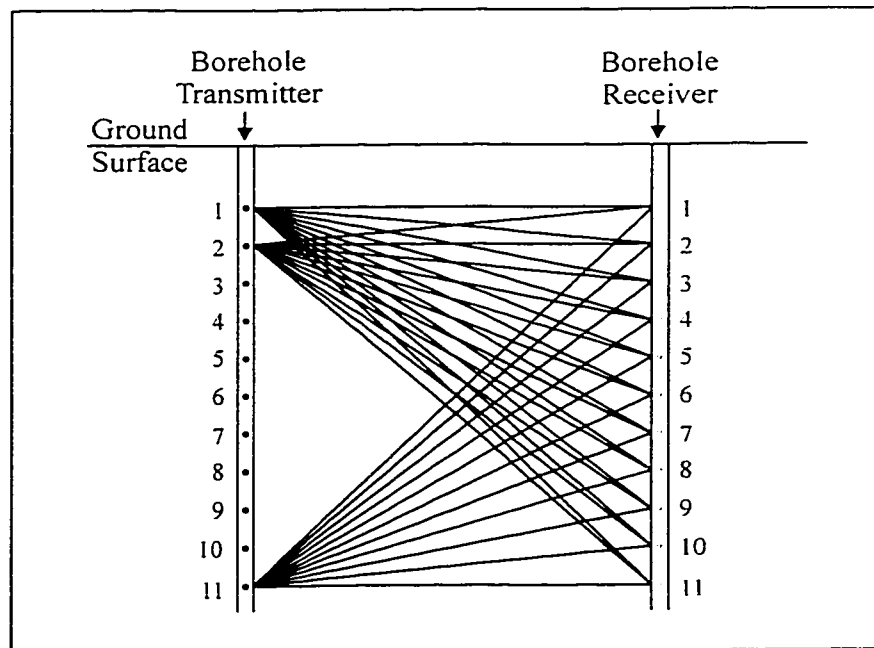
Figure 3-10 Cross-hole radar configuration.

59
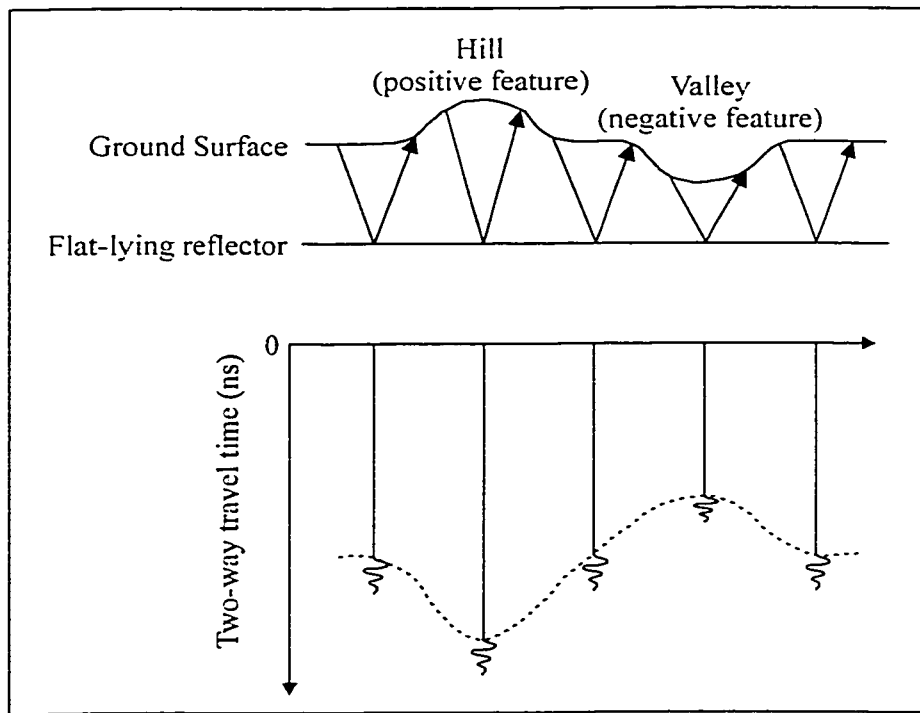
Figure 3-11   Effect of surface topography on the resulting radargram image.
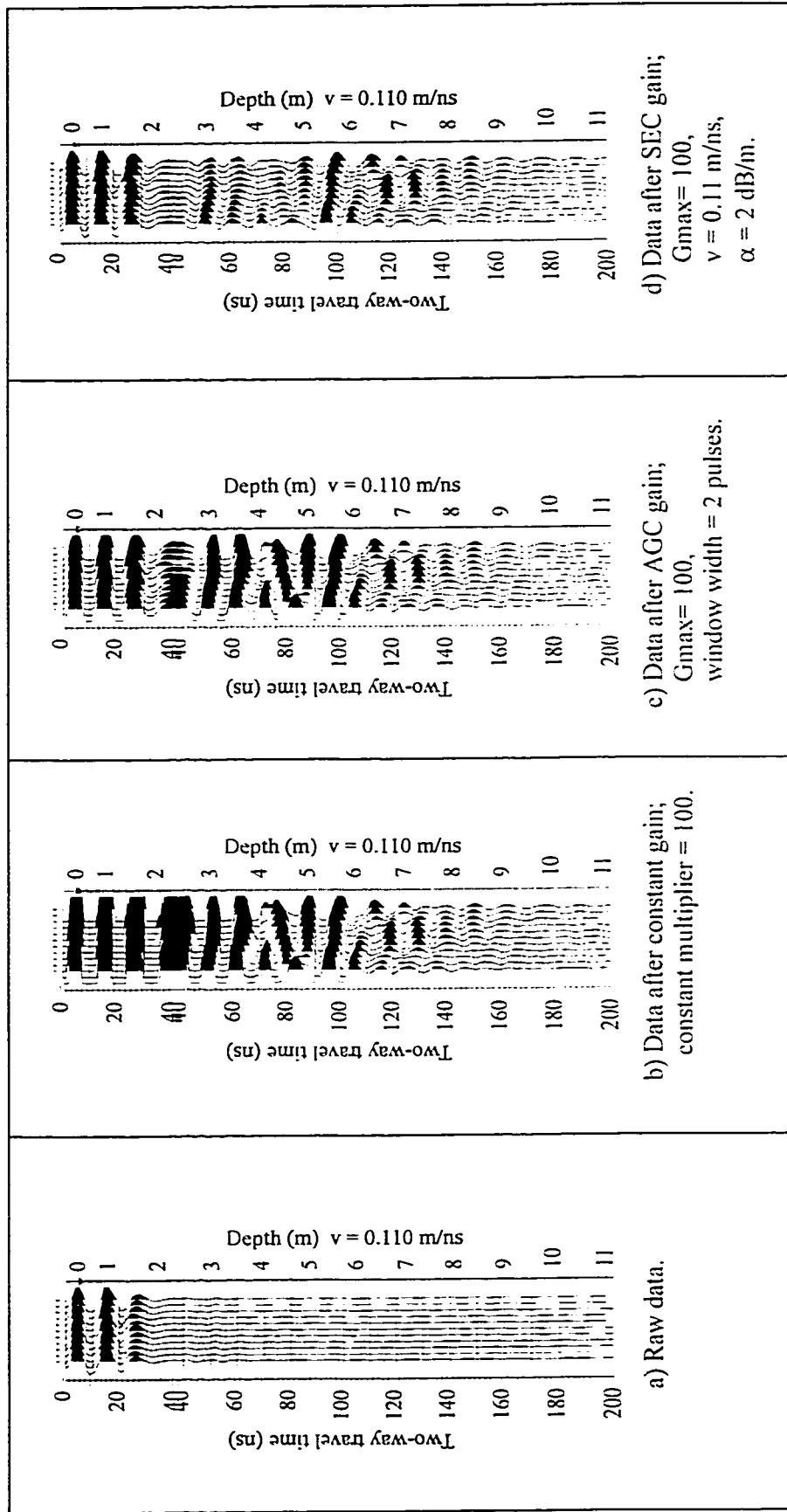
Figure 3-12 Influence of various time gains on a radar data set.

a) Raw data.

b) Data after constant gain; constant multiplier = 100.

c) Data after AGC gain; Gmax= 100, window width = 2 pulses.

d) Data after SEC gain; Gmax= 100, v = 0.11 m/ns, α = 2 dB/m.

b) Trapezoidal bandpass filter in the frequency domain.

a) Amplitude spectrum for 1000 Mhz. data set - before and after bandpass filter.
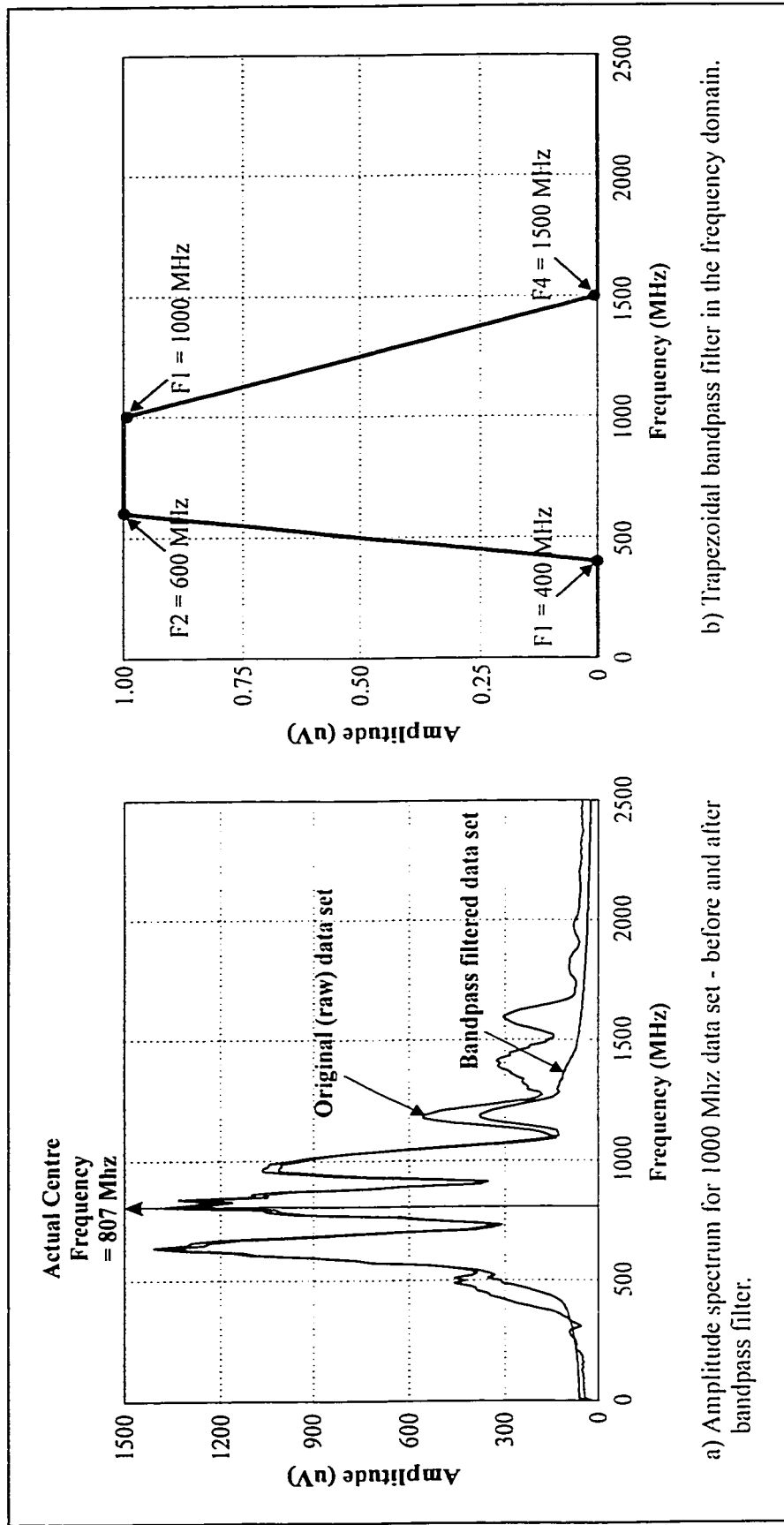
Figure 3-13 Bandpass filter applied to a radar data set.
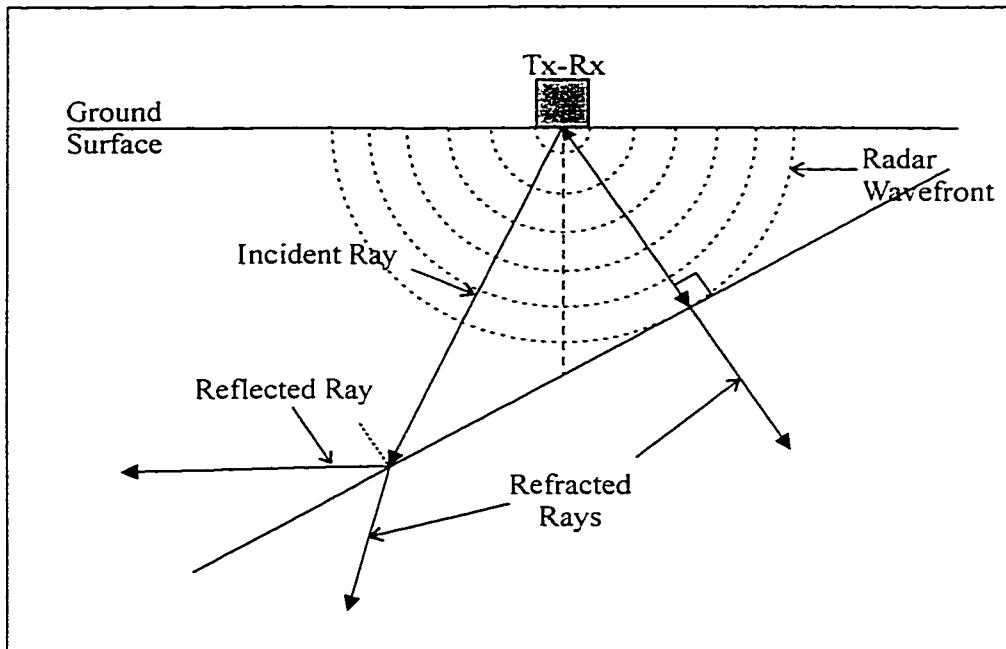
Figure 3-14 Typical radar waves impinging on a dipping planar interface.
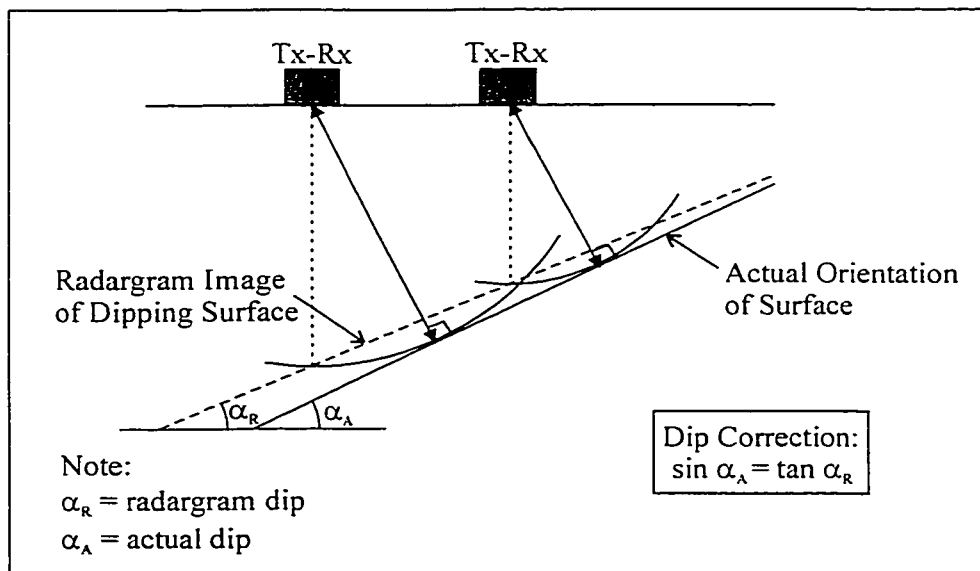
Figure 3-15 Dip correction for inclined reflector surfaces.
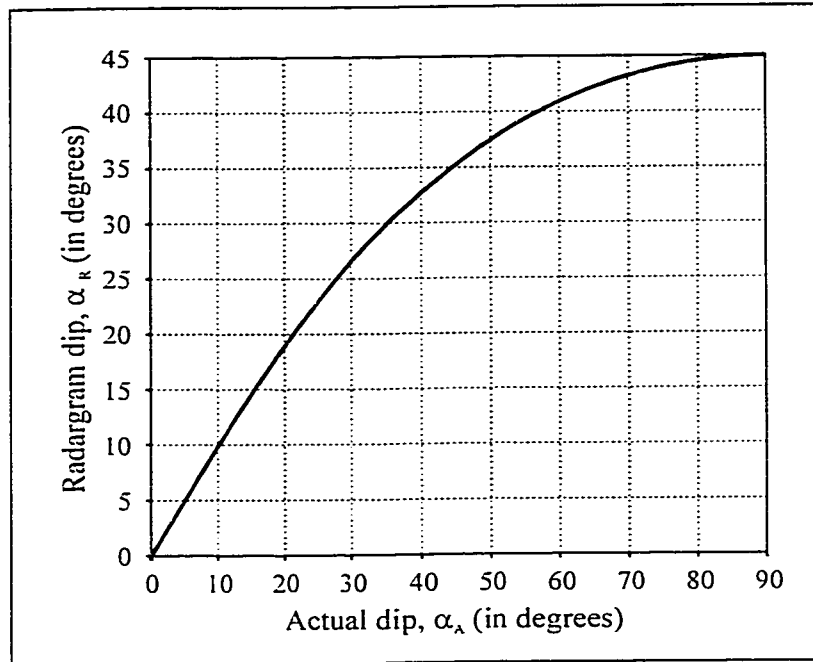
Figure 3-16 Dip correction in graphical form.
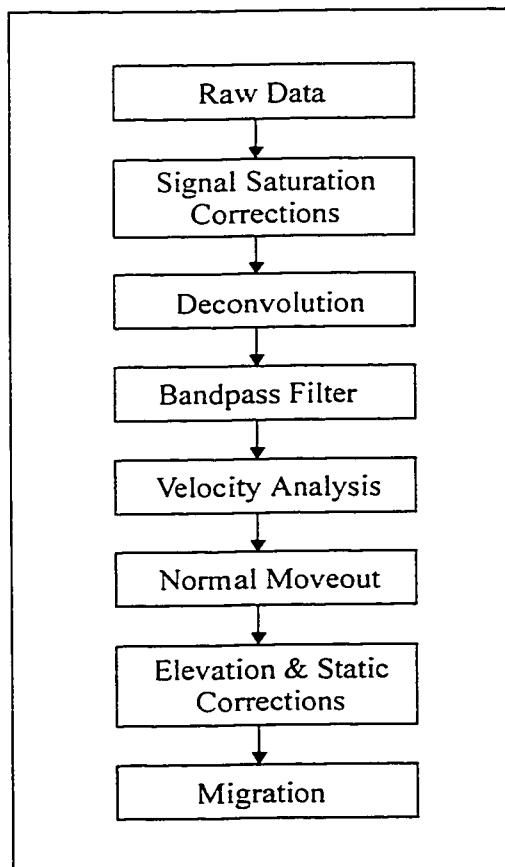
Figure 3-17 Seismic Processing Steps.

64

Figure 3-19 Subsurface synform feature and the resultant 'bow-tie' shape of its reflection event in a non-migrated section. Source: Kearey and Brooks, 1991. Reprinted with permission from Blackwell Science Ltd.

Figure 3-18 Collapse of a point reflector using migration Source: Kearey and Brooks, 1991. Reprinted with permission from Blackwell Science Ltd.

a) Non-migrated section (with bow-tie reflection events).

b) Migrated section.
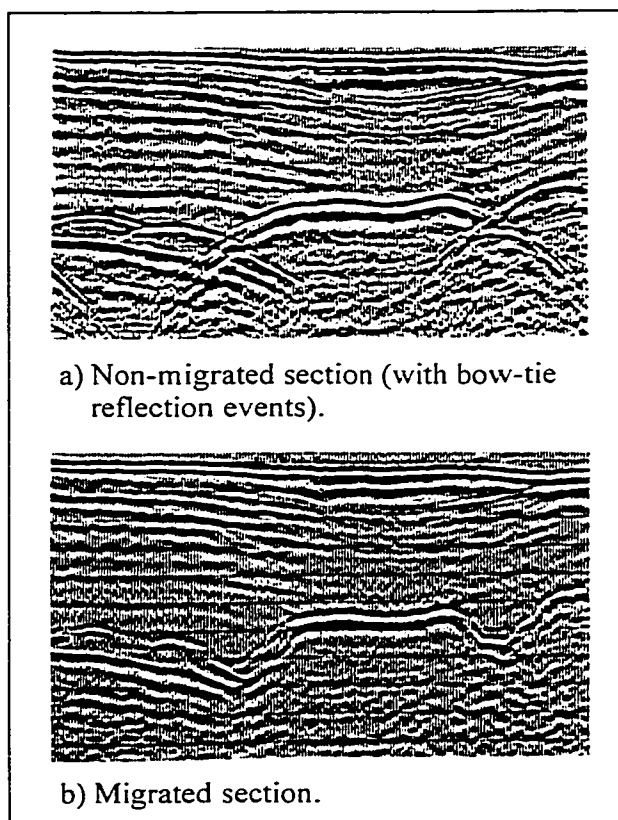
Figure 3-20 Synform feature before & after migration.

Source: Kearey and Brooks, 1991. Reprinted with permission from Blackwell Science Ltd. Courtesy of Prakla Seismos GmbH.
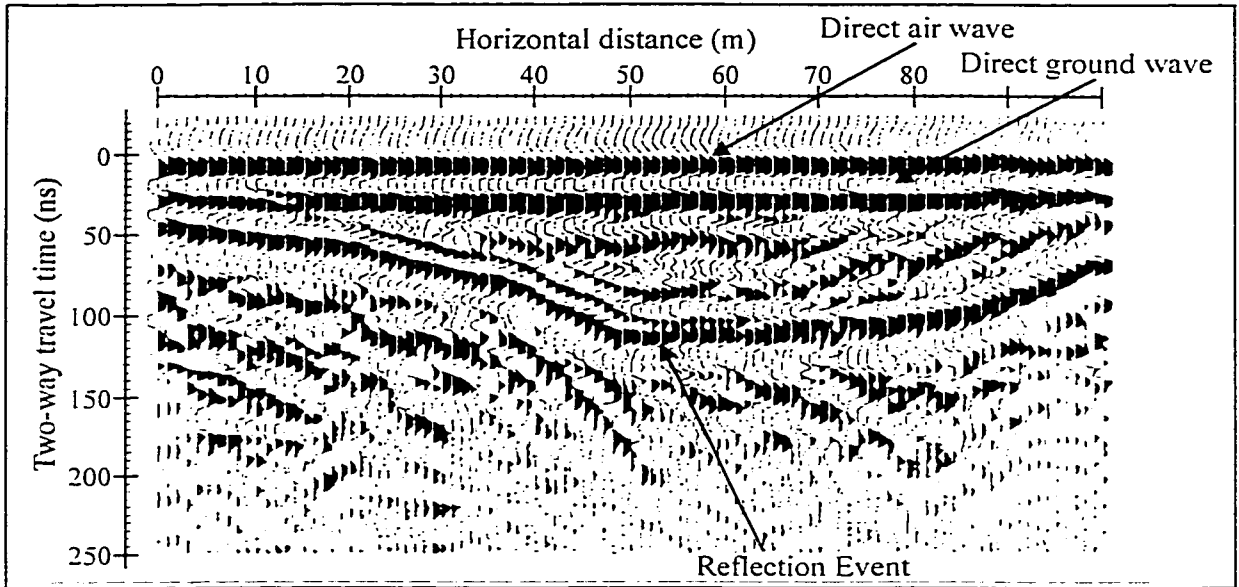
Figure 3-21 Direct waves in a reflection radargram
Source: Robinson and Michaud, 1999. Reproduced with the permission of the Minister of
Public Works and Government Services Canada, 2000 and Courtesy of the Geological
Survey of Canada.
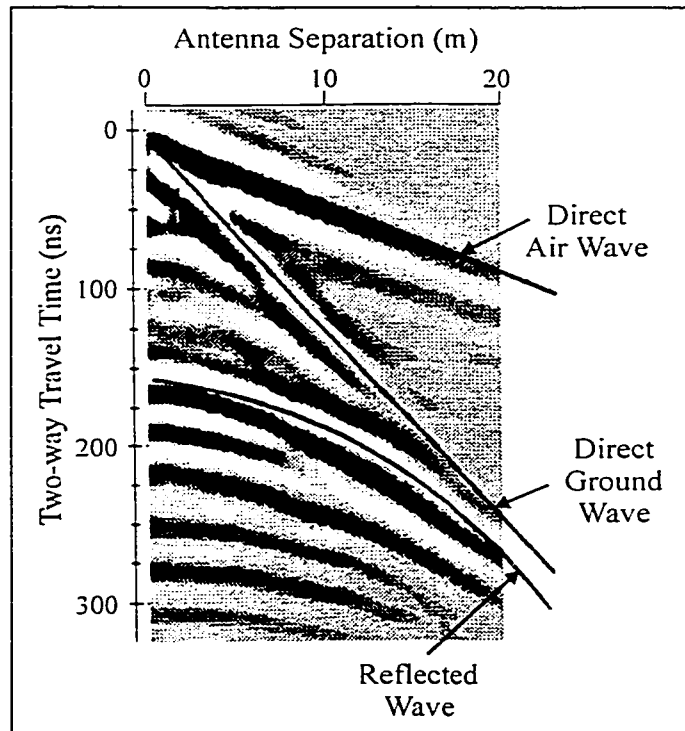
Figure 3-22 Direct waves in a CMP radargram.
Source: Annan, 1999. Reprinted with permission
from Sensors & Software Inc.

67
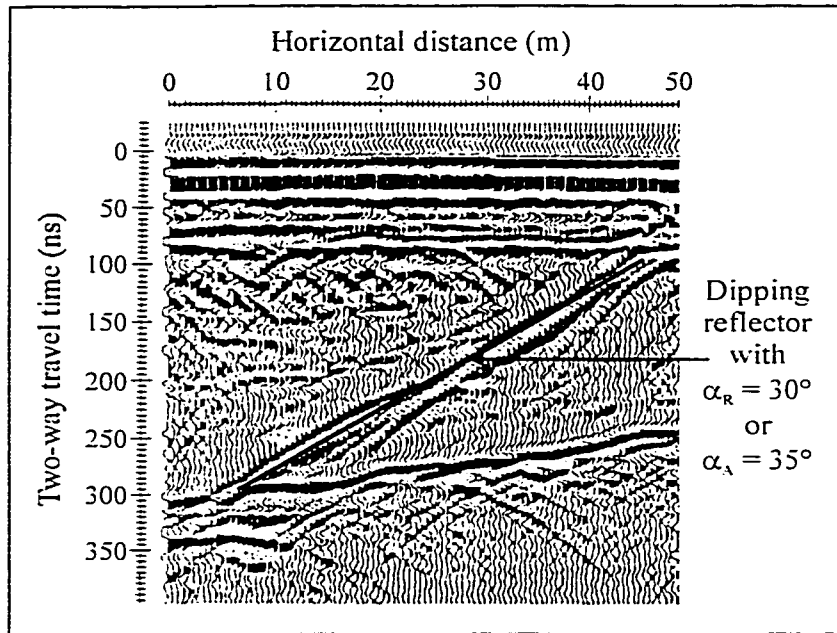
Figure 3-23 Reflection survey radargram with a dipping event.
Source: Robinson and Michaud, 1999. Reproduced with the permission
of the Minister of Public Works and Government Services Canada,
2000 and Courtesy of the Geological Survey of Canada.
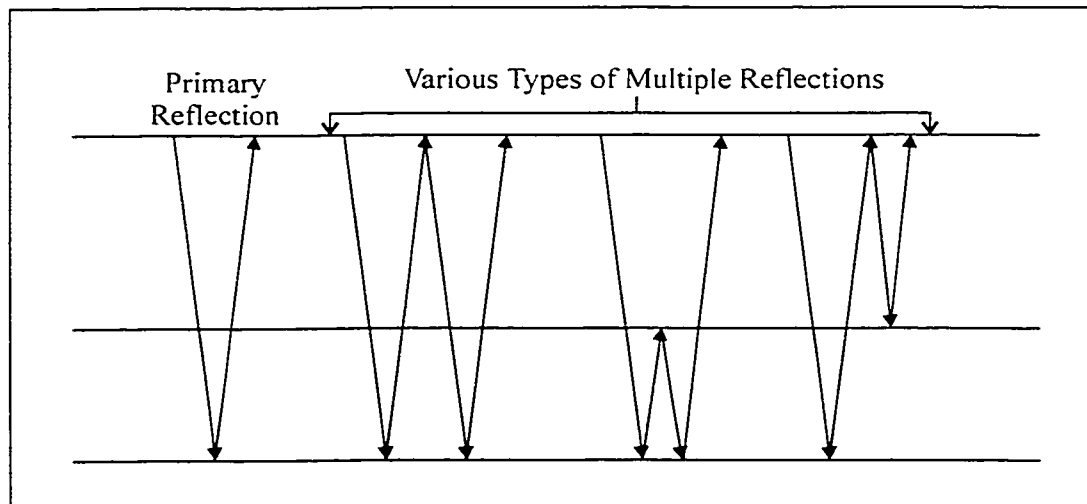
Figure 3-24 Multiple reflections.
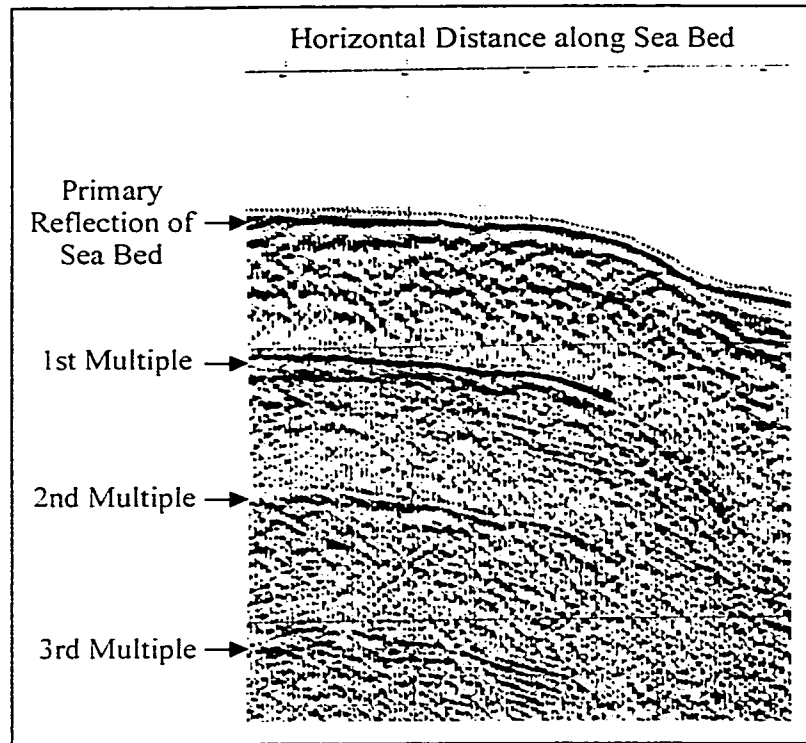
Figure 3-25 Example of multiple reflections in a radargram
(modified from Coffeen, 1986).
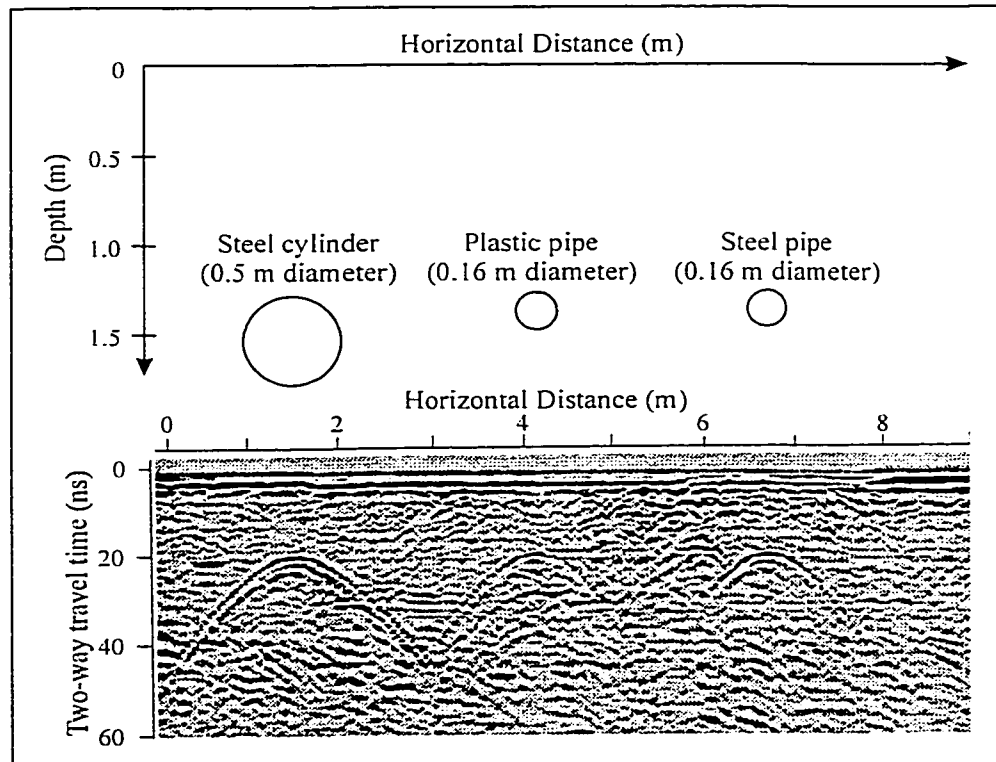
Figure 3-26 Characteristic hyperbolic shape of point targets
(modified from Annan, 1999).
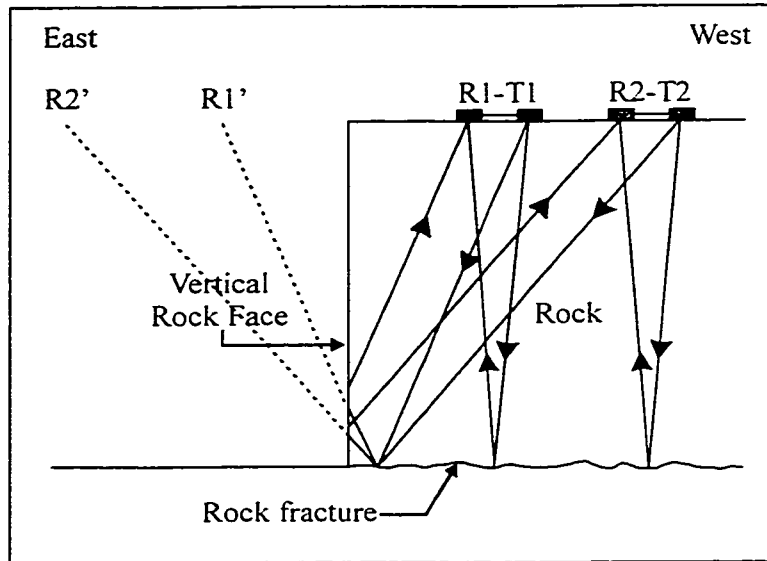
Figure 3-27 Radar paths with vertical boundaries.
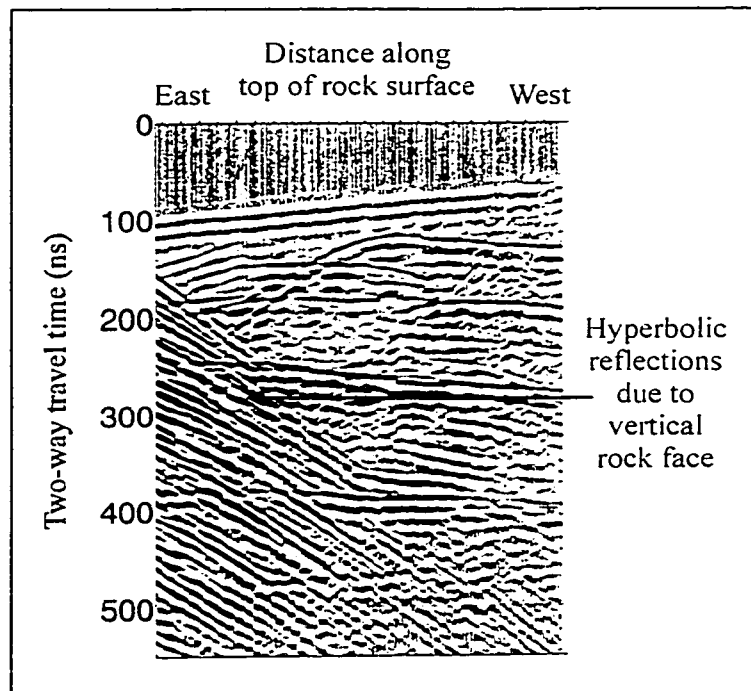
Figure 3-28 Radargram showing hyperbolic events caused by vertical boundaries (modified from Grasmueck, 1996).

CHAPTER 4: GPR APPLICATIONS

4.1 INTRODUCTION

Chapter 4 is a comprehensive literature review of GPR. This chapter begins by examining the advantages to using GPR as a site investigation tool – Section 4.2. Next, common GPR applications in the area of geotechnical engineering are discussed in Section 4.3. The remainder of the chapter focuses on the main objective of this thesis, using GPR for rock structure detection. Section 4.4 summarizes why GPR is being considered a tool for location and possibly characterizing various types of rock structure. Then the importance of rock structure in geotechnical engineering is considered for mining, foundations, nuclear-waste disposal sites, and stability of surface slopes in Section 4.5. Case studies where GPR has been used for detection of both small and large-scale fractures are critically examined in Section 4.6. Based on these past studies and literature on seismic reflection surveys, identification of rock structure in GPR radargrams is discussed in Section 4.7. In the last section (Section 4.8) summary remarks and conclusions are made for this chapter.

4.2 GPR AS A SITE INVESTIGATION TOOL

Site investigation is the process of collecting information about the ground in order to properly design and construct structures on or within the ground. Part of this investigation involves locating and characterizing geological hazards such as faults and cavities. To detect such hazards, ground penetrating radar can be used as a site investigation tool. GPR is favored over other geophysical techniques because the resulting radar profile is nearly a direct image of the subsurface (Annan, 1997). As well, it can provide information over a wide area more quickly and often at lower cost than conventional investigation techniques such as drilling and sampling. GPR is also considered superior at locating lateral subsurface variations since conventional methods are inherently localized (Clayton and Hope, 1997).

GPR's effectiveness at providing a general overview of the site makes it an excellent tool at the reconnaissance stage (prior to drilling and test pitting). At this stage, GPR may be able to identify critical or anomalous zones. This information can help the engineer optimize layout of boreholes and test pits for the main ground investigation. GPR can also be used at later stages in the project to interpolate and extrapolate between borehole data, in order to create subsurface cross-sections. In fact, if a GPR grid survey is conducted over a site, a three-dimensional ground model can be produced from a compilation of radar profiles and ground samples. Using conventional techniques, accurate sectioning can only be done using closely-spaced boreholes and thus at considerable expense.

Recent GPR advances have contributed to making it a more desirable tool for site investigation. Significant improvements in radar instrumentation and field procedures have made soundings to 20 m depth more reliable (Davis and Annan, 1989). The price of instrumentation has dropped while the performance has increased (Annan, 1997). There is a wider range of antenna frequencies plus borehole antennas are now available. The introduction of digital processing techniques has increased data quality and allows for more advanced data processing. There have been substantial improvements in data presentation due to an improved understanding of the engineer's needs and decreased costs in computer technology (Annan, 1997). Finally, technology specific for engineering is now being developed (Annan, 1997).

Today, GPR can be described as a rapid, non-contact, non-destructive, high-resolution method for detecting and mapping geological features in-situ (Davis and Annan, 1989). The equipment is lightweight and portable making it easy to use in difficult field conditions. There are also no known health risks to the people required to conduct the radar surveys (White et al., 1996). Notwithstanding this praise, it is important to remember that GPR only provides the engineer with guidance to where potential problems may lie but does not preclude the use of the more conventional methods (McCann et al., 1997). The results from drilling and test pitting are required to help calibrate the geophysical data for proper interpretation (McCann et al., 1997).

4.3 GEOTECHNICAL APPLICATIONS FOR GPR

The applications of GPR as a site investigation tool in geotechnical engineering are many and diverse (Clayton and Hope, 1997). Table 4-1 summarizes the more common geotechnical applications and rates them according to their general level of success. In this section each of these applications is briefly described and examples given when appropriate.

Locate & Characterize Buried Objects

GPR is recognized for locating and characterizing buried objects according to Table 4-1. In geotechnical engineering, radar would therefore provide information regarding the depth and location of buried utilities in urban areas. Detection of buried utilities has in fact been developed and tested in several countries including the U.S. (Peters et al., 1994). Based on this testing, it has been determined that GPR can detect both plastic and steel pipes (Peters et al., 1994). Since pipes would be point targets to radar, they would have the characteristic hyperbolic shape in the radar profile (Figure 3-26). Unfortunately, radar sometimes detects the trench but not the pipe. This happens because pipeline installation alters soil and drainage properties creating contrasts in dielectric properties picked up by the radar system (Peters et al., 1994).

Void Detection

GPR is also an appropriate tool for detection of both natural and man-made cavities or voids. Because these features are generally filled with either air or water, they provide an excellent contrast in dielectric constant with the surrounding soil or rock. Detection of voids is important for geotechnical projects, as they are geologic hazards. In karstic terrain, identifying natural subsurface cavities prior to construction of buildings and other structures is very important. In surface mining environments, unknown underground workings or natural cavities can cause catastrophic failures when heavy mining equipment breaks through the surface. In these situations, failures can cause considerable damage, delays, and possibly loss of life (Fenner, 1995). Drilling techniques have been traditionally used to detect such subsurface voids however drilling can interfere with mining activities and provides only line or point information (Fenner, 1995). GPR however has the ability to detect cavities ahead of mining operations so that steps can be taken to minimize or eliminate their impact (Momayez et al., 1996).

An example of where GPR was used for void detection is at the Zortman Gold Mine in Montana (Daniels et al., 1992). At this site, GPR surveys were conducted across various levels of the open pit to detect old underground workings from past mining operations. GPR proved successful in the detection of drifts, stopes, and other vertical features to depths greater than 10 metres. Radar provided valuable information on the size and location of hazardous underground conditions with a minimum delay to mining operations.

Stratigraphic Mapping

Stratigraphy involves studying the arrangement of strata in order to determine their geologic history (Bates and Jackson, 1984). It is important for a geotechnical engineer to understand the ground's stratigraphy for creation of a geologic model required for design purposes. GPR has been used successfully to map soil and rock stratigraphy, however seismic reflection and refraction are considered slightly better techniques (McCann et al., 1997). Annan et al. (1988) describes the successful use of radar to map the stratigraphy of the salt beds in various Saskatchewan potash mines. Thin clay seams, potash-rich zones, and anhydrite beds were detected in both the roof and floors of the mine tunnels. Detection of such features allowed for more effective mining of the potash.

Estimating Fault Displacement

Faults are another type of geologic hazard that are often concealed at the surface but can be detected by GPR (Benson, 1995). Knowledge of the location and amount of displacement along an individual fault is important in order to mitigate the effects of possible future earthquakes through adequate engineering design (Benson, 1995). GPR been given a good rating of success for estimating the amount of displacement along a fault, but similar to stratigraphy, seismic reflection and refraction are regarded as better techniques for this application (McCann et al., 1997). Benson (1995) however provides an example of where GPR surveys were conducted across a section of the Wasatch Fault in Utah for estimating displacement. The results of the study showed that the calculated fault offset and dip angle were close to the actual values determined from a nearby trench: the fault offset was calculated to be 3.3 m with a dip angle of 77°W. whereas the actual offset and dip angle were found to be 3.5 m and 76°W respectively.

Locating and Characterizing Fracture Zones

Fracture zones or faults can be located and sometimes characterized using radar but often seismic or EM (electromagnetic) methods are more successful (McCann et al., 1997). Because this application is partly the focus of this thesis it will be discussed in more detail in Section 4.6.2.

Estimating Depth to Bedrock

Determining the depth of bedrock is important when designing foundations for heavy structures such as bridges or high-rise buildings. Seismic refraction/reflection techniques are the best geophysical techniques to use for this application because depth and/or type of overburden can limit GPR (McCann et al., 1997): for example, if the overburden is too deep or has a high clay content, the bedrock surface is not detected. Despite these problems, Davis and Annan (1992) give an example of where GPR was used to determine the depth to bedrock under a shallow lake. Surveys were conducted during the winter when the surface was covered in ice and low frequency (12.5 MHz) antennas were used to minimize the attenuation effects caused by the clayey overburden. GPR at this site was successful at locating a bedrock knob to be used as the base of a proposed cofferdam.

Locating and Characterizing Erosional and Structural Features

Delineation of erosional and structural features in rock or soil prior to the main site investigation or construction allows the engineer to adapt the design accordingly (Li, 1998). GPR may not be the best geophysical technique for this application but at the Three Gorges Project in China, GPR quite effectively delineated non-uniform layers in granite and outlined the extent and attitude of weathering interlayers. Information from the radar surveys allowed the excavation elevation to be redesigned and in the more weathered sections, high pressure grouting was used to strengthen the foundations. For this study, GPR proved to be a cost-effective means of mapping buried geological defects that would have had large influences on construction procedures.

Assessing the Integrity of Mine Pillars

In an underground mining environment, GPR may be an effective tool for assessing the integrity of pillars in coal, salt, and gold mines (Fenner, 1995). For example at a coal mine in West Virginia, GPR was used successfully to map the thickness and geometry of coal pillars that were approximately 15 m thick (Fenner, 1995). And at a gold mine in South Africa, fractures were detected in quartzite pillars when transillumination surveys where being conducted to calculate propagation velocities (Fenner, 1995).

Locating the Water Table & Groundwater Contamination

Locating the phreatic surface or characterizing a contaminant plume may be thought of as more geoenvironmental applications, but they do have an impact on geotechnical projects as well. Annan et al. (1991) and Van Overmeeren (1997) give examples of GPR used to accurately detect and map the water table. For groundwater contamination, Benson (1996) provides two excellent case studies of how GPR was used in Arizona and Utah to map contaminant plumes produced by leaking underground fuel tanks. Benson (1996) also describes how radar was able to determine the lateral extent of the plumes allowing monitoring wells to be installed at strategic locations at both sites.

Distinguish Lithological Changes

The final geotechnical application to be considered is lithology. Lithology is distinct from stratigraphy, as it involves identifying the physical characteristics of the ground including color, mineralogy, and grain size (Bates and Jackson, 1984). Lithology is important because knowledge of the ground's physical characteristics allows the engineer to determine how it will perform under various loads and stresses. Unfortunately, GPR has limited use in assessing the lithology of both soil and rock (McCann et al., 1997). Because GPR measures changes in dielectric properties, it cannot distinguish geologic media based on color but may have some success with mineralogy and grain size. Recall from Section 2.5.1 that mineralogy is one of the main factors in determining the dielectric constant of a rock. As for grain size, large particles such as boulders and cobbles can often be detected by radar and appear as hyperbolic features in the resulting profile.

Aside from detection of buried objects, for all other engineering applications there are other geophysical techniques that are either equivalent or better to use than ground penetrating radar. So, before using GPR for a specific application, consult a geophysical advisor to ensure the correct technique is used for the given application and site conditions (McCann et al., 1997).

4.4 GPR FOR ROCK STRUCTURE DETECTION

The main object of this project is to evaluate whether GPR can be used to detect features that result from processes such as faulting, folding, stress relief, metamorphism, and igneous intrusion – or rock structure. These structural features represent a discontinuity of mechanical properties with a rock mass (Herget, 1977). In this thesis, rock structure is a term used to represent joints, fractures, foliation and bedding planes, faults, fracture and shear zones, dykes, and veins.

Detection and mapping of rock structure often requires both geological and geophysical techniques due to the inherent complexity of the ground (Dowding et al., 1981). Discontinuities, for example, have dimensions, orientations, spacings, and physical properties. It is also important to remember that mapping structure is a three-dimensional problem. The traditional approach to creating a three-dimensional subsurface model is to correlate information from surface geologic mapping with borehole information (Dowding et al., 1981). These conventional investigation techniques acquire information regarding the characteristics of individual structural features (i.e. spacing, surface roughness, aperture, color, orientation, etc.) can be acquired. Unfortunately, the main disadvantage to surface mapping is that the information is not applicable to anything greater than a few metres from the rock surface. For drilling, the associated high costs and localized information are two big disadvantages. Because of these problems, remote techniques such as ground penetrating radar are being considered a cost-effective, non-intrusive means for mapping structure in the interior of a rock mass.

4.5 IMPORTANCE OF STRUCTURE IN GEOTECHNICAL ENGINEERING

Locating and characterizing structural features such as joints is vital for all geotechnical engineering projects because they influence rock properties which in turn affects the engineering behavior of the rock mass (Dowding et al., 1981). Structure can affect important properties such as permeability, porosity, deformability, and rock-mass strength (Dowding et al., 1981). Porosity and permeability for example will both increase as fracturing increases.

This section describes the importance of rock structure for mining projects (both surface and underground), construction of underground chambers for nuclear waste disposal, foundation investigations and slope stability assessments. Examples where GPR has been used for detection of rock structure in each of these areas are also provided.

4.5.1 Underground Mining

To improve global competitiveness, the Canadian mining industry is presently trying to identify technologies for remote characterization of rock masses (Momayez, et al., 1996). Geophysical tools such as ground penetrating radar are being considered for locating rock mass structure and assessing stability. GPR is an attractive technique for locating potential problems in underground environments because of its portability and compactness (Momayez, et al., 1996). As well, radar is more beneficial to use in comparison to the more costly and sometime hazardous intrusive examination methods such as drilling (Momayez, et al., 1996). Detection of geologic structure in advance of mining would help to decrease dilution, increase safety, minimize exposure to workers, and allow more efficient mine planning, which translates to lower production costs (Momayez et al., 1996).

At present, routine use of GPR in the mining industry is limited by difficulties with interpretation (White et al., 1996). Despite this, there has been (and still is) a lot of research done on the use of radar in Canadian mines. Many feel that a number of current and future mining problems that are structure-related may be identified by GPR. For example, GPR is being considered as a monitoring tool during tunneling because rock structure can cause deviation in drilling sequences. so prior warning using GPR would be beneficial (Momayez et al., 1996). The issue of underground safety is still an important topic because most structural failures result from undetected discontinuities, voids, faults, and other inclusions (Dennen and Stroud, 1991).

Related to mining safety, radar is a tool that could help identify stress fractures that form parallel to an underground opening. These fractures are often formed in deep mines due to high devatoric stresses but also in shallow mines due to stress-relief. Fracturing in the back poses the greatest risk to personnel and equipment because loose rock blocks are created and may fall without warning if there is not adequate tunnel support. These types of fractures are especially dangerous because their orientation prevents them from being observed visually; therefore radar is potentially a good tool for assessing the extent of this fracturing. Should radar have the ability to identify where the fractures are opening with time and the height of the fracture above the tunnel. this will help the engineer design adequate support.

A future mining problem that is also related to mining safety is the use of spray-on linings as underground support instead of the traditional wire mesh and/or shotcrete. These linings are applied to the back of an underground opening following blasting. The rapid application of these linings will likely conceal the rock structure before it can be observed and mapped. Radar may be able to detect stress or structurally controlled fractures before they become a problem.

Radar has been successful in fracture detection in soft rock mines but has only limited success in hard rock mining environments. Annan et al. (1988) and Unterberger (1978) describe examples of where radar has been used successfully to probe salt mines for fractures and faults. Annan et al. (1988) conducted experiments at various Saskatchewan potash mines to prove that stress-relief cracks surrounding underground excavations can be detected and mapped. Unterberger (1978) describes how radar has been successful in the detection of discontinuities by conducting radar soundings at various mines in Canada and the United States.

Based on the successes in these soft rock environments, researchers such as Annan (1989) and Momayez et al. (1996) looked at using radar in hard rock mining environments. Unfortunately, Annan (1989) concluded that hard rock environments are more difficult for radar because of their increased complexity and high signal attenuation characteristics. Annan (1989) attempted to detect small fractures and joints at the Denison Uranium Mine in Ontario but experienced limited success due to their tight nature. Seven years later, Momayez et al. (1996) was also unsuccessful in detecting closed discontinuities in a sill pillar at Kidd Creek Mine, Ontario. Nevertheless, much of the research presented in this thesis is motivated by the desire to assess the applicability of GPR for rock structure identification in hard rock environments. In particular, guidelines of what should or should not work based on the physical principles of GPR and the material properties associated with rock structure are clearly explained.

4.5.2   Surface Mining (including ornamental building stone quarries)

For surface mining, understanding the natural fault/fracture system within the rock mass is essential for slope design. Fractures that do not daylight in the slopes often go undetected and can cause unforeseen failures. Using radar to help delineate structure for surface mining has the

same advantages as described in Section 4.5.1 for underground mining. Unfortunately, no case studies that used radar for mapping rock structure in surface mines could be located. however Grasmueck (1996), Piccolo (1992) and Unterberger (1992) all provide examples of where radar has been used in ornamental building stone quarries.

In the mining of ornamental building stone, structure often dictates block thickness and can make the extraction of larger blocks difficult to impossible (Grasmueck, 1996). Radar has the ability to look ahead of the mining process to sense flaws or boundaries allowing the distinction between high and low-quality rock to be made (Grasmueck, 1996). This information allows quarry personnel to focus on only the good-quality rock thereby reducing the accumulation of commercially unattractive broken material that can potentially obstruct quarry operations (Grasmueck, 1996). Identifying structure such as bedding can also allow more efficient blasting procedures (Momayez et al., 1996).

Field studies have been conducted at various quarries around the world using radar for fracture mapping. Piccolo (1992) describes a case study where GPR surveys were conducted across marble blocks that had already been cut on the walls of a quarry in Italy. The objective was to map artificial fractures, natural stratifications, cavities and altered zones of carbonate within the blocks using radar (Piccolo, 1992). The results of the study showed that GPR could detect both natural and artificial fractures less than 1 cm wide using 500 and 900 MHz centre frequency antennas (Piccolo, 1992).

GPR surveys have also been conducted in a granite quarry in Marble Falls, Texas (Unterberger, 1992) and across the floor of a gneiss quarry in Switzerland (Grasmueck, 1996). At the granite quarry, a natural fracture approximately 6-7 m deep was mapped for 50 m along the surface (Unterberger, 1992). At the gneiss quarry, reflections from three water-filled fractures (2-4 cm thick and oriented parallel to the floor) plus a steeply dipping fault was clearly identified in the radar profiles (Grasmueck, 1996). This information helped to determine which rock blocks could be released from the quarry (Grasmueck, 1996).

4.5.3 Foundations on Rock Masses

The first step in the design of buildings, bridges, or dams on rock requires proper characterization of the rock mass. This includes determining the frequency and distribution of discontinuities which ultimately influences the engineers' evaluation of settlement and bearing capacity. Similar to soil, displacements within the foundation generally control foundation design. but all settlement estimates require a geomechanical model which can only be established with some knowledge of the subsurface discontinuities (Kulhawy and Carter, 1992). As for bearing capacity, the failure mode is highly dependent on the orientation and spacing of the discontinuities.

Radar would be helpful in identifying the major discontinuities at the preliminary foundation design stage and later, to help correlate information between boreholes. Pilon et al. (1996) describe a study where GPR was used across the foundations of a proposed containment dam construction site on the Little French River in Ontario (Pilon et al., 1996). The radar surveys were successful in delineating joints, fractures, and faults to depths of approximately 15 m in the gneiss foundations (Pilon et al., 1996). At this site, fracture detection was important for assessing the integrity of the rock under the dam and to detect problem areas that required further investigation (Pilon et al., 1996). Ultimately the radar information aided in the selection of the optimum site for the new dam (Pilon et al., 1996). The main disadvantage of this study was that

there was no ground-truthing information available to help interpret the data or confirm the presence of the identified fractures.

4.5.4   Underground Chambers in Hard Rock Masses

Rock mass structure influences the location, size, shape, excavation sequences, and reinforcement of large underground openings (or chambers) in hard rock environments (Stephansson, 1992). In fact, evaluating the rock mass characteristics is important at an early stage in the project to identify conditions that might cause problems during and after construction (Stephansson, 1992). Characterization of igneous and metamorphic shield rock has received considerable attention as it is considered a media for permanent disposal of nuclear waste. Research evaluating radar for rock mass characterization has been done at underground research labs such as Stripa in Sweden, Grismel in Switzerland, and Pinawa in Canada. At all three sites, both surface and borehole GPR surveys have been conducted.

At the Stripa project site, borehole radar was successfully developed and tested for characterization of major fracture zones (Olsson and Falk, 1990). The fracture zones within the granite ranged from 1 to 8 m wide and consisted of brecciated and mylonitized rock (Olsson and Falk, 1990). Fracture detection is so important because these features are potential pathways for the waste to escape in either fluid or gas form (Olsson and Falk, 1990). Through the radar research at Stripa, it was concluded that borehole radar in unweathered shield rock could achieve a penetration of more than 100 m using antenna frequencies between 20-60 MHz (Olsson and Falk, 1990).

Two years later, similar radar surveys were conducted at the Grismel Rock Laboratory in the Swiss Alps and are described in Olsson et al. (1992). Again borehole radar was proven to be capable of characterizing shear zones in granite to 90 m away from the borehole using antenna frequencies similar to those used at Stripa (Olsson et al., 1992).

Closer to home, from 1984 to the mid-1990's, radar was used extensively at the Underground Research Laboratory (URL) in Manitoba for the characterization of granite (Holloway, 1992; Holloway et al., 1986; Holloway and Mugford, 1990; Stevens et al., 1994). The objective of the many GPR studies conducted at the URL was to assess radar as a non-destructive technique to be used during siting, design and construction of the waste disposal vault (Holloway and Mugford, 1990). Both surface and borehole surveys were conducted using frequencies ranging from 22 MHz up to 500 MHz for the detection of large moisture bearing fault zones through to small-scale fractures or joints (Stevens et al., 1994). The results of this testing showed that radar could be used as a quick and reliable tool for locating and orienting zones of significant fracturing 5 to 50 m away from the surveyed face in granite (Holloway, 1992). The URL was particularly useful for evaluating GPR because the rock at this site has been extensively mapped and drilled, allowing for proper calibration of the geophysical data (Holloway, 1992).

78

4.5.5 Slope Stability

In excavations and natural rock slopes, the engineer needs to identify and evaluate all potential failure mechanisms. Because rock slopes generally fail along geological defects (or rock structure) an engineering assessment of a slope includes proper identification of all possible planes of weakness. Only with the knowledge of the major structural discontinuities can the rock slope be designed based on a kinematic analysis. Primarily, surface structural mapping is conducted to identify these discontinuities, however sometimes features are missed due to limited rock exposure or weathering. Because any undetected structure(s) can have disastrous consequences, GPR is being considered a tool that may help locate them.

In order to examine the applicability of GPR to map the surface distribution and extent of internal fracturing, Toshioka et al. (1995) describes the results of reflection profiling surveys conducted at a welded tuff quarry in Japan. Toshioka et al. (1995) used 100, 300, 500, and 900 MHz antennas and compares the results of each survey with geological observations. The major conclusion of this study was that fractures with clay or water infilling were identifiable on the radar profile, so GPR may be useful for assessing the potential of rock fall hazards (Toshioka et al., 1995).

4.6 ROCK STRUCTURE CASE STUDIES

One of the first investigators to consider the use of radar propagation through rock for structure detection was Unterberger (1978). Based on the results of GPR surveys conducted at various salt mines in North America, Unterberger (1978) found that radar successfully detected discontinuities[10] ahead of mining. Since then a number of researchers have conducted field investigations assessing GPR's potential for fracture detection in hard rock environments (Annan, 1989; Buursink and Lane, 1999; Davis and Annan, 1989; Grasmueck, 1994; Grasmueck, 1996; Holloway, 1992; Holloway et al., 1986; Momayez et al., 1996; Olsson and Falk, 1990; Olsson et al., 1992; Piccolo, 1992; Pilon et al., 1996; Unterberger, 1992) – most of which were mentioned throughout Section 4.5. For the majority of these references, either large-scale features such as faults or small-scale features such as joints were observed. As for other types of rock structure, Davis and Annan (1989) and Olsson et al., (1992) provide examples of the detection of dykes and Grasmueck (1996) gives an example of foliation-fracture[11] detection.

Despite the fact that the vast majority of these case studies claim that radar was successful in delineation of fractures in the millimetres to metres thickness range, most researchers (including geophysicists) tend to advertise successes and not failures (Clayton and Hope, 1997). Throughout the remainder of this report, it is important to keep in mind the five factors that influence success of any GPR survey (McCann et al., 1997):

1. required penetration in the geologic medium,
2. required resolution for the anticipated target(s),
3. contrast in dielectric properties between the target and host,
4. signal to noise ratio, and
5. available site information (i.e. ground-truthing).

---

[10] In Unterberger (1978) discontinuities were any distinct features within the salt such as anhydrite, carbonate rock, lenses of sand, fractures and faults.

[11] A foliation-fracture is a parting that has occurred along a foliation plane.

Sections 4.6.1 and 4.6.2 will discuss and compare the results of various GPR case studies such that more definite conclusions can be made regarding the use of GPR as a tool for detection of rock structure in hard rock environments. Section 4.6.1 will describe small-scale fracture detection and Section 4.6.2 will describe large-scale fracture detection. Recall from the introduction that small-scale discontinuities in this thesis refers to features will an aperture less than 1 cm, whereas large-scale discontinuities are features will an aperture significantly greater than 1 cm.

4.6.1   Small-Scale Fracture Detection (i.e. Joint Detection)

Should radar have the capability to detect discontinuities less than 1 cm in width (or aperture) both quickly and accurately, the geotechnical community would be extremely pleased. However, delineation of small, individual, discrete fractures in a rock mass is particularly challenging for radar because of the following limitations:

1. *Amplitude fidelity* – Current commercial radar systems are designed to measure time delays but have very poor amplitude fidelity (Parry and Davis, 1992) – Section 2.7.1.
2. *Energy losses in the media* – There are energy losses due to inclusions (i.e. veins, dykes) and moisture within the rock.
3. *Target dimensions* – Detection of small fractures is governed by the thin layer concept, so as the thickness of the feature decreases the reflectivity decreases (Section 2.6.4).
4. *Target roughness* – The surface of most discontinuities ranges from rough to smooth to slickensided. As the surface roughness increases the attenuation increases due to higher amounts of scattering. This effect has more impact on the higher frequency antennas (Parry and Davis, 1992).
5. *Insufficient contrast in dielectric constant* – If there is an insufficient contrast in dielectric constant between the target and host medium, the reflectivity may be too low to be detectable using radar (Section 2.6.3). For example if a fracture is dry and infilled with broken rock fragments, there may not be sufficient contrast in ε_r with the surrounding host rock.

In spite of these problems, a number of researchers have taken on the difficult task of evaluating detection of small-scale fractures using GPR (Annan et al., 1988; Annan, 1989; Buursink and Lane, 1999; Grasmueck, 1994; Grasmueck, 1996; Holloway et al., 1986; Momayez et al., 1986; Piccolo, 1992; Pilon et al., 1996, Toshioka et al., 1995). Unfortunately, there are clear discrepancies between the various case studies as the results vary from being not successful to highly successful. In order to try to understand the different levels of success, a comparison of the ten case studies will be made with respect to the following conditions: antenna frequency, host rock, survey environment, fracture (or target) characteristics, and data processing.

4.6.1.1   Antenna Frequency

Selecting the proper antenna frequency is vital for the success of GPR, however it is often a difficult task because there are a number of factors to be considered (i.e. required resolution, required depth of penetration, etc.). For all ten case studies, a variety of GPR systems from different manufacturers and a range of antenna centre frequencies (from 100 MHz to 900 MHz) were used. In fact, both Toshioka et al., (1995) and Piccolo (1992) used more than one frequency to conduct the radar surveys. Unfortunately, there was no real consensus as to which antenna frequency is most appropriate for joint detection.

For surveys conducted with the lower frequency antennas (i.e. 100 and 200 MHz) - Buursink and Lane (1999), Grasmueck (1994 & 1996) and Pilon et al., (1996) - all concluded they successfully detected jointing planes in surface outcrops. Yet, Annan (1989) and Momayez et al., (1996) concluded that the low frequency antennas were inadequate for detecting these targets. In fact, Annan (1989) recommends that 1000 MHz be used for future investigations of thin fractures.

Where higher frequency antennas were used (Holloway et al., 1986; Piccolo, 1992; and, Toshioka et al., 1995) there are also conflicting views. Holloway et al. (1986) used 500 MHz antennas to survey the walls during excavation of a shaft but had limited success. However, Piccolo (1992) and Toshioka et al. (1995) claimed successful detection of discontinuities using both 500 MHz and 900 MHz antennas. Toshioka et al. (1995) was the only researcher to evaluate and compare a full range of centre antenna frequencies - 100 MHz, 300 MHz, 500 MHz and 900 MHz. Based on the results of this study, Toshioka et al. (1995) concludes that the 500 MHz antennas were superior in terms of operating depth and resolution. Unfortunately, Piccolo (1992), who tested both 500 and 900 MHz antennas, makes no reference to which antenna frequency was more effective.

To help compare the ten case studies, each was rated according to the level of success for detecting small-scale structure. The rating scale is from 0 (no success) to 4 (high success). The level of success was somewhat subjectively assigned to each case study based on conclusions given by each author. Figure 4-1 is a plot of the success level versus the antenna centre frequency for the various case studies. The figure shows that despite the advancements in radar instrumentation over the thirteen-year period these ten case studies were conducted, it is difficult to conclude that the level of success has increased over time. As well, there is not an obvious correlation between the level of success, the antenna frequency, and the reference date of publication. Hence, the question of what antenna centre frequency is most effective for detection of joint-sized fractures remains unanswered.

4.6.1.2 Host Rock

The dielectric properties of the host rock control how radar energy propagates and attenuates in the subsurface, so the type of host rock influences the success of a GPR survey. Table 4-2 shows the level of GPR success for each case study versus the type of host rock and the associated dielectric properties in terms of signal propagation velocity in m/ns and attenuation constant in dB/m (if determined).

Table 4-2 shows that although a variety of rock types were tested, half of the sites were in shield rock - specifically granite and gneiss. These rocks are considered good media for ground penetrating radar surveys because they are relatively uniform and have a low conductivity (< 1 mS/m) in their unweathered state - Figure 2-2. Rocks composed of predominantly one mineral (i.e. quartzite, marble, and salt) may also be good media because they characteristically have low absorption and high homogeneity which allows electromagnetic waves to easily penetrate the medium.

Knowledge that the rocks in Table 4-2 are generally considered to have a low conductivity perhaps partially explains why the attenuation constant was only determined for two of the case studies. Holloway et al. (1986) gave the reasoning that because the granite at the URL site had a low porosity, they assumed the effect of rock saturation on the value of the dielectric constant was negligible. Annan et al. (1988) also explains the difficulty in attaining reliable estimates of attenuation - which is primarily due to instrumentation limitations.

Unlike attenuation, a value for the signal propagation velocity was determined for each rock type. The velocities are either slightly lower or higher than the values given in Table 2-2. The average propagation velocity is 0.120 m/ns (or ε_r = 6.25) for all the rock types listed in Table 4-2 (excluding the welded tuff). For the majority of the case studies, the velocity was estimated from a CMP or WARR survey. Annan et al. (1988) however determined the velocity by conducting transillumination surveys through a salt pillar and Holloway et al. (1986) conducted reflection surveys on a outcrop then back-calculated the signal velocity using the known distance to a parallel reflector.

The site in welded tuff[12] (Toshioka et al., 1995) had a significantly lower signal velocity in comparison to the other nine. Silica (or quartz) has a dielectric constant around 4 to 5, so the high ε_r of 19.5 for the tuff is likely due to the presence of water. Recall that tuff is a pyroclastic rock so there may have been significant water between the grains. Evidence to support this hypothesis was the mention of water flowing out of some of the joints in the surface outcrop.

In all ten case studies, the geologic conditions were relatively simple (i.e. one rock type) except for the study conducted by Buursink and Lane (1999). The outcrop used for this study had heterogeneous conditions with metamorphic gneisses and schistose rocks intruded by dykes of granite and pegmatite. Buursink and Lane (1999) conclude that radar is successful in detecting fractures but neglects to mention if radar detected any changes in lithology. Perhaps this is explained by Table 4-1 which shows radar has limited use in detecting changes in rock types. But despite their claim of success, it is recommended that further testing be conducted in geologically complex environments because large variations in dielectric constant exist between various rock types.

To summarize, there is increased potential for a successful radar survey for detection of rock fractures when the host rock is relatively uniform and non-conductive. Since the host medium at all ten research sites adequately fit this criterion, it is unlikely that the different host rocks can explain the variation in success between the case studies.

4.6.1.3   Survey Environment

The survey environment also has an influence on the success of GPR because it may contain objects that will cause interference with the radar signals. This interference decreases the signal to noise ratio and hence reduces the chance of target detection. Both surface surveys (i.e. across rock outcrops) and underground surveys (i.e. across sidewalls of mine drifts) can be influenced by a number of factors, but in general underground surveys face even more challenges.

For each of the ten case studies that examined small-scale structure, Table 4-3 lists the survey environment, the location of the survey(s), and the level of GPR success. This table shows that of the ten case studies, four were conducted underground and six were conducted on surface exposures. Considering the level of success with the type of environment, the table reveals that the underground survey environments have a lower level of GPR success in comparison to the surface environments. Some of the problems in underground environments are discussed in Annan (1989) and Annan et al. (1988).

---

[12] A welded tuff is a pyroclastic rock that has been hardened by the welding together of glass shards due to temperature and pressure (Bates and Jackson, 1984). It has a high silica content and is banded or streaked in appearance (Bates and Jackson, 1984).

One of the underground problems is reaching the back of the tunnels for surveying. This was overcome in two case studies by using either custom built adjustable plastic poles (Annan, 1989) or a spring-loaded platform that could be pushed up against the back (Annan et al., 1988). The next major problem associated with using radar in a confined-space are the signal reverberations (Annan et al., 1988). These are undesired signals generated by echoes from the tunnel walls and other mining equipment, causing unwanted multiples in the resulting radar profile (Annan et al., 1988). This problem was only addressed by Annan et al. (1988) who used radio-frequency absorbing[13] material around the antennas to minimize this effect. This technique however worked better for the high frequency antennas because the effectiveness of the material depends on the thickness compared to the signal wavelength (Equation 2-18) – Annan et al., 1988.

Metallic underground support such as wire mesh also causes problems with the use of radar because it causes high signal attenuation. Annan (1989) found that rock bolts did not cause excessive interfere with the radar signals using the 200 MHz antennas, but warned that bolts may have a significant influence on higher frequency antennas. In general, it is recommended that when GPR is used in the presence of metallic support that steps be taken to minimize their influence (Annan, 1989). This can be done by using absorbing material or shielded antennas and proper antenna placement (i.e. locate antennas as far away from sources of interference as possible).

Conductivity problems can also occur when surveys are performed near conductive ore bodies. Figure 2-2 in Chapter 2 shows that massive sulphide ore bodies have undesirable dielectric properties for ground penetrating radar. In fact, Momayez et al. (1996) was able to identify zones of rich sulphides in a sill pillar because of the signal saturation that was clearly visible on the radar profile. At the Denison mine, Annan (1989) determined that the attenuation constant in mineralized rock was 10 to 50 times greater compared to unmineralized rock. It is therefore important to understand that success in fracture detection will decrease if the surveys are performed near conductive ore bodies.

Lastly, there are problems with surveying across the rough surfaces found in underground environments. These surfaces, created by blasting, make it difficult to achieve close contact between the antennas and the surveyed surface (Annan et al., 1988). In fact, when using higher antenna frequencies (i.e. 1000 MHz), Annan (1989) recommends that the radar data be compensated, however any compensation for roughness may be costly and increases the complexity of the survey. Annan (1989) unfortunately, does not reveal by what means the compensation should occur (i.e. topographic correction?).

Focusing now on the surface environments, Table 4-3 shows that three sites were rock quarries and the other three were outcrops. The higher success rate of these case studies may be due to the fact that the sites were relatively ideal for conducting radar. The majority of the sites had no overburden, were located in non-populated areas (i.e. minimal sources of background noise), and the surveyed surfaces were all relatively planar. Despite these favorable conditions, there were still problems. In the case studies presented by Buursink and Lane (1999) and Pilon et al. (1996), the surveyed surfaces were so irregular that topographic corrections had to be applied. Topographic irregularity is often viewed as a problem because it adds to the cost and complexity of the GPR survey (Annan. 1989).

---

[13] Annan et al. (1988) did not mentioned what type of absorbing material was used.

Another problem with surface environments is the presence of water bodies at a site. Pilon et al. (1996) overcame this difficulty by conducting radar surveys across a small river using an inflatable raft. Unfortunately though, the steep banks along the water's edge prevented them from conducting continuous surveys across the site (Pilon et al., 1996). As a result, no information was collected at the transition zones from water to land on either side of the waterbody (Pilon et al., 1996).

The last surface problem was the influence of vertical to sub-vertical boundaries in stone quarries. At the marble quarry, Piccolo (1992) found that the vertical sides of the marble blocks caused hyperbolic reflections of varied intensity depending on the thickness of the artificial cut. As well, in the gneiss quarry, Grasmueck (1996) had hyperbolic reflections caused by a buried vertical face. In both cases, the steeply dipping noise was successfully removed from the radargrams using migration (Piccolo, 1992) and two-pass f-k filtering with triangle-shaped passbands (Grasmueck, 1996).

4.6.1.4   Fracture Characteristics

A fracture is a separation or break in a rock mass that may signify a joint, fault, slickenside, foliation or cleavage plane (Bates and Jackson, 1984). In this thesis, the term small-scale fracture is restricted to joints with an aperture or filled width less than one centimetre. Small-scale structures are normally characterized by their continuity, spacing, aperture, infilling, orientation, surface roughness, and flow of water. This discussion focuses on the aperture, infilling, and orientation of the fracture relative to the survey line and how they influence the level of success of GPR detection.

Joint aperture/width depends on the degree of weathering of the rock mass but tends to range from being closed (zero thickness with no infilling) to wide (> 10 mm). Table 4-4 shows a commonly used engineering aperture classification. Typically, most joints have apertures less than half a millimetre (Barton, 1978), but in underground environments, stress fractures and natural joints are normally classified as tight with apertures ranging from 0.1- 0.3 mm (Personal communication, Dr. D. D.Tannant, University of Alberta, February 2, 2000).

Joints apertures may contain air or water, or may be filled with soil, gouge, minerals, and/or broken fragments of local rock. Infilling of these small-scale fractures is important because insufficient contrast between the infilling material and the host rock significantly reduces the chance of detection by GPR.

Fracture planes exist at various orientations to the surveyed surface. Planes that are parallel to the surface have the most favorable orientation for detection whereas planes that are perpendicular are the least favorable. Table 4-5 summarizes the fracture characteristics for the ten case studies and the associated level of GPR success.

Comparing all the case studies, Table 4-5 shows that a range of fracture widths were examined - from closed to up to 4 cm. (Note: Due to the limited number of case studies available. Grasmueck (1996) was included as a small-scale case study despite the fact the fracture apertures were likely larger than 1 cm). Unfortunately, three of the case studies did not mention any values and two others failed to be any more specific that 'less than 1 cm'. Failure to report fracture width may be because there was not direct observation of the fractures. Selecting a site where the fracture characteristics are visible is advantageous, especially when assessing the potential of radar for fracture detection. But even with direct observation there can be problems. Measuring or estimating fracture aperture is difficult because the surface aperture is normally the maximum value. As well, orientations can sometimes be difficult to measure and can even change over short distances. As a result, fracture characteristics recorded from surface mapping are subject to error.

Considering these joint characteristics and calculating the Fresnel Reflection Coefficient when possible, an assessment of target influence on the level of success for each case study can be made. First of all, the unsuccessful detection of closed joints at the Kidd Creek Mine is not surprising because it is not theoretically possible to detect these features using the 100 MHz antennas - the R_t value approaches zero as the joint aperture approaches zero.

Holloway et al. (1986) and Annan (1989) both had limited success - rating of 1 - detecting small-scale fractures in hard rock underground environments. Holloway et al. (1986) was only able to identify two major sub-vertical joints up to 5 m behind the walls of an underground shaft using an antenna centre frequency of 500 MHz. Unfortunately, the joint characteristics are not mentioned in the paper so the R_t value could not be calculated. However, the air-filled fractures that were weakly detected at the uranium mine had a R_t value of 0.004-0.04 for the 200 MHz antennas (Annan, 1989). Annan (1989) concludes that the limited success at this site was in fact due to the tight nature of the joints and recommends that higher frequency antennas be used to increase resolution.

Annan et al. (1988) was given a rating of marginal success (rating of 2). This case study is unique from the other nine because it is an example of a soft rock environment. The importance of this study is that stress-relief cracking was detected in an underground environment (Annan et al., 1988). Although this is a positive result, the fractures that were detected would be classified as moderately wide to wide according to Table 4-4 (i.e. 10 mm wide). The R_t was calculated to be 0.06 under air-filled conditions and using 300 MHz antennas. However, in this soft rock mine the conditions were far better than those in the hard rock mine described by Annan (1989). In these potash mines, the tunnels generally run parallel to the bedding and so the roofs are relatively flat. It is therefore recommended that additional testing be conducted in soft and hard rock environments.

Buursink and Lane (1999), Grasmueck (1996), Piccolo (1992), and Toshioka et al. (1995) were all given a success rating of 3 - good success. The most recent paper by Buursink and Lane (1999) is an excellent case study on fracture detection. The major conclusion of this study is that fractures can be characterized in heterogeneous bedrock (Buursink and Lane, 1999). This finding was based on the identification of 18 potential fractures in the radar profiles (Buursink and Lane, 1999). It is likely that the majority of the fractures contained water because the radargram reflections were consistent with numerical modeling results for saturated fractures (Buursink and Lane, 1999). Although this is a positive result, the fracture thickness is not mentioned. so R_t cannot be calculated.

For the case studies described by Grasmueck (1996), Piccolo (1992) and Toshioka et al. (1995) the positive results were of no great surprise. Grasmueck (1996) successfully detected three sub-horizontal fractures beneath the floor of a gneiss quarry but detection of the fractures was to be expected since they had a favorable orientation to the surveyed surface and were water-filled. As well, the fracture apertures were 2 to 4 cm and would be classified as large-scale discontinuities. The R_t using the 100 MHz was determined to be (-)0.585 to (-)1.17 for these large water-filled fractures.

Piccolo (1992) concluded that high frequency antennas (500 & 900 MHz) could be used successfully to detect dry fractures less than one centimeter in marble. Assuming the centre antenna frequency of 500 MHz, the corresponding R_t value under these air-filled conditions is 0.22.

Toshioka et al. (1995) also claims success using the 500 MHz antenna frequency, however only water-filled joints approximately 1-2 mm were detected, not closed or dry joints of similar thickness. Under these conditions, the undetected air-filled fractures have a R_t value of 0.02 to 0.11, whereas the detected water-filled fractures have a R_t value of (-)0.07 to (-)0.14.

Grasmueck (1994) and Pilon et al. (1996) are the remaining two case studies and were given a high success rating. Interestingly, both case studies claimed they were successful in detecting fractures using low frequency 100 MHz antennas. Grasmueck (1994) conducted surveys across a gneiss outcrop and concluded that GPR could be used to detect sub-horizontal moisture-filled fractures less than one centimetre thick. With the assumption that the aperture was 1 cm, the corresponding R_t value is (-)0.30 using these low frequency antennas.

Pilon et al. (1996) successfully detected minor and major fractures in the rock foundations for a proposed dam. Like Grasmueck (1994) there were no excavations in the foundations to provide a direct visual observation of the sub-surface GPR fracture targets so there is no mention of the fracture apertures or infilling and the Fresnel Reflection Coefficient cannot be calculated. It is however highly probable that at least some of the fractures contained water since the surveys were conducted across and adjacent to a stream. Pilon et al. (1996) also discusses that the categorization of minor versus major fractures was strictly subjective and based on relative signal amplitude and strength recorded on the various radar profiles: furthermore these observed differences are likely due to the type of fracture infilling, fracture size, and/or orientation.

Not knowing the fracture aperture at a site is a disadvantage to this study because the reflectivity of these features is governed by the thickness (Section 2.6.4). If the target thickness is unknown the Fresnel Reflection Coefficient cannot be calculated, and the R_t threshold for detected versus undetected rock structure remains a mystery. Table 4-6 summarizes the R_t values for the case studies where they could be calculated.

The results shown in Table 4-6 suggest that successful detection under dry conditions occurred with a Fresnel Reflection Coefficient between 0.06 and 0.12. Under saturated conditions, detection corresponded to a R_t between (-)0.07 and (-)1.2. In terms of fracture apertures, the results of the case studies suggest that air-filled fractures $\geq$ 10 mm and water-filled fractures $\geq$ 1 mm can be detected in hard rock under the right conditions (i.e. non-conductive host rock, appropriate antenna centre frequency, etc.). With these positive results, it is recommended that addition testing be conducted under both wet and dry conditions, with fracture apertures less than 1 cm, and using commercially available antenna frequencies within the range of 100 to 1000 MHz.

In summary, the comparison of fracture characteristics for the ten case studies clearly shows that thickness and infilling are likely the most important controls on the success of GPR. The general conclusions from this comparison are as follows:

- There is significantly more success in detecting water-filled fractures than dry fractures due to the increased contrast in dielectric constant.
- Using low frequency antennas (i.e. 100 MHz –300 MHz) there has been successful detection of dry and wet open fractures in rock ≥ 10 mm. Unfortunately, the lower limit has not be determined.
- Using high frequency antennas (i.e. 500 MHz – 1000 MHz) there has been successful detection of water filled fractures ≥ 1 mm thick, but closed or dry fractures ≤ 2 mm thick cannot be detected.
- In terms of the Fresnel Reflection Coefficient, the criterion for successful detection in rock (assuming a rock ε_r of 6.25) based on these ten case studies is as follows:

$$for\ air\text{-}filled\ fractures \qquad R_t > 0.06\ MHz$$
$$for\ water\text{-}filled\ fractures \qquad R_t > (\text{-})0.07\ MHz$$

4.6.1.5   Processing

A range of radar processing - from no processing to advanced processing - was conducted for the ten case studies, and the only case study that had no mention of processing was Momayez et al. (1996). For the two oldest studies (Annan et al., 1988; Holloway et al., 1986) analog GPR systems were used so no processing was conducted on this data. However, either basic or advanced processing was conducted on the remaining seven case studies.

Annan (1989) used basic processing in the form of spatial and temporal filters (i.e. low-pass and high-pass) to enhance either flat-lying or dipping reflections. The high pass Fourier transform filter seemed to enhance the weaker reflections from the joints, but it also enhanced the noise making the data appear less coherent and more erratic. Toshioka et al. (1995) also used frequency filters to eliminate noise not related to fracture reflectors. Lastly, Pilon et al. (1996) used time gains, time zero drift correction, and topographic corrections to improve the data.

The remaining case studies all used advanced processing techniques to bring out the weaker rock fracture reflections in the radar profiles. Grasmueck (1994 & 1996) applied standard seismic processing techniques such as f-k filtering, amplitude recovery, velocity estimation, stacking and migration to enhance fracture reflections. Piccolo (1992) mentions little of the processing, but does state that unwanted lateral events and diffraction hyperbolas were removed by migration. Finally, Buursink and Lane (1999) used dewow and spatial/temporal filters to remove noise and preserve true GPR reflections. Time gains were also applied to compensate for signal attenuation effects and migration was used to correct the locations of subsurface reflectors.

4.6.2 Large-Scale Fracture Detection (i.e. Fault Detection)

Detection of fracture zones or faults using GPR is far-less confusing than small-scale fracture detection because researchers seem to be in agreement that radar is successful in both soft and hard rock environments (Davis and Annan, 1989; Grasmueck, 1996; Holloway and Mugford, 1990; Holloway, 1992; Momayez et al., 1986; Olsson et al., 1992; Pilon et al., 1996; Stevens et al., 1994; Unterberger, 1978). Because of this, an exhaustive comparison of the various case studies for large-scale fracture detection is not warranted. However, the success of detecting these structural features will be discussed with reference to the same conditions considered for small-scale fracture detection (excluding data processing): antenna frequency, host rock, survey environment, and fault characteristics. Table 4-7 summarizes the GPR system and site conditions for each of the case studies that examined fracture zone detection.

A fracture zone is considered to be a large-scale discontinuity having a minimum width of at least 1 cm and a maximum width of several metres, so often lower antenna frequencies are used for their detection – as seen in Table 4-7. As well, borehole antennas are favored in hard shield (igneous or metamorphic) rock environments because the depth of penetration is improved due to less sources of interference. Because locating fracture zones is often more important at the preliminary site investigation stage (rather than characterization), penetration is desired over resolution in most cases. This helps to explain why the borehole antennas are often used, because antenna frequencies between 20-60 MHz give penetration ranges of 50-100 m from the borehole in gneiss and granite type rocks (Olsson et al., 1992; Stevens et al., 1994).

Considering the host rock at each of the sites, Table 4-7 shows that large-scale fracture detection has been conducted in similar rock types to those for small-scale fracture detection. The nature of these typically highly resistive, homogeneous rocks such as granite and gneiss allows large fracture interfaces to be detected because they cause electrical discontinuities in the rock mass.

The successful detection of fracture zones in all the case studies - most of which occurred in an underground environment - suggests that perhaps the survey environment does not have such a large impact on the success of GPR for large-scale fracture detection. This may be because the targets are geometrically larger and/or because borehole radar was used in three of the nine case studies.

Finally, examining the fracture zone characteristics, the few widths that were mentioned in the case studies shows that zones 0.5 to 8 m wide were successfully detected; however, the presence of water infilling in the fracture zones improved their identification in the radar profile. In regards to orientation, although interfaces sub-parallel are the easiest to detect, the results of the case studies clearly show that zones oriented at various angles to the survey line were detected as well.

4.7 ROCK STRUCTURE IDENTIFICATION IN RADAR PROFILES

The difficulty with interpretation is one of the biggest downfalls to ground-penetrating radar. Because the geophysical measurements are generally ambiguous and imprecise, a number of models can fit a single data set. As well, interpretation is often based on the assumption that the geological units are isotropic and homogeneous with clear distinct boundaries meaning the electrical properties are constant. Unfortunately, in a real geological medium, this is never the case. To help with interpretation the following key steps are required: 1) accept the fact that the complexity of rock structure will give complicated profiles; 2) have an understanding of the types

of structure at the site and how they should appear in a radar profile: and 3) use site information from boreholes or geologic field mapping to calibrate the data. Only after all these steps are taken can someone begin to properly interpret subsurface GPR profiles.

To aid in the second step, this section provides general descriptions on some of the more common types of rock structure and their associated visual appearance on radargrams. Comments regarding the possible GPR reflection characteristics are based primarily on the case studies on fracture detection discussed in Section 4.6. The following structures will be considered:

- bedding planes,
- dykes/veins,
- faults/fracture zones,
- foliation, and
- joints.

Bedding Planes

In sedimentary rocks, bedding planes - or the contacts between rock units - are the most important structural features. Bedding planes are more continuous compared to joints and faults and usually have a strong physical expression both in nature and in a radargram. For example, bedding planes in sandstones are often distinguished by changes in color and grain size, but can also be characterized by a zone of weak material such as lignite or montmorillonite clays (Hunt, 1984). Annan et al.(1989) gives an example of where radar was used to detect thin clay seams and anhydrite beds in a salt environment.

Radar detection of these small-scale structural features may be improved under near-surface rock conditions since fracturing often occurs parallel to bedding planes. Should these bedding fractures contain water, the reflectivity will further increase because of the increased contrast in dielectric properties.

Dykes/Sills/Veins

Dykes, sills, and veins are grouped together because they are all sheet-like bodies of igneous origin that intrude into the host rock. The three main differences between these three features are how the body intrudes into the host rock, and their size, orientation, and composition. Dykes crosscut through bedding or structural planes, sills intrude along bedding or structural planes, and veins intrude along joints. Comparing sizes, dykes and sills are measured in metres whereas veins are measured in centimetres. Finally, dykes and sills are composed of igneous rock but veins are composed of one or more mineral(s).

Although dykes, sills, and veins are geologically distinct from each other, in terms of GPR these large-scale structural features are similar. They all likely yield strong and continuous reflections depending on their size, orientation, and electrical contrast from the surrounding rock. In fact, if the width of these features is large enough (i.e. width > $\lambda/4$), the radar system may be able to unambiguously resolve the structure. Figure 4-2 shows an example of where a pegmatite dyke with a dielectric constant of 5 was detected in the granite host rock with a dielectric constant of 6.

Faults/Fracture Zones

A fault is often a large-scale discontinuity along which there has been a considerable amount of observable shear displacement due to tectonic activity. They generally have widths in the range of several centimetres to metres and lengths of several metres to kilometres. Faults usually contain either fault gouge (clay-rich material) or fault breccia (rock fragments) depending on the rock strength and are preferential pathways for groundwater. Faults also often reside in groups, occurring as sub-parallel to parallel sets of fractures, and are referred to as fracture (fault) zones.

Fault recognition in a radargram is easiest when there is a distinct offset of relatively planar continuous reflectors caused by fault displacement – Figure 4-3. Most of the criteria for fault identification are from seismic profiling since it has been used for fault detection much longer than GPR; in fact, criteria for fault interpretation developed as early as 1965 (Campbell, 1965). Aside from observing reflector displacements, additional fault criteria include: the observation of abrupt reflector terminations, direct fault plane reflections, diffractions at the fault ends, visible drag and rollover, and loss of coherency under a fault plane or distorted dips seen through the fault plane (Wyatt and Temples, 1996). Also, faulting patterns differ from jointing patterns because they are usually not repetitive and have horizontal offsets (Wyatt and Temples, 1996). Similar to dykes, sills, and veins, faults have the opportunity to be both detected and resolved depending on the width of the structure, the antenna centre frequency, and the signal velocity. However, based on this literature review there are no examples showing where the width of a fault has been delineated.

Foliation

Foliation is the strong directional structure or fabric in metamorphic rocks. Generally, it is the parallel alignment of platy minerals or mineral banding in rock. In schistose rocks, the parallel alignment of mica is termed the schistosity. Because schistosity is rarely planar but instead exhibits kinks and folds, it is unlikely that schistose foliation will produce clear reflections in a radar profile. However, fracturing can occur parallel to the schistosity, which can be detected. Grasmueck (1996) is an example of where radar successfully detected continuous schistosity-parallel fractures that were found to be rich in mica and chlorite and saturated.

Gneiss is formed by the segregation of minerals into felsic and mafic bands. This banding in the rock's foliation is referred to as gneissosity. The dark-colored mafic bands are rich in biotite and hornblende, whereas the light-colored felsic bands are rich in quartz and feldspar. The banding generally has a wavy or undulating expression but may also be folded. Detection of gneissic banding by GPR may be easier than schistosity because it is more distinct. The difference in dielectric constant between the mafic and felsic banding may be sufficient to be detected. However the change in dielectric properties may be too gradual to cause radar energy to reflect. If the banding is distinct enough to be reflected, it will likely appear as strong, continuous reflectors. Despite the many case studies that used radar in gneiss, there was no mention if whether the gneissosity was detected.

Joints

Joints are regular fractures with no observable displacement on either side of the interface. Joints normally appear in sets with similar orientations. In most rock masses, there is a minimum of three joint sets all approximately perpendicular to each other. Typical joint characteristics in terms of aperture, infilling, and orientation relative to the GPR surveyed surface are described in Section 4.6.1.4. For GPR, changes in any of these three characteristics will influence the signal amplitude and strength of their reflection events (Pilon et al., 1996).

90

Research conducted by Buursink and Lane (1999) is important for understanding the influence of aperture and water infilling on the reflectivity and detection of these small-scale targets. Buursink and Lane (1999) attempted to establish the GPR reflection characteristics of small-scale fractures by conducting one and 2.5 dimensional numerical modeling and physical modeling using laboratory-sized rock blocks of granite.

The numerical modeling consisted of simulating dry and water-filled fractures of various apertures for simple geologic conditions and assuming a centre antenna frequency of 100 MHz (Buursink and Lane, 1999). The primary conclusions were that water-filled fractures had higher amplitudes and of opposite phase to the dry fractures with the same thickness – Figure 4-4 (Buursink and Lane, 1999). The modeling results also showed that when the fracture aperture increases the amplitude increases and the waveform changes (Buursink and Lane, 1999) – Figure 4-4 a).

The physical modeling consisted of conducting surveys using 500 MHz antennas over two-granite rock blocks approximately 2.3 m³ with the objective of detecting an artificial fracture between the two blocks (Buursink and Lane, 1999). The fracture was completely sealed except for a single valve that allowed water to enter or flow out, in order to simulate dry and saturated conditions (Buursink and Lane, 1999). The conclusions from the physical modeling were the same as the numerical modeling, the amplitude from the saturated fracture is higher and opposite in phase to the unsaturated fracture (Buursink and Lane, 1999) – Figure 4-5. Unfortunately, the thickness of the artificial fracture was not mentioned in the paper, but changes in the aperture is the likely cause of the variation in reflection amplitude seen across Figure 4-5 a & b).

These conclusions are not surprising because the thin layer concept can be used to show the same general conclusions regarding amplitude and phase. Table 4-8 summarizes the calculated Fresnel Reflection Coefficient, R_t for the same conditions used in the one-dimensional numerical modeling described by Buursink and Lane (1999).

The higher amplitudes and phase change for the water-filled fractures are clearly observed in R_t values shown in Table 4-8. (Recall from Section 2.6.3, that a negative R_t indicates the reflector will have the opposite polarity to the incident signal.) The actual values for the normalized Fresnel Reflection Coefficient are lower than the values presented in Figure 4-4 a). This may be because the equation does not account for conductivity, whereas Buursink and Lane (1999) used a conductivity of 300 μS/cm for the water filled fracture.

Although Buursink and Lane (1999) conducted numerical modeling using fracture apertures of 1, 4 and 16 mm, these authors provided no concrete evidence that radar can detect these thicknesses. Based on the results of the case studies which examined small-scale fracture detection, it is likely that absolute R_t values < 0.06 to 0.07 correspond to non-detection. If this is true, it is unlikely that air-filled fractures 1, 4, and 16 mm thick and water-filled fractures 1 mm thick can be detected using 100 MHz antennas.

In summary, joints will likely produce straight reflectors that extend for a couple of metres. Joints that are parallel to sub-parallel to the surveyed surface will likely produce relatively flat-lying continuous events in a radargram. Conversely inclined joints will produce dipping reflections. In addition, as the aperture decreases, the reflection amplitude decreases making it more difficult to identify joint reflection(s) in the radar profile. Finally, if there is knowledge that water-filled fractures may exist, the interpreter should look for polarity changes.

4.8 SUMMARY AND CONCLUSIONS

Ground penetrating radar clearly has some advantages (e.g. lower cost, non-intrusive) as a site investigation tool over the more traditional drilling and sampling. It is because of these attributes that GPR has been examined for a number of applications, some of which work well and others not as well. Regardless of this, the engineering community is continuing to look for more applications to use this tool.

As stated in Chapter 1, looking at GPR for fracture detection is not a new concept and the case studies compared in Chapter 4 are evidence of this. Large-scale fracture detection, such as fault and fracture zones, have been proven successful in non-weathered, shield rock environments. This is a positive result, however depending on the depth of the fault, seismic methods can work just as effectively.

Small-scale fracture detection is where the confusion lies. The general consensus on the basis of the ten excellent case studies is that radar can be used successfully to detect discontinuities ≤ 1 cm. However, there is critical information missing from the majority of these references. For example, Buursink and Lane (1999) and Pilon et al. (1996) successfully identified numerous fracture reflections in the resulting profile but neither have any evidence to back up the claim. No drilling was conducted at either site so their interpretation of the radar results cannot either be accepted or rejected.

There was also no mention of the exact fracture apertures or infillings in a majority of the references. From an engineering perspective, stating these small-scale structural features can be detected but not giving the size for the appropriate antenna frequency is not adequate. It is therefore recommended that additional testing be done to determine what minimum aperture can be detected using typical antenna frequencies under average rock conditions (i.e. $\varepsilon_r \approx 6.25$ and σ < 10 mS/m). Noting the type of infilling in the fractures is also a requirement because there is strong evidence to suggest that water-filled fractures are much easier to detect than air-filled fractures.

For the fracture sizes that are mentioned, they would be classified as open to wide based on Table 4-4. Of interest to many engineers are fractures between 0.1 to 0.5 mm – classified as tight to partly open. This substantiates the recommendation for addition GPR testing with smaller fracture apertures.

So on the basis of this literature review, if 'detection of small-scale fractures' became a new GPR application for geotechnical engineering it would receive a rating of 2 (Table 4-1). The definition in this case would be that 'the technique has potential but is not fully developed'.

Table 4-1 Geotechnical applications for GPR (modified from Anon, 1997).

Application	Rating
Locate & characterize buried objects (i.e. old foundations, pipelines)	4
Void detection (both natural and man-made)	3
Stratigraphic mapping	3
Estimate fault displacement	3
Locate & characterize fractures zones	2
Estimate depth to bedrock	2
Locate & characterize erosional and structural features (i.e. buried channels, faults, dykes)	2
Assess integrity of mine pillars	2
Locate the water table & groundwater contamination	2
Distinguish lithological changes	1

4 = Excellent, well-developed technique; 3 = Good, but not fully developed:
2 = Not the best technique for this application: 1 = Limited use.

Table 4-2 Host rock versus level of GPR success.

Reference	Host Rock	Signal Propagation Velocity (m/ns)	Attenuation Constant (dB/m)	Level of GPR Success
Annan et al., 1988	Salt	0.120 - 0.130	0.4 - 2	2
Annan, 1989	Quartzite	0.120	0.1-1	1
Buursink and Lane, 1999	Gneiss, schist, dykes of granite & pegmatite	0.117	n/a	3
Grasmueck, 1994	Gneiss	0.120	n/a	4
Grasmueck, 1996	Gneiss	0.116	n/a	3
Holloway et al., 1986	Granite	0.118	n/a	1
Momayez et al., 1996	Andesite	0.110	n/a	0
Piccolo, 1992	Marble	0.110	n/a	3
Pilon et al., 1996	Gneiss	0.120	n/a	4
Toshioka et al., 1995	Welded tuff	0.068	n/a	3

0 = No success; 1 = Limited success; 2 = Marginal success; 3 = Good success: 4 = High success
n/a = not available

Table 4-3 Survey environment versus level of GPR success.

Reference	Survey Environment	Location of Survey(s)	Level of GPR Success
Annan et al., 1988	Underground	Back of tunnel	2
Annan, 1989	Underground	Back of tunnel	1
Buursink and Lane, 1999	Surface	Top of outcrop	3
Grasmueck, 1994	Surface	Top of outcrop	4
Grasmueck, 1996	Surface	Floor of rock quarry	3
Holloway et al., 1986	Underground	Walls of shaft	1
Momayez et al., 1996	Underground	Floor of sill pillar	0
Piccolo, 1992	Surface	Top and sides of quarry blocks	3
Pilon et al., 1996	Surface	Top of outcrop	4
Toshioka et al., 1995	Surface	Top of vertical quarry wall	3

0 = No success; 1 = Limited success; 2 = Marginal success; 3 = Good success; 4 = High success

Table 4-4 Fracture aperture classification (modified from Barton, 1978).

Classification	Aperture Width
Very tight	< 0.1 mm
Tight	0.1 - 0.25 mm
Partly open	0.25 - 0.5 mm
Open	0.5 - 2.5 mm
Moderately wide	2.5 - 10 mm
Wide	> 10 mm

Table 4-5 Fracture characteristics versus level of GPR success.

Reference	Aperture	Infilling	Orientation (with respect to survey line)	Level of GPR Success
Annan et al., 1988	1 cm	n/a (likely air)	parallel	2
Annan, 1989	1 mm to 1 cm	n/a (likely air)	inclined	1
Buursink and Lane, 1999	n/a	n/a (likely some water filled)	highly variable orientations	3
Grasmueck, 1994	< 1 cm	n/a (likely water)	sub-parallel & steeply inclined	4
Grasmueck, 1996	2 cm to 4 cm	water	sub-parallel	3
Holloway et al., 1986	n/a	n/a	inclined (15° off survey line)	1
Momayez et al., 1996	closed	not applicable	n/a (likely variable orientations)	0
Piccolo, 1992	< 1 cm	n/a (likely air)	parallel, perpendicular & inclined	3
Pilon et al., 1996	n/a	n/a (likely some water filled)	sub-parallel & inclined	4
Toshioka et al., 1995	closed to 5 mm	air, water, and/or clay	highly variable orientations	3

0 = No success; 1 = Limited success; 2 = Marginal success; 3 = Good success; 4 = High success
n/a = not available

95

Table 4-6 Fresnel Reflection Coefficient, R_t for the small-scale fracture case studies.

Reference	Antenna Centre Frequency, f_c (MHz)	Host Rock Dielectric Constant, ε_{rt}	Fracture Aperture(s) (mm)	Fracture Classification (based on Table 4-4)	Fresnel Reflection Coefficient, R_t[1]	
					Detected Fractures	Undetected Fractures
Annan et al., 1988	300	5.5	10	Moderately wide to wide	0.06 (air-filled)	–
Annan, 1989	200	6	1 to 10	Open to moderately wide	–	0.004-0.04 (air-filled)
Buursink and Lane, 1999	n.e.i.	–	–	–	–	–
Grasmueck, 1994	100	6.25	10	Moderately wide to wide	-0.30 (water-filled)	–
Grasmueck, 1996	100	6.7	20 to 40	Major discontinuities	-0.585 to -1.17 (water-filled)	–
Holloway et al., 1986	n.e.i.	–	–	–	–	–
Momayez et al., 1996	n.e.i.	–	–	–	–	–
Piccolo, 1992	500	7.5	10	Moderately wide to wide	0.12 (air-filled)	–
Pilon et al., 1996	n.e.i.	–	–	–	–	–
Toshioka et al., 1995	500	19.5	1 to 5	Open to moderately wide	-0.07 to -0.14 (water-filled)	0.02 to 0.11 (air-filled)

n.e.i. = not enough information provided in the reference to allow calculation of R_t

Table 4-7 Summaries of the case studies for fracture zone/fault detection.

Reference	Location	Antenna Centre Frequency (MHz)	Host Rock	Survey Environment	Fracture Zone Characteristics		
					Width	Infilling (dry vs. wet)	Orientation (w.r.t. survey line)
Davis and Annan, 1989	n/a	n/a	granite	underground	0.5 m	dry & water-filled	sub-parallel
Grasmueck, 1996	Gneiss Quarry, Switzerland	100	gneiss	surface	5-7 m	n/a	steeply inclined
Holloway and Mugford, 1990	URL, Canada	120	granite	underground	n/a	water-filled	sub-parallel (5° to 27° off survey line)
Holloway et al., 1992	URL in Manitoba, Canada	120	granite	surface & underground	n/a	water-filled	sub-parallel (15° to 30° off survey line)
Momayez et al., 1986	Kidd Creek Mine, Canada	500	andesite & massive sulphide	underground	< 1 m	n/a	steeply inclined
Olsson et al., 1992	Klipperas, Sweden	20 & 60	granite	underground	n/a	n/a	steeply inclined
Olsson et al., 1992	Stripa, Sweden	20 & 60	granite	underground	1-8 m	water-filled	inclined
Pilon et al., 1996	Outcrop in Ontario, Canada	100	gneiss	surface	n/a	n/a	inclined
Stevens et al., 1994	URL in Manitoba, Canada	22 & 60	granite	underground	n/a	water-filled	sub-parallel
Unterberger, 1978	Salt Mines in U.S. & Canada	230, 440, & 4300	salt	underground	n/a	n/a	n/a

n/a = not available

97

Table 4-8 Calculated Fresnel Reflection Coefficient, R_t for similar fracture conditions used in Buursink and Lane's (1999) one-dimensional numerical modeling.

Fracture Aperture (mm)	Fresnel Reflection Coefficient, R_t [1]		Normalized Fresnel Reflection Coefficient, R_t [1,2]	
	Air-filled ($\varepsilon_{r2}=1$)	Water-filled ($\varepsilon_{r2}=81$)	Air-filled ($\varepsilon_{r2}=1$)	Water-filled ($\varepsilon_{r2}=81$)
1	0.002	-0.03	0.004	-0.06
4	0.009	-0.12	0.02	-0.25
16	0.04	-0.48	0.08	-1

Notes
1. Used antenna centre frequency of 100 MHz and a host rock dielectric constant ($\varepsilon_{r1}=6.5$).
2. Values normalized with respect to saturated fracture with aperture of 16 mm.
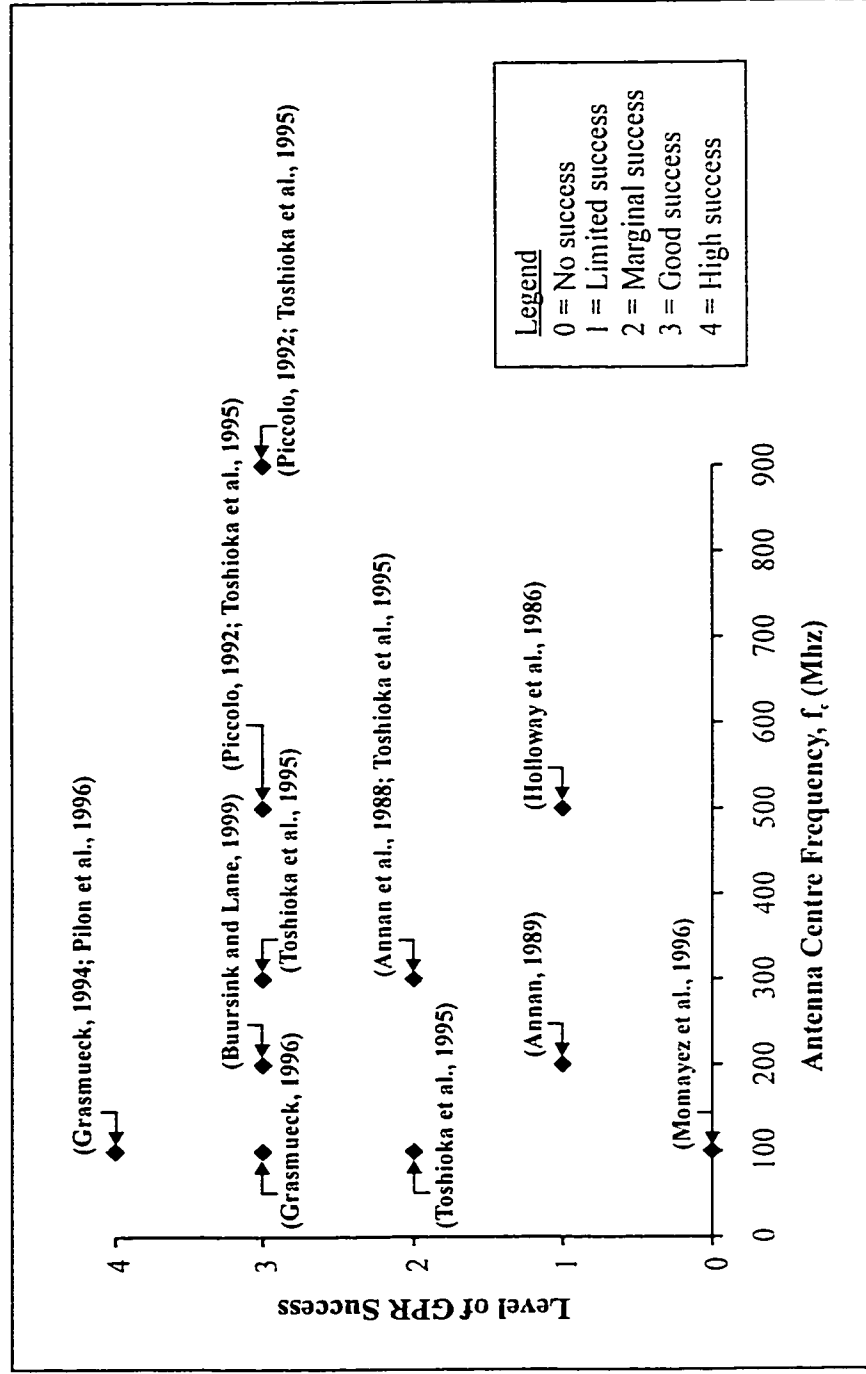
Figure 4-1 Level of GPR success for detection of small-scale fractures versus frequency and publication date for ten case studies.

a) Radargram image.

b) Geological interpretation.
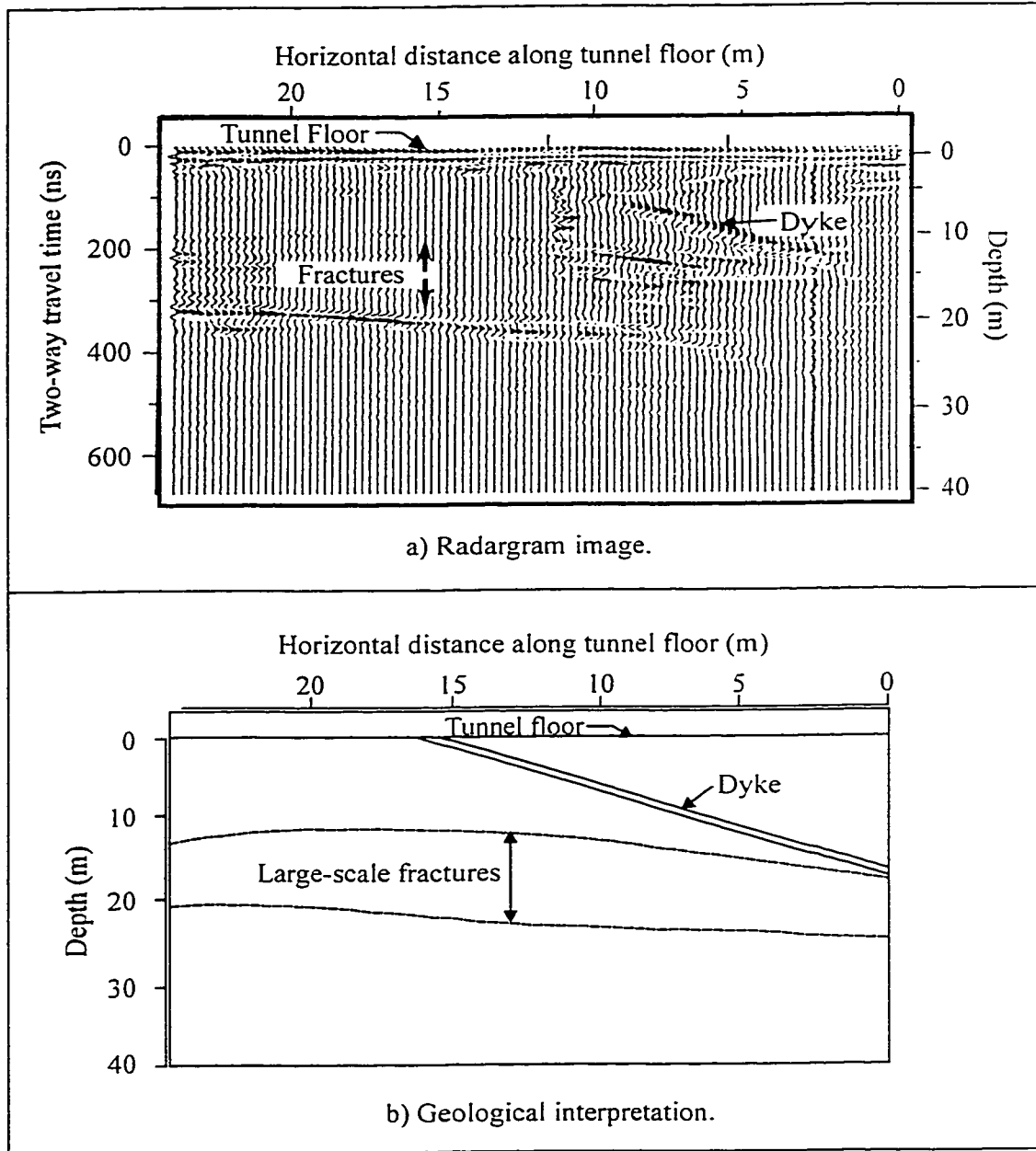
Figure 4-2 Detecting a pegmatite dyke in a hard rock underground environment (modified from Davis and Annan, 1989).
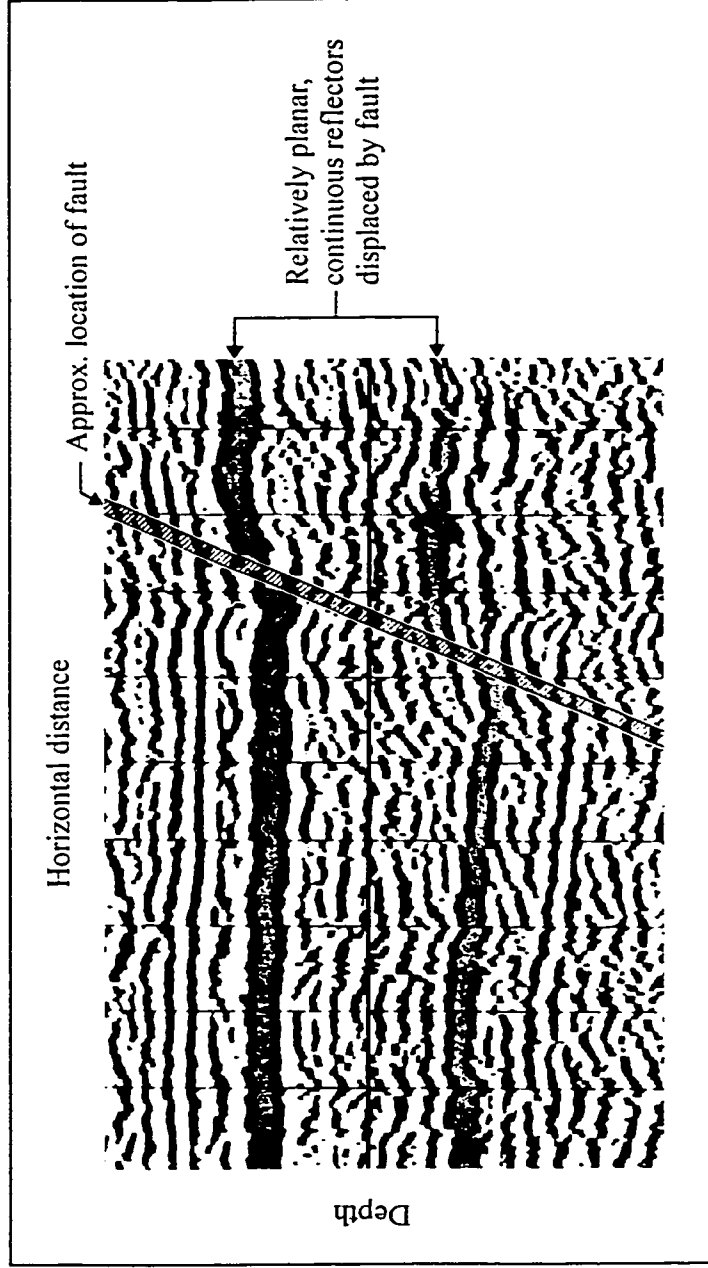
Figure 4-3 Recognizing a fault in a radargram based on observed displacement of continuous planar reflectors (modified from Campbell, 1965).

101
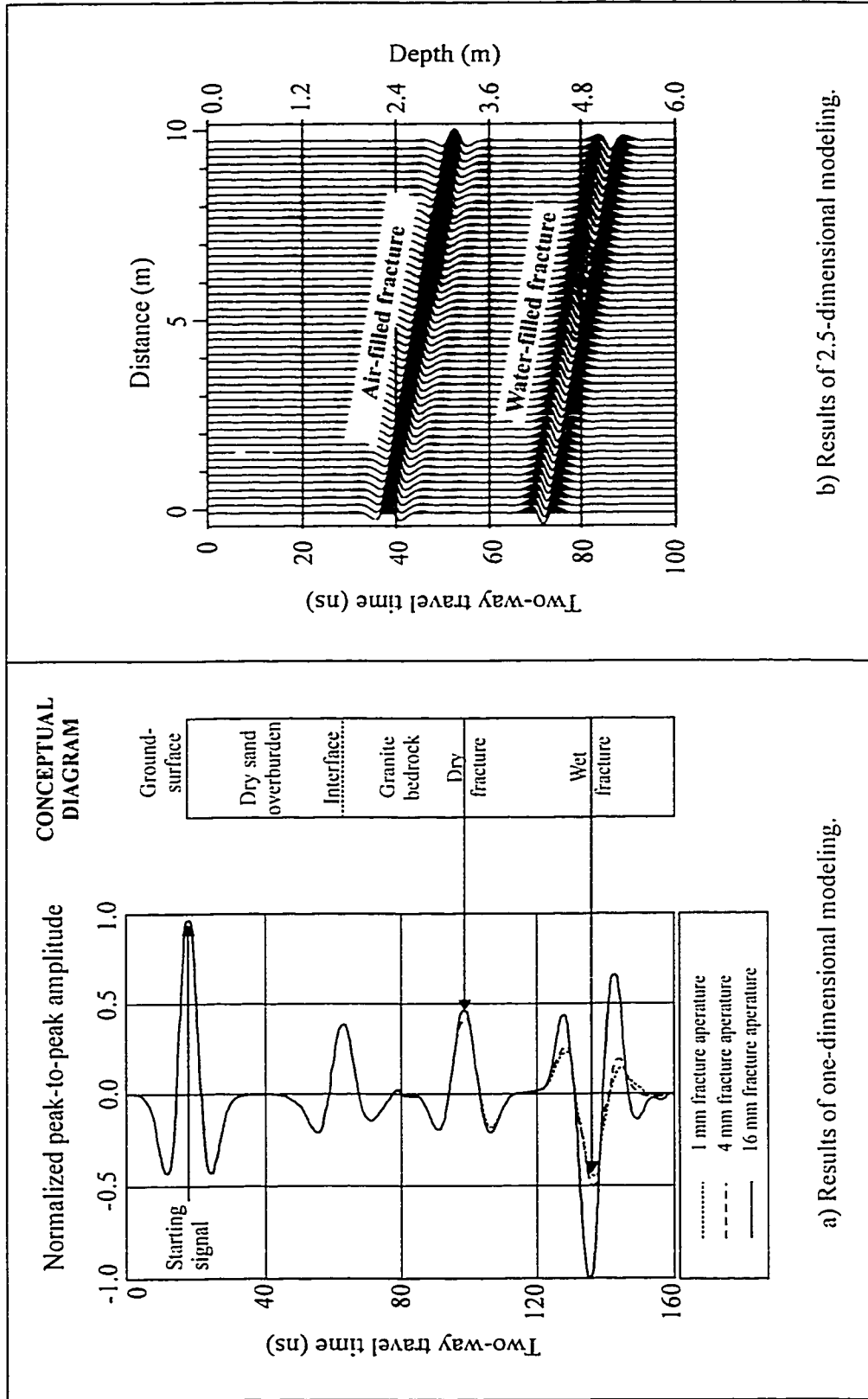
Figure 4-4 Numerical modeling results of air & water-filled fractures (modified from Buursink and Lane, 1999).

b) Results of 2.5-dimensional modeling.

a) Results of one-dimensional modeling.
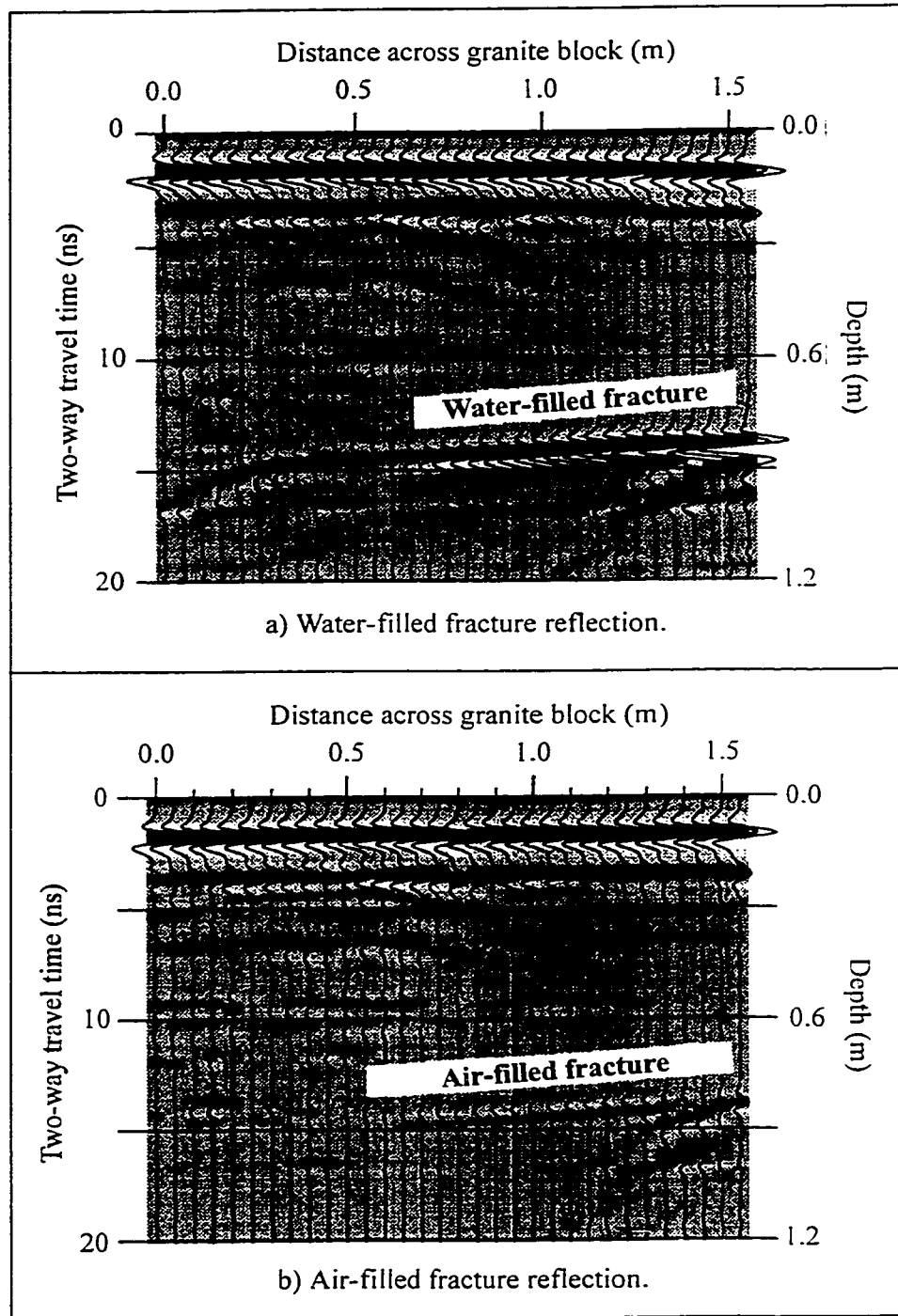
Figure 4-5 Physical modeling results for air and water-filled fractures (modified from Buursink and Lane, 1999).

CHAPTER 5: FIELD PROGRAM

5.1 INTRODUCTION

Chapter 5 describes the field component of this thesis, specifically the GPR surveys conducted within the region of Sudbury, Ontario. Section 5.2 describes the regional geology of the Sudbury District to gain insight as to the types of rocks and their structural history, however there is a focus on the rock types encountered at the various project sites. The geology background is followed by a description of the RAMAC/GPR system, specifically the antenna frequencies that were used – Section 5.3. Problems with the antennas are included in this section. Section 5.4 includes detailed descriptions of both the site conditions and radar surveys that were conducted at each of the nine project sites. Lastly, Section 5.5 contains summary remarks and conclusions about the GPR field surveys.

5.2 REGIONAL GEOLOGY OF SUDBURY, ONTARIO

During the 3-month field study in the Sudbury region, GPR surveys were conducted on a variety of Precambrian rocks of the Canadian Shield (specifically from the Grenville and Southern Provinces). The regional geology of the Sudbury region, and thus the 'project area[14]', lies within a complex part of the Shield. This region is particularly fascinating because of the famous Sudbury Structure located at the junction of Ontario's three geological provinces – Superior, Southern and Grenville Provinces. To the immediate north of the Sudbury Structure are the Archean gneiss, metavolcanics, metasedimentary, and granite of the Superior Province. To the south and northeast of the Structure are the Early Proterozoic metavolcanic and metasedimentary rocks of the Southern Province's Huronian Supergroup.

Table 5-1 summarizes the important Precambrian rock units and events that reflect the Sudbury region. Sections 5.2.1 to 5.2.3 will briefly describe the rocks within each of these three Provinces. Because it is also important to understand the tectonics of the project area, sub-sections 5.2.2.2 and 5.2.2.3 describe the more important tectonic events of the Southern Province and the Sudbury Structure respectively. Note that all these geology sections were written based on the work by Card et al. (1984) and Dressler (1984).

5.2.1 Superior Province

The Superior Province lies north and east of the Sudbury Structure (Figure 5-1) and is composed of Late Archean supracrustal (greenstone) belts, granitic plutons, metasedimentary belts, and granulite rocks. To the immediate north of the Sudbury Structure (or the footwall) are Archean grey-banded gneisses of granodiorite, tonalite, and quartz-diorite composition. These granulite and amphibolite gneisses are called the Levack gneisses.

Further discussion of this Province is beyond the scope of this thesis since none of the GPR field sites were conducted on rocks of the Superior Province. Refer to Card et al. (1984) and Card (1979) for a more complete description of the major lithological units within this province.

---

[14] For this thesis, any reference to the 'project area' represents the region that encompasses all nine GPR project sites.

5.2.2 Southern Province

The Southern Province lies immediately to the south of the Sudbury Structure (Figure 5-1). In fact, the Sudbury Structure is generally classified as a part of the Southern Province. This Province is composed of Early Proterozoic sedimentary rocks, volcanic rocks, and mafic/felsic intrusions. The rocks of the Southern Province are subdivided into four supergroups: Huronian Supergroup, Animikie Supergroup, Sibley Supergroup and Keweenawan Supergroup. Only the Huronian Supergroup will be described because it is the only supergroup on which GPR surveys were conducted for this thesis.

5.2.2.1 Huronian Supergroup

The Huronian Supergroup is a predominately thick sequence of clastic sedimentary rock of conglomerate, mudstone, siltstone and sandstone with local volcanics. These rocks were deposited during the Early Proterozoic, between 2500-2150 Ma. This assemblage shows southward and eastward variations in thickness (10700 m to 8000 m respectively) and in facies. Deposition in fluvial, deltaic, and shallow marine conditions produced distinctive cyclic repetitions of conglomerate, mudstone, wacke, and quartz-feldspar arenites. Based on this characteristic cyclicity, the Huronian Supergroup is subdivided into four groups: Elliot Lake, Hough Lake, Quirke Lake and Cobalt Groups (Table 5-2). For this project, there are two formations of importance: 1) McKim Formation of the Elliot Lake Group and 2) Mississagi Fm. of the Hough Lake Group. Four GPR project sites were composed of these rocks and thus will be the only formations described in detail.

The Elliot Lake Group is the oldest of the four groups and is composed of a heterogeneous assemblage of sedimentary and volcanic rocks. In the Sudbury area, the McKim Formation is characterized as a very thick sequence (i.e. several thousand's of metre's) of greywacke and mudstone. These sediments were likely deposited below wave base and are immature and poorly-sorted. Elsewhere the Elliot Lake Group has interfingering sequences of sandstone, conglomerate, siltstone, and greywacke with minor volcanics.

The Hough and Quirke Lake Groups are both major sedimentary cycles which overly the Elliot Lake Group. Each group has a lower conglomerate unit, a middle shale unit, and an upper sandstone unit. Both groups also show a northwest to southeast thickening from 1500 m to over 6000 m. This formation has poorly-sorted quartz-feldspar arenites that indicate rapid deposition in a high-energy environment.

Finally, the youngest group is the Cobalt Group. This group is composed of a heterogeneous assemblage of conglomerates, siltstones, sandstones and greywackes. Its thickness ranges from 3500 to 5000 m.

5.2.2.2 Important Tectonic Events of Southern Province

Initially, the Huronian sediments experienced early folding due to compressional tectonics about 2460 Ma. Deformation was followed by intrusion of three Early Proterozoic granitic plutons (Creighton, Murray, and Skead Plutons) between 2388-2333 Ma, to the south and east of the Sudbury Structure. Next, mafic (gabbroic) intrusions emplaced into rocks throughout the Southern Province. These rocks are called the Nipissing Diabase or Sudbury Gabbro and have been dated at 2100 Ma.

Correlative with the Penokean Orogeny between 1850-1900 Ma, metamorphism and deformation caused additional faulting and folding of the Huronian sequences. Rocks that lie within the project area and south of the Sudbury Igneous Complex have been subjected to greenschist to lower amphibolite facies metamorphism.

Deposition of the Early Proterozoic rocks of the Southern Province between 2500-1900 Ma and orogenic activity between 1900-1700 Ma was controlled by a zone of faulting and dislocation. This zone is termed the Great Lake Tectonic Zone (GLTZ) – Murray Fault (MFZ) System. The GLTZ-MFZ separates the contrasting northern and southern sequences. The northern sequences (i.e. Huronian rocks) rest unconformably on stable Superior Province Archean basement. They are characterized as thin, sedimentary units with minor deformation and metamorphism (Card et al., 1984). In contrast, the southern sequences overlie Archean gneiss basement or basement of unknown character. These southern units are much thicker than the northern units and contain a high percentage of volcanics. These units have experienced more deformation, more metamorphism and are intruded by felsic plutons.

Around 1750 Ma, intrusion of the Culter, Chief Lake, and Eden Lake plutons occurred in the south. This was later (1500 Ma) followed by intrusions of felsic plutonic complexes - Killarney, Croker, and Manitoulin Island Plutons. The Killarney Igneous Belt separates the Southern Province from the Grenville Province. This pie-shaped wedge of land attached to the Southern Province 1.74 billion years ago. It is characteristic for its large pink granite batholiths and volcanic rocks.

Several phases of igneous activity took place between 1849 to 1000 Ma. The Sudbury Structure was created and swarms of northwest trending dykes emplaced. The Southern Province was subjected to deformational events that created moderate to tight folding and vast faulting.

5.2.2.3   Sudbury Structure

The Sudbury Structure is well-known because it contains one of the world's most significant concentrations of nickel and copper ores. The structure straddles the main contact between the Huronian rocks of the Southern Province and the Archean plutonic rocks of the Superior Province. It is composed of three lithological units: Sudbury Breccia, Sudbury Basin, and Sudbury Igneous Complex (SIC). In plan view, this Early Proterozoic feature has roughly an oval shape (27 km * 60 km) with the Sudbury Basin in the middle, the SIC rimming the basin sediments, and a collar of brecciated and shatter-coned country rocks (Sudbury Breccia) around the intrusion - Figure 5-2.

The Sudbury Basin is a large elliptical shaped depression, elongated in the NE-SW direction, containing the rocks of the Whitewater Group. This group is a lithostratigraphic sequence of heterolithic breccias of the Onaping Formation, mudstones of the Onwatin Formation and wackes of the Chelmsford Formation.

The Sudbury Igneous Complex is a basin-shaped body that holds the sediments of the Whitewater group and intrudes into Archean rocks of the Superior Province and Huronian Rocks of the Southern Province. It is composed of a Main Mass and Sublayer. The Main Mass is further divided into three zones based on rock type - a Lower Zone of norite, a Middle Zone of gabbro, and Upper Zone of granophyre.

The Sublayer or the basal unit of the SIC is of most importance because its hosts many of the nickel and copper ore bodies in the Sudbury area. The Sublayer is a noritic rock containing disseminated or massive sulphides. The Sublayer also has offset dykes of quartz diorite that intrude into the footwall rocks. The 175-Orebody project site (Section 5.4.8) is a part of the Copper Cliff offset dyke of the Sublayer. Refer to Grant and Bite (1984) for a complete discussion of the Copper Cliff offset dyke.

The Sudbury Breccia is found within a 50-80 km wide zone around the SIC. Three types of breccia have been identified: massive breccia, fluidal breccia, and igneous textured breccia. The dark fine-grained matrix holds the rock fragments that range from millimetres to tens of metres in size.

The genesis of the Sudbury Structure (dated around 1849 Ma) is a great geologic mystery and is still heavily debated, however it is clear that the feature formed from a catastrophic event. There are two main theories regarding its formation – a volcanic or meterorite impact origin. Theory 1 proposes that a violent volcanic eruption formed a crater, which afterwards filled with sediments. Theory 2 is the more interesting theory because it involves an extraterrestrial origin. This theory proposes that a gigantic meteorite hit the area forming a crater that later filled with sediments eroded from the surrounding lands. Undisputed evidence for the meteorite origin is the presence shatter cones that are found all around the Sudbury Igneous Complex and in the arkoses and wackes of the Huronian Supergroup. Shatter cones are shock metamorphic features that could only have been produced from a meteorite.

5.2.3 Grenville Province

Approximately 10 km southeast of the Sudbury Structure lies the faulted northwestern boundary of the Grenville Province called the Grenville Front Boundary Fault (GFBF). The GFBF is a geological feature used to distinguish the low-grade metamorphic, cataclastic rocks of the Southern Province from the high-grade metamorphic gneiss of the Grenville Province.

This Province is characterized by a complex history of metamorphism, deformation and plutonism between 1200-1000 Ma therefore a complete description is beyond the scope of this thesis. During the Middle Proterozoic and after intrusion of the major plutons, the rocks were subjected to high rank regional metamorphism between 1400-1200 Ma. The Grenville sedimentary gneisses reflect this metamorphism and have typical mineral assemblages of plagioclase, quartz, biotite, hornblende, and garnet. As well, in many areas the Grenville gneiss are migmatitic. The Elbow Lake project site (Section 5.4.6) has migmatic biotite gneiss rock of the Grenville Province.

5.3 LOW VS. HIGH FREQUENCY ANTENNAS (100 MHZ VS. 1 GHZ ANTENNAS)

The field component of this thesis was conducted in co-operation with the mining research company MIRARCO, who owned a RAMAC/GPR system. The RAMAC/GPR system is a typical commercially available impulse radar system that can be used with a range of antenna centre frequencies in both shielded and unshielded mode. In order to assess GPR performance for the detection of rock structure at various surface and underground sites, two antenna frequencies were used – 100 MHz (unshielded) and 1 GHz (shielded).

5.3.1 General Description of Low Frequency (100 MHz) Antennas

The 100 MHz unshielded antennas - referred to in this thesis as the 'low frequency' antennas - are more apt to deeper penetration surveys and are designed such that they can be used in rugged terrain field surveys (Figure 5-3). The most common applications for the 100 MHz antennas are detection of soil/bedrock contacts, buried utilities, voids, and bathymetry surveys.

The 100 MHz system has separate transmitter and receiver antennas which is advantageous for conducting velocity (i.e. CMP or WARR) or transillumination soundings. Table 5-3 summarizes the dimensions and weights of both the 100 MHz and 1 GHz antennas.

5.3.2 General Description of High Frequency (1 GHz) Antennas

The shielded 1 GHz antennas (Figure 5-4) are high-resolution antennas for higher-quality radar measurements. As such the 1 GHz antennas are referred to as the 'high frequency' antennas in this thesis. These particular antennas are more useful in urban investigations where the shielding helps to minimize the influence due to external sources (i.e. power lines) which can affect the quality of the measured data.

Unfortunately because the frequency is higher the depth of penetration is lower, so the 1 GHz antennas are more suitable for quite shallow GPR surveys (between 0.5-2 m depth). The most common applications for the 1 GHz antennas are quality inspections of pavement and concrete.

The shielded 1 GHz antennas were housed in a single module and as seen from Table 5-3 are more lightweight and compact in comparison to the 100 MHz antennas. This design is advantageous when surveys are conducted in small and narrow places, however they were more difficult to use on rugged and irregular surfaces than the 100 MHz antennas.

5.3.3 Observed Problems with the Low/High Frequency Antennas.

a) Personnel Requirements

The RAMAC GPR systems claim to be operated by one person; however, these systems were ultimately designed for conducting surveys along planar and horizontal surfaces. Unfortunately, this is not always the case because vertical surveys are sometimes conducted (e.g. along sidewalls of underground mine). For vertically oriented surveys, having a single person carry all the equipment, plus move the antennas and record traces is impossible. In fact, even on horizontal surfaces the one-man system is cumbersome. As a result, it was found to be more efficient to have one person carry and move the antennas along the survey line while another carries the backpack control unit and PC. Using two people, the radar surveys can be conducted more quickly and with less discomfort to the operators.

b) Contact between Antennas and Ground Surface

Antennas should be placed directly on or as close to the ground surface as possible (Davis and Annan, 1989) so that more of the energy is transmitted into the ground and less is lost to the atmosphere. However, the RAMAC/GPR antennas are designed in a plastic non-flexible casing, making it difficult to get achieve close contact when the ground is rough. For example, in an underground environment, the surfaces are often very irregular so achieving close contact is

nearly impossible. For this thesis, outcrops that had at least one relatively flat surface were chosen for GPR surveying in order to minimize contact problems.

c) Fibre Optic Cable Connections

All RAMAC/GPR systems are designed with fibre optic cables that link the antennas to the control unit. Using fibre optic cable reduces the noise level resulting in improved data quality however, these cables are the weakest component of the system. As a result, much care needs to be taken when using them. The cables cannot be stepped on or twisted and the ends have to be kept free of dirt and dust while attaching and dismantling the system. As well, the cables can easily be broken, so while performing the surveys the surveyor should be careful to ensure the cables do not snag on nearby vegetation.

The design of the RAMAC/GPR 1 GHz antennas is better than for the 100 MHz antennas because all the fibre optic cables were contained within a single piece of 1.27 cm (or ½") diameter plastic tubing, to reduce the chances of cable breakage. However a disadvantage of having the fibres being inseparable (for the 1 GHz module) is that CMP or WARR surveys cannot be conducted.

Another problem is that fibre optic cables degrade over time due to common handling of the cables. This means they have to be replaced and fibre optic cables are expensive.

5.3.4   Reflection Surveys Using Low vs. High Frequency Antennas

Section 3.4.1 discussed the seven important parameters required for conducting GPR reflections surveys. Within this section the influence of the antenna centre frequency, f_c on the majority of these parameters as described. High and low frequency antennas were used to conduct surveys at several different sites and Table 5-4 summarizes the effects of using a higher antenna centre frequency, f_c (e.g. increasing from 100 MHz to 1 GHz antennas).

Table 5-4 shows that there is an advantage to using the 1 GHz antennas rather than the 100 MHz antennas. The higher frequency antennas may be better able to detect the small-scale discontinuities and the equipment is smaller and easier to handle. The biggest disadvantage is that the depth of penetration is significantly reduced so the target has to be in the near surface (< 2 m) in order to be detected.

Sections 2.6.1 and 2.6.2 describes how the centre antenna frequency influences both signal velocity and attenuation. Generally, the signal velocity increases with increasing antenna frequency; however, for this thesis it was assumed that the conductivity of the ground was < 10 mS/m and the velocity was constant between the 100 MHz to 1 GHz frequency range (Figure 2.3). Attenuation also typically increases with increasing frequency. This is an undesirable effect because it decreases the depth of penetration into the media. Figure 2.5 shows that assuming the attenuation remains constant in the range of 100-1000 MHz may not be entirely correct but this assumption had to be made for this thesis since were no estimates of the actual conductivity at any of the field sites.

5.4 Site & Survey Descriptions and Objectives

Ground penetrating radar field surveys were conducted, from June to August 1999, to test the use of radar reflection methods to detect rock structure. All fieldwork was done in co-operation with the mining research company, MIRARCo, who provided the use of their RAMAC/GPR system. plus assistance in terms of field personnel.

During the three months, GPR reflection surveys were conducted with low frequency unshielded (100 MHz) antennas and with high frequency shielded (1 GHz) antennas at nine different project sites within 100 km of the city of Sudbury, Ontario. The majority of the surveys were conducted on surface- on highway outcrops or bedrock exposures or blocks of quarried rock - with the exception of the underground surveys conducted at INCO's underground research facility - 175-Orebody.

Table 5-5 lists the nine project sites, the survey environment, the primary radar target(s) and the surveys presented in this thesis. Over 70 surveys were conducted at the various sites but due to size limitations of this thesis only the results of 32 surveys will be presented.

Appendix A contains GPR survey tables for each project site. These tables give details for each of the 32 surveys that will be presented – i.e. survey date, file name. total survey length. trend of survey line, station spacing, survey direction, etc. Refer to these tables for additional information, as these details may not be presented in their corresponding sections.

Sections 5.4.1 to 5.4.8 are detailed descriptions for each project site. The descriptions include general site conditions, local geological and structure conditions, general GPR survey conditions. GPR objectives, and field procedures. Note that for all the structural orientations presented in these sections (and for the entire thesis), the convention is strike and dip, using the right-hand rule.

5.4.1 Rock Blocks – Artificial Fracture Surveys

GPR surveys were conducted across pieces of cut rock for the purpose of detecting air-filled artificial fractures or gaps between blocks of rock. The motivation behind conducting such surveys was that the radar targets or fractures were more controlled. Their orientation. location. and aperture/width could be recorded far more accurately than natural fractures in an outcrop. On natural outcrops, there can also be problems due to outcrop size and poor accessibility. Hence by conducting GPR surveys on rock blocks, some of these problems were likely minimized or eliminated.

Another advantage of conducting surveys across blocks of rock was that metallic reflectors could be inserted between the blocks. A conductor dissipates electromagnetic waves because conduction currents dominate over displacement currents. So, when a wave strikes a conductor, nearly all the energy is reflected. For this thesis, aluminum foil was used a reflector to improve detection of a gap. Assuming the dielectric constant of aluminum is infinitely higher in comparison to rock, it was anticipated that reflections off the foil would be obvious in the radargram: the waveform would have a high amplitude and polarity reversal.

Reflection surveys on rock blocks were conducted at Jarvis Resources Ltd. and along the WGMC walkway as described in Sections 5.4.1.1 and 5.4.1.2. Note, however, that due to the size of the

rock blocks and the depth of the air-filled gaps, only the high frequency (1 GHz) antennas were suitable for radar surveys.

5.4.1.1   Jarvis Resources Ltd.

Jarvis Resources Ltd., located approximately 10 km southwest of downtown Sudbury, sells limestone and marble products. Jarvis Resources graciously allowed us to conduct GPR surveys across blocks of limestone and marble that were piled in their stockyard. In the yard, blocks of cut rock were piled vertically and generally separated with pieces of wood ($\approx$ 3.8 cm $\times$ 10.2 cm in cross-section). Three specific block sites within the yard were chosen for GPR testing.

5.4.1.1.1   Block Site 1 Surveys

The first block site consisted of eight limestone slabs angled up against a massive block of marble, creating a triangular opening (Figure 5-5). The limestone slabs were 1.6 m in length, 0.85 m high and 4.4 cm wide. The slabs had a distinct mottled appearance of light grey and beige - the light grey zones were likely areas of dolomitization. In contrast, the marble block was stark white with thin grey stringers.

Three high frequency surveys were conducted along the face of the limestone slabs with the primary radar target being the wide air gap between the slabs and the marble block. The gap itself was a triangular opening which increased from 0 to 17.5 cm wide from the top of the slabs to the bottom (Figure 5-5 b). Table 5-6 lists these three high frequency surveys conducted at Block Site 1 and the important survey details pertaining to each.

All three surveys were conducted along the smooth face of the first limestone slab; however, as shown in Table 5-6 there was a variation in the elevation of the survey line and station spacing. The change in survey line elevation changed the width of the artificial fracture, but the distance to the top of the fracture remained unchanged at 35.2 cm.

For the first survey 'Jarvis 1h', the survey line was located in the middle of the slab and station spacing of 1 cm was used. However, for 'Jarvis 1e' survey line was moved 22 cm up the slabs and the station spacing was increased to 2.5 cm. For these two surveys the influence of station spacing, if any, can be evaluated. Recall that the change in station spacing alters the resolution of the final radar profile, as discussed in Section 2.7.2.1.

For 'Jarvis 1f' the survey parameters (including the survey line) were identical to that of 'Jarvis 1e' except aluminum foil was inserted between the 4th and 5th slabs (or at a depth of 17.6 cm). These two surveys (Jarvis 1e and Jarvis 1f) can be directly compared to observe the influence of a strong reflector (or conductor) within rock.

5.4.1.1.2   Block Site 2 Survey

The second block site consists of eight, long rectangular limestone blocks, as shown in Figure 5-6. The blocks were all 230 cm long, 33 cm high, and 32 to 37 cm wide. The two bottom blocks labeled Block 1 and Block 2 in Figure 5-6 b) are most important since a single survey was conducted along the entire vertical face of Block 1 (File name: Jarvis2).

The objective of the radar survey 'Jarvis2' was to detect the vertical air-filled gap between Blocks 1 and 2. The width of the gap varied from 0.4-4.5 cm but at the elevation of the survey line, the gap was approximately 3 cm wide. Because Block 1 was not perfectly cut, the gap width - and therefore the distance to this primary radar target - varied from 30 cm at the south end to 35 cm at the north end. Additional details concerning this survey are included Table A-2 in Appendix A.

5.4.1.1.3 Block Site 3 Surveys

The last block site was composed of three rectangular limestone blocks. The blocks were vertically stacked with 7.5 cm wide air gaps in-between (Figure 5-7). Two GPR surveys were conducted along the top of the first limestone block and approximately in the middle of the block (File names: Jarvis4 & Jarvis4f). The objective of both surveys was detection of the first 7.5 cm artificial fracture and, possibly, the second 7.5 cm artificial fracture. The only difference between these two surveys was that for 'Jarvis4f' a 1.5 m long piece of aluminum foil was placed on the top of the second block. From elevation of the survey line, the foil existed at a depth of ≈ 39.5 cm. So as in the surveys at Block Site 1, 'Jarvis4' and 'Jarvis4f' show the influence of having a small target with a high contrast in dielectric constant (or a conductor within a dielectric medium).

5.4.1.2 WGMC Walkway

Along the front walkway of the Willet Green Miller Centre at Laurentian University are blocks of gneiss. For conducting GPR surveys, two gneiss blocks stacked vertically on top of each other were chosen. Both rock blocks were rectangular shaped with approximate dimensions of 1.3 m × 0.5 m × 0.5 m (length × width × height). Figure 5-8 shows digital photos of the two gneiss blocks used for the high frequency GPR surveys.

Two surveys were conducted using the high frequency antennas (File names: Reflect1 & Reflect2) along the relatively flat top of the upper block and across its entire length. Details of both surveys are contained in Table A-4 of Appendix A. Figure 5-8 shows the start and end points across Block 1. The objective of both surveys was to detect the air-filled gap between the two blocks. This man-made fracture was irregular with a maximum aperture of 3 cm. If the horizontal fracture were detected with the 1 GHz antennas, it would appear on the radargram as a continuous horizontal reflector at a depth of 0.5 m.

The two reflection surveys were in fact identical except foil was inserted between Block 1 and Block 2 for 'Reflect 1'. Due to the large gap width, the foil was easily inserted and extended across nearly the entire fracture surface (≈ 1 m). The reason for using the foil is the same as for the surveys at Jarvis Resources Ltd., the foil was to increase the reflectivity of the gap. 'Reflect 1' and 'Reflect2' can therefore be directly compared and the influence of a metallic target can be evaluated.

5.4.2 Hwy 17 Bypass Outcrop

The Hwy 17 Bypass project site was a meta-sedimentary highway outcrop located along the southern side of the Hwy 17 Bypass, 5 km east of the intersection between Highway 17 and Highway 69 (Figure 5-9). The outcrop was only 8 km southeast of the downtown Sudbury core.

The outcrop was tens of metres long in an east-west direction and approximately 4.5 m high. A 6.5 m long section was chosen for GPR surveying because it protruded approximately 1.5 m from the face. This allowed the structure from the western edge of the outcrop to be measured (Figure 5-10).

The host rock is subarkose of the Mississagi Fm, part of the Hough Lake Group (Section 5.2.2.1). These sediments are of the Southern Province and have been subjected to at least low rank metamorphism. The rock is recrystallized and distinctive mineralogical banding is observed parallel to the bedding. Deformation has caused the bedding to dip approximately 75° to the north and strike parallel to the highway. This structure is important because well-defined jointing occurs along bedding planes (i.e. along the chlorite-rich surfaces).

The side of the outcrop (facing the highway), being relatively flat, was the most suitable surface for GPR surveying. The top of the outcrop was irregular and vegetated with grass and small bushes – unsuitable for the purposes of surveying.

For the first 1.5 m into the rock, bedding joints and a fracture zone were measured and recorded from the exposed western edge of the outcrop because the structure was not clearly visible from the top or eastern edge. The joints existed at a depth of 20-50 cm and a 5 cm wide fracture zone of broken rock existed at a depth of 95 cm to 105 cm. From this surface these discontinuities all had an average orientation of 244/75. Figure 5-11 shows the locations of the discontinuities at the elevation of the GPR survey line. Note that at the time the surveys were conducted, all fractures appeared to be dry.

The objective of the GPR surveys was therefore to detect these bedding fractures contained within the first metre of the rock face, specifically the two open joints at depths of 20 cm and 50 cm and the fractured zone at 95 cm. If these discontinuities were detected by GPR, they would appear as flat-lying reflections in the radargram; however, because these surfaces had an undulatory nature due to metamorphism, any fracture reflections may not be perfectly planar.

Only three GPR surveys conducted across the northern face of the outcrop are discussed and the details are contained in Table A-5 in Appendix A. Table 5-7 lists these three surveys with their file name, antenna frequency, and important survey details.

Only high frequency surveys were conducted across the northern face of the outcrop because structure could only be seen for the first 1.5 m - the low frequency antennas would not provide worthwhile information within this very near-surface region. All the surveys were conducted along the same survey line and hence can be compared directly to each other. Chalk markings were used as a guide for station spacing along the steeply dipping surveyed surface.

To evaluate the influence of sampling frequency on the GPR results, two high frequency surveys were conducted (File names: BY-1G-2a & BY-1G-2c) using sampling frequencies of 6.6 GHz and 10.8 GHz respectively. As Section 4.1 discussed, the recommended sampling frequency for the 1 GHz centre frequency antennas was $\geq$ 6 GHz, however the time window shortens as the sampling frequency increases. As such, the 6.6 GHz frequency used for 'BY-1G-2a' is close to the minimum sampling frequency, however the 10.8 GHz frequency used for 'BY-1G-2c' is 1.6 times larger.

At this project site, the influence of station spacing can be evaluated because a station spacing both above and below the recommended value was used. (Section 4.1 discusses the importance of using a station spacing lower than the Nyquist sampling interval.) Assuming the host rock has

a dielectric constant of 6.25, the station interval should be less than 3 cm, however for relatively planar features that lie parallel to the survey surface this condition can be relaxed. The two high frequency surveys 'BY-1G-2c' and 'BY-1G-2d' used station spacings of 2.5 and 5 cm respectively and can be compared directly to assess the influence of station spacing.

5.4.3   Vermilion River Outcrop

The Vermilion River project site was a highway outcrop on the north side of the divided section of Highway 17 heading westbound – located 0.4 km east of the Vermilion River crossing (Figure 5-12). With respect to the city of Sudbury, the site was located approximately 27.4 km southwest of the downtown core.

The host rock is a dark grey, recrystallized, argillite of the McKim Fm and Huronian Supergroup of the Southern Province (Section 5.2.2.1). Subjected to low rank metamorphism and deformation, the host rock has been recrystallized and contains white, en-echelon quartz veins running through it. From the highway, the outcrop has a brownish weathered surface and a dark grey appearance on the unweathered surfaces.

The outcrop is at least 100 m long and in the vicinity of the GPR surveys is ≈ 7 m high. On the top of the outcrop, the first 2-3 m away from the highway was bare rock, excellent for GPR surveys; however, progressing away from the highway, the outcrop became covered with small bushes followed by deciduous trees. Surveys could not be conducted on the side of the outcrop because blasting had created a very irregular surface.

A 6 m survey line along the top of the outcrop and parallel to the highway was used for conducting two radar surveys using the 1 GHz antennas. The survey line was 0.5 to 2.2 m away from the rock cliff. At this section of the outcrop, the GPR objective using the high frequency antennas was to detect a well-developed sub-horizontal joint that deepened from 0.7 to 1.8 m, in an west to east direction, along the 6 m survey line (Figure 5-13). The dip of the joint was measured to be 10° to the east. The open joint had a maximum aperture of 2-3 mm at the surface and was dry at the time of the survey.

Because this primary radar target existed at a depth of less than 2 m from the survey line, only the high frequency antennas were used at this site. Table 5-8 lists the two surveys ('VM-1G-3' and 'VM-1G-5') presented for this project site. Table A-6 in Appendix A contains the detailed descriptions of these two surveys.

Surveys 'VM-1G-3' and 'VM-1G-5' were conducted parallel to the highway and along the top of the outcrop. They were also both conducted along the same survey line, starting from the same location, but the second survey was double the length and used a larger station spacing. Figure 5-14 is a sketch of these two surveys in plan view. This figure also shows the locations of quartz veining along the survey lines. Figure 5-15 and Figure 5-16 are digital photos showing each individual survey line from the highway. Both figures show that the ground surface has a dip of 5° to the east for the first 3 m along both surveys. This information is important because topographic corrections to the resulting profiles were required.

5.4.4 Willet Green Miller Outcrops

The next project site was located behind the Willet Green Miller Centre (WGMC) at Laurentian University (Figure 5-17). At this site, two areas of outcrop were selected for GPR surveying. Outcrop 1 was west of the WGMC building and immediately north of the WGMC parking lot. Outcrop 2 was immediately behind the WGMC building – between a paved access road and the building. As the outcrops were less than 200 m apart, the host rock and structure were essentially the same.

The host rock was from the same formation as at the Hwy 17 Bypass project site – from the Mississiagi Fm. of the Hough Lake Group. The rock can be described as a light brown to light grey, recrystallized, subarkose or feldspathic sandstone. Similar to the Hwy 17 Bypass Outcrop, tilting of the beds and grain recrystallization can be explained by the deformation and metamorphism that has influenced rocks of the Huronian Supergroup. The main difference between these rocks and the rocks at the Hwy 17 Bypass, is that the beds are thicker (0.5-1 m).

The topography in this area is irregular, with linear vegetated depressions in-between bare sandstone highs. The distance between the depressions and highs range from 1 to 3 metres. The geological maps of the area suggest the presence of both feldspathic sandstone and siltstone (or wacke). Layers of siltstone which have been preferentially weathered and now covered with vegetation help to explain the undulating topography but these layers could not be confirmed.

Both low and high frequency surveys were conducted at both outcrops. All surveys were conducted along the top of both outcrops, nearly perpendicular to the strike of the bedding. The bedding planes had an average dip of 40° to the northwest. Unfortunately because of weathering and patches of soil (thin veneer) and vegetation (grass and low bushes), the thickness of the beds along the survey lines was obscured. Figure 5-18 and Figure 5-19 show the inferred structure at Outcrops 1 and 2.

The objective of the GPR surveys at both outcrops was therefore to detect bedding planes or possibly contacts between layers of sandstone and siltstone. The surveys were also conducted perpendicular to the bedding strike, so any structure detected by GPR would appear as reflections dipping with an angle of 33° in the radargram.

Table 5-9 lists the Willet Green Miller surveys conducted at the two outcrops with the antenna frequency and RAMAC file name. Tables A-7 and A-8 in Appendix A contains the details of all the surveys performed at Outcrops 1 and 2.

5.4.4.1 Outcrop 1 Surveys

Outcrop 1 was surveyed across the top of the outcrop, perpendicular to the strike of the bedding. Figure 5-18 shows a cross-sectional sketch of Outcrop 1 along the survey line. Two surveys were conducted along this survey line using both the 100 MHz and 1 GHz antennas (File names: WGMC1 & WGMC1G1). The surveyed surface was relatively level - the maximum difference in elevation along the survey line was 10 cm - so no topographic correction is required. The type of ground cover along the survey line was noted (i.e. bare rock vs. soil covered rock). Unfortunately, the depth of the soil-covered areas was not confirmed and no structure measurements could be taken along the survey line.

5.4.4.2 Outcrop 2 Surveys

Across the top of Outcrop 2, a low frequency survey 'WGMC2' and a high frequency survey 'WGMC1G3c' was conducted. Outcrop 2 had a more irregular topographic surface along the survey line so elevations along the line were recorded for future processing of the data. Again, the surface cover along the survey line was recorded. Figure 5-19 shows a sketch of Outcrop 2 along the survey line.

Similar to Outcrop 1, the depth of the soil cover was not confirmed but the presence of the grass does suggest that the soil was deeper than at Outcrop 1. As well, there was likely to be moisture in the grass-covered areas whereas, the bare rock sections appear relatively dry. Structural measurements along the survey line were again impossible at this outcrop due to weathering or overburden.

5.4.5 Hwy 637 - Killarney Outcrop

The Hwy 637 – Killarney project site was a granite outcrop located along Hwy 637, approximately 100 km southwest of the city of Sudbury. From the town of Killarney, the outcrop is located 30.8 km east or 400 m east of the Bell Lake Access Road (Figure 5-20). The granite outcrop is part of a felsic intrusion within orthogneiss of the Grenville Province. The host rock can be described as a pink, medium to coarse-grained granite.

The outcrop has sub-horizontal jointing, possibly due to stress relief. Dimensions of the outcrop are 5 m high, 21 m wide, and greater than 30 m long (Figure 5-21). No dykes, sills or veining was observed, hence it can be assumed that the host rock is relatively homogeneous. The top of the outcrop proved excellent for GPR surveys, as it was nearly planar with sparse vegetation.

The sub-horizontal fractures could not be reached without the aid of a ladder so orientations and apertures could not be measured. Sub-vertical fractures were found to have an average orientation of 059/84 however these were not the main radar targets of the survey. From the highway, the vertical rock face shows an obvious fracture zone 20-25 cm wide containing broken granitic rock. The zone lay 2.5 to 3.1 m below the top of the outcrop – Figure 5-22. All joints including the fracture zone appeared to be dry.

The objective of the GPR surveys was to detect the sub-horizontal fracture zone. If this zone were detected by GPR, it would appear as a relatively strong flat-lying reflection in the radar profile at approximately 3 m depth.

Two perpendicular GPR surveys were conducted across the top of the outcrop using the 100 MHz centre frequency antennas (File names: Kilarney & Kilar-2). The first survey line shown in Figure 5-21 ran parallel to the Highway. The 24 m long survey line was an average of 4 m from the vertical rock face. The second survey line, which ran perpendicular to the highway, was 21 m long and intercepted the first survey line at 11.60 m. Figure 5-22 shows a close-up photo of the start of this second survey line. The second survey line ran across the entire width of the outcrop so there were vertical rock faces at the start and end of the survey. Table A-9 in Appendix A shows the details of these two surveys.

5.4.6 Elbow Lake Outcrops

The Elbow Lake project site also lies within the Grenville Province, similar to the Hwy 637 – Killarney site. Elbow Lake is located in the Burwash District, 20 km southeast of the city of Sudbury (Figure 5-23). At this site, three outcrops along the eastern shoreline were selected. Outcrops 1, 2, and 3. All three outcrops are of a migmatitic biotite gneiss with mafic dykes parallel to the gneissic foliation (or gneissosity).

Table 5-10 lists the Elbow Lake GPR surveys with the RAMAC file name, antenna centre frequency, primary GPR target(s) and any important survey detail(s). Additional survey details are included in Tables A-10, A-11, A-12 in Appendix A.

Identifying gneissic foliation and/or mafic dykes that intersected the survey line were considered the primary radar targets at all three outcrops. Due to the characteristic undulatory nature of the foliation, its orientation ranges from 030/62 to 048/66 within the project site. The foliation also had a spacing of 0.5-1 m and the dykes had widths between 15-75 cm.

5.4.6.1 Outcrop 1 Survey

Outcrop 1 was a section of gneiss along the shoreline of Elbow Lake (Figure 5-24). During the summer months, this outcrop was 1.4 to 4.3 m above lake level. A low frequency GPR survey was conducted across the top of the outcrop, parallel to the shoreline - File name: Camp-1. Figure 5-24 shows the approximate start and end points for this 18.6 m long survey line. Traversing the survey line from south to north, the southern end was higher in elevation and the surface was relatively bare rock. Towards the northern end, the survey line extended through a vegetated depression. In the west-east direction, the survey line was located approximately 4 m from the western edge.

Along this survey line, the orientation and location of each distinct structural feature was recorded. For Outcrop 1, the foliation had an average orientation of 030/60. With the survey line trending at 321° (nearly perpendicular to the strike) any structure detected by the GPR system would appear as reflectors dipping with an angle of ≈ 41° in the resulting profile.

Conducting surveys across this outcrop was made difficult because of the large topographic changes - the maximum elevation difference along the first survey line was 2.9 m. A crude topographic survey for Camp-1 was recorded for future topographic corrections. Keeping the antennas in a horizontal plane and still maintaining close contact with the ground surface was impossible. As well, structural measurements were difficult to record due to vegetation and weathering. Sources of noise or interference may be from surface irregularity, vegetation, and the sides of the outcrop.

5.4.6.2 Outcrop 2 Surveys

Outcrop 2, located less than 50 m north of Outcrop 1, was another shoreline outcrop – Figure 5-25. Of importance to this outcrop were the distinct, steeply dipping mafic dykes located near the southern end of the outcrop. The first dyke, Dyke 1, had a width of 30 cm and an orientation of 040/66. Dyke 1 appears in Figure 5-25 as two dykes which converge near a coniferous tree. The second dyke was, located 1 m northwest of Dyke 1, had a width of 15 cm with an orientation of 052/62. Although Dyke 2 is not visible in Figure 5-25, both can be seen in Figure 5-26.

In the vicinity of the GPR surveys, the outcrop was relatively bare gneiss except for the isolated bush or small tree. As well, the lake level was approximately 5-7 m below the elevation of the GPR survey line at the time of the surveys.

Two GPR surveys were conducted using the 100 MHz and 1 GHz antennas (File names: Camp-2 & Camp-4). Details of these two surveys are in Table A-11 in Appendix A. The objective for both surveys was detection of these two mafic dykes dipping approximately 62-66° to the south. Both surveys used the same line but the low frequency survey line (Camp-2) was 4 times longer than the 1 GHz survey line (Note that the initial 2.5 m of both lines were the same). The starting position for Camp-2 was also ≈ 0.7 m south of the starting position for Camp-4. Figure 5-25 shows the approximate start and end positions of both surveys. Figure 5-26 shows another view of the high frequency survey line taken from the top of the outcrop.

The primary radar targets for both surveys were the two clearly visible mafic dykes, shown in Figure 5-26. Because the surveys were conducted perpendicular to their strike, the dykes would appear as reflectors dipping at an angle of 41-42° in the radargram.

5.4.6.3 Outcrop 3 Surveys

Outcrop 3 was located less than 10 m upslope or east of Outcrop 2. This area had more vegetation compared with the previous two outcrops, so the rock structure was not as visible. Figure 5-27 shows digital photos with the two survey lines on the side of the outcrop labeled as the upper and lower survey line. For the lower survey line, the structure was not visible because of the small bushes which covered the top of the lower bench. For the upper survey line, structural measurements were recorded from above - Figure 5-28. Figure 5-28 shows the gneissic foliation striking at 43-51° and dipping to the southeast at 68-74°. This figure also shows two open gaps 14 – 29 cm wide. These gaps are likely mafic dykes that have been removed by preferential erosion and weathering, unfortunately the presence of these two dykes could not be confirmed because of vegetation covering the surfaces.

The two high frequency surveys were conducted on the side of the outcrop and parallel to the gneissic foliation: Camp-5c (lower survey line) and Camp-5d (upper survey line). Complete details of both surveys are included in Table A-12 in Appendix A. The survey lines where marked on the outcrop using chalk (Figure 5-27). The surveyed surface was relatively planar - with the maximum difference in elevation along the surface being less than 5 cm. The antennas were in contact with bare rock except for at position 0.7 m along the upper survey line where there was a 9 cm wide gap infilled with vegetation.

118

Assuming the two gaps shown in Figure 5-28 extended down to the depth of the upper survey line, the primary radar targets for this survey were the two dykes – Dyke 1 and Dyke 2. In the radargram, these targets would appear as relatively flat-lying reflectors at approximately 0.5 m (for Dyke 1) and 1.1 m (for Dyke 2) depth from the rock face.

Unfortunately, structure for the lower survey line was not visible. Both survey lines had the same trend and were adjacent to each other, so an assumption that the same structure would appear in both profiles could be made. However, this may not be the case since the mafic dykes within this gneiss were observed to be only continuous over a few metres, as well both the orientation and thickness varied. Because of these observations, the depth of flat-lying reflections (due to foliation or the mafic dykes) for the lower survey line is unpredictable.

5.4.7   Hwy 17 Site

The Hwy 17 project site was also 15 km east of the Vermilion River site, or 1 km west of the Hwy 55 overpass along the divided section of Highway 17 (Figure 5-29). With reference to Sudbury, the outcrop was ≈ 13 km southwest of the city centre. Between the divided highway was an 8.5 m high outcrop at least 100 m in length. Heading eastbound, the northern face of the outcrop was chosen for GPR testing. The geology was the same as at the Vermilion River project site – a dark grey argillite of the McKim Fm.

The Hwy 17 outcrop did however have a different appearance than the Vermilion River outcrop despite the fact they had the same type of host rock. The Hwy 17 outcrop appeared more massive and the weathered surface was more orange than brown in color. This particular outcrop also had three clearly defined joint sets – labeled JS1, JS2, and JS3 on Figure 5-30. The average orientations for these joint sets are 080/60 for JS1, 180/90 for JS 2, and 235/10 for JS 3. The first joint set (JS1) is of most importance because it was parallel to the highway and parallel to the GPR survey surface. The average joint spacing of JS1 ranged from 1.5 to 3 m. The outcrop appeared relatively homogeneous and did not have the quartz veining observed at the Vermilion River site.

Both low and high frequency surveys were conducted along the side of the outcrop because the surface was nearly planar – excellent for GPR surveying. For both surveys, the radar objective was to detect JS1 plane(s) and since the survey surface was parallel to JS1, detection of these fractures would appear as horizontal to slightly dipping reflections on the radargrams.

The low frequency survey (File name: Prof21) was conducted along a west to east survey line approximately 1 m from the bottom of the ditch. Figure 5-30 shows the 100 MHz survey being conducted along the outcrop. JS1 fractures were located at depths of approximately 1.6 m, 3.7 m, 5.7 m, and 8.7 m. The aperture of these fractures along the survey line could not be measured but they were likely dry at the time.

The high frequency survey was conducted along the same face but at a higher elevation. Figure 5-31 shows the vertical line was used for survey 'Hwy171G2'. For the 1 GHz survey, the depth to the first JS1 fracture varied from 1.2 at the starting position to 1.65 m at the survey end position. This joint was clearly visible from the side of the outcrop and the measure aperture was 3-4 cm and dry at the time of the survey. The vertical survey line was ≈ 60 cm from the rock edge (JS2). Table A-13 in Appendix A contains additional details for the low and high surveys conducted at the Hwy 17 Site.

5.4.8 175-Orebody

The 175 Orebody is an underground research facility at INCO Limited's Copper Cliff North Mine. The mine is located in the northwest corner of Sudbury, in the Copper Cliff township (Figure 5-32). Off the portal access lies the western access ramp of the orebody - 7500 Main Access Ramp (Figure 5-33). This access ramp trends at 350°, plunges at 10° (Stochal, 1999) and is approximately 5 m wide in the vicinity of our GPR survey areas.

There are three drifts that are important to recognize for the purpose of understanding the GPR surveys: 7715 Drift, 7630 Drift, and Sungeric Drift (Figure 5-33). 7715 and 7630 drifts are two parallel test drifts (referred to as the Twin Drifts) located to the east of the Main Access Ramp. These two drifts are near-surface (i.e. low-stress environment) excavations separated by a 12.2-10.6 m wide pillar. GPR reflection surveys were conducted along the southwest sidewall of the Main Access Ramp and along both sidewalls of the 7715 Drift. The third drift to note is the Sungeric Drift. This is a service drift that contains a safety station for the underground workers. It may have an influence on the GPR surveys because it is located less than 10 m northwest of the 7715 Drift. Table 5-11 lists the dimensions, orientations, and elevations of these three drifts.

The 175-Orebody is located within the Copper Cliff Offset Dyke. This particular dyke is one of the Offset Dikes of the Sudbury Igneous Complex (Figure 5-34). The host rock is a greenish black, medium-grained quartz-diorite to diorite. The rock is relatively homogeneous in the area of the surveys except for the jointing and minor quartz veins observed.

The small-scale discontinuities were the primary radar targets at this project site. The major joint sets were identified from the detailed structural mapping (Stochmal, 1999) of the Twin Drifts. Table 5-12 summarizes the major and minor joint sets identified from this mapping. Figure 5-35 shows these same joint sets plus the orientations of the Twin Drifts and Main Access Ramp plotted on an equal area Schmidt net. Although the radar surveys were conducted in a low-stress underground environment, the majority of the joints were found to be dry and closed.

GPR reflection surveys were conducted in two areas within the 175 Orebody: 1) along the sidewalls of the 7715 Drift, and 2) along the 7500 Main Access Ramp, between the Twins Drifts. The high and low frequency antennas were used in both these areas. A total of four surveys were conducted within the 7715 Drift (2 surveys along the southeast sidewall and 2 surveys along the northwest sidewall). Two surveys were also conducted across an obvious rock wedge in the southwest sidewall of the Main Access Ramp. Table 5-13 summarizes the six surveys conducted within the 175-Orebody, including the location in the survey area, antenna frequency, and RAMAC file name.

5.4.8.1 7715 Drift Surveys

By conducting radar surveys along the sidewalls of the 7715 drift, we hoped to detect the strike lines for any of the five joint sets defined in Table 5-12. Figure 5-36 shows how these joints would appear in plan view along both sidewalls of the drift considering both the joint spacing and orientation of the joint set relative to the drift orientation. Figure 5-36 also includes a sketch of how each individual joint set may appear in the radargram if detected.

The major sub-horizontal joint JS1 is unlikely to be detected because of its unfavorable orientation relative to the survey line – the dip is too shallow. However the two major sub-vertical joints JS2 and JS3 are more likely to be detected. JS2 and JS3 would appear as

discontinuous (i.e. 2.5-3.0 m long) reflections dipping with an angles between 35-39° in the radargrams. The two minor joint sets JS4 and JS5 have the best orientation for GPR detection because their strike is nearly parallel to the trend of the drift and have dips between 40-90°. Should these minor joints be detected, they would appear as sub-horizontal reflectors approximately 3.0 to 3.5 m long with dips of 4-6°.

Detection of the adjacent underground openings was considered possible for the 100 MHz surveys because assuming the conductivity of the host rock is < 10 mS/m, the depth of penetration into the rock is about 15 m according to Table 2-5. However, for the 1 GHz antennas, the depth of penetration under similar conditions would only be ≈ 2 m. For the low frequency survey along the NW sidewall, detection of the Main Access Ramp and/or Sungeric Drift was considered possible. If detected, the Sungeric Drift would appear as a horizontal reflection at ≈ 9.4 m depth. The Main Access Ramp, if detected, would appear as a dipping reflector with a dip angle of 39° (actual dip of 53°) at 6.7 to 9.0 m into the rock. For the SE sidewall low frequency survey, detection of the 7630 Drift would appear as a discontinuous, horizontal reflector 10.6-12.2 m from the rock surface.

All surveys along the sidewalls of the 7715 Drift were conducted using a fibreglass tape measure placed against the wall as a guide for station spacing. The antennas were held in a vertical orientation at approximately 1 m above the floor. Wire mesh and rock bolts covered a large portion of the roof and sidewalls. Although it was recognized that these types of support would produce high interference with the radar system, avoidance was nearly impossible, so large sections of the survey lines had the antennas in direct contact with the wire mesh.

Along the NW sidewall, a low frequency survey ≈ 27 m long (File name: 175-a) and a high frequency survey ≈ 8 m long (File name: 175-1G-3) was conducted. Figure 5-37 are digital photos of the NW sidewall with 100 MHz survey line marked. Although the structure is nearly impossible to observe in these photos, the tunnel support (i.e. wire mesh, rockbolts) and other metallic objects can be seen in relation to the survey line. Figure 5-38 shows a plan view of the twin drifts with all the survey lines marked.

Along the opposite sidewall, a low frequency survey ≈ 30 m long (File name: 175-d2) and a high frequency survey ≈ 7 m long (File name: 175-1G-1) was conducted. The length of the high frequency survey was restricted because of mining equipment at the end of the drift. Figure 5-38 and Figure 5-39 shows the location of the low frequency survey line along the SE sidewall. Similar to the photos of the NW sidewall, Figure 5-39 helps to show sources of potential noise along the survey line.

5.4.8.2   Main Access Ramp Surveys

To evaluate whether GPR can be used to detect rock wedges in an underground environment, surveys were conducted across a visible wedge in the SW sidewall of the Main Access Ramp. Although three joints are required to form a wedge, only two joints were clearly visible at the surface. The orientations of these two planes were 220/87 and 115/52. At the surface, the wedge had a maximum width of 1.2 m in the horizontal direction, so the maximum depth of the wedge was approximately 0.8 m — Figure 5-40.

Within the Main Access Ramp, radar data was acquired using antennas at central frequencies of 100 MHz and 1 GHz across the sidewall wedge (Figure 5-38). Using the low frequency antennas, a 5.2 m survey (File name: 175-c) was conducted across the wedge using a fibreglass measuring tape as a guide for the station spacing (Figure 5-41).

With the high frequency antennas, a short 1.75 m long survey (File name: Wedge1G2) was conducted across the wedge (Figure 5-42). To achieve an accurate station spacing across the rough mine wall surface, a 10 cm × 10 cm grid drawn on a thin piece of transparent plastic was placed over the wedge. Table A-16 in Appendix A contains details of the surveys in the Main Access Ramp.

5.5 SUMMARY AND CONCLUSIONS

The field component of this thesis consists of 32 reflection GPR surveys conducted at nine project sites using 100 MHz and 1000 MHz centre frequency antennas. These two frequencies were thought to provide a good comparison between the capability of low frequency versus high frequency antennas. Both antenna frequencies were not used at all the project sites because the target(s) depth ultimately dictated which would be more successful to use. Recall that the 100 MHz antennas have a typical penetration of about 15 m into rock versus about 2 m using the 1000 MHz antennas and the radar target has to lie above these depths in order to be detected.

Working within the Sudbury District allowed GPR surveys to be conducted in a variety of host rocks – from limestone to granite to gneiss. Within these rocks, the primary radar targets were not just small-scale structural features (i.e. joints, bedding planes, foliation) but there were also larger-scale structural features (i.e. fracture zones, dykes, and veins). The only type of rock structure that I would have liked to test was large-scale faults, but none existed at any of the selected project sites.

Similar to Buursink and Lane (1999) GPR surveys were conducted on rock blocks since the targets can be well characterized, in addition to testing on natural outcrops. Only a few surveys were conducted in the underground mine because of the limited site access and because of the anticipated problems due a high number of sources of interference.

The characteristics of the primary radar targets (i.e. joints, bedding planes, etc.) were noted if visible at the surface. Both dipping and flat-lying targets, relative to the survey line, were surveyed. The apertures of the small-scale fractures were also measured from the surface when possible, but these apertures were likely larger than what actually existed along the survey line. As for infilling, all the target fractures were dry.

Table 5-1 Important Precambrian rock units and events in the project area (Card et al., 1984).

Precambrian	Event	Rock Unit	Approx. Age (Ma)
Middle Proterozoic (1600-900 Ma)	*Grenville Orogeny*		1000-1200
	Mafic Intrusion	Sudbury diabase dikes	1250
	Felsic Intrusion	Croker, Manitoulin Island, Killarney Complexes	1500
Early Proterozoic (2500-1600 Ma)	*Deformation and Metamorphism*	Cutler, Grenville Front plutons	1750
		Sudbury Igneous Complex, Whitewater Group	1849
	Sudbury Event	Breccia, Shatter cones	
	Metamorphism and Deformation (Penokean Orogeny)		1850-1900
	Mafic Intrusion	Nipissing Diabase	2100
	Felsic Intrusion	Creighton & Murray Granites	2333
	Early deformation, faulting, basin subsidence, volcanism, and sedimentation	Huronian Supergroup	2460
		Unconformity	
Archean	*Mafic Intrusion*	Matachewan dikes	2630
	Felsic Intrusion	Algoman granite Granodiorite suite intrusions	2680
	Deformation and metamorphism		
	Volcanism	Abitibi Subprovince volcanic rocks and sediments	2700-2750
		Levack Gneiss	

Table 5-2 Simplified stratigraphy and sedimentology of the Huronian Supergroup in the project area (modified from Dressler, 1984).

Group	Thickness (approx.)	Formation	Rock Types
Cobalt	1500-2400 m	Lorrain Fm.	arkose. feldspathic protoquartizite. wacke. quartz arenite, conglomerate
	180-1200 m	Gowganda Fm.	polymictic paraconglomerate. orthoconglomerate. laminated
Quirke Lake	180-1500 m	Serpent Fm.	protoquartzite. feldspathic quartzite. arkose. minor siltstone, conglomerate. limestone
	150-550 m	Espanola Fm.	limestone, dolostone. wacke. protoquartzite
	60-460 m	Bruce Fm.	pebbly wacke. conglomerate
Hough Lake	760-3000 m	**MISSISSAGI FM.**	orthoquartzite. arkose. wacke. conglomerate
	60-600 m	Pecors Fm.	wacke. quartz feldspar arenite
	60-180 m	Rasmey Lake Fm.	polymictic paraconglomerate. pebbly sandstone
Elliot Lake	1500-1800 m	**MCKIM FM.**	laminated wacke and mudstone protoquartzite
	180-300 m	Matinenda Fm.	feldspathic protoquartzite. laminated wacke, oligomictic quartz-pebble conglomerate. polymictic conglomerate
	up to 730 m	Copper Cliff Fm.	felsic flows. felsic pyroclastic rocks
	up to 1500 m	Stobie Fm.	mafic flows, pyroclastic rocks. minor wacke
	up to 1000 m	Elsie Mountain Fm.	mafic flows, minor pelitic metasediments, and mafic tuffaceous rocks

Table 5-3 Dimensions and weights of the RAMAC/GPR antennas used for the field surveys.

	100 MHz (each antenna)	1 GHz (single module – both antennas)
Length	104 cm	24 cm
Width	16 cm	16 cm
Height	4 cm	12 cm
Weight[1]	1.10 kg	2.4 kg

Note 1. Approximate weight without battery pack.

Table 5-4 Effects of using higher frequency antennas.

Parameter of Interest	Influence on Parameter	Comment(s)
Suitable Target Size	$\uparrow$ f_c, $\downarrow$ target size detection	increases resolution: system can detect smaller objects
Depth of Penetration	$\uparrow$ f_c, $\downarrow$ depth of penetration	cannot 'see' as far into the rock
Time Window	$\uparrow$ f_c, $\downarrow$ time window	cannot view as much of the recorded signal in the plot of two-way travel time vs. position
Station Spacing	$\uparrow$ f_c, $\downarrow$ station spacing	require more points along survey line
Antenna Separation	$\uparrow$ f_c, $\downarrow$ minimum antenna separation	equipment becomes more compact
Antenna Length	$\uparrow$ f_c, $\downarrow$ antenna length	equipment becomes more compact

Table 5-5 Nine thesis field sites used for GPR reflection surveys.

Site Name	Survey Environment	Primary Radar Target(s)	No. of GPR Surveys
Jarvis Resources Ltd.	rock blocks	artificial fractures	6
WGMC Walkway	rock blocks	artificial fractures	2
Hwy 17 Bypass	highway outcrop	bedding joints & fracture zone	3
Vermilion River	highway outcrop	joint & quartz veins	2
Willet Green Miller Centre	surface outcrops	bedding planes	4
Hwy 637 – Killarney	highway outcrop	fracture zone	2
Elbow Lake	surface outcrops	foliation & mafic dykes	5
Hwy 17 Site	highway outcrop	joints	2
175-Orebody	underground mine	joints	6
		Total	*32*

Table 5-6 High frequency GPR surveys conducted at Block Site 1 — Jarvis Resources Ltd.

RAMAC File Name	Antenna Frequency	Important Survey Detail(s)[1]
Jarvis1h	1 GHz	Horizontal survey 38 cm down from the top of the 1st limestone slab; station spacing of 1 cm
Jarvis1e	1 GHz	Horizontal survey 16 cm down from the top of the 1st limestone slab; station spacing of 2.5 cm
Jarvis1f	1 GHz	Horizontal survey 16 cm down from the top of the 1st limestone slab; station spacing of 2.5 cm; + aluminum foil inserted between 4th and 5th slabs

Note 1. Detailed descriptions of these surveys are contained in Tables A-1, A-2, and A-3 in Appendix A.

Table 5-7 High frequency GPR surveys conducted at Hwy 17 Bypass Outcrop.

RAMAC File Name	Antenna Frequency	Important Survey Detail(s)	
		Sampling Frequency	Station Spacing
BY-1G-2a	1 GHz	6.6 GHz	2.5 cm
BY-1G-2c	1 GHz	10.8 GHz	2.5 cm
BY-1G-2d	1 GHz	10.8 GHz	5 cm

Table 5-8 High frequency GPR surveys conducted at Vermilion River Outcrop.

RAMAC File Name	Antenna Frequency	Important Survey Detail(s)
VM-1G-3	1 GHz	3 m long survey with station spacing of 2.5 cm
VM-1G-5	1 GHz	6 m long survey with station spacing of 5 cm (along the same survey line as VM-1G-3)

Table 5-9 GPR surveys at Willet Green Miller Outcrops.

WGMC Outcrop	RAMAC File Name	Antenna Frequency
Outcrop 1	WGMC1	100 MHz
	WGMC1G1	1 GHz
Outcrop 2	WGMC2	100 MHz
	WGMC1G3c	1 GHz

Table 5-10 GPR surveys at Elbow Lake Outcrops.

Elbow Lake Outcrop	RAMAC File Name	Antenna Frequency	Primary Radar Target(s)	Important Survey Detail(s)
Outcrop 1	Camp-1	100 MHz	gneissic foliation & mafic dykes	survey line ≈ 4 m from western rock edge
Outcrop 2	Camp-2	100 MHz	mafic dykes	surveyed perpendicular to the dykes
	Camp-4	1 GHz	mafic dykes	surveyed perpendicular to the dykes
Outcrop 3	Camp-5c	1 GHz	gneissic foliation & mafic dykes	lower survey line
	Camp-5d	1 GHz	gneissic foliation & mafic dykes	upper survey line

Table 5-11 Important Drifts in 175-Orebody Project Site

Drift Name	Dimensions			Orientation	
	Avg. Width (m)	Length[1] (m)	Height (m)	Trend	Plunge[2]
7630 Drift	3.7-4.3	≈ 38	3.7-4.3	210°	1 to 3°
7715 Drift	4.9-5.5	≈ 40	4.9-5.5	210°	1 to 3°
Sungeric Drift	8.4	≈ 11	5	210°	1 to 3°

Notes:
1. Drift length as of July 1999.
2. Plunge is the angle downwards from the horizontal.

Table 5-12 175-Orebody joint sets.

Joint Ranking	Strike/Dip[1]	Average Joint Spacing (m)	Average Persistence (m)
Major Joint Sets:			
JS1	200/08	0.7	4.5
JS2	345/83	0.6	2.5
JS3	083/81	0.9	3
Minor Joint Sets:			
JS4	206/89	0.7	3
JS5	036/40	1.2	3.5

Note 1. All the structural orientations the convention is strike and dip using the right-hand-rule.

Table 5-13 GPR surveys conducted at 175-Orebody.

Survey Area	Location[1]	RAMAC File Name[2]	Antenna Frequency
7715 Drift	NW sidewall	175-a	100 MHz
	NW sidewall	175-1G-3	1 GHz
	SE sidewall	175-d2	100 MHz
	SE sidewall	175-1G-1	1 GHz
Main Access Ramp	SW sidewall	175-c	100 MHz
	SW sidewall	Wedge1G2	1 GHz

Notes:
1. NW = northwest; SE = southeast; SW = southwest.
2. Tables A-14, A-15, & A-16 in Appendix A contains details on each of the surveys at 175-Orebody.
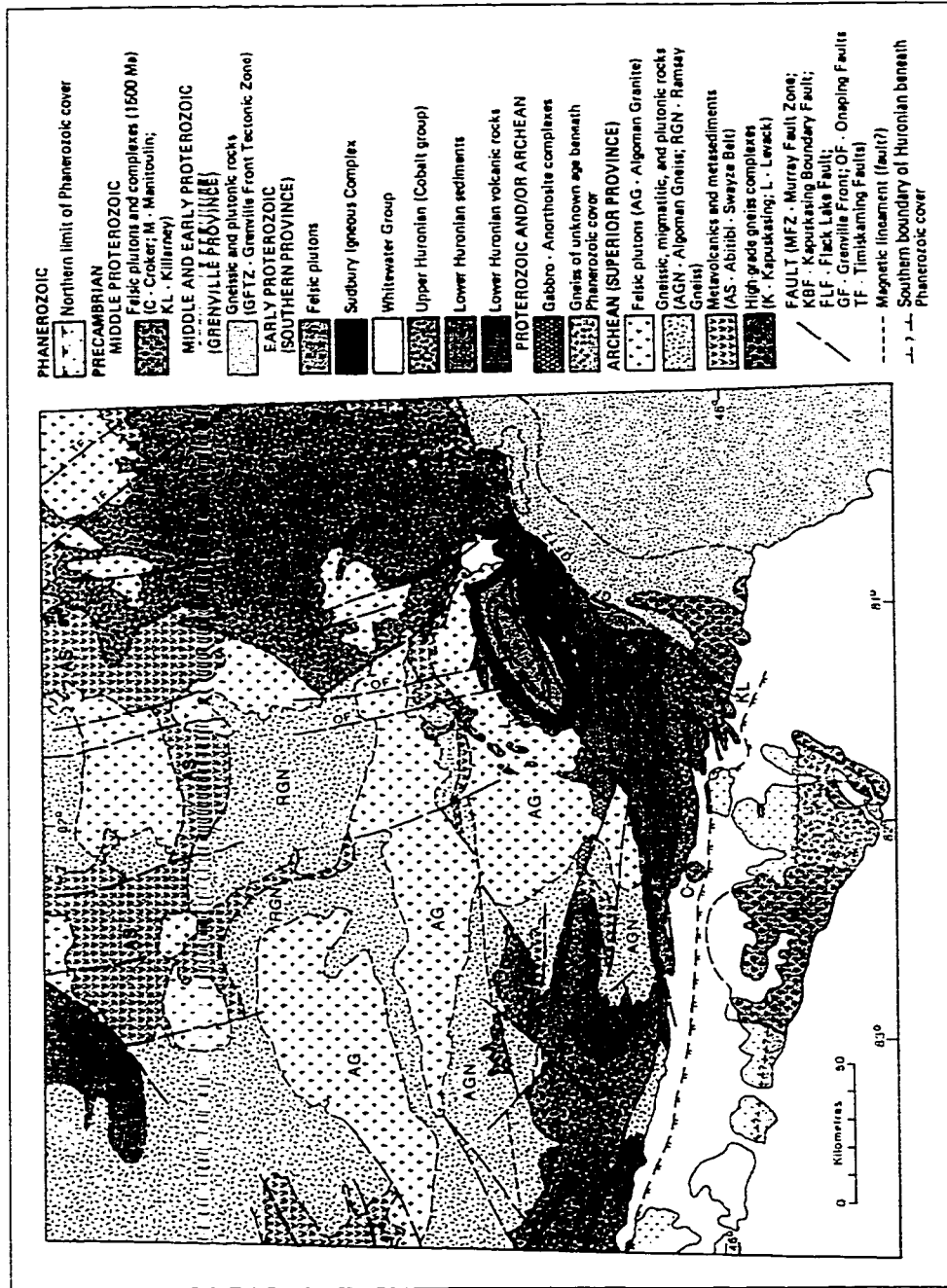
Figure 5-1 Geology of the Sudbury Region. *from* Card et al. (1984, Fig 2.2). © Queen's Printer for Ontario, 1984. Reproduced with permission.

129
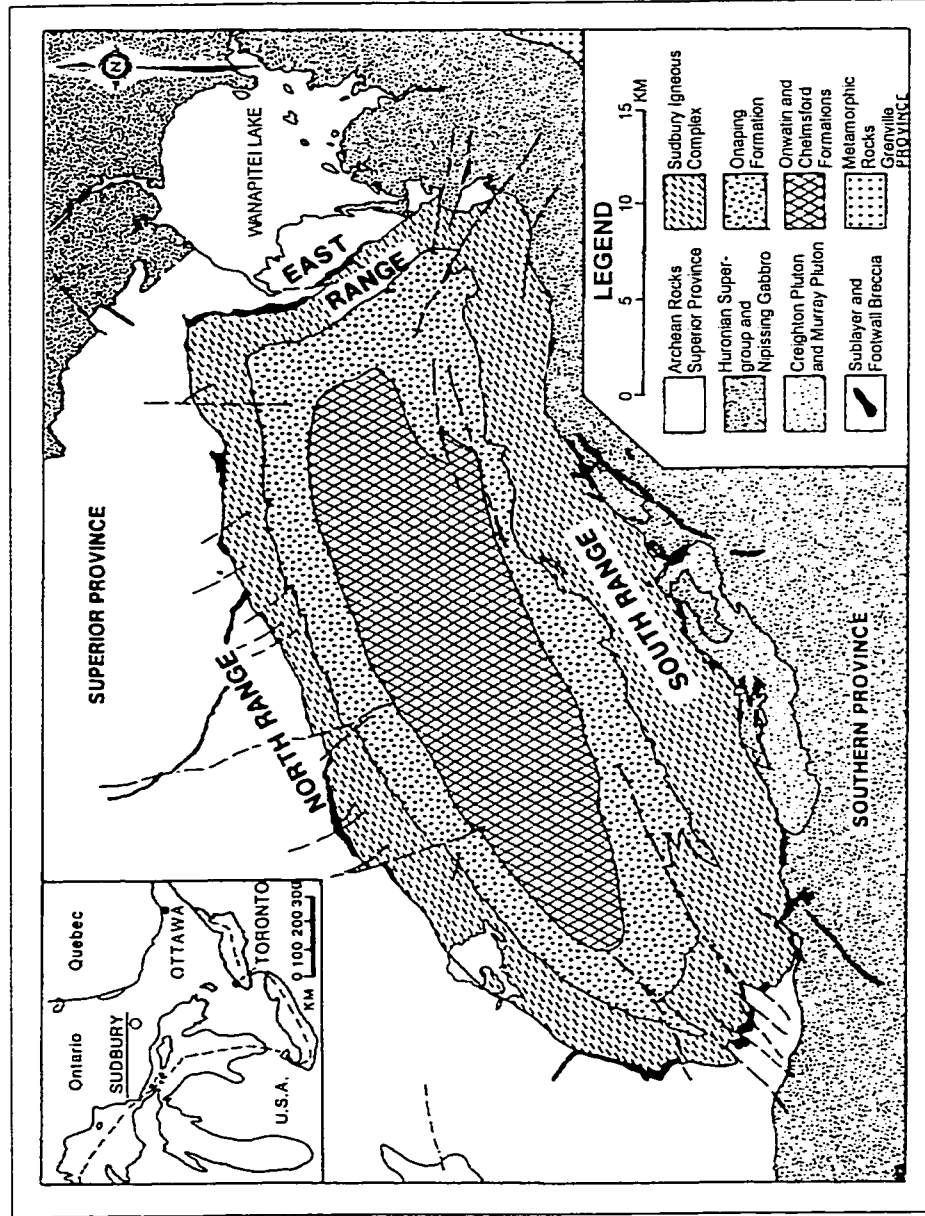
Figure 5-2 Geology of Sudbury Structure.
from Dressler et al. (1992, Fig. 1). ©Queen's Printer for Ontario, 1992. Reproduced with permission.

130
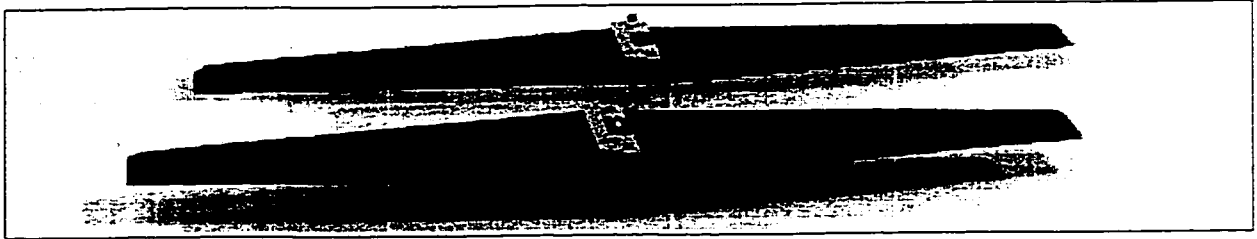
Figure 5-3 Ramac 100 MHz unshielded antennas.
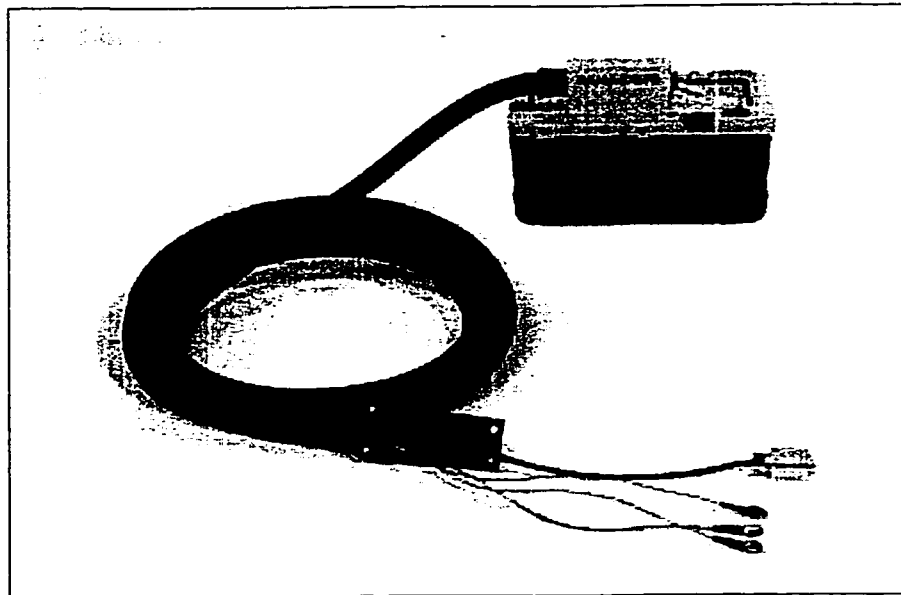
Figure 5-4 Ramac 1 GHz shielded antennas.

West   East
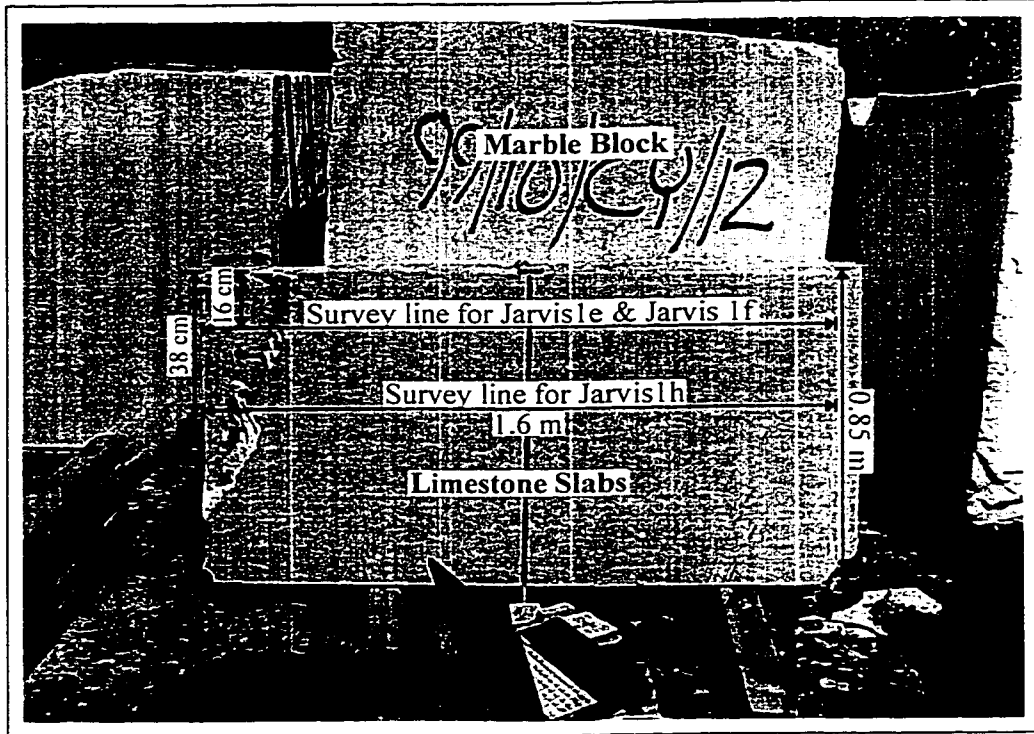
a) Front view of limestone slabs and marble block.

South   North
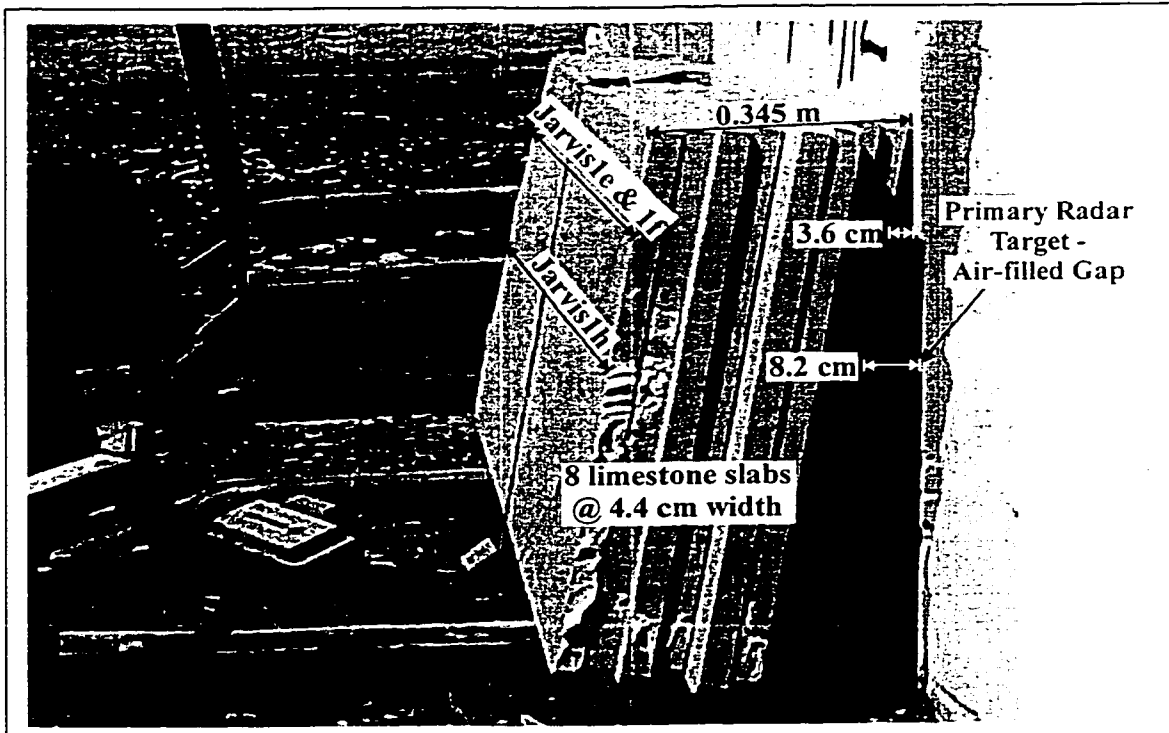
b) Side view of limestone slabs and marble block.

Figure 5-5 Digital photos of Block Site 1 - Jarvis Resources Ltd.
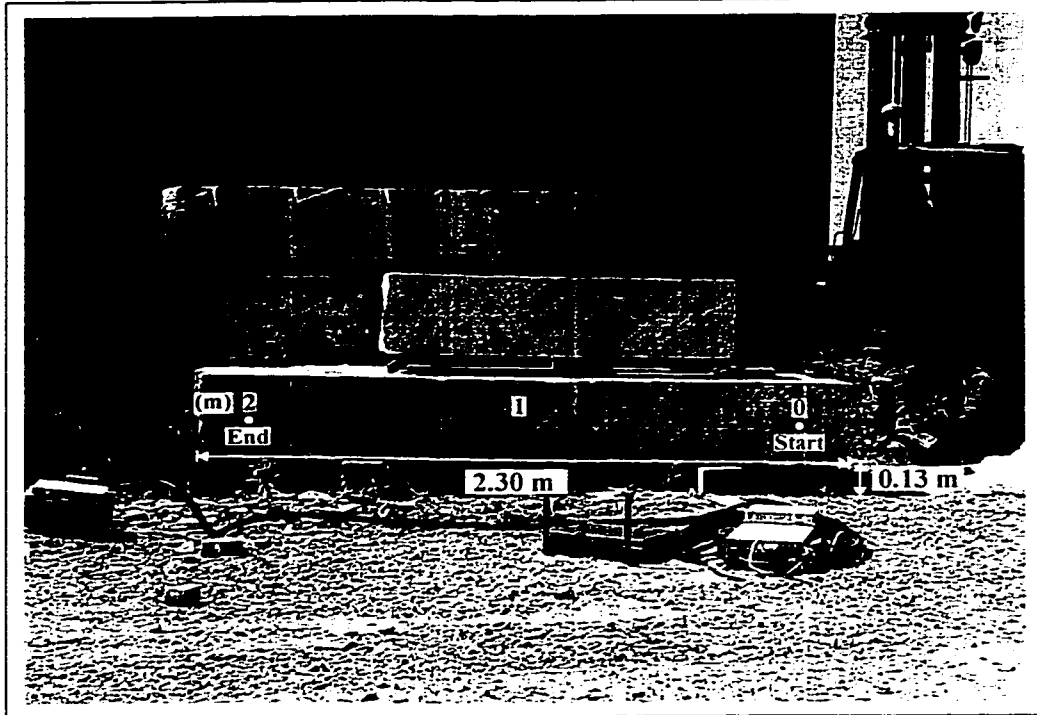
a) Front view of limestone blocks.
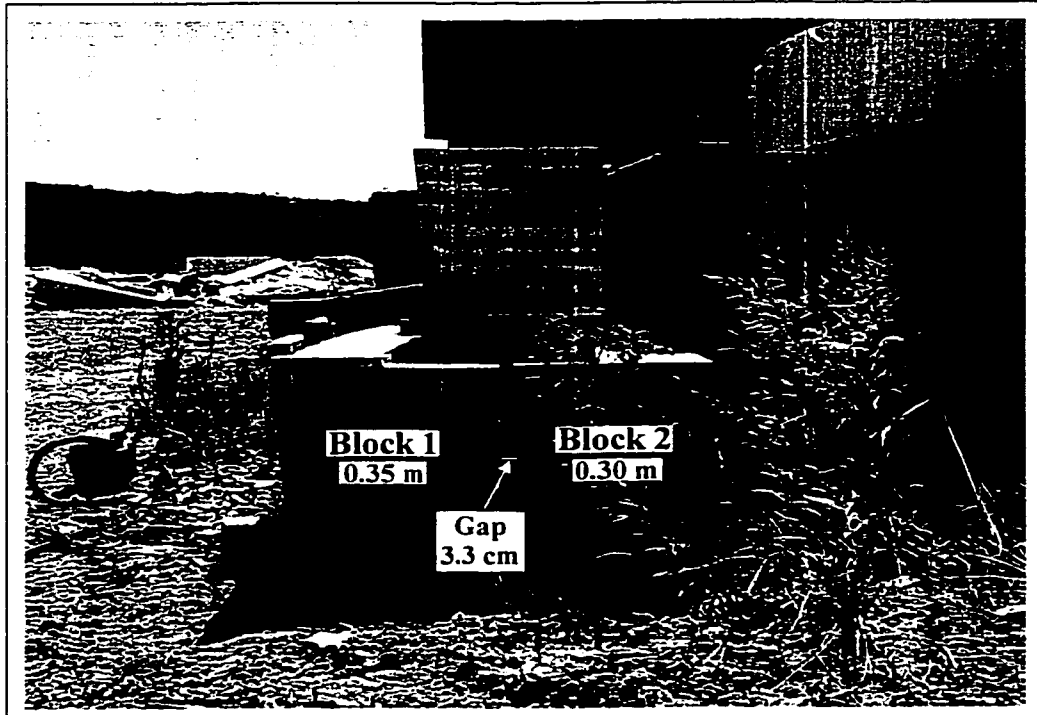
b) Side view of limestone blocks.

Figure 5-6 Digital photos of Block Site 2 - Jarvis Resources Ltd.
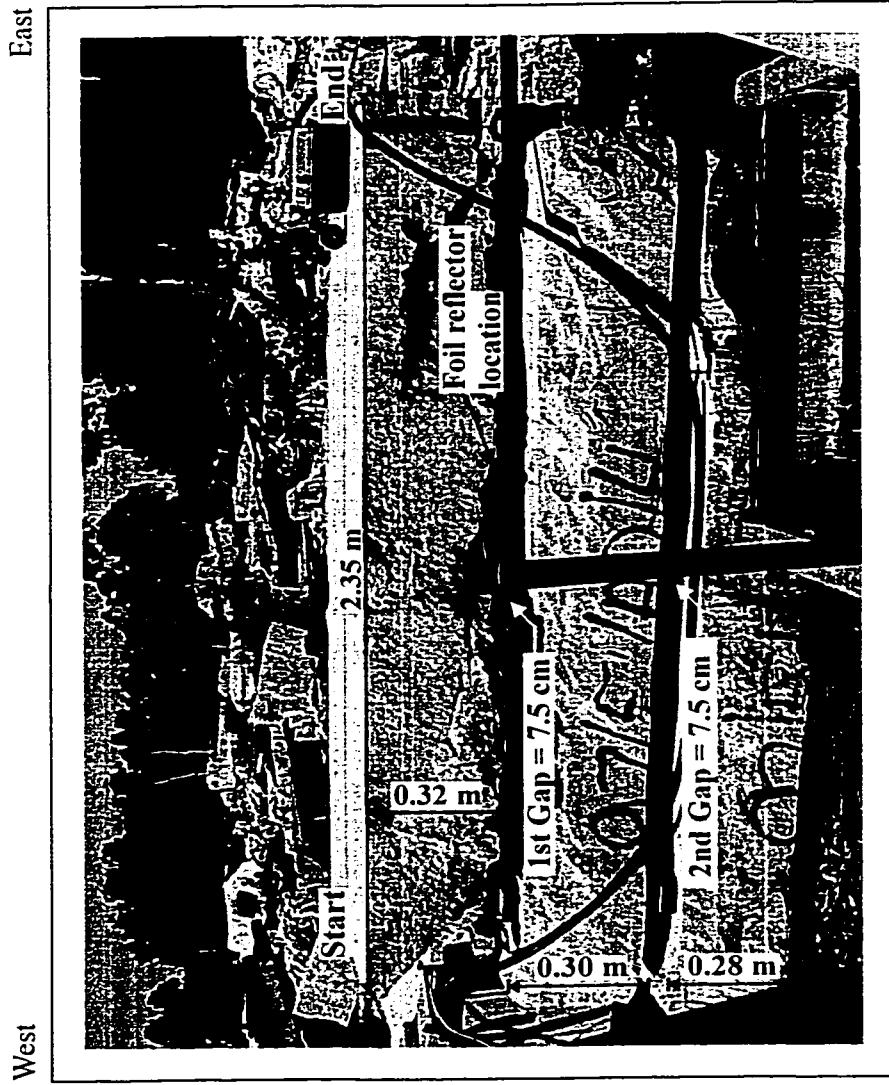
Figure 5-7 Digital photo of Block Site 3 – Jarvis Resources Ltd.
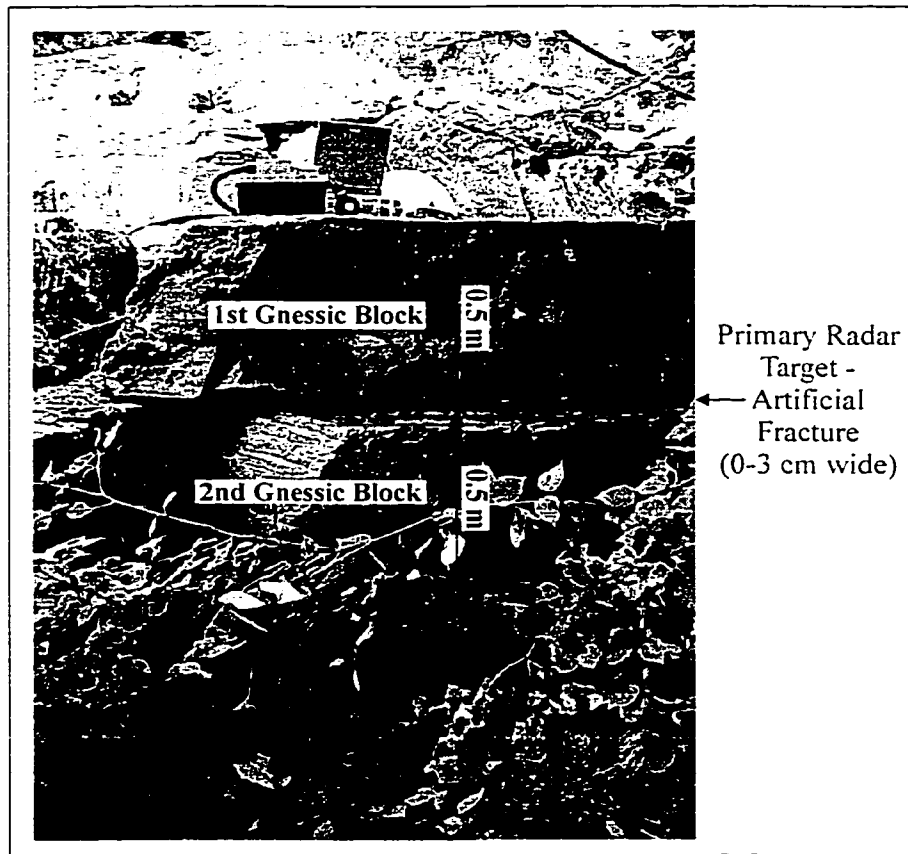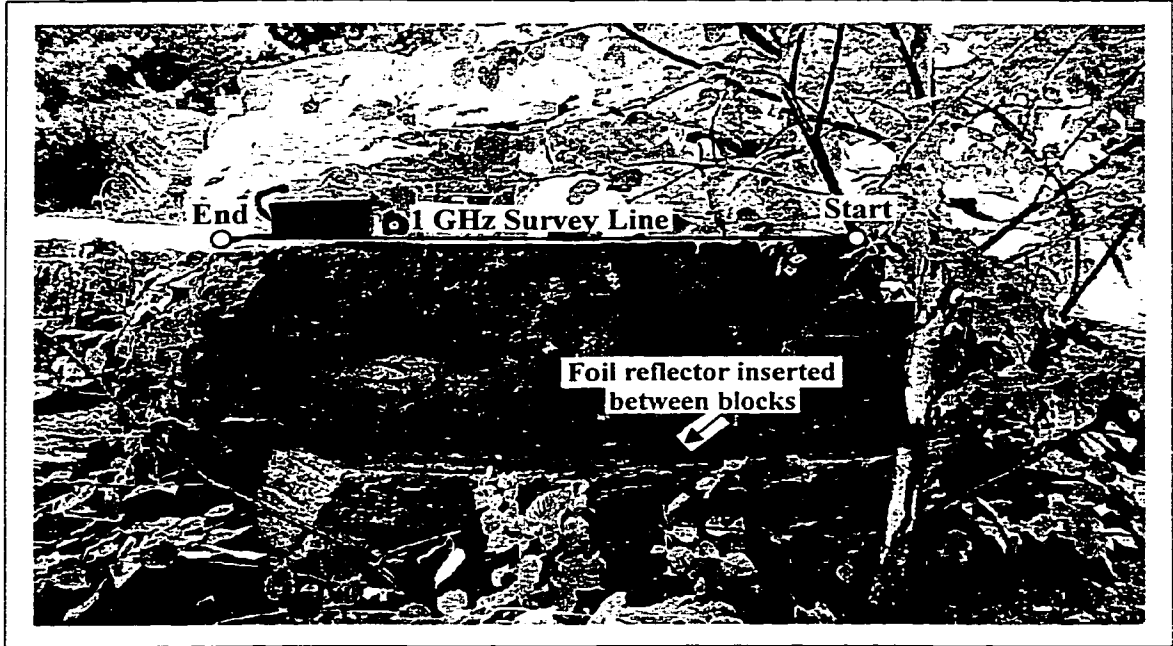
Figure 5-8 Digital photos of the gneiss blocks - WGMC walkway.

Figure 5-9 Location of Hwy 17 Bypass Outcrop.

Modified from:
1: 50,000 Topographic Map; Coniston, Ontario; NTS 41-1/7;
Department of Energy, Mines and Resources; Ottawa, 1995.

Figure 5-10   Digital Photo of Hwy 17 Bypass Outcrop.

a) Close-up digital photo of rock structure.
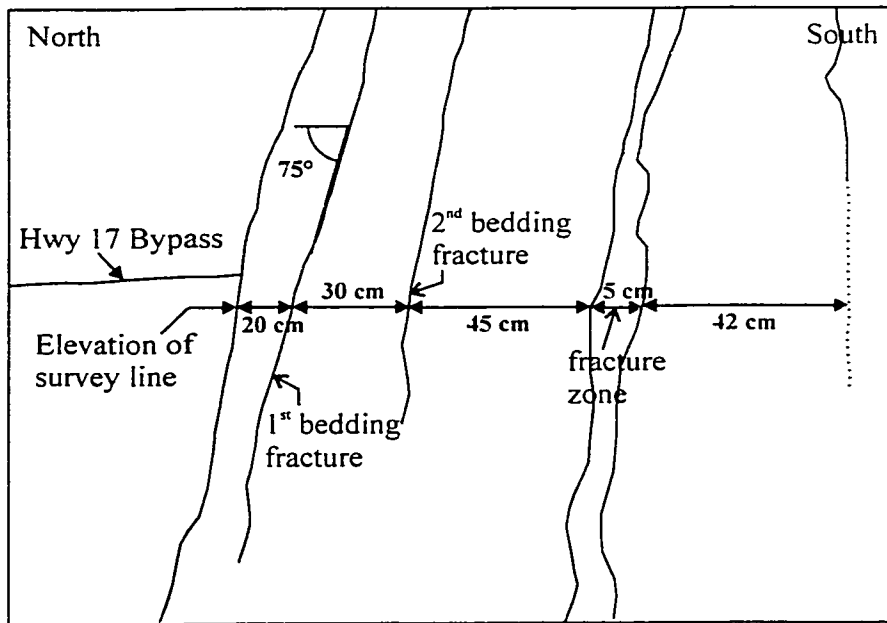
b) Sketch of rock structure (with approximate dimensions).

Figure 5-11 Rock structure from western edge of Hwy 17 Bypass Outcrop.
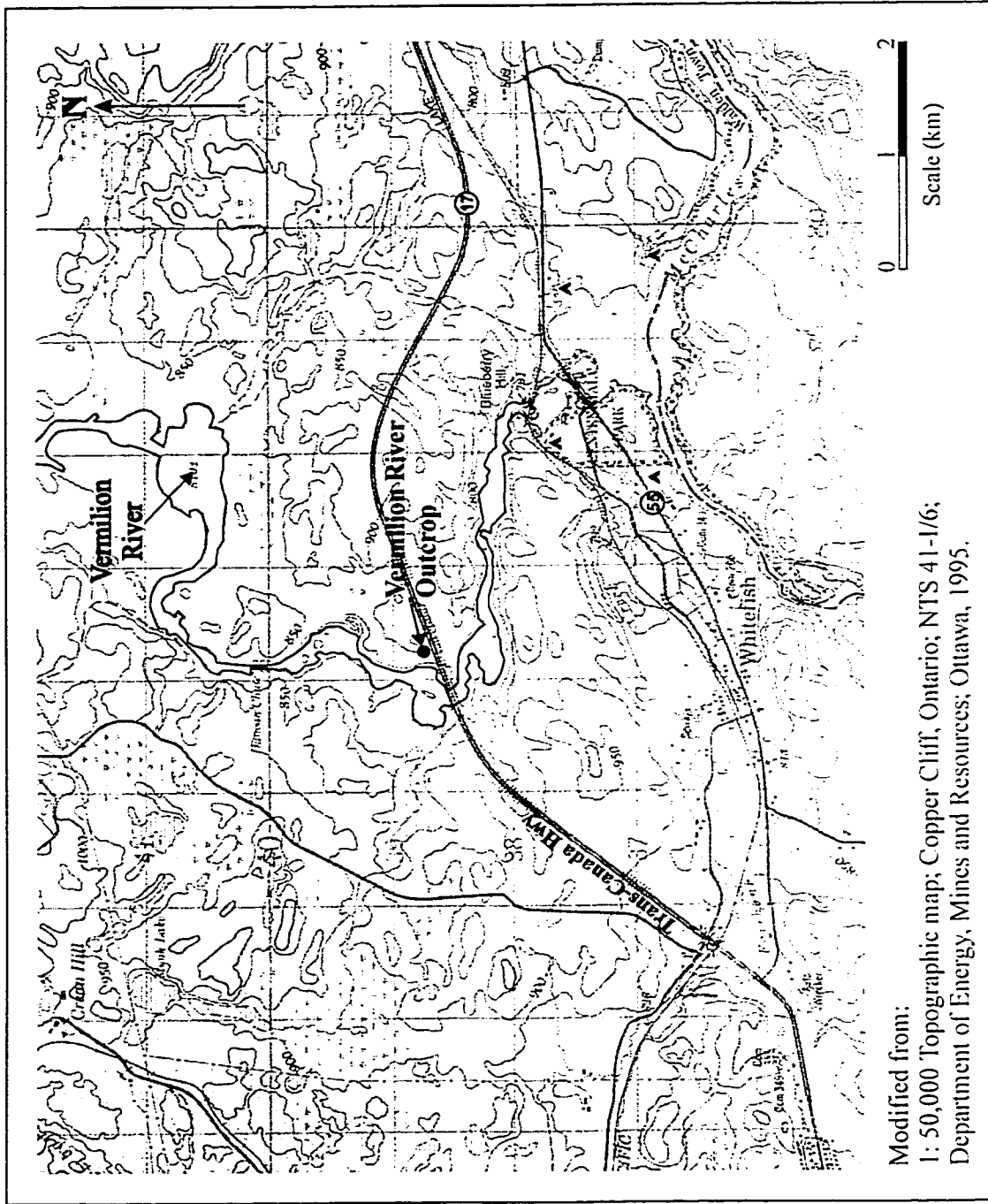
Figure 5-12 Location of Vermilion River Outcrop.

Modified from:
1: 50,000 Topographic map; Copper Cliff, Ontario; NTS 41-1/6;
Department of Energy, Mines and Resources; Ottawa, 1995.
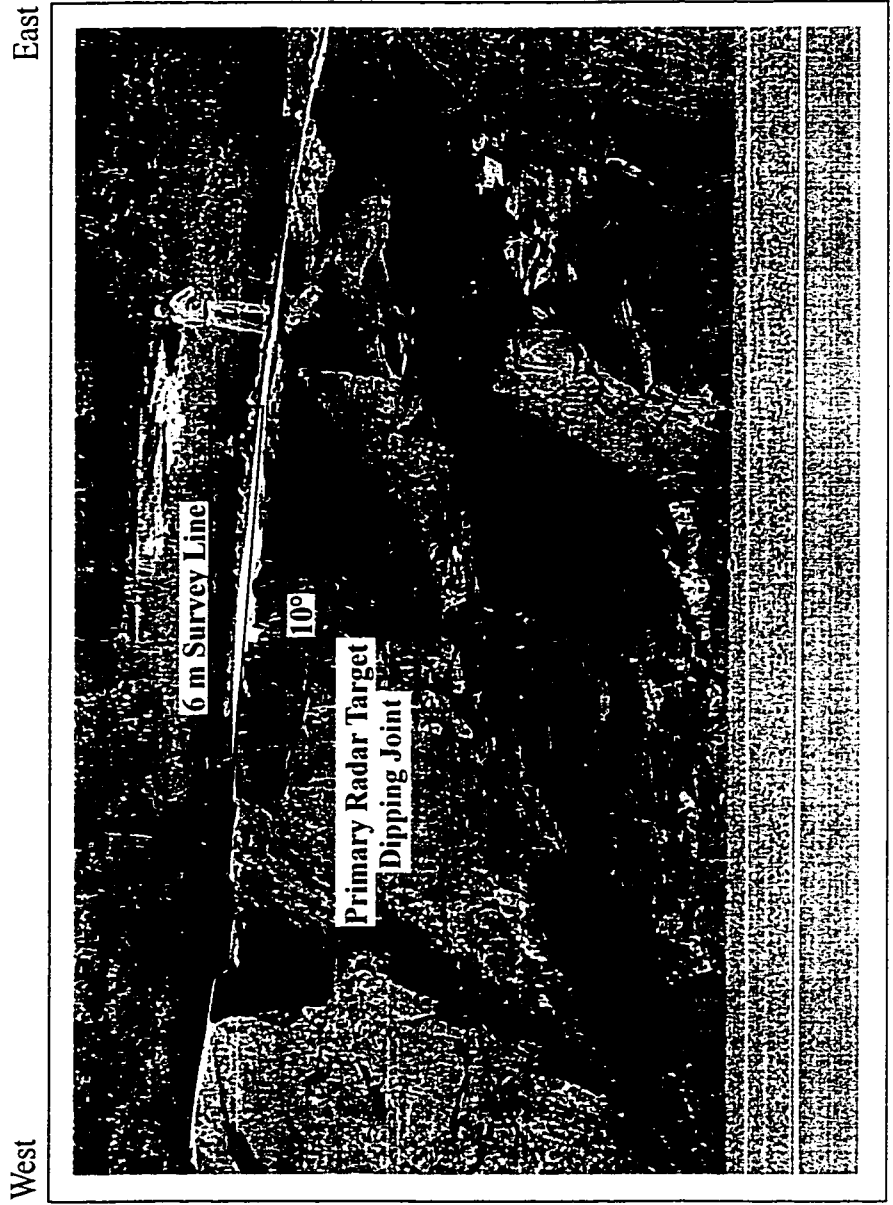
Figure 5-13 Digital photo of Vermillion River Outcrop.
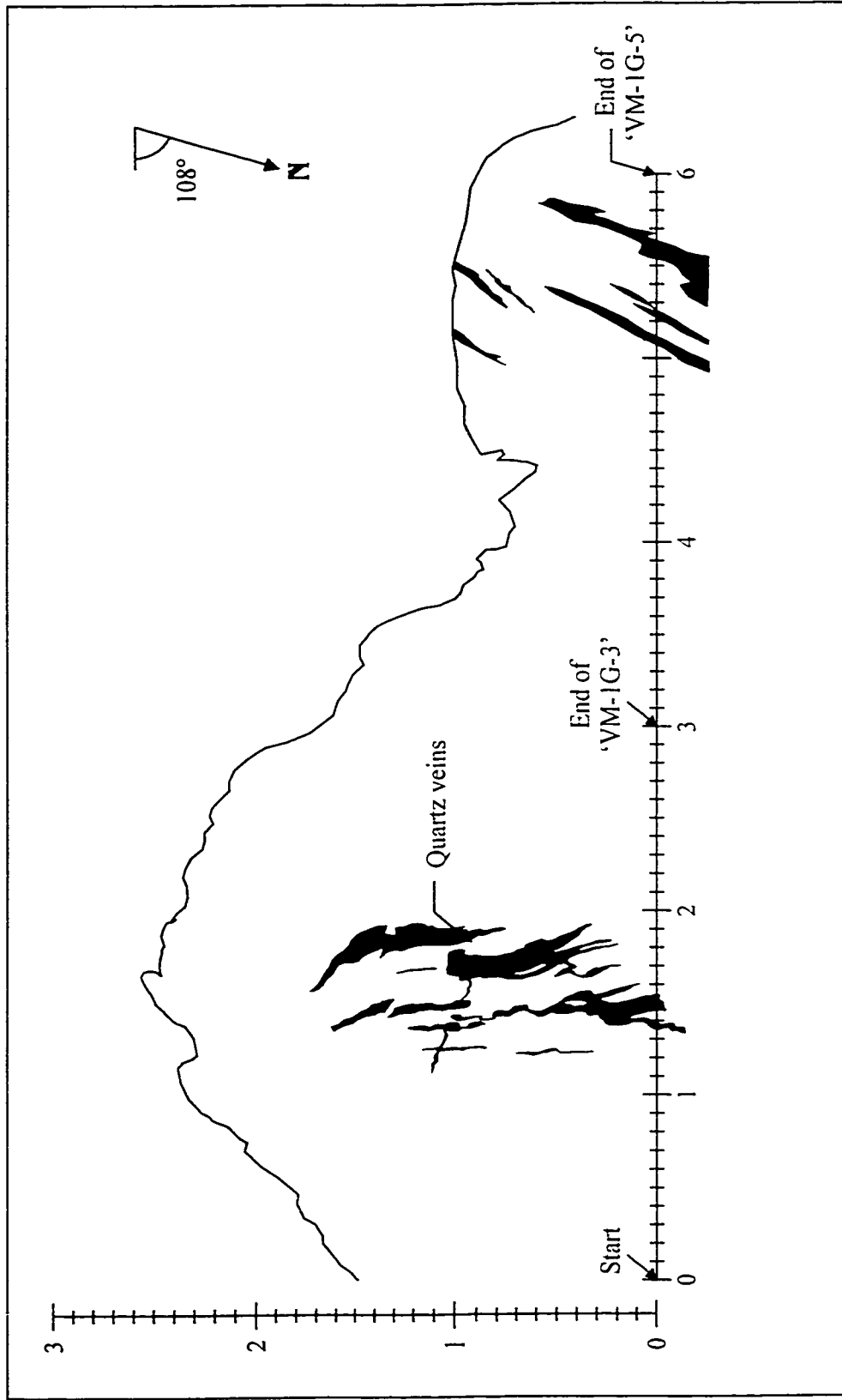
Figure 5-14 Sketch of the high frequency surveys lines at Vermilion River Outcrop - Plan view.
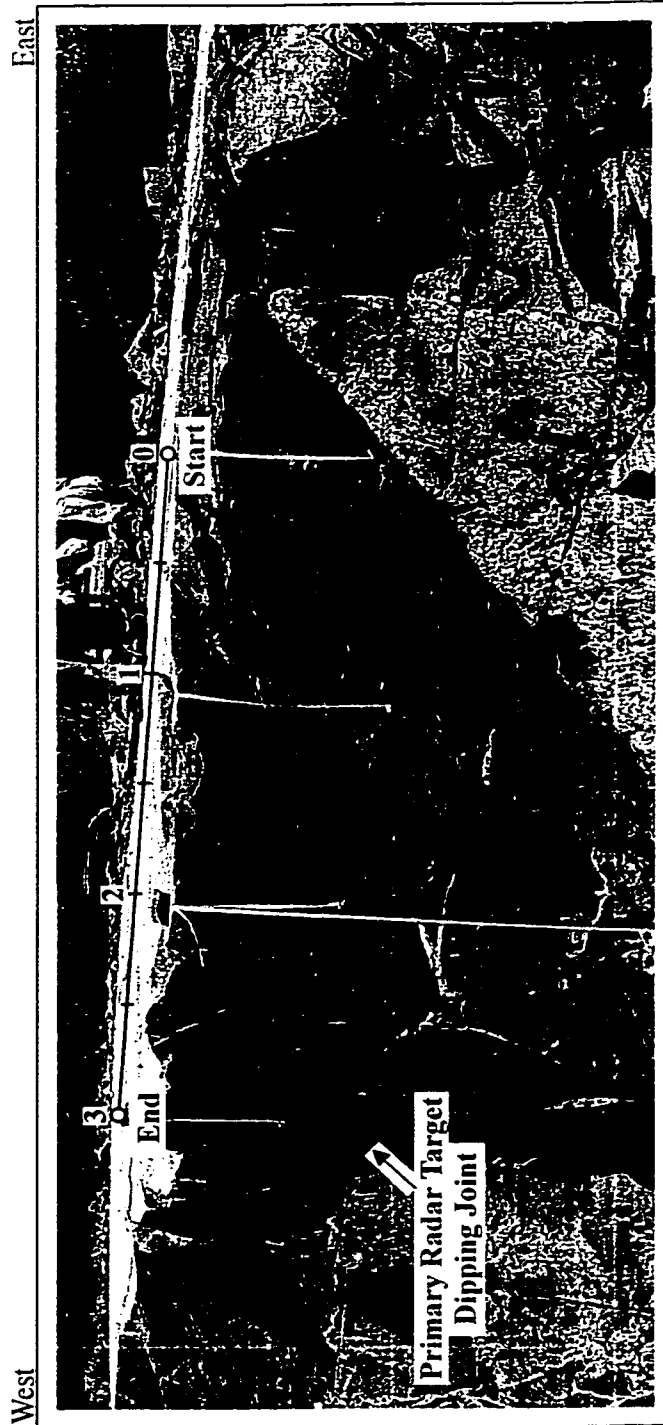
Figure 5-15 Digital photo of the high frequency survey line 'VM-1G-3' at Vermilion River Outcrop.
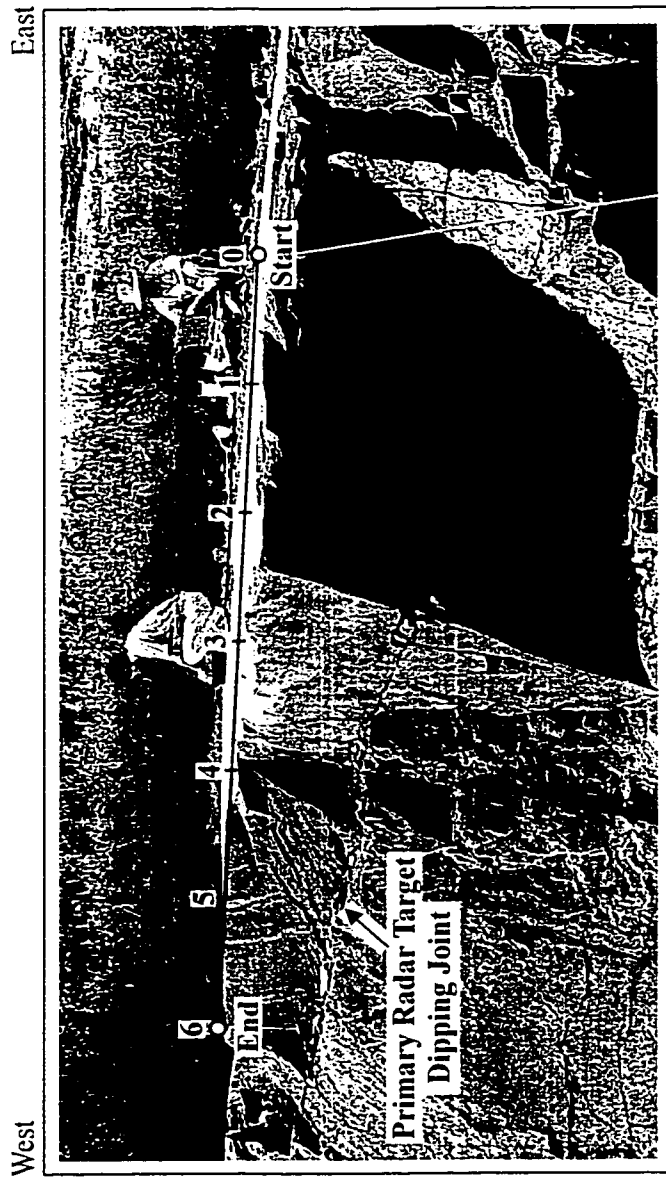
Figure 5-16 Digital photo of the high frequency survey line 'VM-1G-5' at Vermilion River Outcrop.
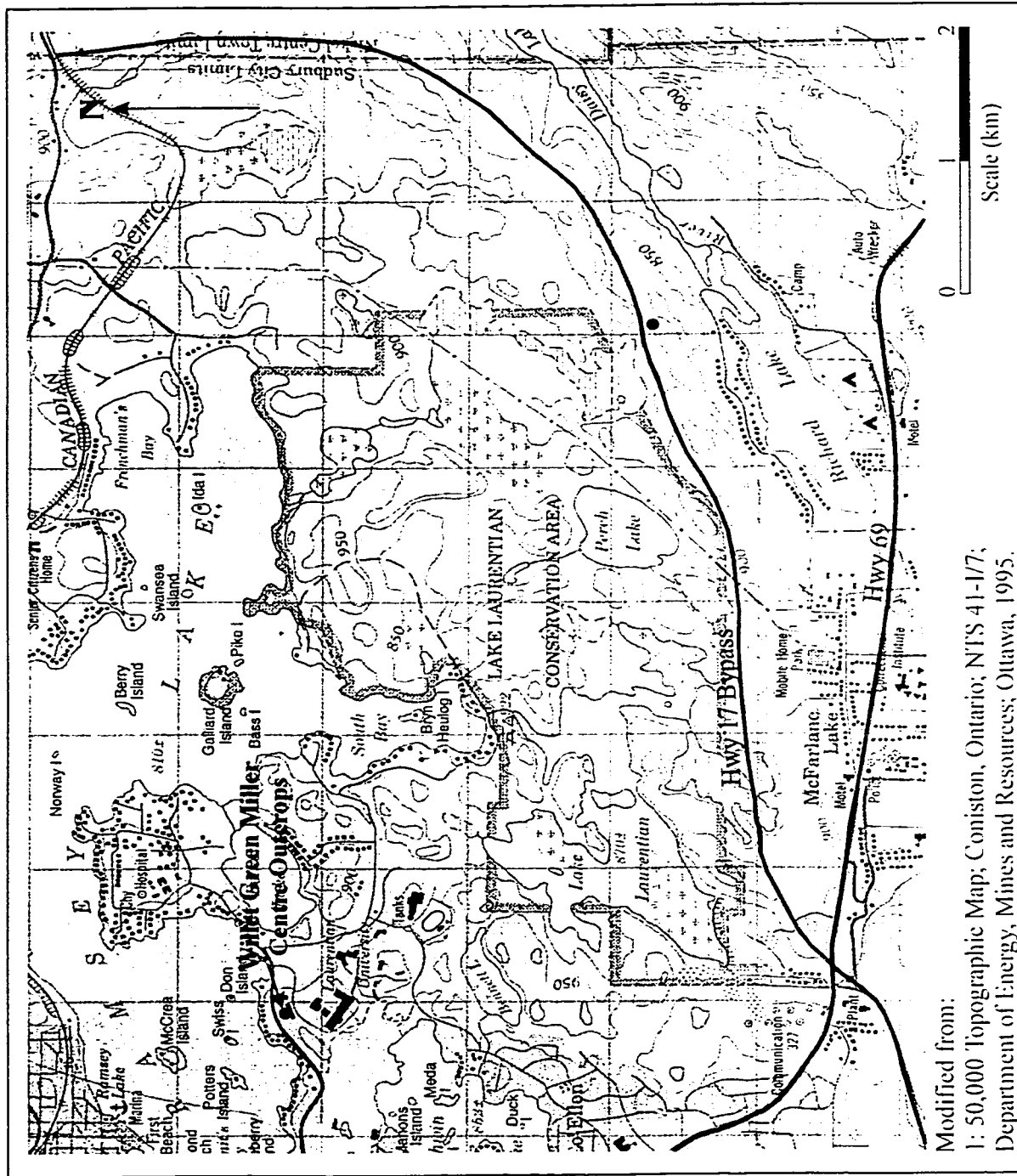
Figure 5-17 Location of Willet Green Miller Centre Outcrops.

Modified from:
1: 50,000 Topographic Map; Coniston, Ontario; NTS 41-I/7;
Department of Energy, Mines and Resources; Ottawa, 1995.

144
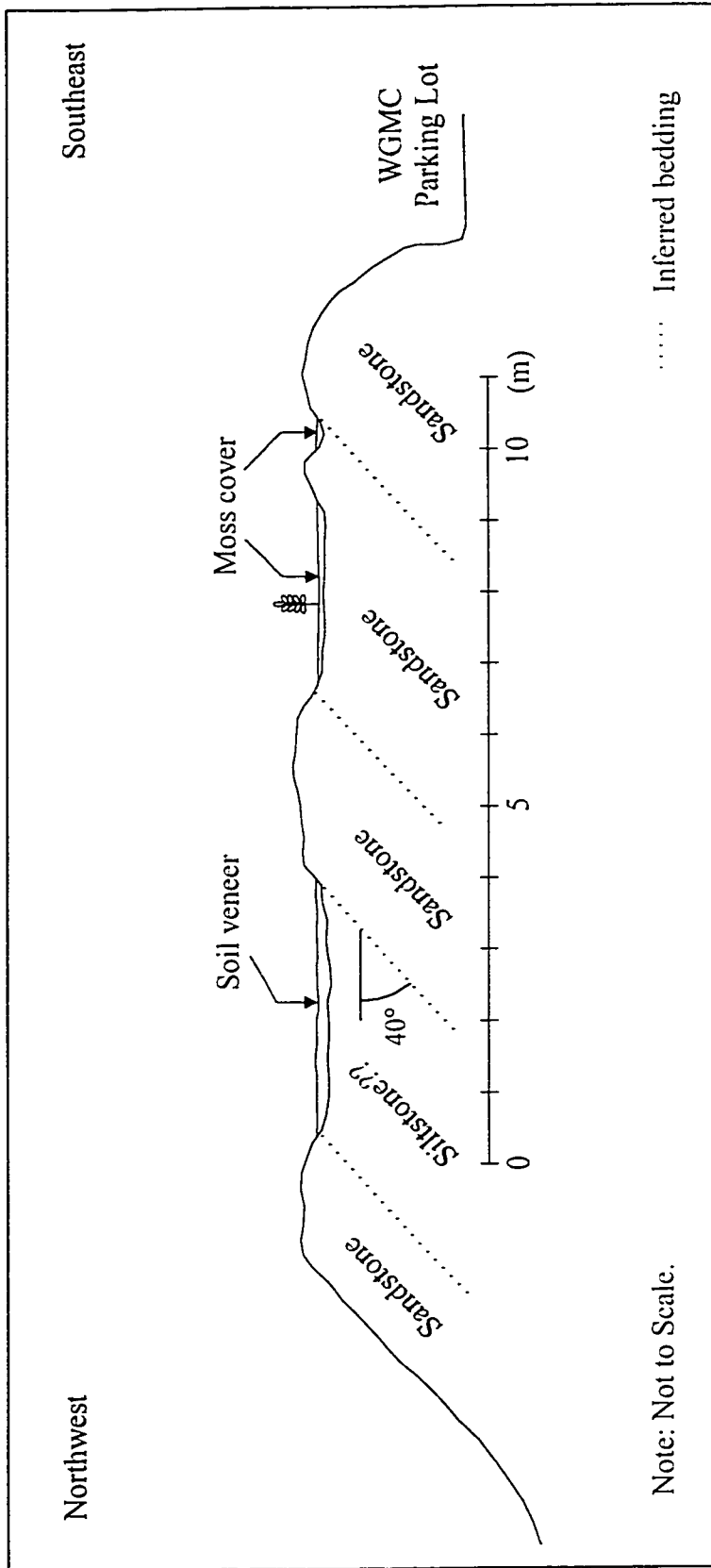
Figure 5-18 Cross-sectional sketch of WGMC Outcrop 1.
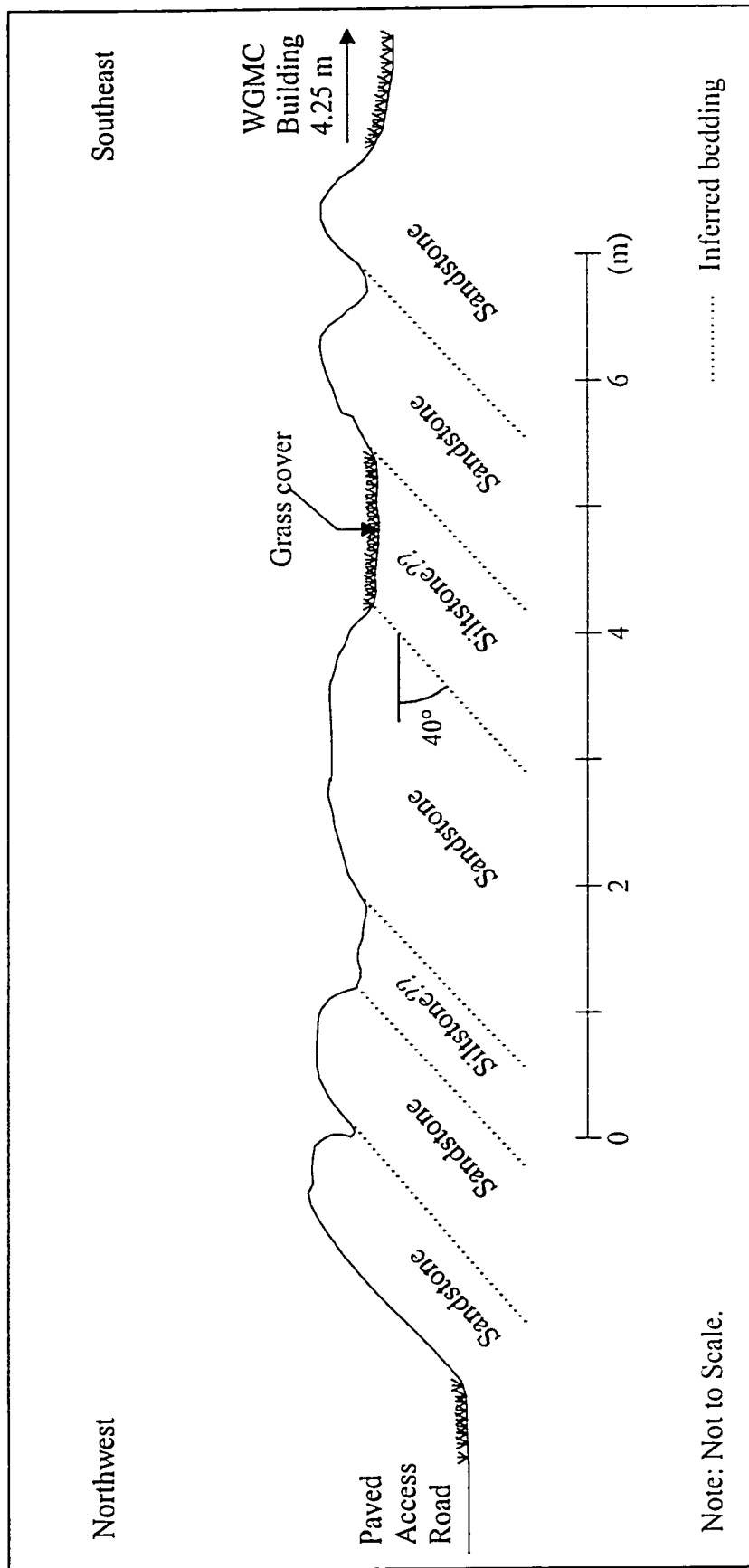
Figure 5-19 Cross-sectional sketch of WGMC Outcrop 2.

Northwest

Southeast

WGMC
Building
4.25 m

Grass cover

Paved
Access
Road

Sandstone

Siltstone??

Sandstone

Siltstone??

Sandstone

Sandstone

Sandstone

40°

0   2   4   6   (m)

.... Inferred bedding

Note: Not to Scale.
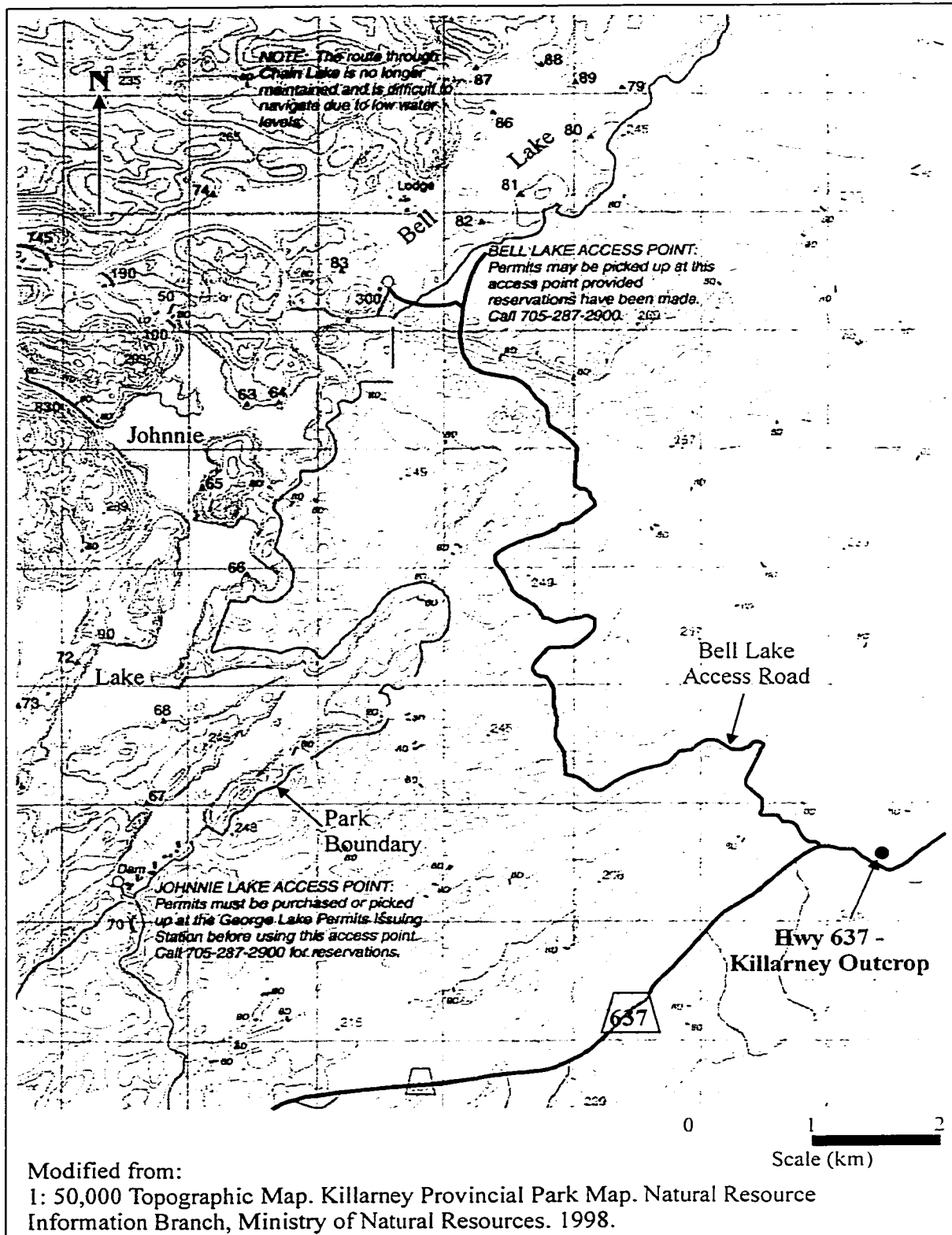
Figure 5-20 Location of Hwy 637-Killarney Outcrop.
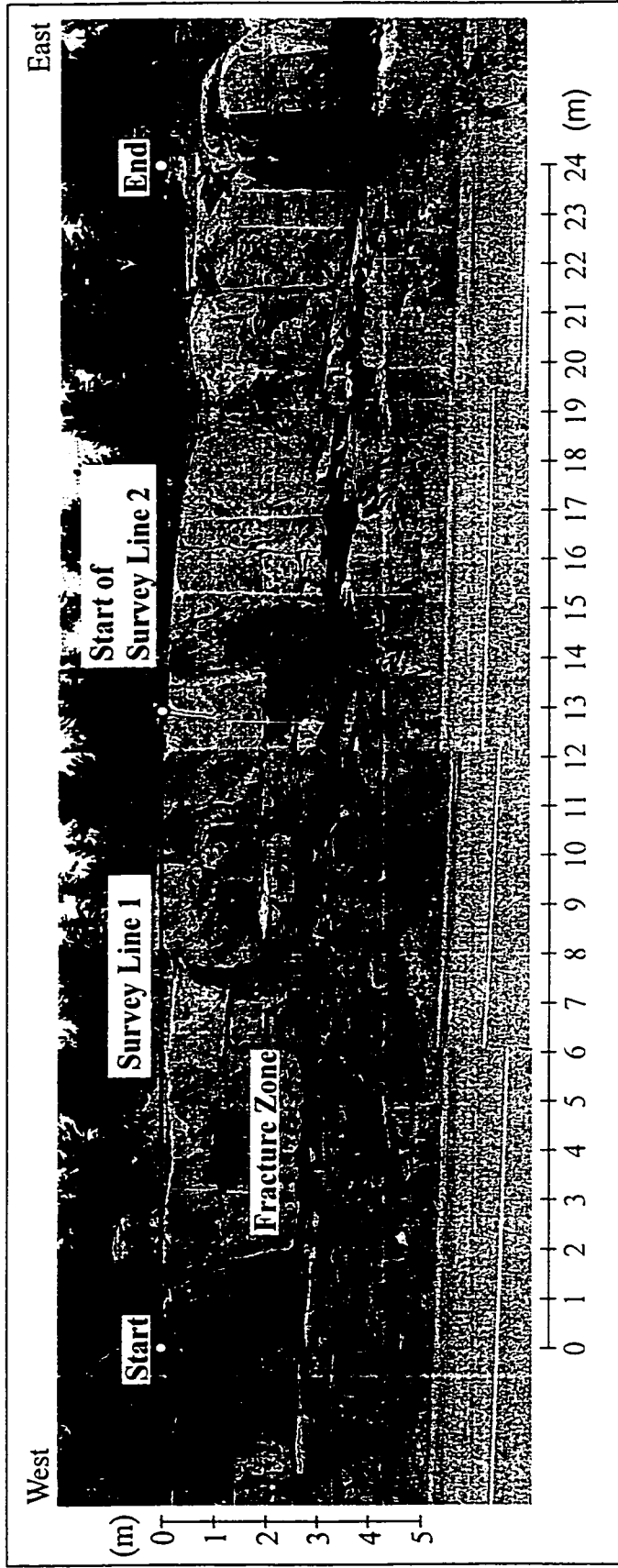
Figure 5-21 Digital photos of Hwy 637 - Killarney Outcrop; including Survey Line 1.
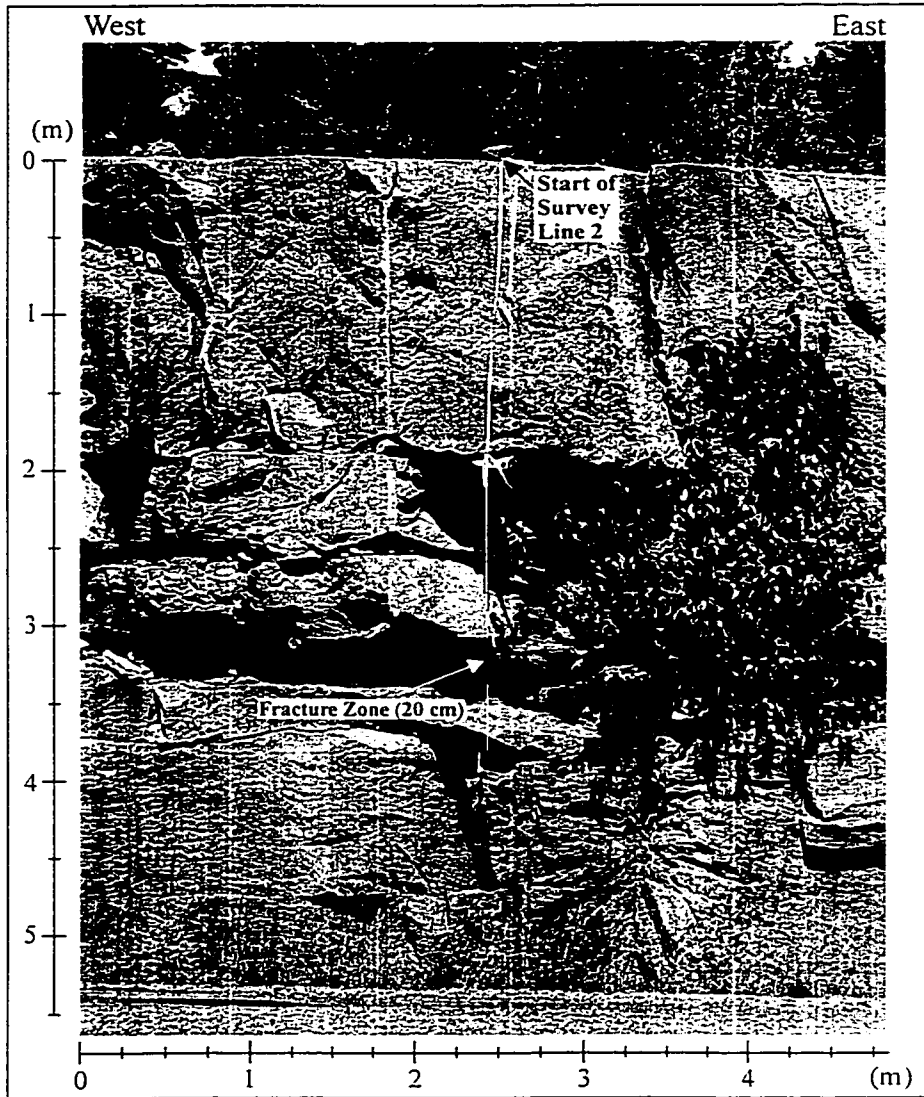
Figure 5-22 Close-up digital photo of Hwy 637-Killarney Outcrop;
including start of Survey Line 2.

Modified from:
1: 50,000 Topographic map; Coniston, Ontario; NTS 41-I/7;
Department of Energy, Mines and Resources; Ottawa, 1995.
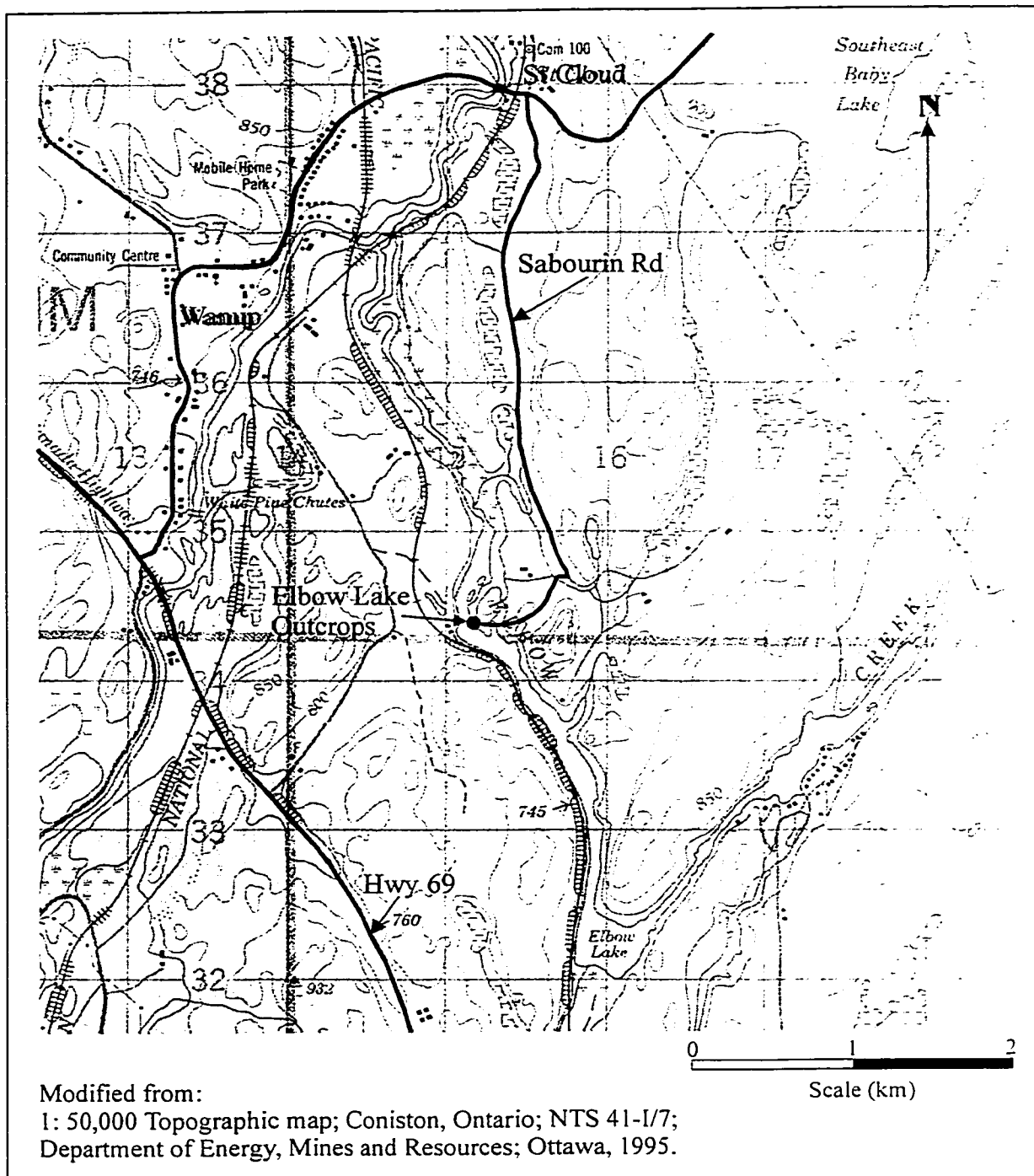
Figure 5-23 Location of Elbow Lake Outcrops.

Figure 5-24 Digital photos of Elbow Lake Outcrop 1.
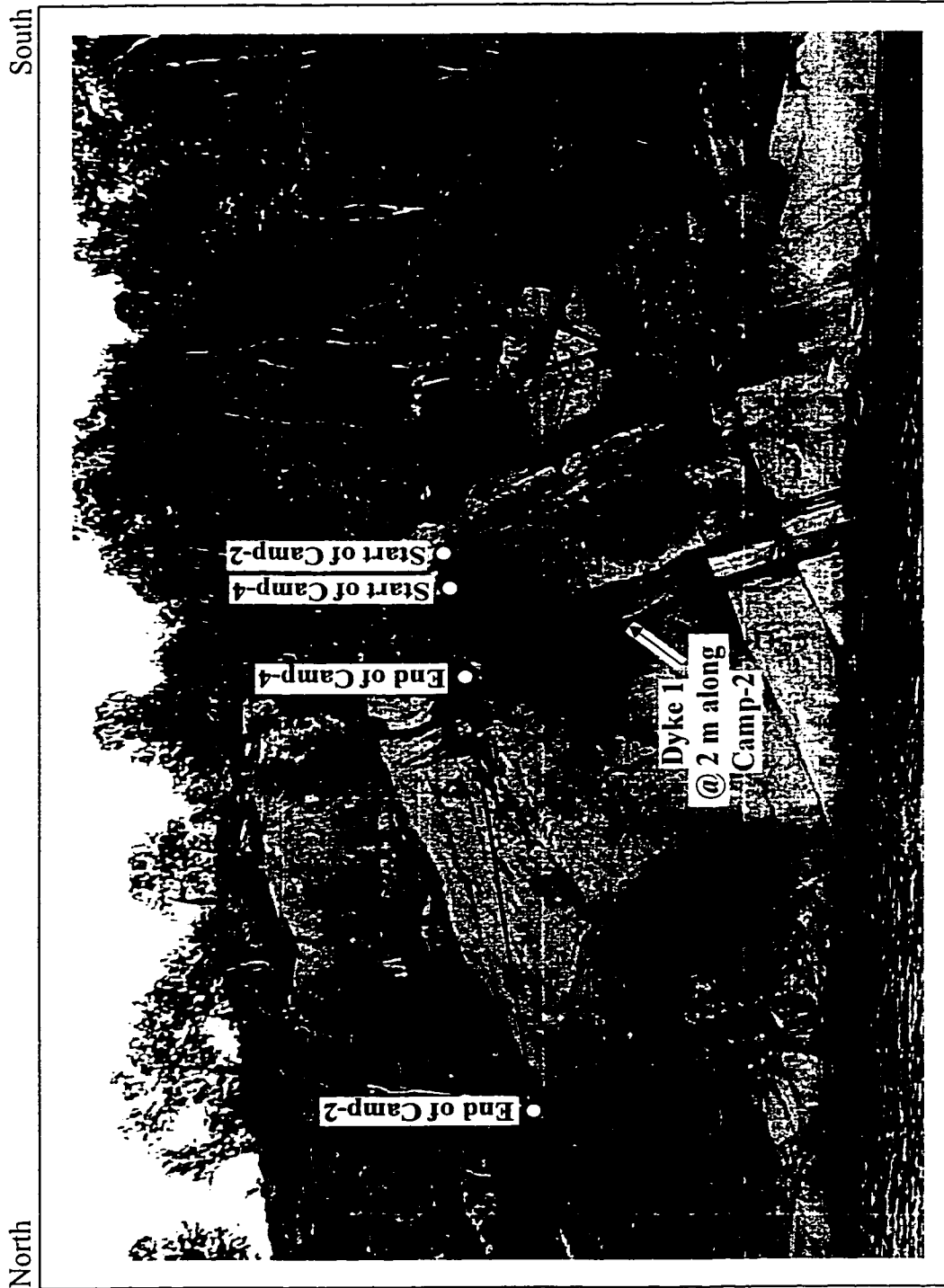
Figure 5-25 Digital photo of Elbow Lake Outcrop 2.

South

North

End of Camp-2

End of Camp-4

Start of Camp-4

Start of Camp-2

Dyke 1
@ 2 m along
Camp-2

Figure 5-26 Digital photo of the high frequency survey line 'Camp-4' at Elbow
Lake Outcrop 2.

Northeast

Southwest
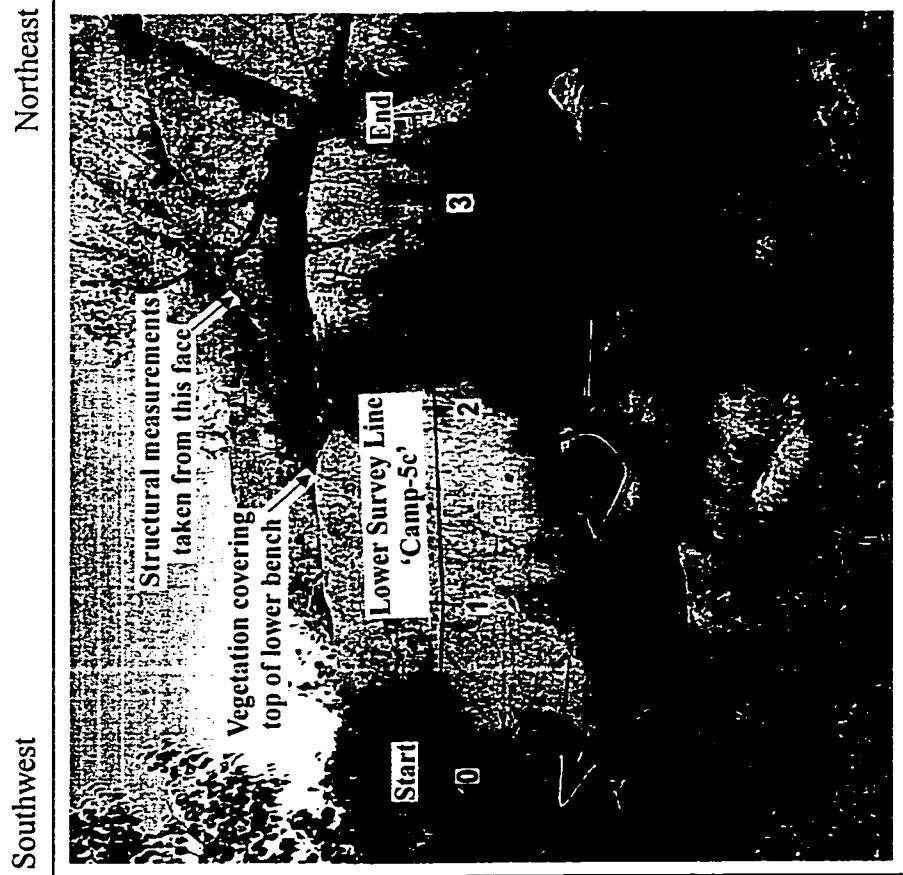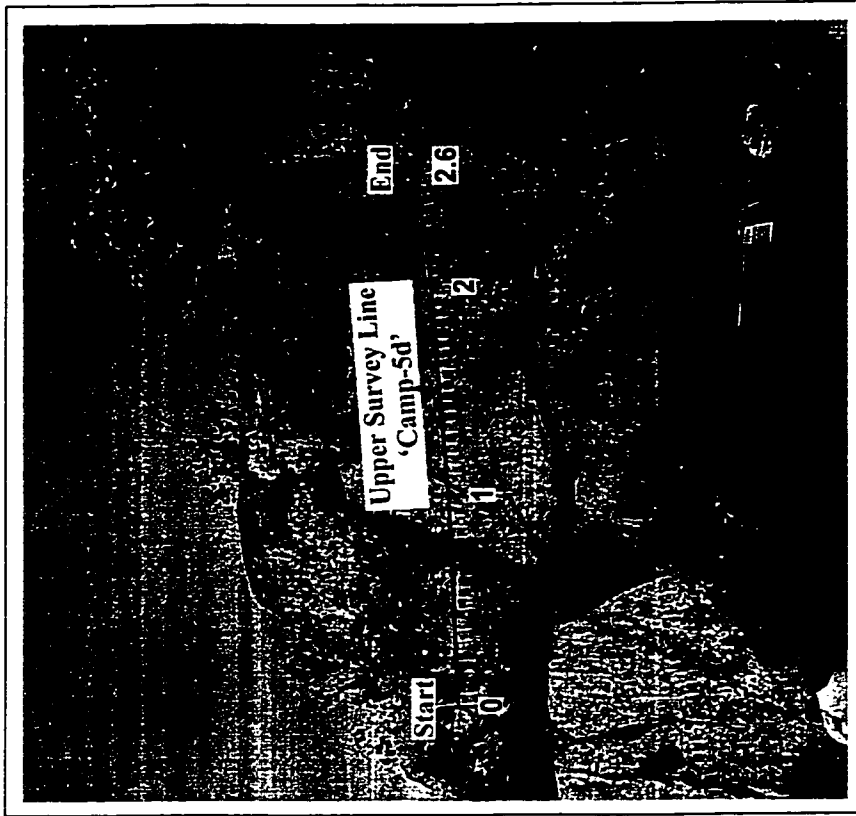
Figure 5-27 Digital photos of Elbow Lake Outcrop 3.
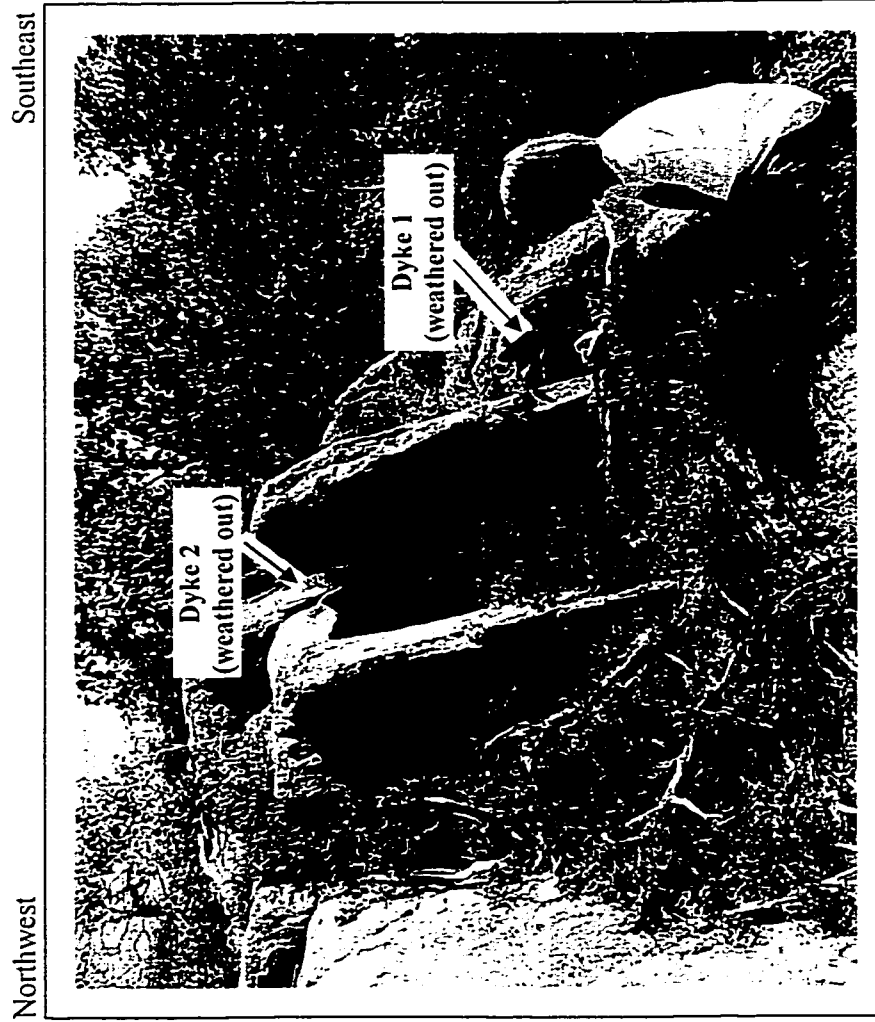
Figure 5-28 Digital photo of rock structure for upper survey line at Elbow Lake Outcrop 3.

155
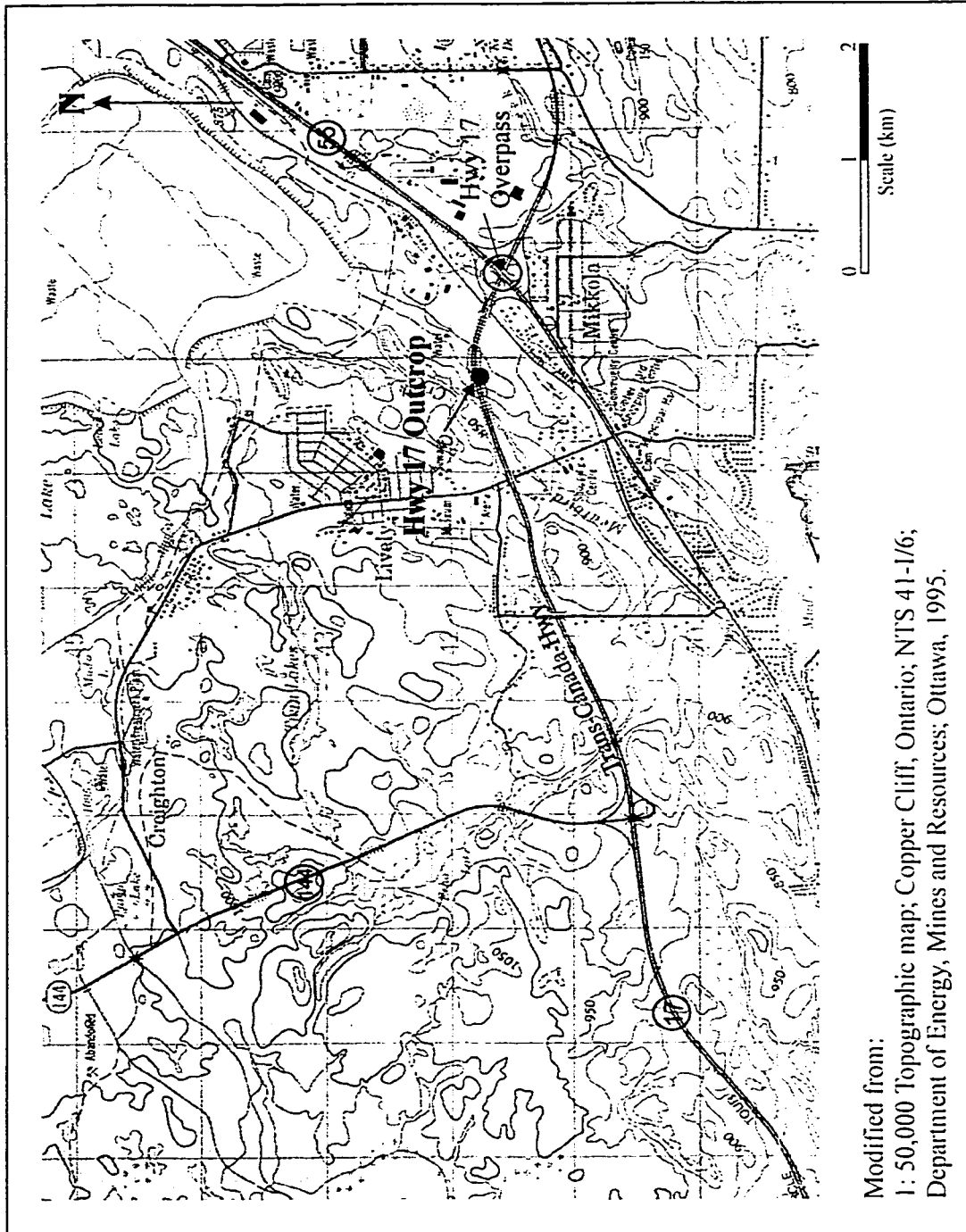
Figure 5-29 Location of Hwy 17 Outcrop.

Modified from:
1: 50,000 Topographic map; Copper Cliff, Ontario; NTS 41-I/6;
Department of Energy, Mines and Resources; Ottawa, 1995.

156

South

North

JS 1 = 080/56

1.6 m

JS3 = 235/10

JS2 = 180/90

2.1 m
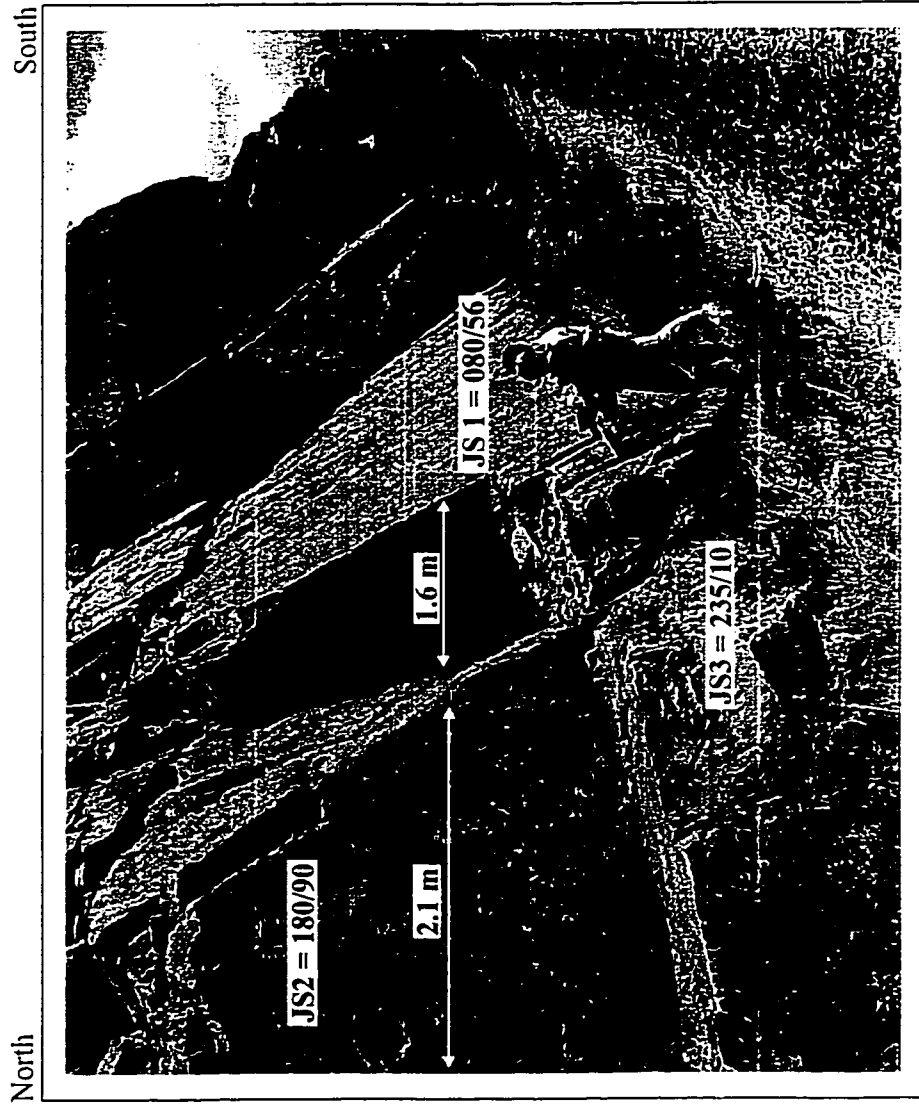
Figure 5-30 Digital photo of Hwy 17 Outcrop.

157

North   South
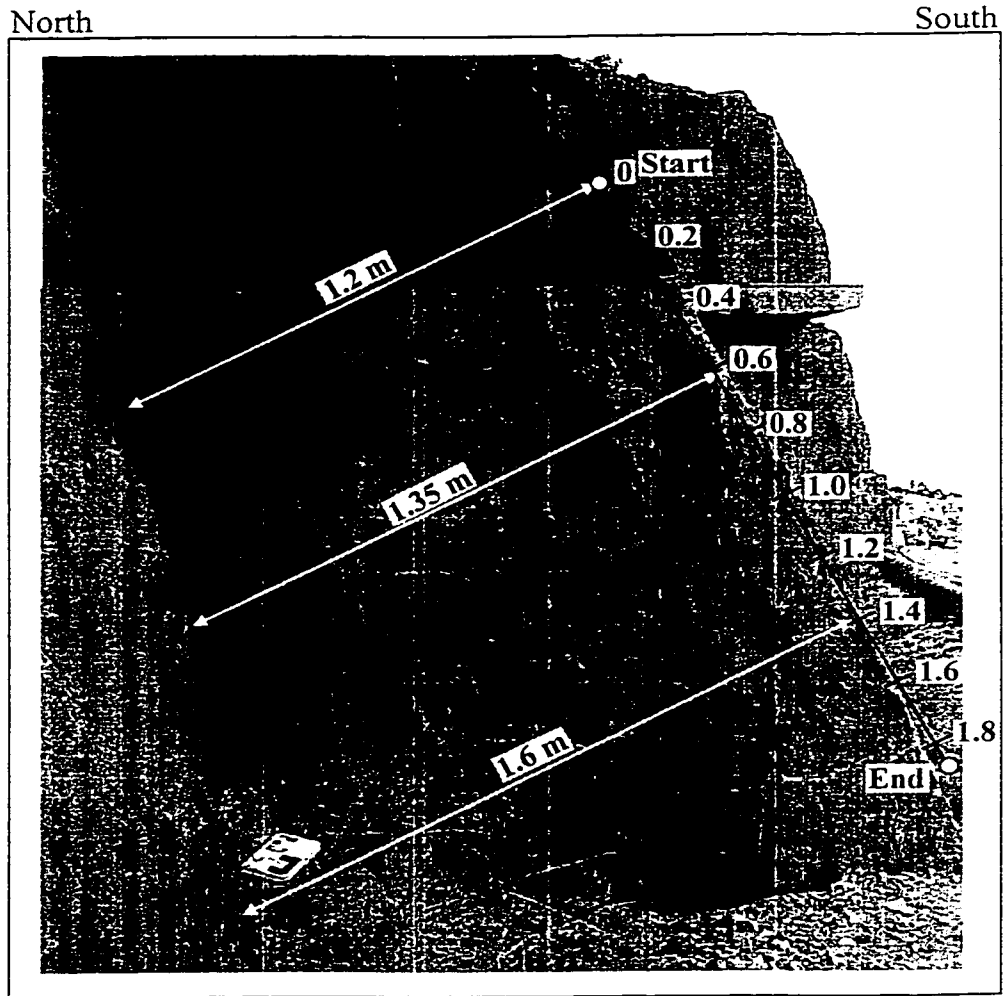
Figure 5-31 Digital photo of high frequency survey line at Hwy 17 Outcrop.
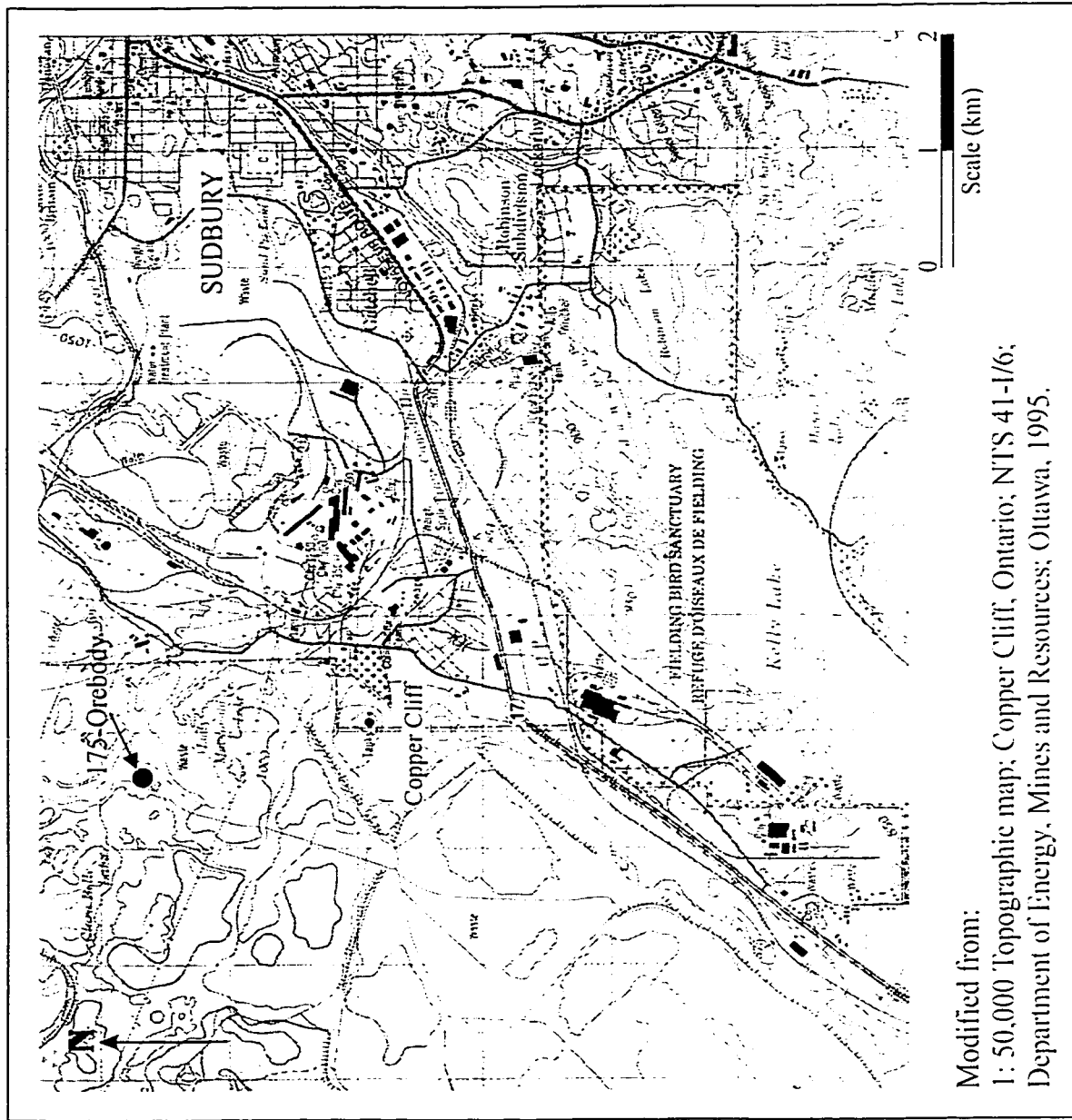
Modified from:
1 : 50,000 Topographic map: Copper Cliff, Ontario; NTS 41-1/6;
Department of Energy, Mines and Resources; Ottawa, 1995.

Figure 5-32 Location of 175-Orebody.

159
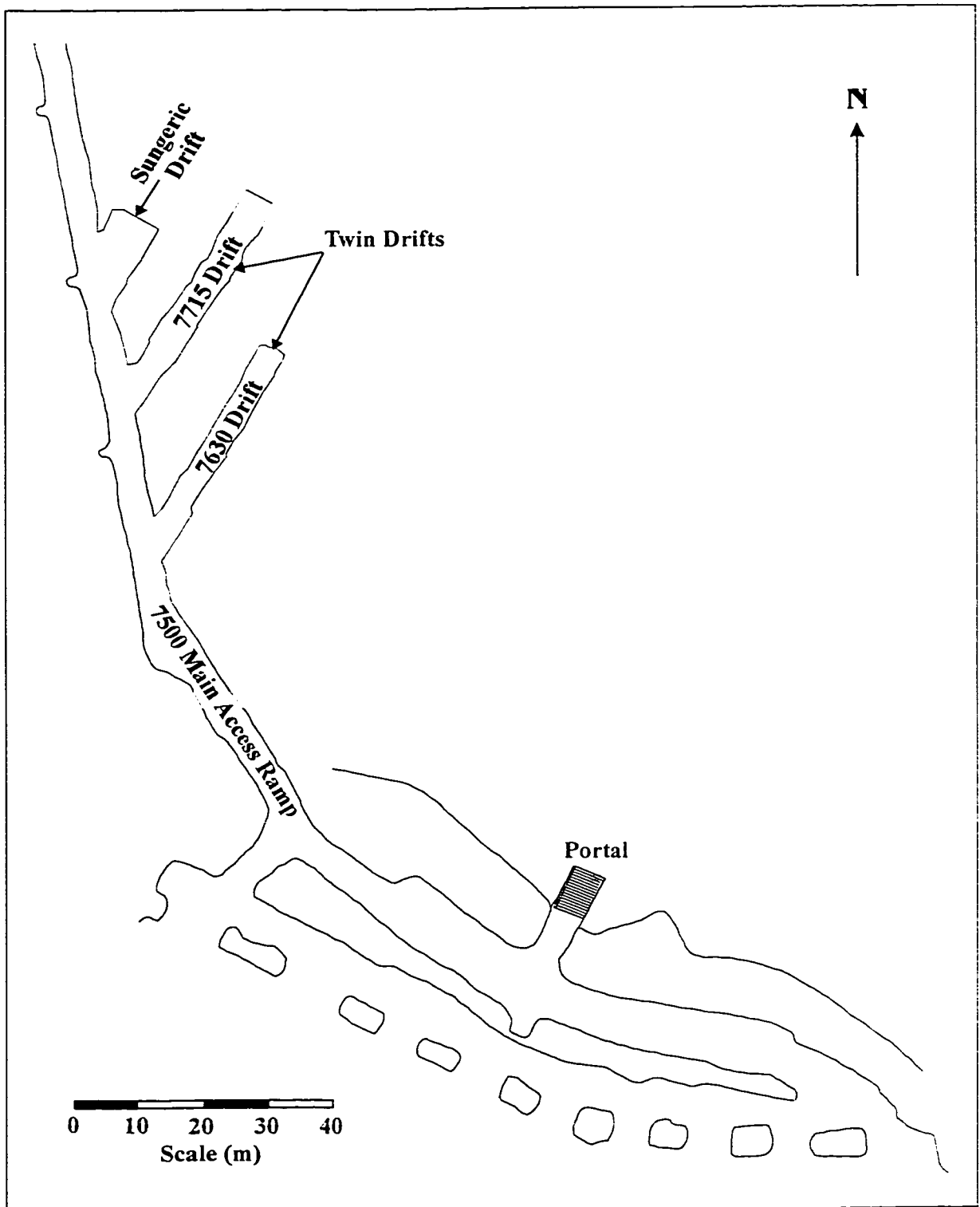
Figure 5-33 Section of 175-Orebody.

160

LEGEND

- ■ Sudbury Igenous Complex
- ▨ Nipissing Diabase
- ⊞ Creighton Pluton
- ▤ Quartzite and Conglomerate
- ▦ McKim Greywacke
- ▨ Felsic and Mafic Metavolcanics
- ⌇ Fault
- ⌇ Olivine Diabase
- ⌇ Quartz Diabase
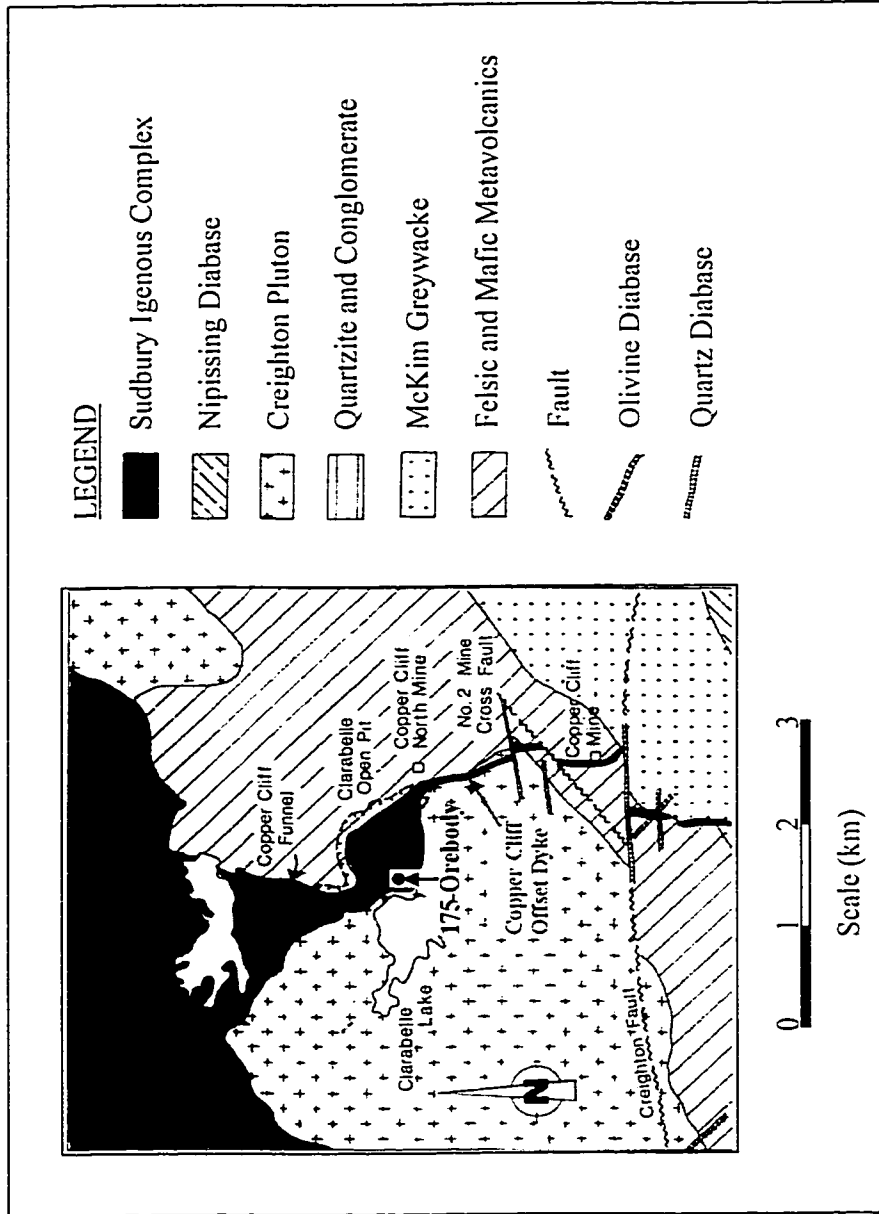
Figure 5-34 Copper Cliff Offset Dyke. Modified from Cochrane, 1984.

161
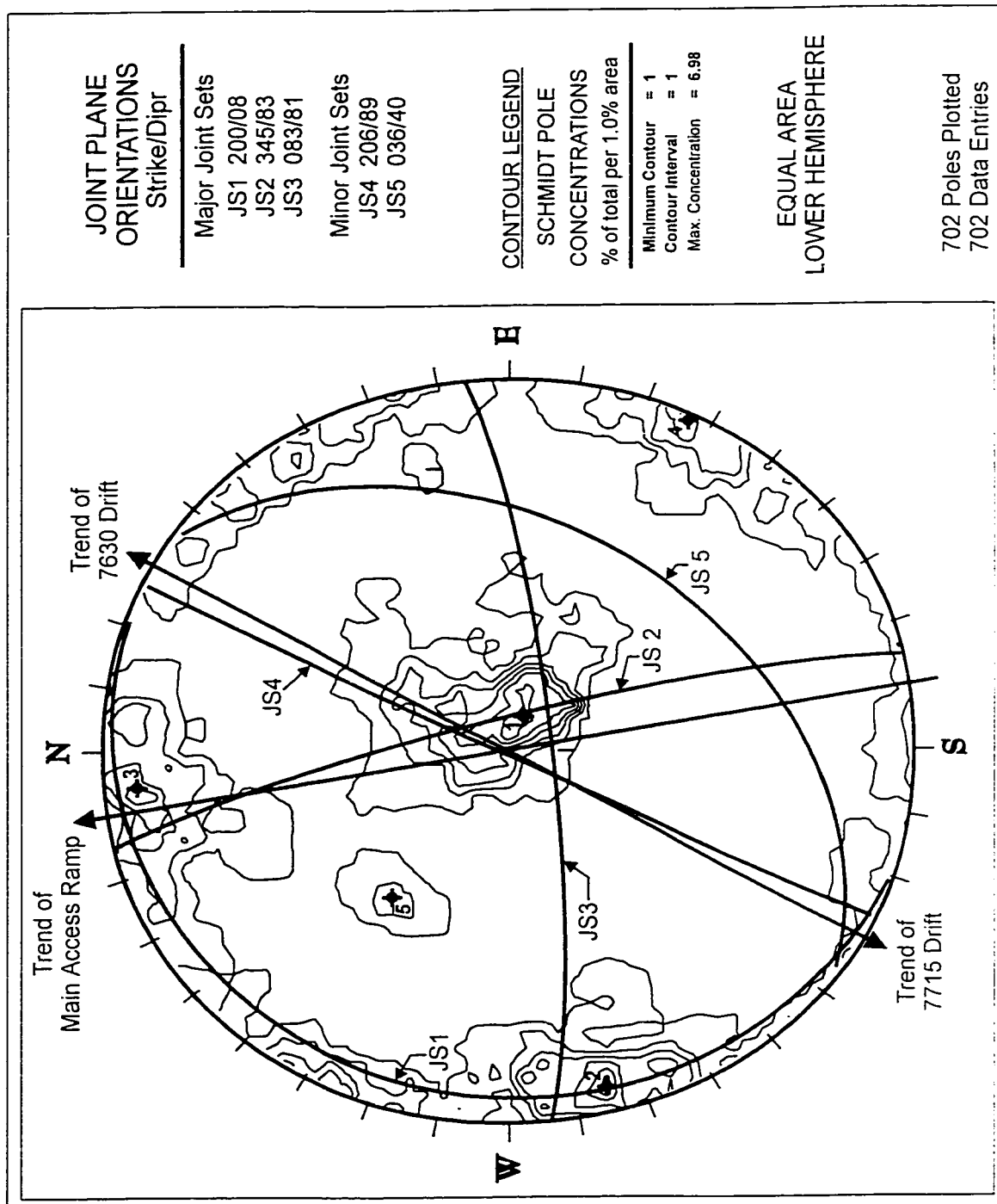
Figure 5-35 Stereonet of joint sets at 175-Orebody.

PLAN VIEW OF JOINT (STRIKE) ORIENTATIONS IN WALLS OF 7715 DRIFT

N 30°

NE
(End of Drift)

JS5

JS4

JS3

7715 Drift

JS2

JS1

SW
(Start of Drift)

JS5

JS4

JS3

JS2

JS1

IMAGE OF JOINT (STRIKE) ORIENTATIONS RADARGRAMS

Rock Face

JS5   6°   4°   JS4

JS3   39°

35°   JS2

10°   JS1

Depth

Radargram dip, $\alpha_R = 10°$	$\alpha_R = 35°$	$\alpha_R = 39°$	$\alpha_R = 4°$ $\alpha_R = 6°$
Actual Dip, $\alpha_A = 10°$	$\alpha_A = 45°$	$\alpha_A = 53°$	$\alpha_A = 4°$ $\alpha_A = 6°$
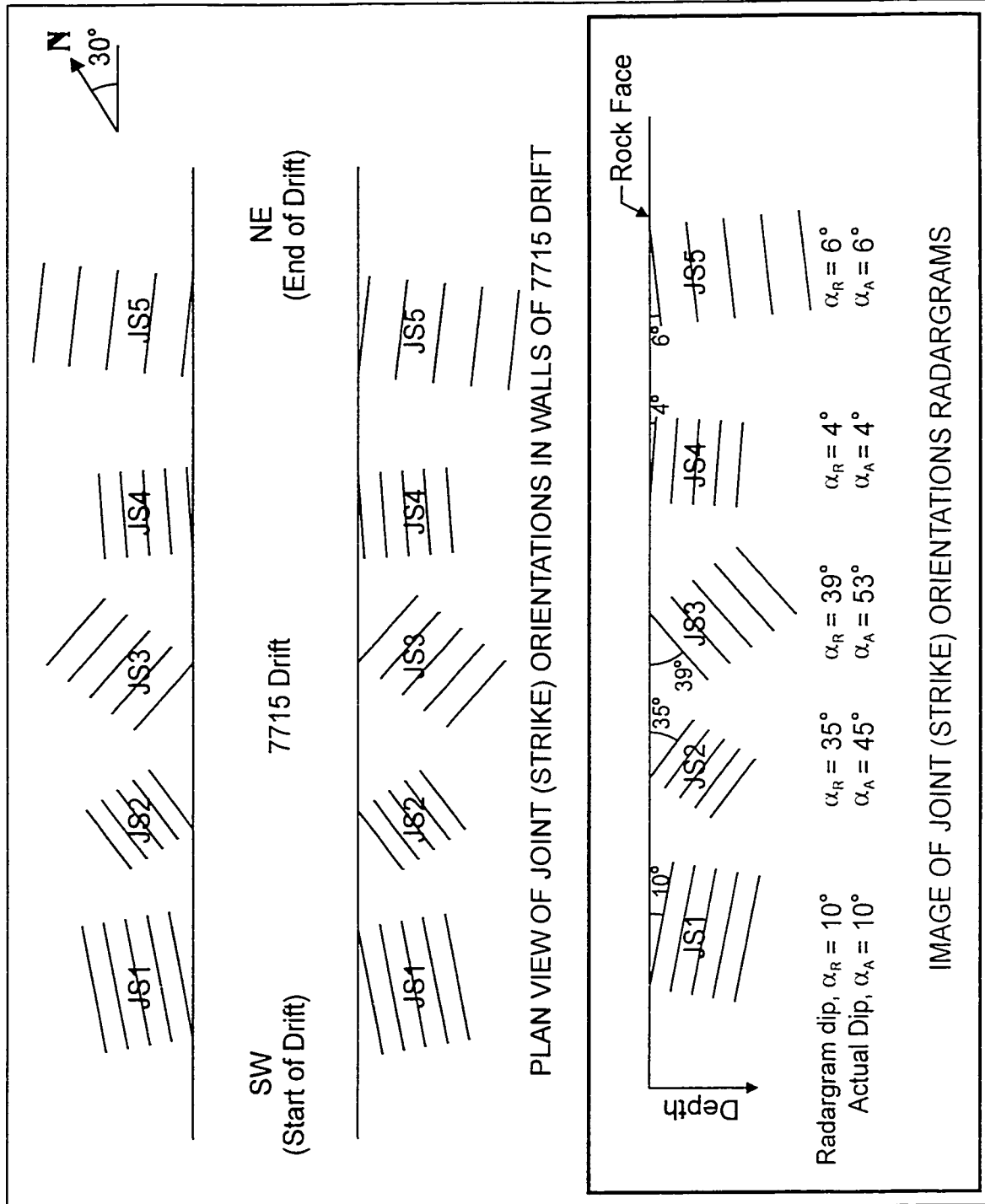
Figure 5-36 Images of joints in 7715 Drift - Plan view & radargram image.

163
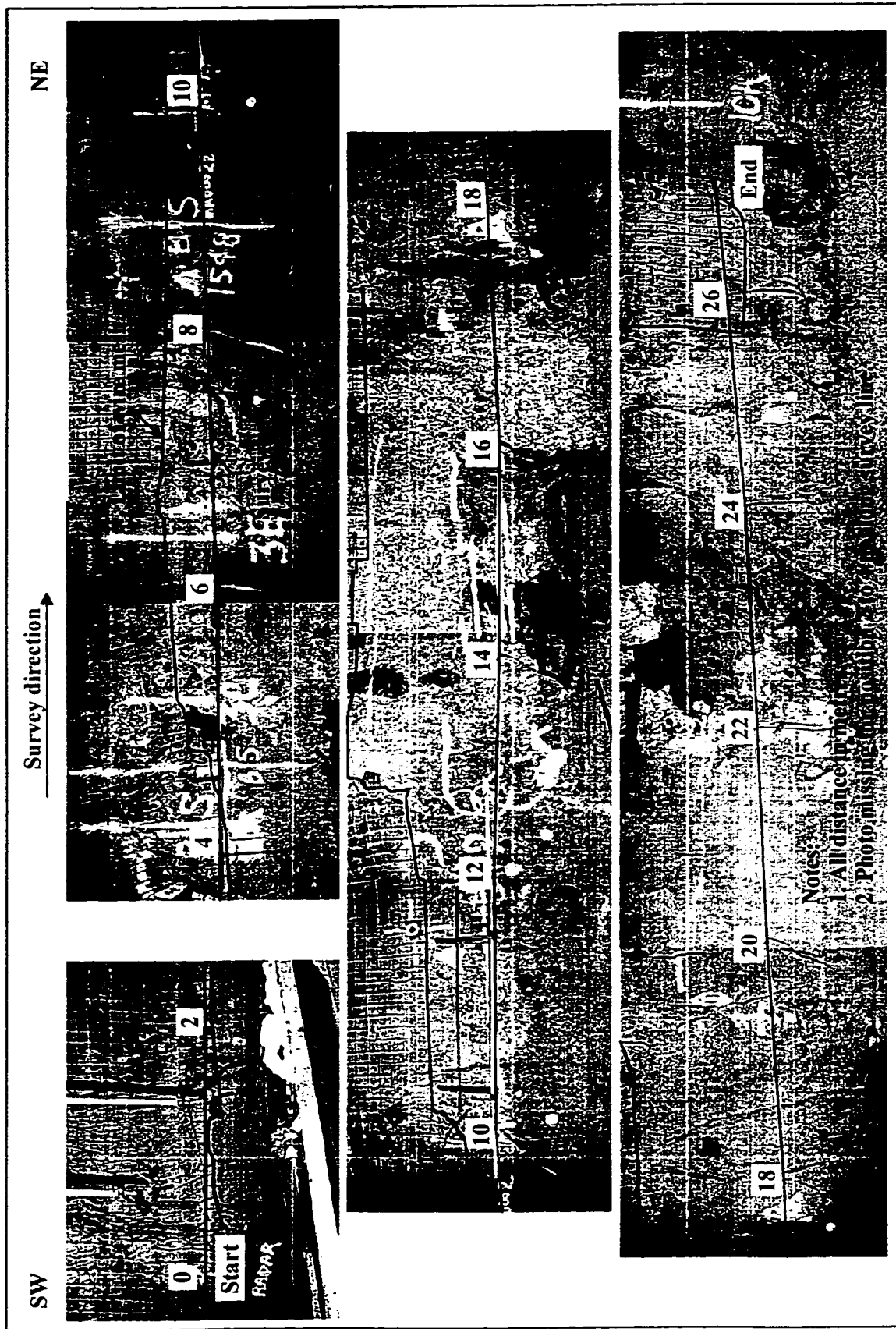
Figure 5-37 Digital photos of NW Sidewall; including low frequency survey line.

164
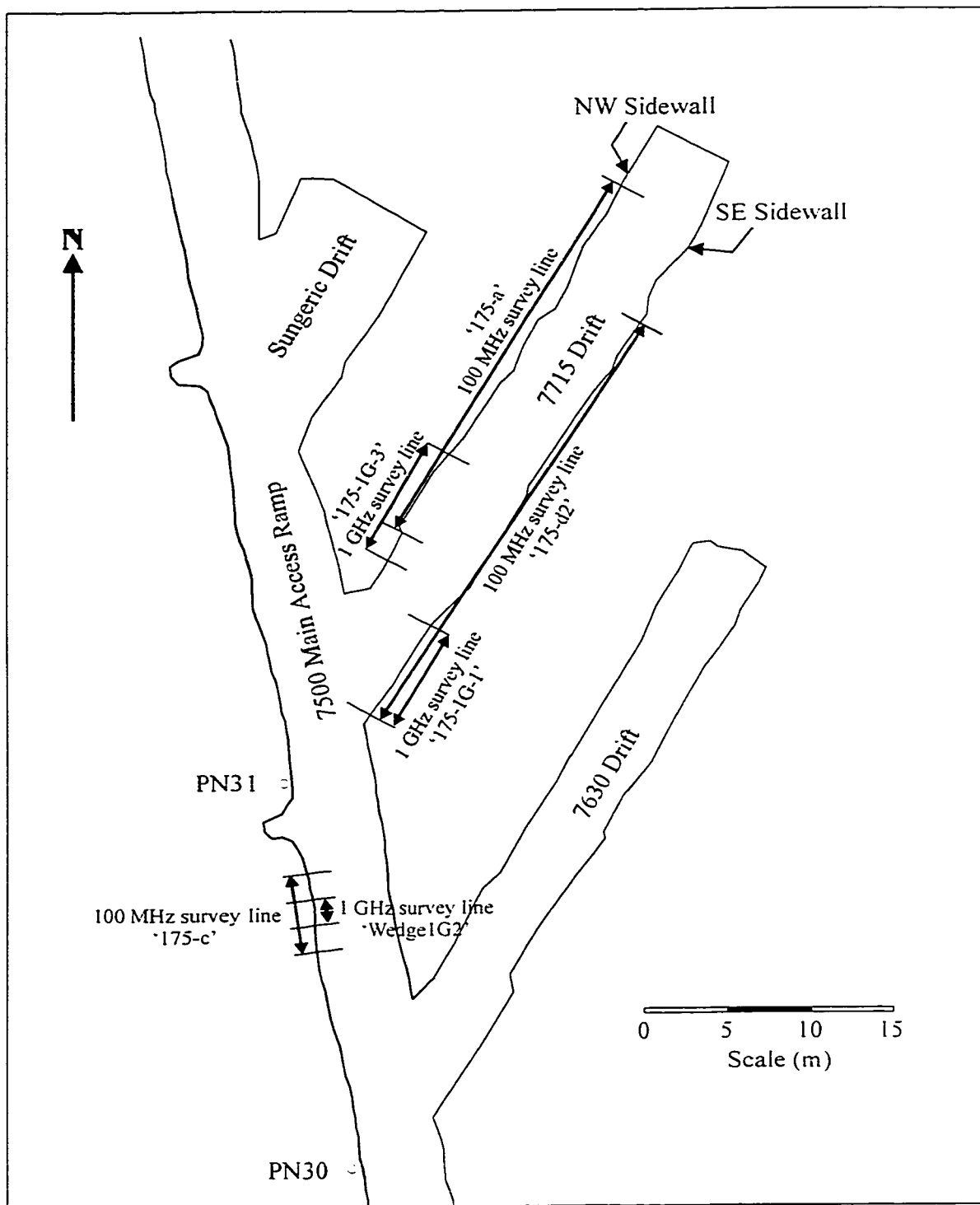
Figure 5-38 High and low frequency survey lines at 175-Orebody.
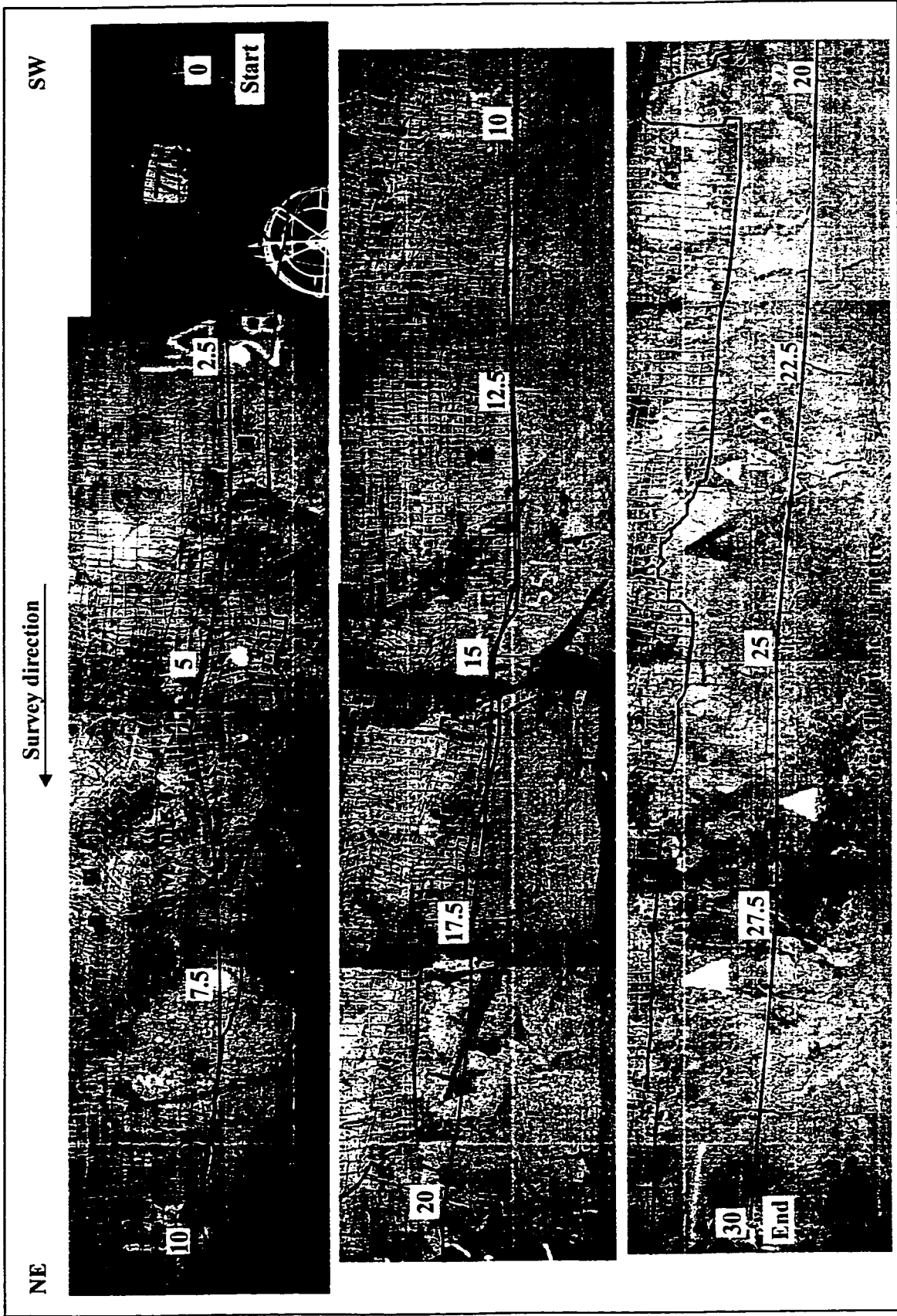
Figure 5-39 Digital photos of SE Sidewall; including low frequency survey line.

166
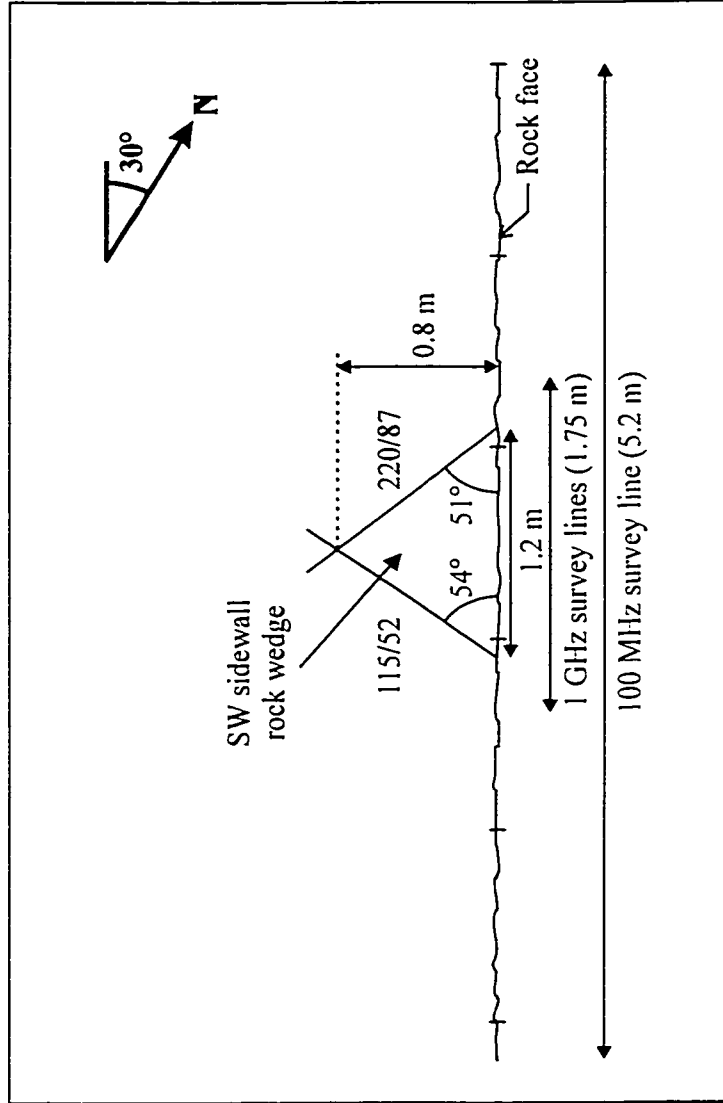
Figure 5-40 Plan view sketch of wedge in SW sidewall of 7500 Main Access Ramp; including locations of the low and high frequency survey lines.
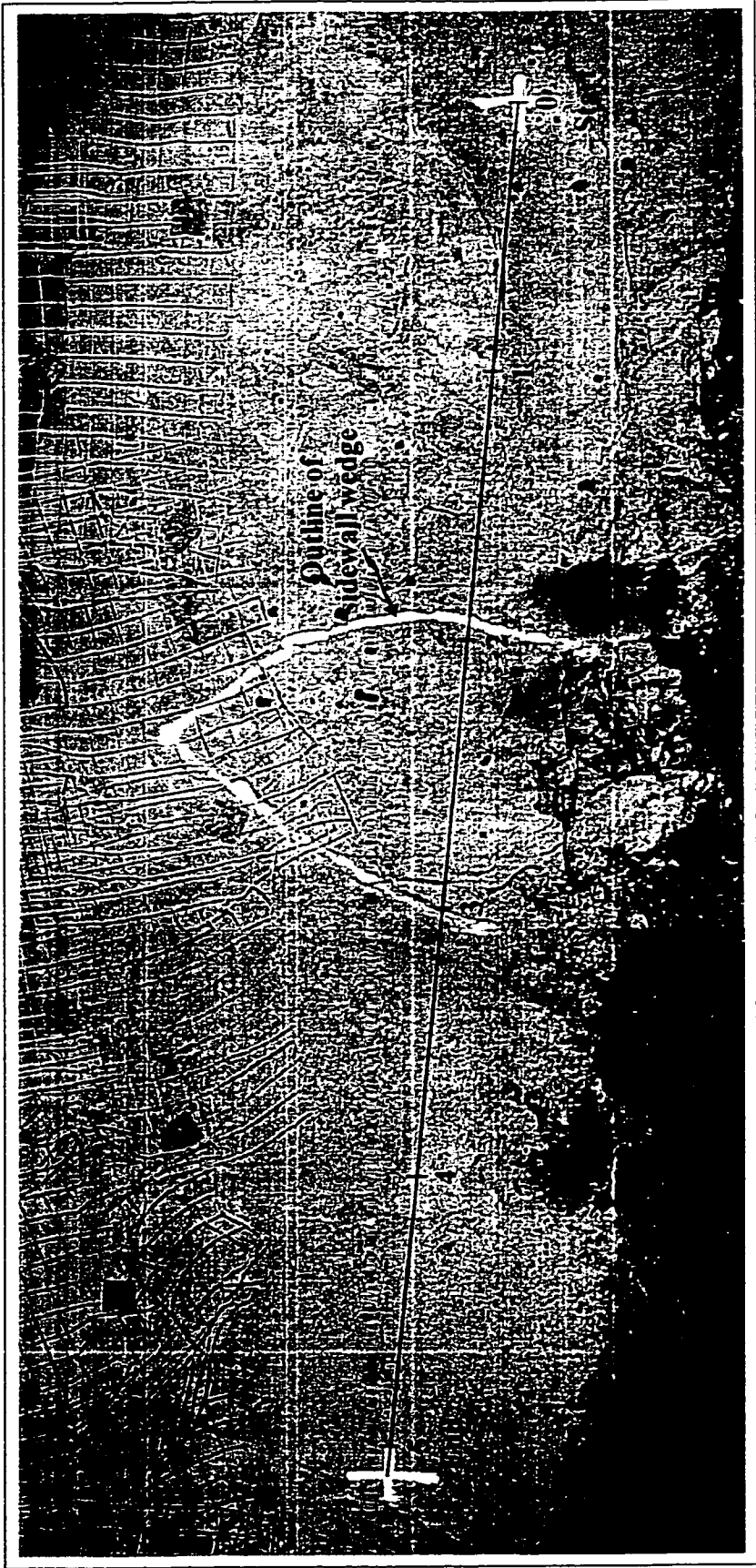
Figure 5-41 Digital photos of low frequency survey line ('175-c') across wedge in 7500 Main Access Ramp.
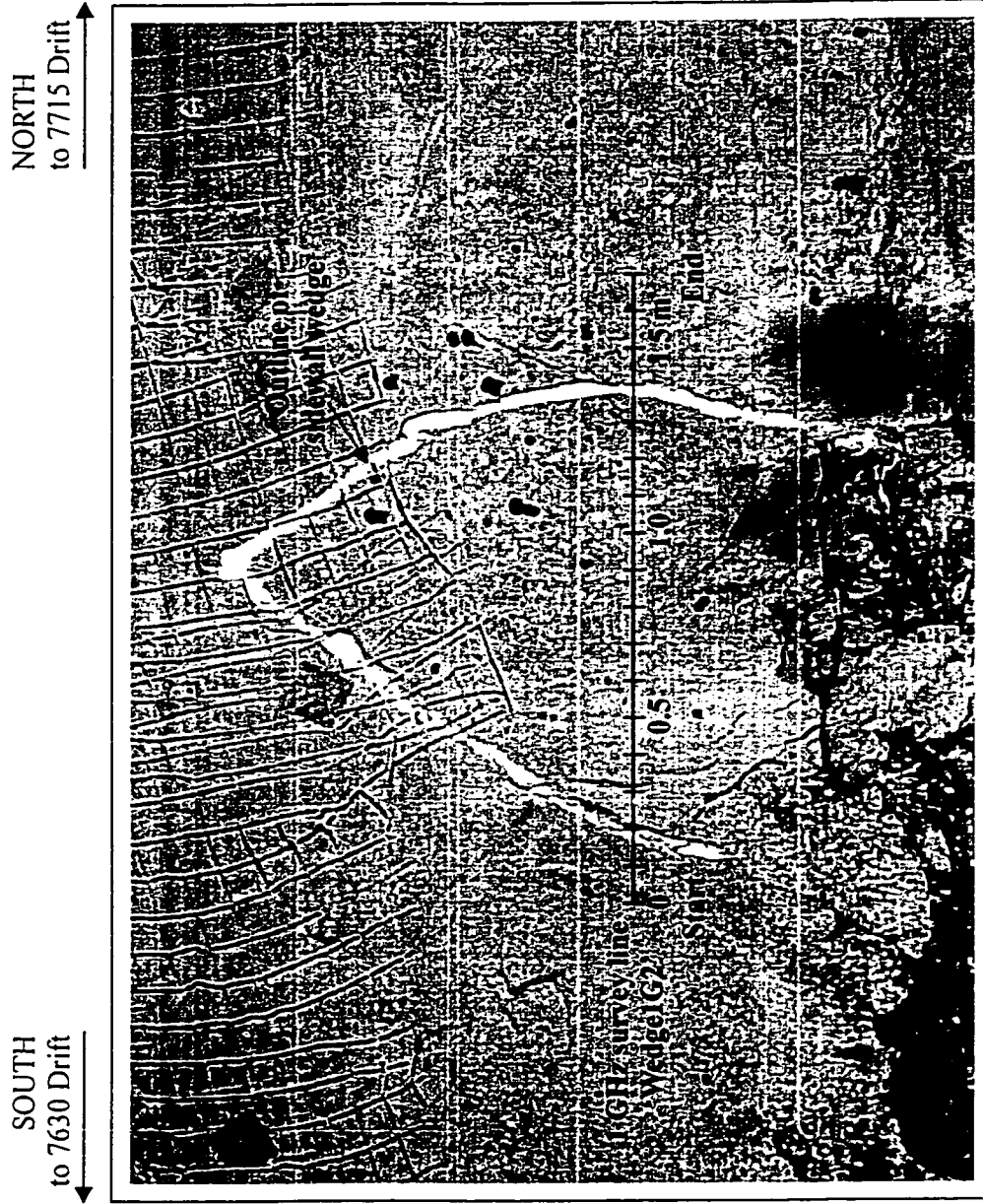
Figure 5-42 Digital photos of high frequency survey line ('Wedge1G2') across wedge in 7500 Main Access Ramp.

169

CHAPTER 6: FIELD DATA RESULTS

6.1 INTRODUCTION

Chapter 6 presents the results of the GPR field study conducted at nine project sites described in the previous chapter. Section 6.2 describes the basic processing that was conducted on the various radar data sets. Section 6.3 discusses how the survey results are presented in this chapter and notes some of the problems associated with presentation of the data and interpretation. Section 6.4 discusses the processing of each low and high frequency survey at each project site with representative profiles and amplitude spectrums included. After processing and interpretations have been made for the various site surveys, preliminary conclusions and recommendations are given. Sections 6.5 and 6.6 contain summary remarks and conclusions for Chapter 6.

Throughout this chapter, it is important to keep in mind the five factors that influence the success of a GPR survey: depth of penetration, resolution (both vertical and lateral), contrast in dielectric constant between the host rock and the target, signal to noise ratio, and available ground truthing information.

6.2 GENERAL PROCESSING COMMENTS

Processing was conducted on all 32 data sets in order to minimize the noise and correct for topography if necessary. The RAMAC/GPR system recorded all the data digitally, different types of processing could be conducted but only basic processing techniques (Section 3.7.1) were used on the radar profiles. In general, this simpler processing allowed the radargrams to be 'cleaned up' which facilitated the interpretation and identification of continuous reflectors.

The RAMAC software that came with the GPR system was used for data collection but not for processing because of the limited processing functions available. GRADIX software by Interpex Ltd. and pulseEKKO software by Sensors & Software was used instead. Both software packages were designed specifically for processing and interpretation of ground penetrating radar. GRADIX (Version 1.11) is the more sophisticated of the two software packages because it has more processing functions (both basic and advanced techniques) and is quite flexible. PulseEKKO (Version 4.1) was however easier to use and was used for most of the processing.

Using both software packages, the processing steps for the GPR reflection surveys included:

1) editing the header files;
2) removal and/or shift of individual traces (i.e. trace removal, trace shift);
3) reversing the polarity of the profile, if necessary;
4) adjust all traces to an appropriate time zero datum (i.e. 1st Shift; 1st Pick);
5) topographic corrections to compensate for elevation changes along the survey, if necessary;
6) application of signal saturation corrections to account for large amplitude air and ground waves (i.e. dewow, DC shift);
7) application of time gains to correct for geometrical spreading of the radar signal (i.e. constant gain & SEC gain);
8) application of temporal and spatial filtering to minimize random noise, equipment noise, and clutter (i.e. trace-to-trace averaging, down-the-trace averaging, spectral analysis, bandpass filtering, low-pass spatial filtering, high-pass spatial filtering, and trace-difference filtering).

Refer to Section 3.7.1 for descriptions of these basic processing techniques.

Aside from selecting the most appropriate time gain and filter, these basic processing steps were relatively straightforward. Each survey was treated as being unique because of the large variations between the sites and survey conditions. Nearly all the surveys required trace removal and/or shifting of individual traces however the topographic correction was only necessary at three of the nine sites. Signal saturation corrections or dewow was applied to all data sets as well as a time gain. The SEC gain was found to give the clearest image however the constant gain was also used when appropriate.

Selecting the time and/or spatial filter proved to be the most difficult processing task. Filter selection primarily depends on whether the targets are dipping or parallel to the surveyed surface and the software manuals all give recommended filters depending on this classification of target orientation. An amplitude spectrum was created for each survey as an aid for filter selection, however only some of the filters actually produced a detectable improvement to the radar profile. Note that the profiles presented in this chapter are based on my own personal bias and other processing techniques may show results that are equivalent or perhaps better.

6.3 DISPLAY AND INTERPRETATION

The radar profiles (or radargrams) presented in this chapter are plotted with both a time and depth scale. The two-way travel time (in nanoseconds) is on the left-hand y-axis, the approximate depth (in metres) is on the right-hand y-axis, and the distance along the survey line (in metres) is along the x-axis. Because all raw data contains no signal information in the uppermost portion of each trace, all radar profiles have also been shifted down to the first radar event - the direct air wave. The direct air wave serves as a datum from which to measure two-way travel time – or the 'time zero marker'. Selection of time zero was made either manually or by using the 1st Pick and 1st Shift options in the pulseEKKO software.

The time scale was converted to a depth scale to help interpret the data, despite the fact no CMP surveys were conducted to determine the radar wave velocity. This data conversion was accomplished by assuming a signal propagation velocity for each project site, based on either literature values or back-calculated using the distance to a known reflector. All depth scales presented in the radar profiles were generated using the pulseEKKO software.

It is important to realize that the depth scale is only approximate because it does not account for velocity variations in the ground. However, the project sites have relatively simple geologic conditions - i.e. the sites were generally composed of single host rock with minimal/no overburden – so using a constant velocity may not be a large concern. One problem that could not be avoided is the fact the depth scale is non-linear. The depth scale is compressed nearest the surface because at shallow depths most of the signal travel time is from the horizontal component of the signal path. This non-linearity is a disadvantage to surveys that require a topographic correction. With this in mind, an attempt was made to minimize the vertical exaggeration in the plotted profiles where possible but obviously there are difficulties in doing this.

The problems with interpretation of GPR data have been mentioned, however the fact that I was involved in both data collection and interpretation proved was advantageous. Interpretation of the processed radar images was also greatly aided by reviewing the results of other case studies in similar hard rock environments (Section 4.6). Identification of rock structure was difficult

because the quality of some of the surveys was lower than desirable due to difficult site conditions – e.g. limited room to conduct the survey, numerous sources of interference, or rough survey surfaces. However, to help identify radar reflections of rock structure, the criteria described in Section 4.7 were used, as well as direct observations of surface structure.

6.4 Field Data Results

For each of the nine project sites, the surveys have been subject to basic processing and interpretation. The following sub-sections describe these two steps for each of the 32 surveys. A processed radar profile for each of the surveys is included, however these are only selected examples, as numerous types of processing were applied to each data set. The details of the processing and gain parameters for each of these radargrams are given in the figure captions. As well, the radar wave velocity used to create the depth axis is noted beside the depth scale. Interpretation of the geophysical data profiles is based on experience and is therefore subject to bias. Each of the survey profiles was reviewed and assessed to identify the primary radar targets described in Chapter 5.

The sites are presented in order of the degree of successful detection of rock mass structure. The artificial fracture surveys are thus presented first because the radar targets were well-defined, whereas the underground surveys at 175-Orebody are discussed last because of the unsuccessful detection of rock structure observed with both antenna frequencies.

6.4.1 Jarvis Resources Ltd

All the air-filled artificial fractures (or air gaps) between the limestone/marble rock blocks were oriented parallel to the surface, so the objective of processing was to enhance flat-lying reflection events. Spatial filtering was used to remove or minimize hyperbolic events created by the vertical ends of the rock blocks. In fact, the apex of the hyperbola seemed to coincide with the gap separating the two blocks. Piccolo (1992) noted similar observations when conducting GPR tests at a marble quarry.

The electromagnetic waves penetrated the limestone and marble blocks easily, so knowing the exact distance to the gap, the signal velocity was calculated to be approximately 0.110 m/ns ($\varepsilon_r =$ 7.4). This velocity is within the accepted range of 0.106-0.113 m/ns (Piccolo, 1992) for this rock type. With this velocity and knowing the gaps were dry, the reflection and transmission coefficients were calculated to be 0.46 and 0.54 respectively. The positive reflection coefficient indicates the reflections from the gaps have the same polarity as the incident signal.

No topographic corrections were required and because the rock blocks had been cut with a saw, the smooth surfaces enabled excellent contact between the shielded 1 GHz antennas and the host medium. Even the smoothness the fracture surfaces were also beneficial because smooth interfaces reduce the amount of energy that is scattered. Because of these conditions the target fractures were easily identified in the radar profiles and appeared continuous across the survey and perfectly planar.

In general, basic processing such as dewow, constant gain, trace-to-trace average, down-the-trace average, spac_low, and bandpass were examined; however, many of the techniques produced similar results. As a result, the processed sections presented contain little to no gain and have been trace-averaged.

6.4.1.1   Block Site 1 Surveys

For the first survey (File name: Jarvis1h), the objective was to detect an 8 cm wide gap between limestone slabs and a marble rock block. Figure 6-1 b) shows the geologic section to help aid in the interpretation of the radargram. No topographic correction was required for this or any other survey across the carbonate rock blocks. No gain was applied to the data set because the gap reflection was clearly identifiable without it. Only trace-stacking was used to minimize the hyperbolic events at the start and end of the survey line.

In the processed radar profile for 'Jarvis1h' - Figure 6-1 a) - the strong horizontal reflection at approximately 35 cm depth is clearly representative of the air-filled artificial fracture. There is a second reflection of moderate amplitude at approximately 42 cm, but it is does not represent the bottom of the gap. The energy that travels through the 8 cm gap is moving at a velocity of 0.3 m/ns (radar velocity through air) but the radar profile is plotted with a velocity of 0.110 m/ns (radar velocity through limestone). As a consequence, the top and bottom of the air gap would only be 3 cm apart on Figure 6-1 a), not 8 cm. Reverberation within the gap is therefore the cause of the reflection at 42 cm, as well as other moderate to weak reflectors below 35 cm.

Aside from the large air-gap, the contacts between the eight limestone slabs were thought to be potential reflecting surfaces. The distance between the slabs ranged from 0-1.5 mm, however these measurements where taken from the top of the slabs and not at the survey line elevation. On Figure 6-1 a), there are three very weak continuous reflections between the direct wave reflection at 7 cm depth and the fracture reflection at 35 cm. It is uncertain whether these reflections are caused by the contacts between the limestone slabs or not.

There are also very weak hyperbolic events seen at the ends of the profile (between 0.35 to 0.9 m depth). As discussed in Section 3.8, the vertical sides of the rock blocks caused these events. These reflections generally have high amplitudes but for this particular profile they remain small because of trace-averaging and the absence of any time gain.

The second and third surveys (File names: Jarvis1e & Jarvis1f) were identical except that a piece of household aluminum foil was placed between the fourth and fifth limestone slab (or at a depth of 17.6 cm) — Figure 6-2. Figure 6-3 show the processed radar profiles of these two surveys. Because the survey lines where higher up the face of the limestone slabs, the width of the artificial fracture was reduced to 3.6 cm. In the survey without the foil (Jarvis1e), the fracture was still clearly detectable in the profile - Figure 6-3 a) - but for Jarvis1f (with foil) the amplitude of the fracture reflector was noticeably smaller. Figure 6-4 is a plot of an average of five traces taken from approximately the middle of the each of the two surveys. As anticipated, the reflection off the foil is has the highest amplitude (or is the strongest reflector in the profile). The presence of the foil appears to have scaled down the amplitude of the direct air wave, direct ground wave, and fracture reflector.

Comparing next the profiles of the first survey (Jarvis1h with a 1 cm station spacing) to the second survey (Jarvis1e with a 2.5 cm station spacing), the clarity or resolution of the profile has improved with the smaller station spacing. Despite this effect, the station spacing does not have a dramatic effect on the overall results because the target is flat-lying, as well, both station spacing remain below the Nyquist sampling interval of $\approx$ 3 cm.

6.4.1.2   Block Site 2 Survey

Figure 6-5 shows the processed radar profile of 'Jarvis2' for the high frequency survey at Block Site 2 and the associated geologic section. A small SEC time gain was applied in order to 'see' reflections to a depth of 1 m, but even without a gain, a high amplitude continuous reflection at 35 cm depth can be easily identified in the radargram. This reflection represents the top of the 3.3 cm wide artificial fracture, but the bottom cannot be distinguished for the reasons discussed in Section 6.4.1.1. At this block site, the target gap at 35 cm would have a reduced width of 1.2 cm when plotted with a velocity of 0.110 m/ns.

Unfortunately, this profile is more cluttered than the Block Site 1 profiles. This is primarily because the time gain emphasizes all reflections, including the flat-lying reflections below the gap (created due to reverberation) and the hyperbolic reflections (created due to the sides of the blocks). Although a trace-to-trace averaging was applied, the hyperbolic reflections remain strong. Notice that the peak of the hyperbolic events mark the breakage between Block 1 and Block 2.

In the field, the first block was not cut perfectly rectangular but had a width of 35 cm at the starting position of the survey and 30 cm at the survey end. This explains why the fracture reflection is not perfectly horizontal. The gap width also varied from approximately 3.3 cm to 1.5 cm from the survey start to end position. This observation is justification for the observable decrease in the gap reflection amplitude along the profile.

In addition to the gap between Blocks 1 and 2, the radar system may have detected the gap behind Block 2. If this second opening were detected, it would appear at a depth between 61-66 cm depending on the location along the survey line. Figure 6-5 does show some weak horizontal reflections at 92 cm and 100 cm but these are likely from some complex radar path through the limestone blocks and not from the base of the second block.

6.4.1.3   Block Site 3 Surveys

The last block site shows similar results to the previous sites. Figure 6-6 is a geologic section with two air-filled gaps at 32 and 65 cm depth. Aluminum foil was again used in hopes of increasing the amplitude of the first fracture reflection. However unlike at the first block site, foil was placed in a wide air gap (Figure 6-6). 'Jarvis4' and 'Jarvis4f' were two identical surveys conducted across the top of Block 1, except 'Jarvis4f' had aluminum foil placed along the top of Block 2.

Figure 6-7 shows the profiles for Jarvis4 and Jarvis4f after trace-averaging. This figure shows that the influence of the foil is by far less dramatic in comparison to the 'Jarvis1f' profile (Figure 6-3) from Block Site 1. In both Jarvis4 and Jarvis4f, there is a strong, continuous high amplitude reflector at 32 cm depth which is representative of the top of the first air gap. Below this is a reflection at 40 cm depth that is caused by energy bouncing within the 7.5 cm wide gap. The amplitude is marginally higher in the reverberation reflection of 'Jarvis4f' because some energy is reflecting off the foil.

Figure 6-8 is a plot showing an average of five traces taken from the middle of each of the two surveys. The influence due to the introduction of the foil is less dramatic than compared to Figure 6-4 from the Block Site 1. Figure 6-8 shows a small increase in amplitude in the reverberation reflection and a smaller decrease in amplitude in both the direct waves. There even appears to be a small increase in amplitude at the top fracture reflector but this increase cannot be detected in the radar profile.

A representative amplitude spectrum for the high frequency surveys conducted at the Jarvis Resources Ltd. project site is shown in Figure 6-9. The centre frequency of the transmitted pulse should be around 1000 MHz, but this is a value quoted for a signal propagating through air. Because geologic media attenuates the radar energy, the centre frequency is generally reduced. For the carbonate rock, the actual centre frequency was closer to 828 MHz, a 17 % reduction from the manufacturer's design frequency of 1000 MHz.

The amplitude spectrum shown in Figure 6-9 is also not a typical spectrum (Figure 3-2). A typical spectrum has a normally distributed shape about a specific centre frequency, but for this project site, the spectrum has multiple peaks within the 1000 MHz bandwidth. This effect is associated with either poor antenna design and/or ground filtering[15], neither of which can be remedied (Personal communication, Mr. N. S. Parry, EBA Engineering Ltd., March 10, 2000).

Conclusions

The results from this project site show that radar can be used to identify dry open artificial fractures between 3 to 8 cm wide – or large-scale structural features. As well, fractures less than 1.5 mm wide are likely not detectable with the equipment that was used. This statement is based on the unsuccessful detection of the contacts between the limestone slabs at Block Site 1.

Considering the factors that influence success of a radar survey, detection of these larger fractures was not surprising. First of all, survey conditions at all three block sites were nearly ideal. The carbonate host rock allowed good propagation of the radar energy due to low absorption and high homogeneity. The primary radar targets existed above a depth of 1 m, well within the depth penetration of the high frequency antennas. The blocks also had smooth surfaces so excellent contact between the antennas and surveyed surface was achieved and no topographic corrections were required.

As for the radar targets, they were all continuous and well-defined targets. The targets also had a favorable orientation – parallel to the surveyed surface. Finally, the smooth fracture surfaces reduced the amount of energy scatter.

Since the artificial fracture apertures ranged between 3.3 to 8.2 cm, they would be classified as large-scale discontinuities according to the definition used in this thesis. However the gap widths were still smaller than the dominant wavelength of the high frequency antennas so detection of these large-scale features was still governed by the thin layer concept. The R_t was determined to be 0.08 to 0.20 for these widths, which is higher than the value for detection quoted in Chapter 4 – R_t for successful detection needs to be greater than about 0.06 to 0.07. This explains why these targets were detected.

The influence of target thickness versus the contrast in dielectric constant is examined when testing with aluminum foil and the rock blocks. Aluminum foil has a thickness of approximately

---

[15] As radar energy moves through the subsurface, geologic media will act as a filter and remove certain frequency components.

175

0.03 mm however the dielectric constant of aluminum is infinity large because it is a conductor. Using the thin layer concept and assuming ε_r for foil is 10000, the Fresnel Reflection Coefficient is (-)0.1; however, if the target is an air or water filled fracture the Fresnel Reflection Coefficient reduces to 0.0007 or (-)0.008 respectively. Clearly, these values suggest very thin targets can be identified but they require a large contrast in dielectric constant. The maximum contrast for a rock fracture occurs when it is water-filled (i.e. ε_r = 80 for water).

Although the large gap widths allowed detection, they also had a disadvantage: they caused a masking effect. At any of the three block sites, once the radar energy encountered the first gap, the energy stayed and bounces within it. This energy dissipating mechanism prevented detection of deeper targets. It is for this reason that when interpreting a profile, the interpreter should always work from the surface down, because travel times and amplitudes associated with any reflector are affected by overlying material (McMechan, 1981). The masking effect explains why deeper opening were not detected at any of the block sites.

As for the signal to noise ratio, the surveys were conducted in a quarry yard with nearby buildings, pieces of equipment, and other stacked blocks of rock all which may have been sources of interference, but the shielded antennas minimized their influence. As well, a stacking value of 16 was used for all the surveys. The one source of noise that was unavoidable was the near-vertical sides of the blocks. When a survey is conducted such that the antennas are moved away from the vertical edge the characteristic hyperbolic signature appears, but when antennas are moved parallel to a vertical edge, flat-lying reflections are appear. The problem is that reflection caused by edge effects need to be identified in the profile. Luckily for this project site, these effects did not inhibit identification of the flat-lying reflectors from the air-filled gaps.

Recommendations

Although conducting GPR surveys across blocks of cut rock is not entirely representative of natural fractures, which are not as planar or possibly as smooth, it would be beneficial to conduct further testing on such blocks. Because we already know that large-scale fractures ≥ 3 cm wide can be detected, it would advantageous to examine smaller-scale fractures (i.e. less than 1 cm). It is also recommended that in order to reduce edge effects, blocks as large as can be managed be used.

6.4.2 WGMC Walkway

Two surveys were conducted across the top of two vertically piled gneiss blocks along the WMGC walkway. The objective was to detect the man-made fracture (or gap) between the two blocks. The two surveys were conducted under identical conditions except aluminum foil was inserted between the two blocks for one of the surveys. Figure 6-10 shows a processed radargram for the survey without foil (File name: Reflect2) and with foil (File name: Reflect1). Although the fracture had an undulatory nature and varied in aperture, processing was conducted knowing the target would appear relatively flat-lying in the radargram.

A small SEC time gain was applied in order to 'see' reflections above 1 m depth more clearly. For the gneiss host, a typical signal propagation velocity of 0.12 m/ns (or dielectric constant of 6.25) was used for the SEC gain and depth scale. A reasonable amplitude constant of 1 dB/m was also used as input for the gain. Trace-averaging was also used to emphasize horizontal reflections and minimize dipping reflections. This site was different from the previous site (limestone/marble rock blocks) because the sides of the gneiss block were both rough and

irregular, not smooth and vertical. As a result, there were virtually no hyperbolic reflections seen in either profile even before the spatial filter was applied.

Knowing breakage between the blocks existed at a depth of 0.5 m, the corresponding fracture reflection has been labeled on each of the surveys (Figure 6-10). The fracture reflection has the same polarity as the incident signal and is continuous across the profile. The reflection amplitude does however vary due to the change in aperture. The exact aperture along the survey line could not be measured, but the fracture was definitely open for the majority of the distance because the aluminum foil was inserted between the blocks with little difficulty. Comparing the survey profiles with and without foil, the amplitude at the location of the fracture is slightly higher. Figure 6-11 provides addition support of the increase in amplitude at the fracture location and a corresponding decrease in amplitude in both the direct air and ground wave.

Unfortunately, aside from the reflections due to the air-filled gap, there are other sub-horizontal reflections between 0.1 to 0.5 m depth. Some of the reflections are continuous and others are discontinuous across the profile. It is likely that these are caused by reflections off the gneissic foliation that was parallel to the gap. Because foliation generally has an undulating nature, this would explain why the reflections are not perfectly planar.

The average amplitude spectra for these surveys show that the actual centre frequency is again reduced to 827 MHz from the manufacturer's value of 1000 MHz – Figure 6-12. Comparing the representative spectra from the gneiss blocks (Figure 6-12) to the spectra for the limestone rock blocks (Figure 6-9), the shape has clearly changed. The depressions are not as pronounced which is evidence that the spectra is likely changing due to a ground response and not due to poor system design. As well, peaks are occurring at different frequencies. Since the peaks can correspond to reflections at certain depths and because artificial fractures existed at different depths at the two project sites, the spectra peaks would show this.

Conclusions

The high frequency antennas successfully detected the man-made fracture between two gneiss blocks with and without the aid of the aluminum foil, however detection was not surprising. In fact, Pilon (1996) and Grasmueck (1994 & 1996) are examples of where GPR was claimed to be successful in delineating fractures in gneiss outcrops. At this project site, the rock blocks were a good medium for radar because they were unweathered, relatively homogeneous, and non-conducting.

With the high frequency antennas having a penetration depth of at least one metre, the air-filled gap was well above the depth of penetration. Considering the system resolution, the dominant wavelength for the high frequency antennas was ≈14.5 cm using a dominant frequency of 827 MHz (from the amplitude spectra – Figure 6-12). Because the fracture aperture was much smaller than this value, the thin layer reflectivity concept again has to be used. Although the exact aperture is unknown, if it is assumed that the value ranged between 3 mm to 3 cm, then the calculated Fresnel Reflection Coefficient is 0.07 to 0.66 respectively. These values were obviously high enough such that detection across the entire block was possible.

Because the gneiss blocks were a part of a walkway with a building less than 10 m away, there was a concern that this would introduce noise into the data. Fortunately, because the antennas were shielded and there was relatively close contact with the top of the upper gneiss block, the interference due to external sources was not a concern. A somewhat lower stacking value of 8 was used for both surveys but based on a review of the data, this value proved adequate.

Conducting radar surveys across the gneiss blocks in hopes of detecting a dry open fracture was more realistic in comparison to the surveys across the limestone rock blocks. The surfaces of this structural feature were more irregular and the aperture varied across the profile. similar to the expression of a natural discontinuity. The radar successfully detected the desired target, but the fracture reflection was not distinct from the other sub-horizontal reflection events. Not knowing how many fractures existed within the gneiss host, the interpreter likely would suggest that more than one fracture existed at this site. As a result, this project site is an example of showing the non-uniqueness in the interpretation of the radar reflections.

The fracture reflection within the gneiss blocks was not as strong (or lower amplitude) in comparison to the limestone fracture reflections. This is likely due to a number of reasons: the aperture was smaller, the fracture surface was more irregular causing more scattering, and more energy was lost due to reflections off near-surface foliation.

Recommendations

Additional testing at this site is not warranted, however if the surveys were to be redone, it would be more beneficial to somehow measure the aperture along the survey profile. This is because based on the results of this study, all that can be said for certain is that an open fracture less than 3 cm was detected using 1 GHz antennas.

6.4.3 Hwy 17 Bypass

The three primary targets at this highway outcrop of meta-sedimentary rock were two bedding joints at approximately 20 and 50 cm from the rock face and a fracture zone at a depth of 95 to 100 cm – Figure 6-13. The radar surveys were conducted vertically across the side of the outcrop, so the objective of data processing was to enhance flat-lying reflectors to a depth of at least 1 m. This was accomplished by applying a SEC time gain and a spatial filter such as a low-pass spatial filter or trace-to-trace averaging. A signal propagation velocity of 0.120 m/ns was assumed for construction of the depth scale and as input for the gain function. For the attenuation constant, a value of 1 dB/m was assumed. Luckily the surveyed surface was relatively planar, no topographic corrections were required.

Figures 6-14 to 6-17 are processed radar profiles for the three high frequency surveys using different spatial filters. (Note that only survey BY-1G-2c has been processed using trace-averaging and a low-pass spatial filter for proper comparison with the other two surveys: BY-1G-2a & BY-1G-2d). Because the rock structure was only visible from the western edge of the outcrop and to show the surveys without a vertical exaggeration, only the last 3 metres of the survey line was plotted for each of the surveys.

All the profiles show numerous undulating reflections between 0.2 and 1.2 metres depth. As an aid for locating the three target fractures, the approximate locations have been marked on all the profiles with arrows. Both the 1st and 2nd open joints at 20 and 50 cm depth appear as relatively continuous, wavy reflectors that vary in amplitude. At approximately 95 cm lies a very weak, discontinuous reflector that may or may not represent the fracture zone. The presence of several continuous and discontinuous reflections - of similar amplitude - that exist in between the potential fracture reflections make interpretation difficult. Because these reflections exist parallel to bedding, they are likely created by changes in mineralogy or are other fractures not visible from the exposed western edge of the outcrop.

From these three GPR surveys, the influence of sampling frequency and station spacing can be examined. Using trace-averaging to improve resolution, Figures 6-14 and 6-15 show the influence of the sampling frequency. Survey BY-1G-2a used a sampling frequency of 6.6 GHz whereas survey BY-1G-2b used a higher frequency of 10.8 MHz. Clearly the profile with the higher sampling frequency shows more detail in the subsurface. Using a different type of spatial filter, Figures 6-16 and 6-17 show that a decrease in the station spacing produces a similar increase in resolution.

The corresponding amplitude spectra for the high frequency surveys at this project site is shown in Figure 6-18. The actual centre frequency is approximately 810 MHz – a 19% reduction from the manufacturer's rating of 1000 MHz. Unlike the high frequency spectrums for the rock block surveys, the spectrum for the Hwy 17 Bypass Outcrop is smoother and has only three peaks within its 1000 GHz bandwidth.

Conclusions

Successful detection of at least three obvious fractures was anticipated at this site for a number of reasons: the surveyed surface was relatively planar and would provide close contact with the rock surface; there were minimal sources of interference; the rock structure for the first 1.5 m depth was visible from the side of the outcrop. It is therefore not surprising that the processed radargrams show reflections at the appropriate depths for the first two bedding joints.

That these two fractures were air-filled and had apertures less than one centimetre at the surface is even more encouraging. These small-scale targets fall under the thin layer concept. This enabled calculation of the Fresnel Reflection Coefficient, which was 0.15 to 0.20 assuming a thickness of 7 to 9 mm respectively. These R_t values are greater than the criteria for detection quoted in Chapter 4 (i.e. R_t needs to be > 0.06-0.07 for detection), therefore these values provide a theoretical explanation of why the fractures were detected.

The large-scale 5 cm fracture zone likely was undetectable because it existed near the limit of the maximum depth of penetration using the 1 GHz frequency antennas. In other words, much of the radar energy had been lost by the time it reached this zone of broken rock.

Notwithstanding the successful detection of two obvious bedding joints, the biggest disappointment is that the fracture reflections in the radar profile are not distinct from other reflections caused by mineralogical changes in the host rock. The heterogeneity of the host rock was not anticipated to be a problem at this site but it clearly was from examination of the final results. As such, when conducting radar surveys in heterogeneous geologic conditions, there has to be acceptance that the resulting profiles may be too complex and confusing to 'see' the target features through the noise.

Recommendations

Although two potential bedding joints were detected, the complexity of the radar profiles suggested that the host rock was heterogeneous for the 1 GHz antennas. As such no addition testing is recommended at the Hwy 17 Bypass Outcrop.

6.4.4 Vermilion River Outcrop

The primary radar target at the Vermilion River Outcrop was a single joint dipping 10° to the east – Figure 6-19. From the highway, this small-scale fracture appeared have an aperture of 2-3 mm at the surface and was dry during surveying. Because of the dipping nature of the target. processing involved enhancing dipping reflections by suppressing flat-lying reflections.

Figures 6-20 and 6-21 are the 3 and 6 m long surveys (File names: VM-1G-3 and VM-1G-5) after basis processing. Unique from the previous project sites, a topographic correction was required since the ground surface had a dip of 5° to the east for the first three metres along the survey line. A SEC time gain was also required in order to enhance reflections between 0.7 and 1.8 m depth. As well, a point-averaging time filter was applied to enhance reflections inclined to the surveyed surface. For the depth scale, a velocity of 0.123 m/ns was back-calculated based on the knowledge of the actual fracture depth.

In both profiles, this dipping joint appears to have been detected in the first 2 m along the survey line. The dip measured off the profile is approximately 13° which is slightly larger than the actual dip of 10° but is within the error of the measurement itself. Figures 6-20 and 6-21 also show irregular noise throughout the profile. It is likely that some of this noise is due to the quartz veining observed within the argillite. From the top of the outcrop, veins were visible between position 1.3-1.6 m and position 5.1-5.6 m but they likely extended to a depth of at least 0.5 m.

The profiles also shows noisy multiples within the first 12 ns (or 1 m depth). These are distinct reflections because they are continuous across the entire profile and appear approximately every 3.3 ns. These multiples were minimized but not eliminated with down-the-trace averaging.

The two surveys were conducted with different station spacings, so by comparing profiles 'VM-1G-3' to 'VM-1G-5' the influence of this variable can be seen. Reviewing these survey profiles. the conclusions are the same as those stated for the previous project site (Hwy 17 Bypass) – the smaller the station spacing improves resolution or sharpens the image. The assumed fracture reflector could be seen in both profiles. but is more difficult to see in 'VM-1G-5'. therefore the 5 cm station spacing should be regarded as the upper limit to the station spacing.

Figure 6-22 is a representative amplitude spectrum for the high frequency surveys at the Vermilion River outcrop. The dominant frequency is 808 MHz, which is approximately a 19% reduction from the reference centre frequency in air. The shape of the spectra is nearly identical to that for the Hwy 17 Bypass (Figure 6-18) except the amplitudes are slightly higher.

Conclusions

Prior to conducting these surveys, there was some uncertainty as to whether the high frequency antennas could detect the dipping joint for a number of reasons. The joint was located at a maximum depth of 1.8 m from the surveyed surface, which is nearing the maximum depth of penetration for the 1 GHz antennas. As well, the argillite host rock likely has a high clay content so the conductivity (or attenuation) may have been high (> 10 mS/m). The third reason was that the aperture may have been too small to be detectable.

Despite these concerns, the resulting radar profiles do appear to show that a portion of this small-scale fracture was detected by radar. Surprisingly, the portion that was detected existed at a depth between 1.6 and 1.8 m. Unfortunately, the fracture was not directly observable at this location along the survey line but can been seen in the digital photos (Figures 5-15 & 5-16). It is unknown why the fracture was detected only within the first 2 m of the survey line, perhaps either the aperture decreased such that this feature could not be detected elsewhere. Using the thin layer concept, an air-filled fracture with an aperture of 2-3 mm would have a Fresnel Reflection Coefficient between 0.04-0.06. These are relatively low values, which may be insufficient for detection, so either the aperture between position 0 and 2 m was greater than 3 mm or the reflection is an artifact.

The success at this site may be because this outcrop had a number of good quantities. The host rock was more homogeneous and massive, especially in comparison to the meta-sedimentary rock at the Hwy 17 Bypass site. This observation and the fact that the rock may not have been as conductive as expected, helps to explain why the maximum depth of penetration achieved was nearly 2 m and thus why a reflector is present between 1.6 and 1.8 m depth in the profile. Success may also have been due to the close contact between the rock and the antennas and minimal external noise.

Recommendations

Despite the possible detection of a single joint within the argillite host rock using the high frequency antennas, further testing at this site is not recommended. This recommendation is because the actual aperture of the discontinuity along the survey line is unknown and because there is a possibility that the reflection between 1.6-1.8 m depth is merely an artifact.

6.4.5   Willet Green Miller Outcrops

The objective of the GPR surveys at both WGMC outcrops was to detect bedding planes (or lithological contacts) in a meta-sedimentary host rock. The host was similar to that at the Hwy 17 Bypass site, except at this site the rock appeared more massive (i.e. thicker bedding). As well, the orientation of the bedding was different – a dip of 40° to the north at the WGMC outcrop compared to a dip of 75° to the north at the Hwy 17 Bypass. Surveys were taken across the top of both outcrops and perpendicular to the strike of the bedding. As a result, data processing focused on enhancing dipping reflectors. For both outcrops, a signal propagation velocity of 0.120 m/ns was used. This is the same value used at the Hwy 17 Bypass site.

6.4.5.1   WGMC Outcrop 1

Both the low and high frequency data was processed with a SEC time gain and a time filter which suppresses flat-lying features - Figure 6-23 a) and Figure 6-24 a). The corresponding geologic section is shown adjacent to the processed radargram to help with interpretation – Figure 6-23 b) and Figure 6-24 b). Both geologic sections are the same sketch as Figure 5.18 but have been scaled appropriately to match the radargram.

The low frequency profile shows relatively strong reflectors from position 0 to 6 m along the survey line and at a depth of 3-7 m – Figure 6-23 a). These reflectors have a radargram dip of 32° or an actual dip of 39° to the northwest and are likely caused by reflections off bedding planes. For the high frequency surveys the depth of penetration was only 20 ns or ≈ 1m – Figure 6-24 a). The bedding plane reflectors are not seen in this profile. There are however some hyperbolic reflections that may be caused by irregularities in the host rock or due to the soil/bedrock interface. Recall that there were areas of a thin soil/vegetation cover but the exact depth of the overburden is unknown.

The amplitude spectra for the low and high frequency surveys are shown in Figure 6-25 and Figure 6-26. The low frequency spectrum has the characteristic 'normal' distribution that centres around 88 MHz, whereas the high frequency spectra has two peaks at 702 MHz and 925 MHz. The centre frequency has been reduced by 12% for the low frequency antennas and 18% for the high frequency antennas. This is to be excepted because higher frequencies attenuate more rapidly.

6.4.5.2   WGMC Outcrop 2

Processing for Outcrop 2 was similar to that for Outcrop 1 except this outcrop required a topographic correction and a higher time gain to see reflections at depth. Figure 6-27 a) and Figure 6-28 a) show the low and high frequency surveys after application of a SEC time gain and point-stacking. The geologic sketch for this outcrop (shown in Figure 5.19) is adjacent to each radargram as an aid for interpretation– Figure 6-27 b) and Figure 6-28 b).

The low frequency data set has a number of noisy multiples which are continuous across the profile and extend to a depth of 5 metres. Unfortunately, these reflections could not be eliminated with the point-stacking filter. Aside from these strong reflections, there does not appear to be any distinct dipping reflections representative of the sedimentary bedding planes. Comparing the amplitude spectra of the low frequency survey for Outcrops 1 and 2 (Figure 6-25 and Figure 6-29), there may have been a problem with this survey. The centre frequency for the low frequency survey at Outcrop 2 appears to be 115 MHz compared to the 88 MHz centre frequency for Outcrop 1. As well, the maximum amplitude for Outcrop 1 is over 3 times smaller than that for Outcrop 2 – maximum amplitude for Outcrop 1 is ≈1170 uV compared to ≈360 uV for Outcrop 2. These observations indicate radar energy was may not have been entering the ground at Outcrop 2 because of either poor contact with the surface or equipment/system problems. Unfortunately, while this low frequency survey was being conducted there were no obvious signs of any problems.

The high frequency profile - Figure 6-28 a) - also shows poor results. There appears to be a few hyperbolic reflections in the profile, but no strong dipping reflections associated with detection of any bedding planes. Unique to this survey was the grass cover between survey position 4.25 and 5.1 m. On the radargram the direct air and ground wave is absent within this same section of the survey line.

The corresponding amplitude spectrum for the high frequency survey for this outcrop (Figure 6-30) is nearly identical to the spectrum for Outcrop 1 (Figure 6-26) except the amplitudes are slightly lower. The dominant frequency for Outcrop 2 was at 819 MHz for the high frequency antennas - the same value determined for the Outcrop 1 spectrum.

Conclusions

I had anticipated the radar would detect bedding planes at both outcrops because the meta-sedimentary host rock was likely non-conductive and the bedding was both pervasive and had a constant orientation throughout the site. However, the results show there was very limited success at detecting this particular rock structure using either the 100 MHz or 1 GHz antennas. Only the low frequency survey at Outcrop 1 shows possible detection of bedding planes dipping at 40° to the north. Unfortunately at both outcrops, the structure was either not visible or only poorly visible due to weathering and/or a thin soil or grass covering.

There could be a number of reasons for the unsuccessful detection of bedding planes at this project site. First of all, at Outcrop 2, the topography along the survey line was quite irregular. These non-planar surfaces made the 1 GHz antennas more difficult to use in comparison to the 100 MHz, which are designed for rougher terrain, but regardless of which antennas was used the contact with the rock was poorer than at other project sites. This poor contact would likely result in less energy entering the rock and thus a reduced chance of detecting rock structure.

Another reason for non-detection of bedding planes at Outcrop 2 may have been due to the close proximity to the Willet Green Miller Centre building, which was ≈ 4 m away from the end position of the survey line. The building may have been a source of noise for the low frequency antennas because they were unshielded.

The final reason that applies to both outcrops and antenna frequencies is the possible insufficient contrast in dielectric constant at the bedding plane contacts. At this site a change in dielectric constant would have been associated with change in mineralogy at the interface. Recall from Section 5.4.4 that it was hypothesized the host rock was composed of both meta-sandstone and siltstone layers. If this is true, I anticipated that the change in mineralogy between sandstone and siltstone would be sufficient for radar detection, but if the site was only sandstone perhaps the contrast in dielectric properties was insufficient to cause reflections off these contact surfaces.

Recommendations

No addition testing is recommended at this project site because there was very limited success at detecting bedding planes in a meta-sedimentary host rock using both 100 MHz and 1 GHz antenna frequencies.

6.4.6   Hwy 637 Killarney Outcrop

The main target at this granite outcrop was a large-scale 20-25 cm wide fracture zone that existed at a depth of approximately 3 m. Without any gain applied to the data, the radar profiles show only the direct ground and air waves. However with application of a constant gain and trace-to-trace averaging, Figure 6-31 and Figure 6-32 show that a maximum depth of penetration of 6 metres was achieved with the low frequency antennas.

At this project site, a constant time gain was selected over a SEC time gain because the primary radar target was relatively close to the surface. Unfortunately, the constant gain caused extreme amplification of reflections in the first 3 metres. Figures 6-31 and 6-32 show four strong reflections that extend across the entire profile. These reflections relate to the direct air wave, direct ground wave, and multiples of the ground wave. Aside from these sub-horizontal events, strong hyperbolic reflections are also observed at the ends of the second survey line (Figure 6-32). Moving the antennas away from the near-vertical sides of the outcrop caused these events. There are also weaker hyperbolic reflections throughout the profile below 3 m depth. The source of these reflections cannot be verified without drilling but may be associated with the intersection of the horizontal stress-relief joints and sub-vertical joints.

Assuming a signal radar velocity of 0.120 m/ns for the granite host rock, there does appear to be a relatively continuous reflector around the 3 m depth with a varying amplitude - the location of the fracture zone has been marked on both profiles with an arrow. For the second survey line (Figure 6-32), the start of the fracture zone reflection event on the south end of the survey is masked by the hyperbolic events but does seem to extend across the entire profile with a varied intensity.

Figure 6-33 shows that the actual dominant frequency of the low frequency antennas was 93 MHz, which is 7% lower than the manufacturer design centre frequency of 100 MHz. The spectrum is similar to the low frequency spectrum at WGMC Outcrop 1 (Figure 6-25) – the spectrum is smooth and has a single dominant peak. Assuming the broadband range extends from 43 to 143 MHz, there appears to be only a small amount of low and high frequency noise outside of the range.

Conclusions

There were high expectations that GPR would work well at this project site. The granite host rock is an ideal medium for radar penetration based on the case studies discussed in Section 4.6. The fracture zone was well within the depth of penetration for the low frequency antennas. As well, the thickness of the fracture zone was at least 20 cm (but appeared to be dry). Unfortunately, the fracture zone reflection could not be clearly identified in either radar profile. The radar may have pick up some areas of the fracture zone but there is so much near-surface noise it is not clearly identifiable.

Knowing the actual centre frequency was closer to 93 MHz, the wavelength for the low frequency antennas was 1.3 m. Because the width of the fracture zone is less than 1.3 m, this large-scale structural feature still meets the 'thin layer' criteria using the low antennas. The fracture zone was composed of broken rock and air, so the dielectric constant was somewhere between 1 and 6.25. The fact that there was no reversal in polarity observed in the radar profile, is evidence that the dielectric constant of the 20-25 cm zone was not higher than 6.25. Assuming that the zone has a dielectric constant of 4, the Fresnel Reflection coefficient is $\approx$ 0.2. This value suggests detection was theoretically possible however the dielectric constant for the fracture infilling was merely an estimate.

184

It is also important to consider the width of the fracture zone. Recall from Section 2.6.3 the rule-of-thumb 'the smallest target dimension should be greater than $1/10^{th}$ the target's depth for successful detection'. If this holds true, this target does not meet the criterion:

i.e. (width of fracture zone = 20-25 cm) < ($1/10^{th}$ the target's depth = 30 cm)

Interference was also a problem for this site since the vertical sides of the outcrop produced the characteristic hyperbolic events at the ends of survey line 2. For the first survey line that remained parallel to a near-vertical boundary there would also likely have been edge effects, but in the profile they would appear as horizontal reflections. Because the first survey line was 3-4 m away from the rock cliff, any horizontal reflections in the depth range of 4-6 m may be due to side effects. These edge effects make interpretation more difficult.

The fracture zone is clearly obvious from Hwy 637 and for the purposes of this study, it was assumed that the zone was laterally continuous across the site. It is most probable that the horizontal fracturing is due to stress-relief, however without drilling there is no certainty that the fracture zone existed below both survey lines.

Recommendations

Although the 100 MHz antennas did not detect the 20-25 cm fracture zone, it would be beneficial to re-test at this site using higher frequency antennas in the range of 200 to 500 MHz. This recommendation is based on the assumption that the zone could not be properly detected because the antenna frequency was too low. If the zone is still not detected at these higher recommended frequencies it is likely the fracture has an insufficient contrast in dielectric constant to cause detection – recall, that the zone was dry and infilled with broken host rock only.

6.4.7 Elbow Lake Outcrops

At the three selected gneiss outcrops near Elbow Lake, both low and high frequency radar surveys were conducted in order to detect either the gneissic foliation and/or the mafic dykes which existed parallel to each other. At Outcrops 1 and 2, processing focused on enhancing dipping reflections because these surveys were conducted across the top of the outcrop and perpendicular to the strike the rock structure. However at Outcrop 3, the surveys were conducted across the side of the outcrop and parallel to the foliation, so processing required enhancement of flat-lying reflections. The profiles shown for this project site were all processed with an appropriate time/spatial filter plus a SEC time gain. For the gain and the depth scale, a signal propagation velocity of 0.120 m/ns was chosen because it is a common value for gneiss (Table 4-2).

6.4.7.1 Outcrop 1

Figure 6-34 shows the radar profile of Outcrop 1 after basic processing. The data set required a topographic correction, a high time gain to magnify deep reflectors, and a point-stacking filter to enhance inclined reflectors. With the large time gain there are at least 2 weakly dipping reflectors between positions 0 and 7 m along the survey line. The reflector closest to the surface has a length of approximately 5 m, a dip of 38° in the radar profile (or actual dip of 51° using the dip correction), and if extrapolated to the surface is located at the 6 m position. The deeper reflection has a length nearly 8 m long a radargram dip of 36° (or actual dip of 47°), and occurs at position 13 m if extrapolated up to the ground surface level.

Unfortunately, these reflections may not be due to the gneissic foliation because their dips are 9-13° lower than the measured foliation dip of 60°. In addition. there were no structural measurements taken at positions 6 and 13 m either because they did not exist or because the weathered surface did not permit it. The radar profile also does not show a 28 cm mafic dyke observed at position 10.3 m. This observed dyke had a dip of 63° along the survey line. In the radar profile this particular dyke should have appeared as a reflector dipping with an radargram dip of 42° to the south.

Aside from the two dipping reflectors seen in Figure 6-34, there are three strong continuous reflections that exist within the first 2 m depth. These high amplitude reflections represent the direct air wave, direct ground wave, and likely a multiple of the ground wave. Recalling from Section 5.4.6.1 that this survey traversed over a vegetated depression as well as over bare rock. the radargram shows addition reflections below direct waves within the labeled depression. These reflections are still relatively parallel to the surface and therefore may be due to moisture in the soil or may represent the interface between the soil cover and the bedrock.

The average amplitude spectra for the low frequency survey at Outcrop 1 is shown in Figure 6-35. The spectra shows a normal distribution with little noise, however unlike any of the other low frequency surveys at the other project sites, the spectra has a centre frequency that matches the manufacturer's value of 100 MHz. This may indicate not as much energy was entering the ground.

6.4.7.2 Outcrop 2

At the second outcrop, a low and high frequency survey was conducted across the top of the outcrop. The primary radar targets were two mafic dykes with widths of 15 and 25 cm. and dipping to the south at 62-66°. Figure 6-36 and Figure 6-37 show the results of these two surveys. To aid in interpretation, the locations where the dykes were visible along the survey line are labeled on both plots. As well, a geologic section accompanies the radar profile for the low frequency survey - Figure 6-36 b).

The low frequency profile shows a number of strong reflections between the depths of 3 to 7 m. The reflections are moderately dipping either to the north or south and have lengths between 1-3 m. Looking at the corresponding geologic section with the radar profile, it is unlikely that the reflectors between position 0-3 m and at a depth of 4-5 m are the two dipping joints shown in Figure 6-36 b) because the dip is too shallow. As such, the source of these reflections is unknown.

As for the primary radar targets – the two mafic dykes at position 2 and 3 m along the low frequency survey line – there are no reflections dipping with radargram angles between 41-42° to the south, so the dykes were obviously not detected. With the high frequency profile. the conclusions are the same because there is an absence of dipping reflections that originate at surface positions 1.3 and 2.3 m.

Similar to the low frequency profile, there are however noisy multiples in Figure 6-37. These reflections are easily identified because they are always parallel to the surveyed surface, they are continuous across the profile, and occur approximately every 3.4 ns. Aside from this noise. there is not much to be seen in this high frequency radar profile.

The amplitude spectra for the low and high frequency survey are shown in Figure 6-38 and Figure 6-39. The low amplitude spectra for Outcrop 2 is similar to Outcrop 1 in that the actual centre frequency is again higher than the reference value of 100 MHz. For the high frequency spectra, the dominant frequency and a distinct depression are seen at a value of approximately 817 MHz. This spectrum has a form similar to the high frequency spectrums of the Hwy 17 Bypass Outcrop (Figure 6-18), Vermilion River Outcrop (Figure 6-22), and WGMC Outcrops (Figure 6-26) and (Figure 6-30).

6.4.7.3 Outcrop 3

Conducting surveys along the side of Outcrop 3, the primary targets were mafic dykes and gneissic foliation that would appear as flat-lying reflections in the radargram. Figure 6-40 and Figure 6-41 show the upper and lower survey line with a time gain and trace-stacking applied to the data. Note that a much lower time gain was required to 'see' deeper reflectors in comparison to the high frequency survey conducted at Outcrop 2 (Figure 6-37).

The profile of the upper survey line (Figure 6-40) shows a high amplitude reflection starting at 0.4 m at the southwest and ending at 0.6 m to the northeast. Because this sub-horizontal reflection is relatively continuous across the profile and exists at approximately 0.5 m depth, it is likely a reflection from Dyke 1. The second dyke (Dyke 2) at approximately 1.1 m depth may also have been detected but the reflector has a much lower amplitude and is only continuous from 0 to 0.75 m along the survey line.

Aside from the possible reflections from these two dykes, there are other moderately strong sub-horizontal reflections between 0.4 and 1.1 m depth. The reflections are likely from the gneissic foliation that is oriented parallel to the dykes.

The lower survey profile also shows many strong reflections – Figure 6-41. These reflections are again sub-horizontal but are more continuous over the profile compared to the reflections in the upper survey line. Below the direct air and ground wave reflections are two high amplitude reflections at 0.25-0.45 m and 0.65-0.75 m which are labeled the 1st and 2nd reflector in Figure 6-41. As mentioned in Section 5.4.6.3, the structure above the lower survey line was not visible, so it cannot be confirmed that the reflections are from either the gneissic foliation or the dykes. Because the orientation of Dyke 1 and Dyke 2 likely varied between the two survey lines, is it probable that these same dykes caused the reflections.

A representative amplitude spectra for these high frequency surveys is shown in Figure 6-42. The centre frequency is at 802 MHz, which is slightly lower than the centre frequency for Outcrop 2. The amplitudes are however higher for Outcrop 3 indicating more energy was propagating through the rock.

Conclusions

From Section 4.6, we know that a number of radar surveys have been conducted on gneiss although these surveys were focused primarily on fracture detection. At this site, the objective was not to detect fractures but to detect foliation interfaces or mafic dykes. The contrast in dielectric constant is therefore dependent on changes in mineralogy either within the gneiss or between the host rock and the dykes. It is likely that the felsic (i.e. quartz and feldspar) rich bands in the gneiss have a lower dielectric constant in comparison to the mafic (i.e. biotite and hornblende) rich bands or dykes but the exact values are not known.

187

Success at the Elbow Lake outcrops varied from none to moderate. The high frequency surveys conducted at Outcrop 3 were the most successful as the mafic dykes likely generated the high amplitude reflections observed in the radar profile. The success of these surveys was predictable for a number of reasons. First of all, the surveyed surface was relatively planar so close contact with the rock was achieved. As well, the structure that was visible existed within the anticipated depth of penetration for the high frequency surveys. Lastly, the dykes may have been easier to detect because they have a sharp change in dielectric constant in comparison to a likely more gradual change for a foliation interface.

At Outcrop 1, it is uncertain whether the dipping reflection events observed in the radar profile are representative of the gneiss structure because the radargrams dip angles do not correspond to those measured in the field. If the reflections are due to foliation, why were so few detected? Recall that the foliation at Outcrop 1 had a spacing of 0.5 to 1 m. Perhaps failure to detect these structural features was because of a low contrast in dielectric constant or a gradual change in ε_r. However, if the reflections in Outcrop 1 were caused by reflections off mafic dykes then why were they not observed at the surface? And why was a 28 cm wide dyke, clearly visible at the surface, not detected? Finally if the reflections are not related to either the foliation or the dykes it is uncertain as to what they were caused by.

Contributing to the low success at Outcrop 1 may have been the extreme topographic changes that cause poor contact with the ground surface. Evidence to confirm this is the high time gain required for processing the data. The processed radar profile failed to show many reflections at depths even with a high SEC gain (Figure 6-34).

Finally, at the second outcrop both the low and high frequency antennas were unable to detect the two mafic dykes that were clearly visible from the surface of the outcrop. Based on the successful detection of dykes of similar width at Outcrop 3, the problems at this location were likely due to a combination of poor orientation of the targets with respect to the survey line or higher amounts of background noise. Recall that the most favorable orientation for detection of a target is when it is parallel to the surveyed surface, whereas the least favorable orientation is a target perpendicular to the surveyed surface. So because the two dykes at Outcrop 3 were inclined at 62-66° to the surface this would have decreased the chance for detection.

Both the low and high frequency surveys conducted at Outcrop 3 also show a lot of noise in the radargrams. The surveyed surface was relatively planar, so contact with the rock surface was significantly better in comparison to Outcrop 1, however the survey line was in close proximity to the western edge of the outcrop. It is highly likely that much of the noise at depth is due to edge effects, however because the edge was not vertical and the survey line did not move away from the edge, the characteristic hyperbolic signature is not seen. The amplitude spectrum for the low frequency survey also provides further evidence that there was a lot of noise in the data – i.e. the centre frequency was greater than 100 MHz.

Recommendations
Conducting GPR surveys at the Elbow Lake project site was difficult because of the irregular topography, weathered surfaces, and vegetation. With these problems and the very limited success at detecting gneissic foliation and mafic dykes using the 100 MHz and 1 GHz, additional testing is not recommended at this site.

6.4.8   Hwy 17 Site

For the massive argillite outcrop along Hwy 17, surveys were conducted along the side using both the low and high frequency antennas. The primary radar target was the major joint set oriented parallel to the surveyed surface.

For the low frequency survey (File name: Prof21), there were four possible flat–lying joints to be detected between 1.6 and 8.7 metres depth - Figure 6-43 b). As such, processing the low frequency data set involved enhancing horizontal reflections within this depth range. Figure 6-43 a) shows the processed data set with a SEC gain and both time and spatial filters applied. Because the host medium (argillite) was the same rock type as at the Vermilion River project site. the same signal propagation velocity of 0.123 m/ns was used for this site.

Both sub-horizontal and dipping reflections can be seen in Figure 6-43 a). Because the target joint set (JS1) is pervasive across the entire length of the outcrop - which is tens of metres long – it is expected that that corresponding reflectors would be continuous across the 15 m long profile. The radar profile shows sub-horizontal reflections between the 1.5 and 4.5 m depth that are relatively continuous across the survey line but have a varied amplitude from start to end. These same reflectors are strongest near the western limit and weaken towards the east. Assuming the radar velocity is correct, any of these reflections may represent the first or second fracture sketched in the corresponding geologic section – Figure 6-43 a). However, the two sub-horizontal reflections at 2.5 and 3 m on the eastern limit of the profile may also be multiples of the direct waves.

Figure 6-43 a) also shows some higher amplitude dipping reflectors between 8.5 and 14 m along the survey line. These reflections have a true dip of 20° to 40° to the east. Unfortunately, the source of these dipping reflectors is unknown because they do not correspond to any of the three major joint sets described in Section 5.4.7.

The amplitude spectrum of this low frequency survey is shown in Figure 6-44. Based on this figure, the corresponding dominant frequency was 81 MHz - a 19% reduction from the manufacturer's quoted frequency of 100 MHz. The spectrum also shows only a minor amount of high frequency noise outside of the upper bandwidth limit of 131 MHz (i.e. 50 MHz + 81 MHz = 131 MHz).

Processing the high frequency survey was different from the low frequency survey because the open fracture was inclined to the surveyed surface – Figure 6-45 a). An open dry joint existed at 1.2 m depth from the starting of the survey and increased to 1.7 m depth at the end of the survey. Aside from this fracture, two bedding planes were observed at 33 cm and 72 cm from the surface – Figure 6-45 b). Figure 6-45 a) shows the 1 GHz radar profile after application of a SEC time gain, trace stacking and point stacking. A higher point stacking was used to enhance dipping reflections.

Because the survey line was only 1.9 m long, any reflections caused by the open joint would be continuous across the profile. Unfortunately, the profile does not have any continuous reflections aside from the direct waves. Between position 0.5 and 1.5 m, there are a least ten short reflections dipping at various angles and orientations. The source of these reflections is unknown.

The amplitude spectrum for the high frequency antennas is similar to those seen at previous sites - Figure 6-46. The centre frequency has shifted down to 828 MHz due to attenuation in the ground. There is also a large depression in the spectra near this centre frequency, caused likely by ground filtering.

Conclusions

The results of both the low and high frequency surveys show that the GPR system was unsuccessful in detecting joints clearly visible from the surface of the outcrop. This was surprising because at the Vermilion River outcrop, the high frequency antennas appeared to detect a dipping joint at approximately 1.6-1.8 m depth. At this project site, the same antennas did not detect a joint within a similar depth range (1.2 to 1.7 m). The survey conditions at the Hwy 17 Site were in fact similar to those at the Vermilion River outcrop. The surveyed surface was relatively planar, which allowed for close contact with the rock surface and there did not appear to be any major sources of interference.

For the low frequency antennas, the joint spacing was approximately 2 m and these features were laterally continuous across the site, so it was surprising that the 100 MHz antennas were unable to clearly detect any of the fractures. This lack of success suggests that either the joint aperture or the dielectric contrast was the problem with detection.

For the high frequency survey, the primary target had a measured aperture of 3-4 cm at the surface and was air-filled. Using the thin layer concept, the associated Fresnel Reflection Coefficient is 0.64-0.85. These values are high enough to suggest detection was possible using the 1 GHz antennas, but along the actual survey line the apertures and corresponding R_t values were likely less.

Recommendations

Because both the low and high frequency antennas were unsuccessful at detecting flat-lying joints within the argillite host rock, no additional testing is recommended at the Vermilion River project site. It would however be beneficial to determine to conduct lab testing to determine the dielectric constant and attenuation of the host rock. Determining the dielectric properties of the argillite rock is recommended because it is my opinion that the conductivity was likely higher than 10 mS/m and hence may have contributed to the unsuccessful detection of these joints.

6.4.9   175-Orebody

Surveys at the 175-Orebody were conducted in order to evaluate whether GPR could be used in a hard rock mining environment to detect small-scale fractures with apertures < 0.5 mm. With the five dominant joint sets identified in the diorite host rock and the surveys conducted along the walls, detection of the strike lines was considered possible using radar. Since the joint sets oriented at various angles to the survey lines, data processing was more difficult because filters are generally designed to enhance either flat-lying or dipping reflections, not both. Because of this problem, processing of these underground surveys was by far the most challenging of all the project sites.

To create the depth scales for processed radar profiles at this underground site, a radar wave velocity of 0.12 m/ns was used. Although this value was not confirmed, it is considered a reasonable value - it is a velocity commonly used for hard igneous rock conditions and is quoted in Table 2-2 for dioritic rock.

6.4.9.1   7715 Drift

Figures 6-47 to 6-50 show example profiles for the low frequency surveys conducted along both sidewalls of the 7715 Drift. For each survey along the NW sidewall (File name: 175-a) and the SE sidewall (File name: 175-c), two plots have been produced showing the influence of a constant gain versus a SEC gain. Comparing Figure 6-47 to Figure 6-48 and Figure 6-49 to Figure 6-50, the profiles show that the constant gain tends to make reflectors in the first 5 m more visible, whereas the SEC gain accentuated reflectors between 5 to 12 m depth. Note that high time gains were required to enhance reflectors below 1 m depth.

In the low frequency profiles, a large number of strong continuous and discontinuous reflections can be observed. Unfortunately, most of these reflections are due to noise making interpretation extremely difficult. Various types of spatial and temporal filters were used to help minimize this noise but none proved satisfactory. As a result, the processed images shown in Figures 6-47 to 6-50 contain both a down-the-trace average filter and a trace-to-trace average filter. Although these two filters have different objectives – to enhance dipping reflectors vs. inclined reflectors - the large amount of background noise in the data sets required both to be applied.

Most of the noise or interference in the profiles is due to the wire mesh support. The antennas unavoidably had to be placed on wire mesh along parts of the survey lines: these areas have been marked on the plots. The profiles clearly show that within these areas the spurious reflections are the strongest and extend right from the surface to depths of at least 10 m.

Aside from the metallic tunnel support, areas nearest the intersection with the main access ramp were more open and caused a large amount of air wave reverberations. This is best seen in Figure 6-49 between position 0 and 6 m. Reverberations are however also seen along the entire survey line (but not to such a great depth) because of the poor contact between the 100 MHz antennas and the drift walls. Both the rough surface created by blasting and the wire mesh prevented close contact from being achieved.

If joints caused reflections in any of the profiles they cannot be distinguished from the noise. The underground sources of interference also prevented possible detection of adjacent underground openings. Recall from Section 5.4.8.1 that the low frequency survey along the NW sidewall had the potential to detect both the Sungeric Drift and a portion of the 7500 Main Access Ramp. As well, the survey on the opposite sidewall could have detected the 7630 Drift. With the locations of these three openings marked on the SEC profiles – Figure 6-48 and Figure 6-50, clearly none of these openings were detected. The unsuccessful detection of these openings suggests penetration by the low frequency antennas was likely less than 10 m into the host rock.

In hopes of minimizing the signal reverberation within this underground setting, shielded 1 GHz antennas were used to conduct surveys across the sidewalls. Figure 6-51 and Figure 6-52 show profiles of the high frequency surveys with different processing applied to the data sets. Unlike the low frequency surveys, a topographic correction was required for the high frequency surveys since the maximum depth of penetration was less than 1.5 m and the changes in topography along the survey line varied up to 0.5 m. Another difference between the low and high frequency profiles is that only a SEC time gain was used to enhance reflections below the direct air and ground wave.

Processing the high frequency data set using a SEC gain and filters similar to that used for the low frequency surveys - Figure 6-51 a) and Figure 6-52 a) – nothing can be seen beyond the noise multiples which exist parallel to the surveyed surface. In order to 'see' beyond these multiples, the same data was then trace-differenced – Figure 6-51 b) and Figure 6-52 b). With trace differencing, no distinct reflections can be identified.

Figure 6-53 and Figure 6-54 show representative amplitude spectra for both the low and high frequency surveys conducted in the 7715 Drift. For the low frequency surveys, the spectrum shows the antennas were operating at a dominant frequency of 87 MHz instead of the manufacturers' quoted frequency of 100 MHz. This corresponds to a reduction of 13% due to ground attenuation of the radar energy. Similarly for high frequency spectrum shows the dominant frequency is 856 MHz. This is a 14% reduction from the quoted reference value of 1000 MHz. Similar to the high frequency amplitude spectra for the other project sites, it has an obvious depression around 800 MHz. The spectrum also shows high frequency noise above 1100 MHz.

6.4.9.2   Main Access Ramp

Two short surveys were conducted along the SW sidewall of the Main Access Ramp in hopes of detecting a clearly visible wedge. Figure 6-55 and Figure 6-56 show a processed radar profile using the low and high frequency antennas. In both profiles, the wedge has been sketched to help identify the two joint planes that were measured at the site.

For the 100 MHz survey, a constant gain was applied because the wedge is located in the near surface; recall, that the two joint sets intersect at a depth of 0.8 m (Figure 5.40). Figure 6-55 clearly shows that the wedge is located too close to the surface to be detected by the radar system. Any reflections by either joint plane are masked by the direct ground wave.

With the unsuccessful detection using the low frequency antennas, the 1 GHz antennas were thought to be ideal for detection of the rock wedge because the resolution in the near surface was far greater. Figure 6-56 shows the results of the high frequency survey after application of a SEC time gain and a point-stacking filter. The profile shows strong and relatively continuous flat-lying reflections from 0.25 to 1.1 m depth, but no strong, coherent dipping events that would be associated with the two visible joint planes. The flat-lying reflections are likely noise and not rock structure.

The amplitude spectra for the low and high frequency surveys conducted within the main access ramp are shown in Figure 6-57 and Figure 6-58. Comparing the low frequency spectrum for the ramp to the drift (i.e. Figure 6-57 to Figure 6-53), the actual centre operating frequency were identical - 87 MHz. However, the spectrum for the ramp shows more noise (both low and high frequency) and slightly smaller amplitudes. Comparing the high frequency spectrum for the ramp to the drift (i.e. Figure 6-58 to Figure 6-54), the conclusions are similar - the amplitudes are again slightly lower, and there is more noise in the data.

Conclusions

The processed radar profiles for this underground site are extremely complex, showing numerous strong reflections. This increased complexity is due to complex underground conditions. Unfortunately, most of these reflectors appear to be caused by noise, not rock structure. Various types of processing were conducted in order to 'see' beyond the noise but none proved successful.

Based on radar surveys conducted in other hard rock environments, this lack of detection was not surprising based on the results of the case studies discussed in Section 4.6.1.3. The host rock was relatively homogeneous, however the actual dielectric properties were unknown, thus it is likely that the conductivity may have been higher than 10 mS/m, which is the recommended maximum conductivity value for successful GPR work. The maximum depth of penetration was lower than anticipated for both the low and high frequency antennas however the joints still existed within these penetration depths.

The tight nature (or small aperture) of the joints was probably the biggest problem at this project site. Most of the joints ranged from closed to tight and were dry. Because these apertures are less than the dominant wavelength for both the low and high frequency conditions, these targets fall under the thin layer concept discussed in Section 2.6.4. Assuming a joint aperture of 0.5 mm under air-filled conditions, the Fresnel Reflection Coefficient ranges between 0.01 to 0.001 for the 1 GHz and 100 MHz frequencies respectively. Based on conclusions given in Section 4.6.1.4, these values are likely too low, therefore it is theoretically not possible to detect these small-scale targets with the GPR antenna frequencies used.

The abundance of noise in this underground environment was also a large problem. The wire mesh, rockbolts, and other metallic objects inside the drift and ramp could not be avoided. As well, the low frequency antennas should have been shielded or some type of radio-frequency absorbing material should have been placed around the antennas to damp the reverberations. The high frequency antennas were shielded however the irregular surfaces prevented close contact being attained with the rock surface.

Recommendations

With no rock structure detected using either the 100 MHz or 1GHz antennas, no addition testing is recommended in underground environments with extensive sources of noise (metallic objects). It would however be advantageous to conduct surveys in a similar underground environment where thin-membrane support was used instead of wire mesh and rock bolts. Because these membranes are non-metallic, the interference should be significantly lower. As well, any additional testing should be done using either shielded antennas or radio-frequency absorbing material should be placed around the antennas. Surfaces that are relatively planar should be sought out rather than rough and irregular surfaces. Finally, higher frequency antennas (>1000 MHz) will likely be required to successfully detect tight air-filled fractures. But the use of very high frequency GPR equipment will further limit the depth of penetration to less than 1 m.

6.5 Summary of the Sudbury Field Surveys

On the basis of the field survey results of Section 6.4, each project site has been rated from 0 – no success at detecting rock structure to 4 – high success at detecting rock structure for the 100 MHz and/or 1GHz antennas (Table 6-1). In order to better understand success in detection of the primary radar targets, it is important consider the host rock, survey environment, antenna centre frequency, and target characteristics at each of the nine project sites. Table 6-1 summarizes these parameters for the various sites.

Table 6-1 shows that the level of success for the field surveys varied from high success for the surveys conducted on the limestone blocks to none at the underground test site. However, unlike the Chapter 4 case studies, the majority of the field surveys (60 to 70 %) experienced no to limited success at detecting rock structure.

Considering the influence of the antenna centre frequency on the level of GPR success. the 1 GHz antennas proved to be more successful in detecting small-scale fractures than the 100 MHz antennas. The 1 GHz antennas detected dry open fractures ≥ 3 mm in aperture. whereas the low frequency antennas only detected unconfirmed bedding and foliation planes in sedimentary and metamorphic rock. Due to these poor results with the low frequency antennas. it is recommended that future GPR surveying be conducted only with frequencies above 100 MHz when detection of interfaces less than 1 cm is required.

The host rock at the nine project sites varied from sedimentary limestone to metamorphic gneiss. At most of the sites, the rock was relatively homogeneous and the conductivity was assumed to be low (< 10 mS/m). however no testing was conducted to confirm this assumption. The meta-sandstone at the Hwy 17 Bypass site and the gneiss blocks along the WGMC walkway may not have been ideal because the rock proved to be more heterogeneous in comparison the other rock types. Aside from primary fracture targets. these two rock types contained additional rock structure that complicated interpretation of the radargram - at both sites. the reflections for the target fractures were indistinguishable from reflections due to mineralogical changes or foliation planes.

The problem found with heterogeneous rock was however experienced only with the high frequency antennas because they have an increased ability to detect smaller changes in dielectric constant. Perhaps this explains why Buursink and Lane (1999) found no problem detecting fractures in a geologically heterogeneous environment using 100 MHz antennas. To clarify whether complex geologic conditions influences detection using GPR. it is recommended that further testing be conducted in similar environments.

There were three different survey environments used for the conducting GPR surveys: surface outcrops, pieces of cut rock, and an underground mining environment. Surveys across the rock blocks were the most successful followed by the surface outcrops and the underground mine. The unsuccessful detection of any rock structure at the underground mine was anticipated based on past studies in similar environments (Section 4.6.1.3). The majority of the drift back and sidewalls was supported by wire mesh and rock bolts which contributed to the high level of noise observed in the radar profiles for both the low and high frequency profiles. As well. the rough surfaces prevented close contact from being achieved between the rock and the system antennas.

Most of the surface outcrops and rock blocks were of limited lateral extent so there was often noise in the data due to nearby vertical rock faces. When the survey lines were oriented such that the antennas gradually moved away from a near vertical face. the noise manifested itself in the radar profiles as hyperbolic events. These hyperbolic events could only be minimized by the basic processing techniques but were never removed entirely from the final image. Fortunately. the desired reflections could still be seen through these noisy reflections. When the survey lines were oriented parallel to a vertical face, the noise appeared as sub-horizontal events in the radar profile. There is presently no guidance as to how to eliminate such events from the radargram. This noise can complicate matters even more so when the targets are also flat-lying.

Similar to the comparison of the Chapter 4 case studies (Section 4.6). it is most likely that the characteristics of the primary radar targets had the most control over the level of detection success for each survey. The targets varied from man-made fractures to natural joints to foliation and bedding planes and finally to mafic dykes. Despite the geologic distinctions among these targets, in terms of GPR they all meet the criteria of a 'thin layer' – i.e. their thickness. aperture or width was always less than the dominant radar wavelength. Another similarity was the fact that all the targets were dry. The angle between the target(s) and the survey line however varied

between the sites. For the majority of the sites, the target had the most favorable orientation for surveying – i.e. flat-lying – however, there were also targets inclined between 10° and 70° to the survey line.

The detected and undetected fractures at the various project sites as well as those from the Chapter 4 case studies have been plotted on graphs of antenna centre frequency versus aperture for air-filled and water-filled conditions – Figure 6-59. This plot was produced in order to determine what threshold R_f value or range of values is required for successful detection of fractures for various antenna frequencies. Because the Fresnel Reflection Coefficient is also dependent on the contrast in dielectric constant, the case study results from Toshioka et al. (1995) were not included because the host rock had a dielectric constant of 19.5, which is significantly different from all other rock types.

Figure 6-59 shows that the R_f threshold is a zone between 0.01 and 0.065 (absolute value). Rock structure with reflectivity values above this identified zone are detectable using GPR and non-detectable below this zone. The 0.01 value is the lower limit and was based on a value quoted from the literature (Sections 2.6.3 & 2.6.4). The upper value of 0.065 is a value the matches what has been obtained in practice. This upper value is therefore a more realistic value however this line is based on relatively limited data and may be subject to error. As such, it is recommended that additional testing be done on a variety of fracture apertures and using different antenna frequencies to improve the position of both limits.

These plots are somewhat conservative because the fracture apertures are likely overestimated since they were measured from the surface of the outcrop and not along the survey line. Surface weathering and loosening of the rock creates wider apertures than would be found at depth. Only the surveys conducted along the perfectly planar limestone blocks at Jarvis Resources Ltd. are the 'true apertures'.

Under these threshold values for R_f, Table 6-2 and Table 6-3 shows the minimum detectable fracture aperture for antenna frequencies between 100 MHz and 1 GHz under dry and saturated conditions. These calculations are based on assuming the host rock has a dielectric constant of ≈ 6.25. Tables 6-2 and 6-3 show there is a large difference between the minimum detectable fracture aperture for the lower bound R_f value of 0.01 compared to the upper bound R_f value of 0.65. This supports the recommendation for additional testing on small-scale fractures. Regardless of this, the values suggest that under dry conditions tight fractures cannot be detected using even the highest antenna frequencies but under wet conditions there is a chance for detection if the antenna frequency is high enough.

6.6 CONCLUSIONS

Of the 32 surveys that were conducted approximately 41 % did not detect any rock structure. 25 % successfully detected the primary radar targets, 22 % detected either some of the targets or detected all the primary targets in addition to other rock structure, and for the remaining 12 % there was some uncertainty as to whether any structure was detected. The surveys conducted with the 100 MHz antennas were particularly disappointing, but based on the results shown in Table 6-2, it comes as no surprise that the 1 GHz antennas were significantly better at detecting small-scale rock structure.

The most successful surveys were those conducted on the rock blocks. Air-filled gaps with widths between 3 and 8 cm (or large-scale structural features) were detected between pieces of

limestone. Despite this high success, these apertures are not typical of natural discontinuities in rock and therefore the success is of limited interest to engineers. The engineering community is more interested in detecting very tight to partly open fractures (i.e. from < 0.1 to 0.5 mm) using GPR technology.

A drawback to the field surveys conducted for this thesis was the fact that all the target discontinuities were dry. As mentioned in this and previous chapters, water-filled fractures have a significantly higher chance of being detected because the reflection coefficient is higher and there is a polarity change in the wavelet. For example, using the 100 MHz antennas, air-filled fractures 30 mm wide or water-filled fractures 2 mm wide should be detected assuming the R_t threshold for detection is 0.065.

The field surveys conducted on the rock blocks where aluminum foil was used are excellent examples which show the influence of fracture aperture and infilling. Foil is extremely thin ($\approx$ 0.03 mm) and most geologic targets with this size would likely not be detected using 1 GHz antennas, however the infinite contrast in dielectric constant between this metal conductor and the rock enabled its detection. In a real geologic environment the highest contrast in dielectric constant would exist for a water-filled fracture.

For the surveys conducted across the gneiss blocks along the WGMC walkway and across the meta-sandstone at the Hwy 17 Bypass, the primary radar targets (i.e. fractures) were identified however the high frequency antennas also detected other rock structure. Because of this, these two project sites are excellent examples of the non-uniqueness of the radar reflections. As for both sites, if the locations of the fractures were unknown, the interpreter could not unambiguously pick them out of the radar profile.

At the Hwy 637-Killarney Outcrop and Vermilion River Outcrop the results were inconclusive even after basic processing. At Killarney, higher frequency antennas were probably required for detection of the fracture zone at the granite outcrop. However, at the Vermilion River Outcrop the dipping reflections observed in the profiles were likely system noise and not caused from reflection off a rock joint. This is based on the fact that at the Hwy 17 Site, where the site and survey conditions were similar to Vermilion River, there was no success using the 1 GHz antennas.

Surveys at the WGMC Outcrops, Elbow Lake Outcrops, Hwy 17 Outcrop, and the 175-Orebody were unsuccessful at detecting rock structure, however these results still contribute to the objectives of this thesis. At many of these sites, I was testing the limits of the equipment knowing detection may not be possible due to either an insufficient contrast in dielectric constant or an inadequate target thickness. These results show the limitations of the radar system and/or the conditions that inhibit detection.

Table 6-1 Summary of thesis field studies for rock structure detection.

Site Name	Host Rock	Survey Environment	Antenna Centre Frequency (MHz)	Rock Structure			Level of GPR Success
				Primary Target (s)	Infilling	Orientation (w.r.t. survey line)	
Jarvis Resources Ltd.	limestone	rock blocks	1000	artificial fractures	air	parallel	4
WGMC Walkway	gneiss	rock blocks	1000	artificial fractures	air	parallel	2
Hwy 17 Bypass	meta-sandstone	highway outcrop	1000	bedding joints & fracture zone	n/a	parallel	2
Vermilion River	argillite	highway outcrop	1000	joint	air	sub-parallel (10° off line)	2
Willet Green Miller Centre	meta-sandstone	surface outcrops	100 / 1000	bedding planes	n/a	inclined (40° off line)	1 / 0
Hwy 637 - Killarney	granite	highway outcrop	100	fracture zone	broken rock	parallel	0
Elbow Lake	gneiss	surface outcrops	100 / 1000	foliation & mafic dykes	n/a	inclined & parallel	1 / 0 to 2
Hwy 17 Site	argillite	highway outcrop	100 / 1000	joints	air	inclined & parallel	0 / 0
175-Orebody	diorite	underground mine	100 / 1000	joints	air	inclined & parallel	0 / 0

0 = No success; 1 = Limited success; 2 = Marginal success; 3 = Good success; 4 = High success
n/a = not available

197

Table 6-2 Minimum detectable fracture apertures for various GPR antenna frequencies under air-filled conditions. (Assuming $\varepsilon_r \approx 6.25$ and $\sigma < 10$ mS/m for the host rock.)

Antenna Centre Frequency	$R_t = 0.01$		$R_t = 0.065$	
	Minimum detectable fracture aperture (mm)	Fracture classification	Minimum detectable fracture aperture (mm)	Fracture classification
100 MHz	4.6	moderately wide	30	major discontinuity
200 MHz	2.3	moderately wide	15	wide
300 MHz	1.5	open	10	wide
500 MHz	0.9	open	6	moderately wide
1000 MHz	0.5	partly open	3	moderately wide

Table 6-3 Minimum detectable fracture apertures for various GPR antenna frequencies under water-filled conditions. (Assuming $\varepsilon_r \approx 6.25$ and $\sigma < 10$ mS/m for the host rock.)

Antenna Centre Frequency	$R_t = 0.01$		$R_t = 0.065$	
	Minimum detectable fracture aperture (mm)	Fracture classification	Minimum detectable fracture aperture (mm)	Fracture classification
100 MHz	0.33	partly open	2.1	open
200 MHz	0.16	tight	1.1	open
300 MHz	0.11	tight	0.7	open
500 MHz	0.07	v. tight	0.4	partly open
1000 MHz	0.03	v. tight	0.2	tight

35.2 cm

8.2 cm

Eight limestone slabs
(v = 0.110 m/ns)

Artificial fracture; air-filled (Note 1.)

Marble block

Depth (m)

Note 1. Due to the higher signal velocity in air, the 8.2 cm wide fracture has a reduced thickness of 3.0 cm in a profile plotted with a velocity of 0.110 m/ns.

b) Geologic section of Jarvis1h from Block Site 1.

Depth (m) v = 0.110 m/ns

Distance across limestone slabs (m)

Artificial fracture

Ringing

Two-way travel time (ns)

a) Processed radar profile. Processing steps included: polarity reversal, dewow, DC shift, & trace averaging of 5. Note that no gain was applied to the data set.

Figure 6-1 High frequency survey 'Jarvis1h' at Block Site 1 - Jarvis Resources Ltd.: with accompanying geologic section.
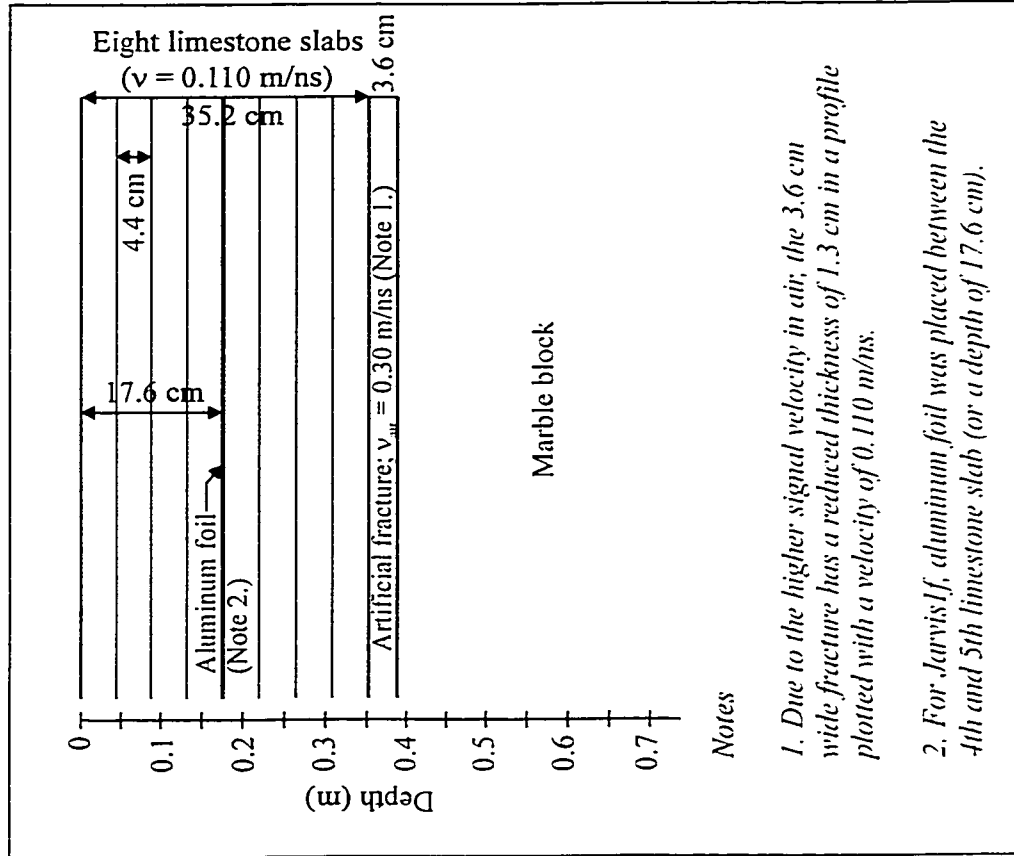
Figure 6-2 Geologic section for high frequency surveys 'Jarvis1e - without foil' and 'Jarvis1f - with foil': Block Site 1 - Jarvis Resources Ltd.

The figure contains the following labels:

Eight limestone slabs (v = 0.110 m/ns)

3.6 cm

35.2 cm

4.4 cm

17.6 cm

Aluminum foil (Note 2.)

Artificial fracture: $v_{air} = 0.30$ m/ns (Note 1.)

Marble block

Depth (m): 0, 0.1, 0.2, 0.3, 0.4, 0.5, 0.6, 0.7

Notes

1. Due to the higher signal velocity in air, the 3.6 cm wide fracture has a reduced thickness of 1.3 cm in a profile plotted with a velocity of 0.110 m/ns.

2. For Jarvis1f, aluminum foil was placed between the 4th and 5th limestone slab (or a depth of 17.6 cm).

Depth (m) v = 0.110 m/ns

Distance across limestone slabs (m)

Two-way travel time (ns)

Foil

Artificial fracture

b) Processed radar profile of Jarvis1f (with foil). Processing steps included: dewow, DC shift, & trace averaging of 2. Note that no gain was applied to the data set.

Depth (m) v = 0.110 m/ns

Distance across limestone slabs (m)

Two-way travel time (ns)

Artificial fracture

a) Processed radar profile of Jarvis1e (without foil). Processing steps included: dewow, DC shift, & trace averaging of 2. Note that no gain was applied to the data set.

Figure 6-3 High frequency surveys 'Jarvis1e' and 'Jarvis1f' at Block Site 1 - Jarvis Resources Ltd.
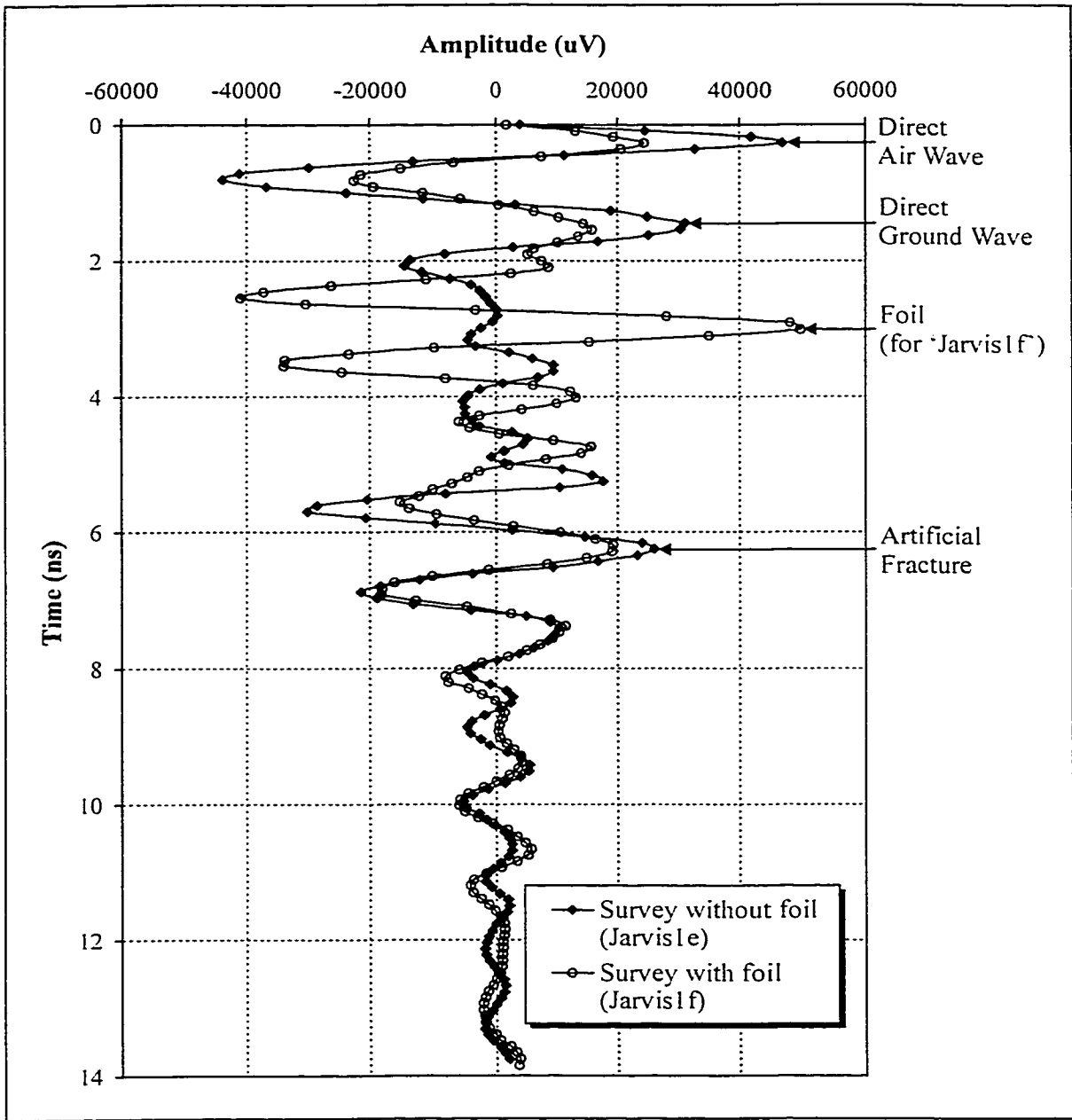
Figure 6-4 Comparison of an average trace from 'Jarvisle - without foil' to 'Jarvislf - with foil'.
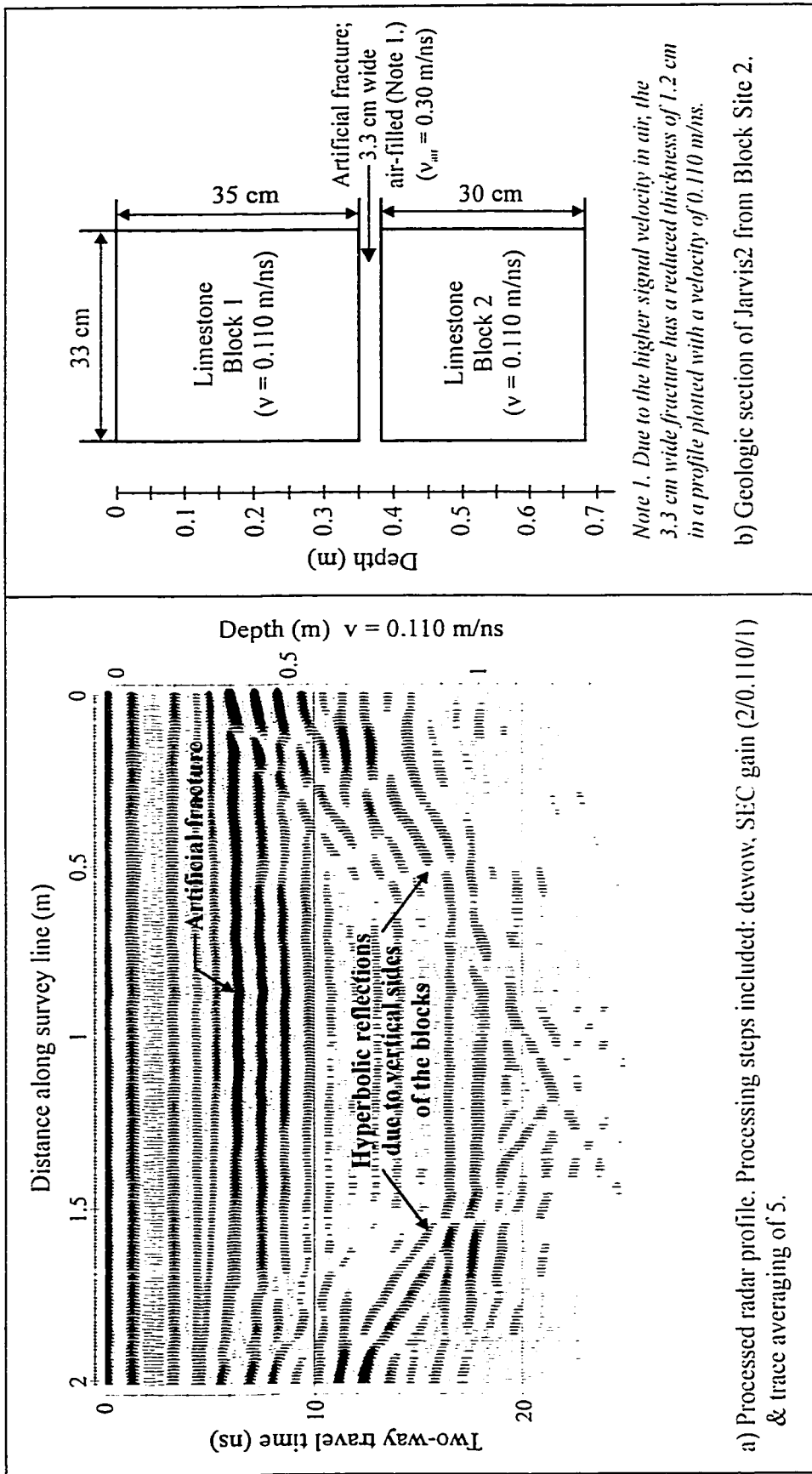
Figure 6-5 High frequency survey 'Jarvis2' at Block Site 2 - Jarvis Resources Ltd.; with accompanying geologic section.

a) Processed radar profile. Processing steps included: dewow, SEC gain (2/0.110/1) & trace averaging of 5.

b) Geologic section of Jarvis2 from Block Site 2.

Note 1. Due to the higher signal velocity in air, the 3.3 cm wide fracture has a reduced thickness of 1.2 cm in a profile plotted with a velocity of 0.110 m/ns.

203
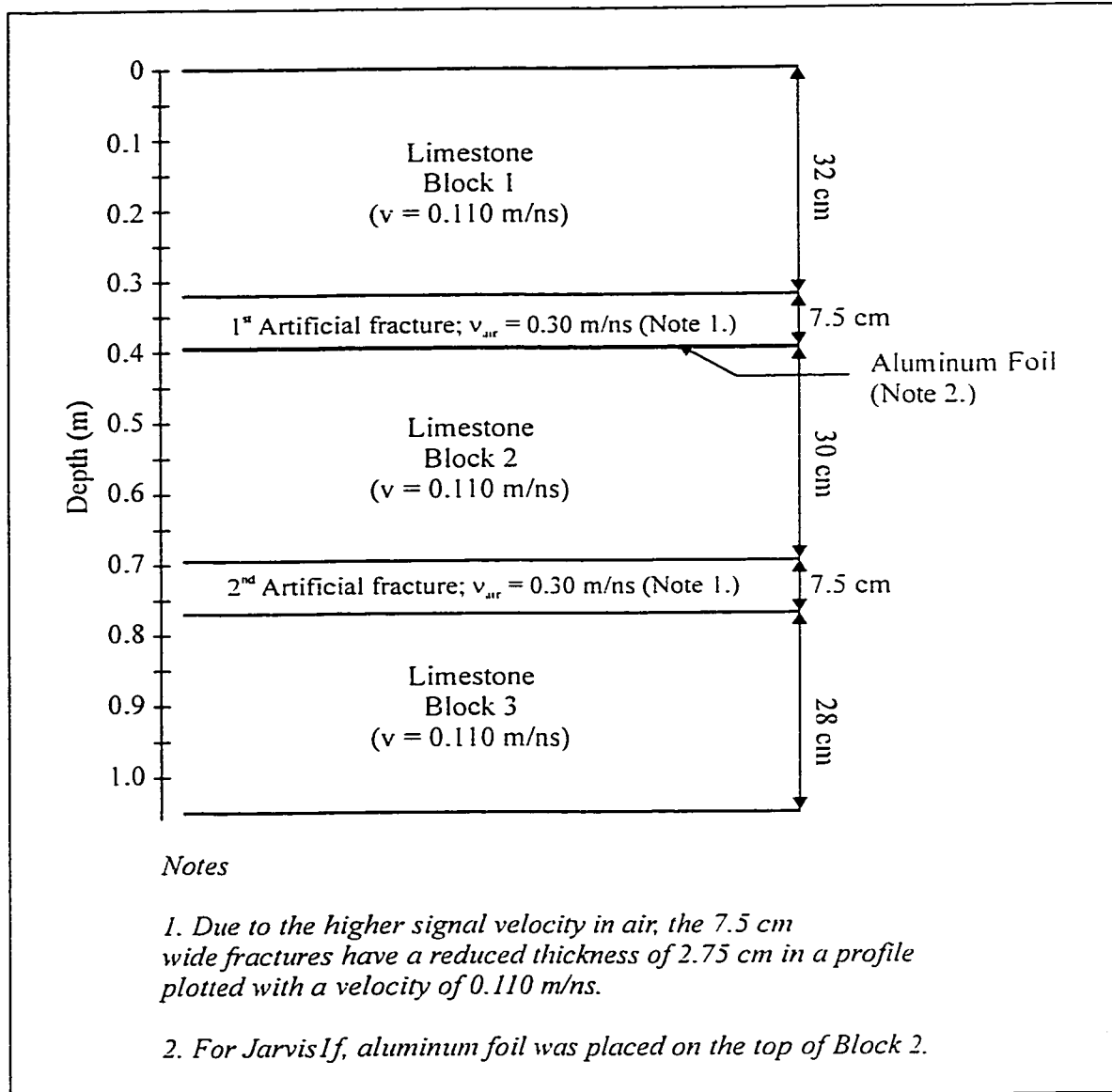
Figure 6-6 Geologic section for high frequency surveys 'Jarvis4 - without foil' and 'Jarvis 4f- with foil'; Block Site 3 - Jarvis Resources Ltd.
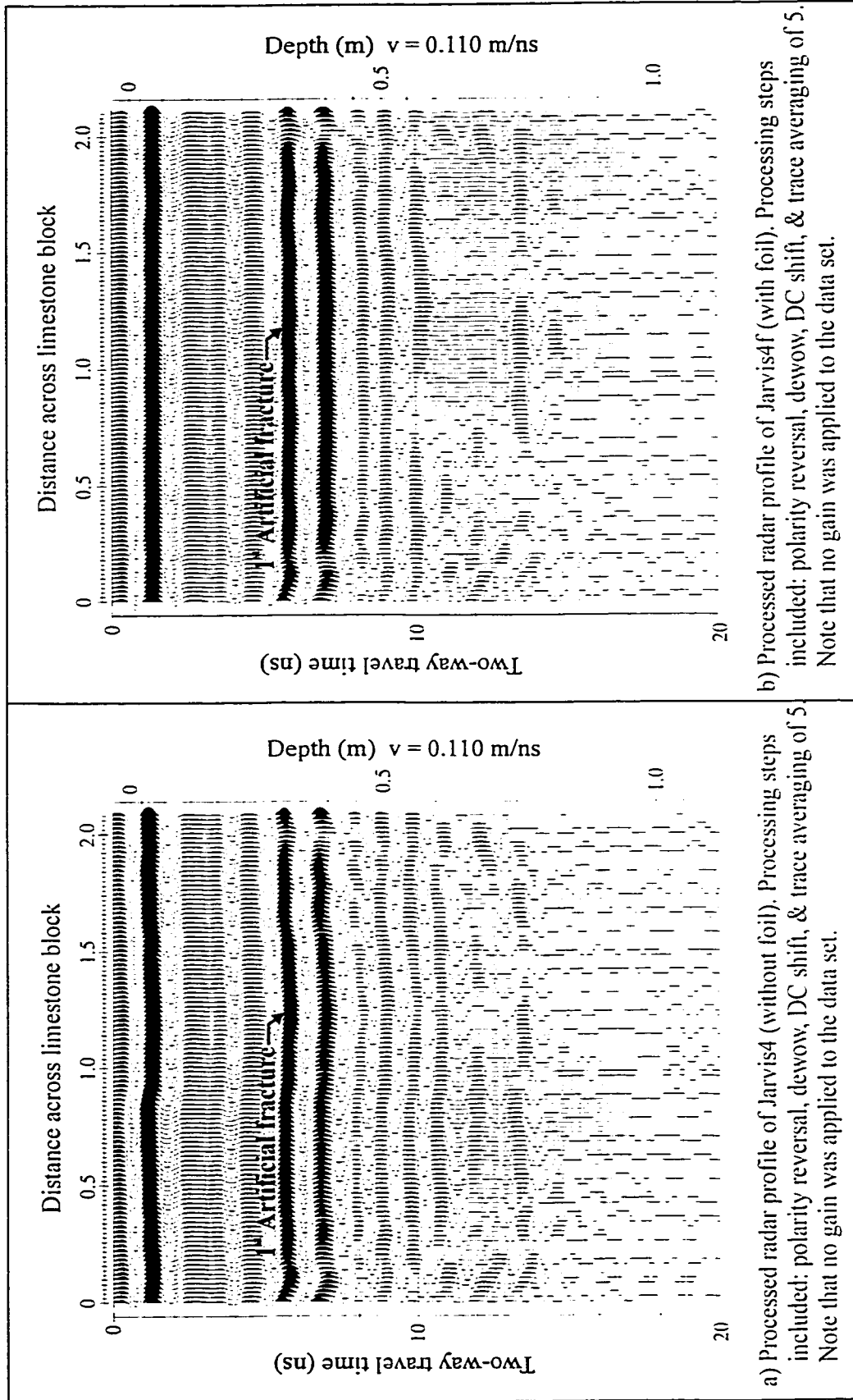
Figure 6-7 High frequency surveys 'Jarvis4' & 'Jarvis4f' at Block Site 3 - Jarvis Resources Ltd.

a) Processed radar profile of Jarvis4 (without foil). Processing steps included: polarity reversal, dewow, DC shift, & trace averaging of 5. Note that no gain was applied to the data set.

b) Processed radar profile of Jarvis4f (with foil). Processing steps included: polarity reversal, dewow, DC shift, & trace averaging of 5. Note that no gain was applied to the data set.
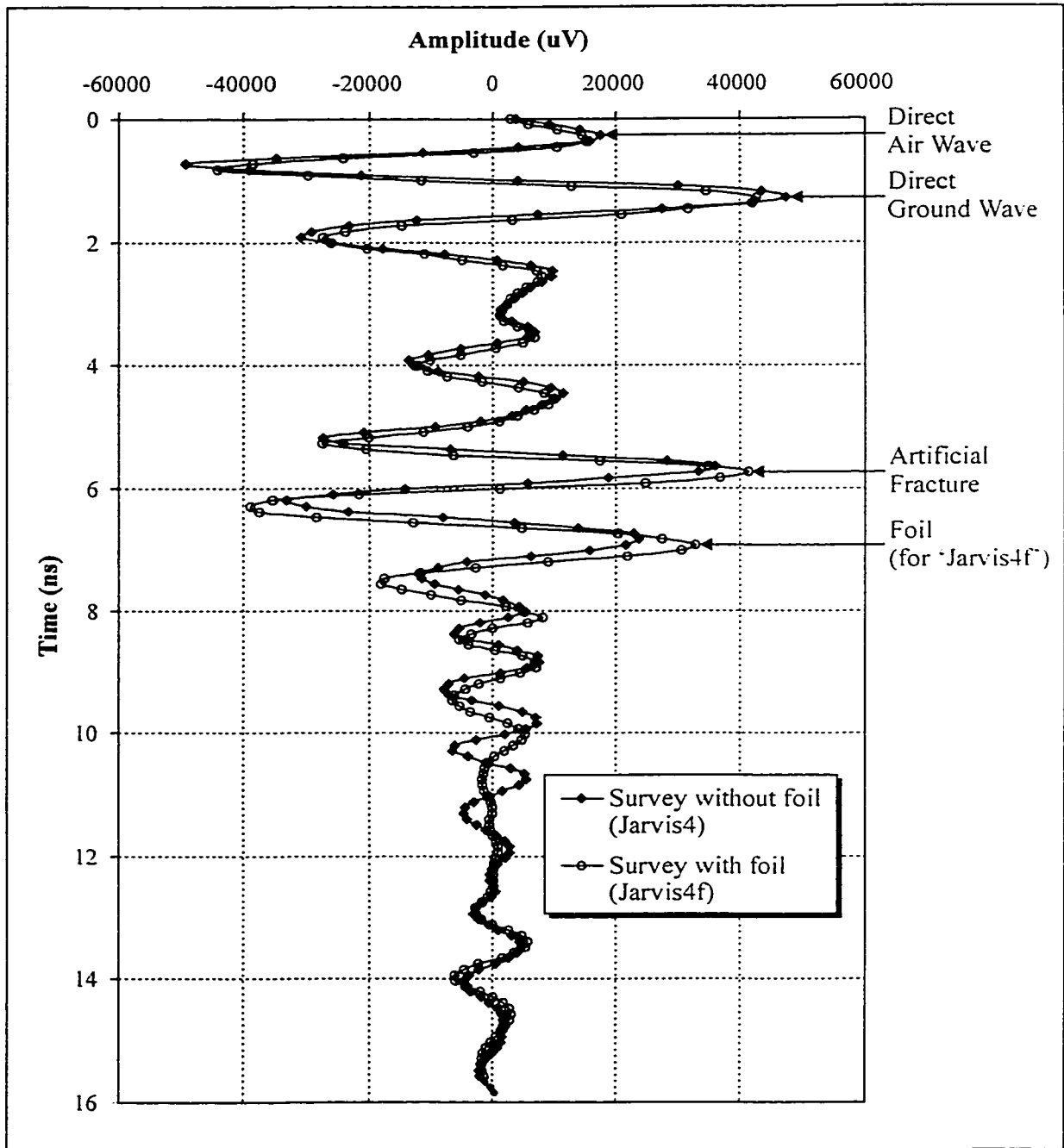
Figure 6-8 Comparison of an average trace from 'Jarvis4 - without foil' to 'Jarvis4f - with foil'.
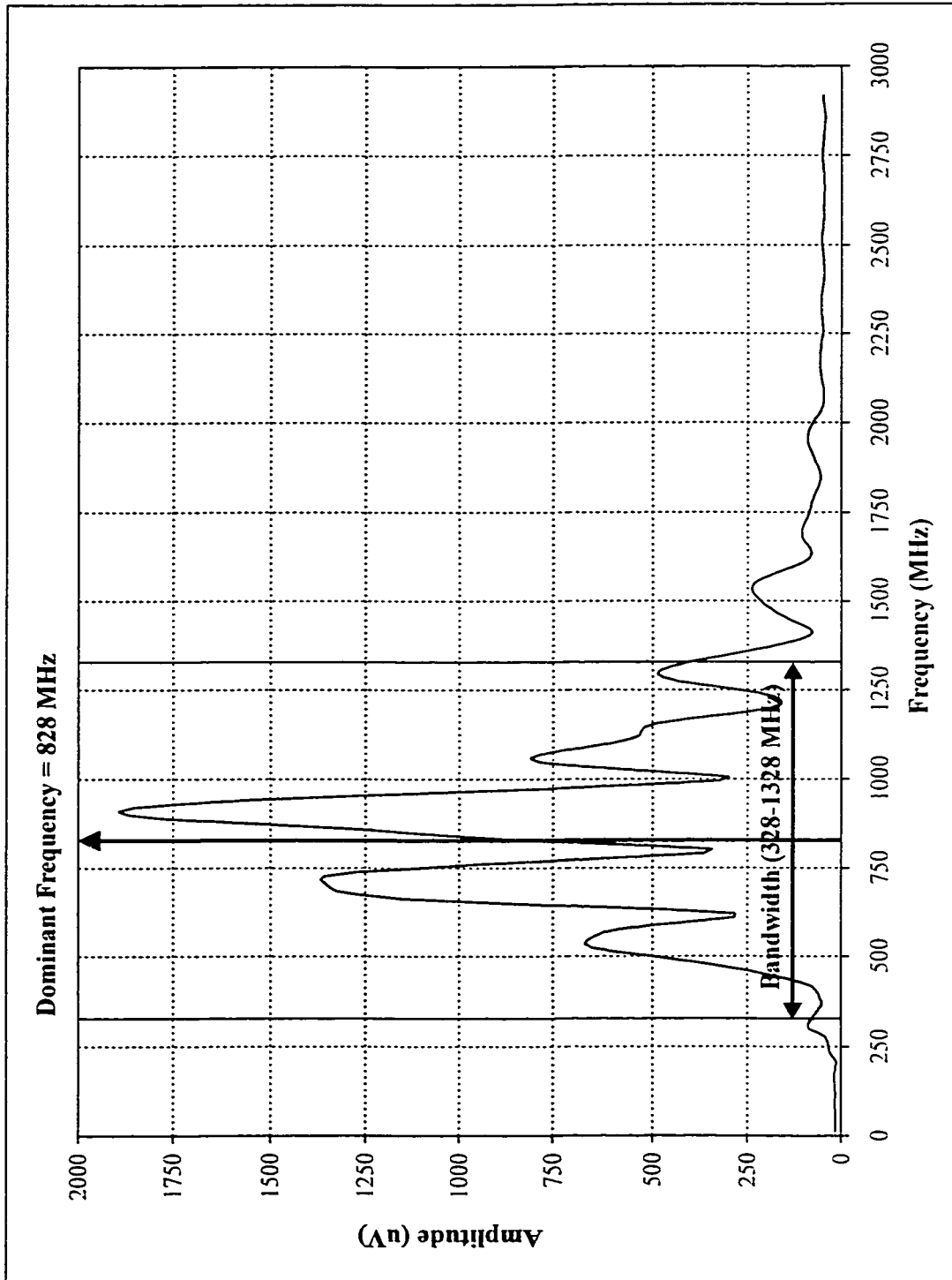
Figure 6-9 Representative amplitude spectrum for the high frequency surveys conducted on limestone/marble rock blocks at Jarvis Resources Ltd.

207
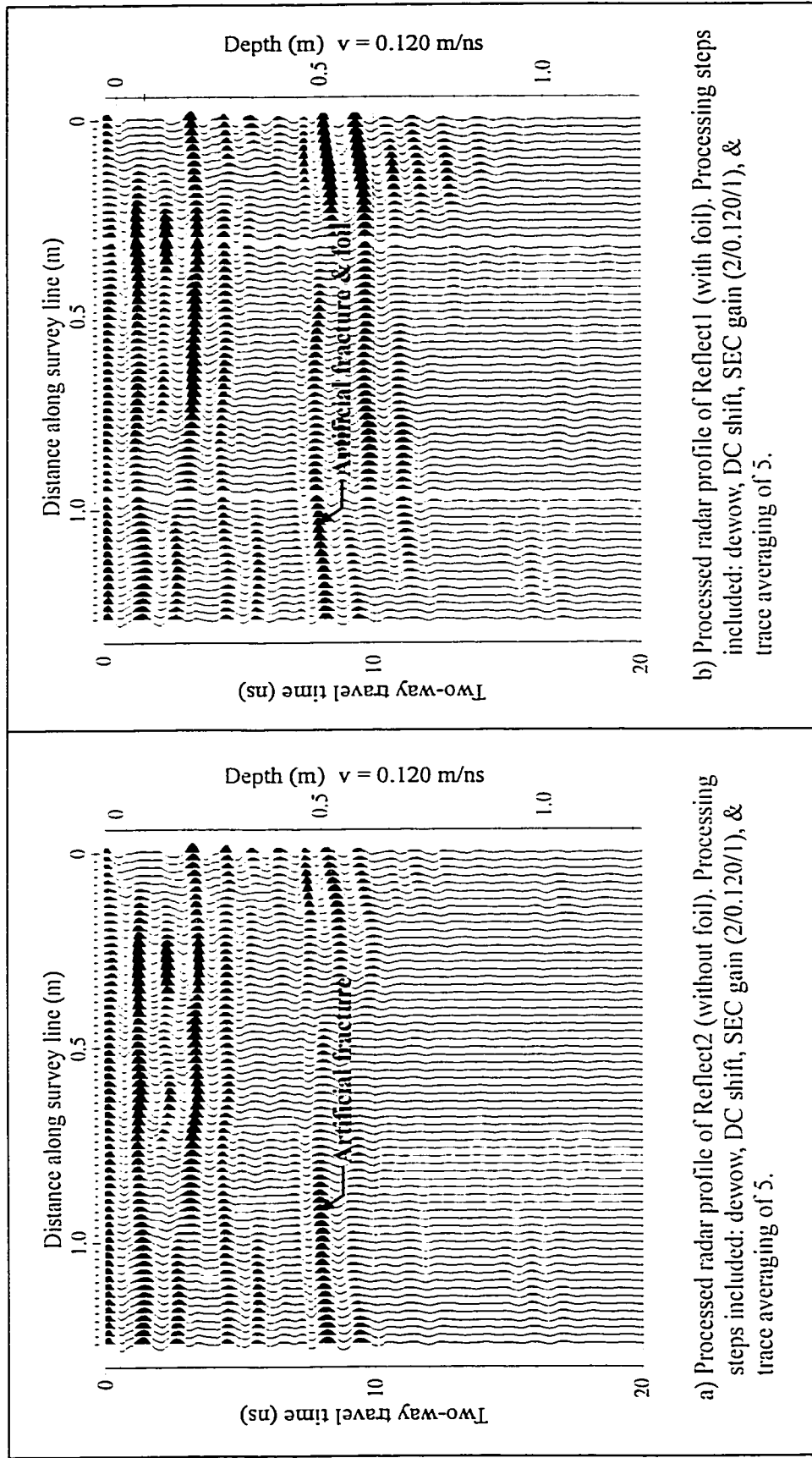
Figure 6-10 High frequency surveys 'Reflect1' & 'Reflect2' on the gneiss blocks along the WGMC walkway. (Note: For 'Reflect1' aluminum foil was placed between the two gneiss blocks).

a) Processed radar profile of Reflect2 (without foil). Processing steps included: dewow, DC shift, SEC gain (2/0.120/1), & trace averaging of 5.

b) Processed radar profile of Reflect1 (with foil). Processing steps included: dewow, DC shift, SEC gain (2/0.120/1), & trace averaging of 5.

208
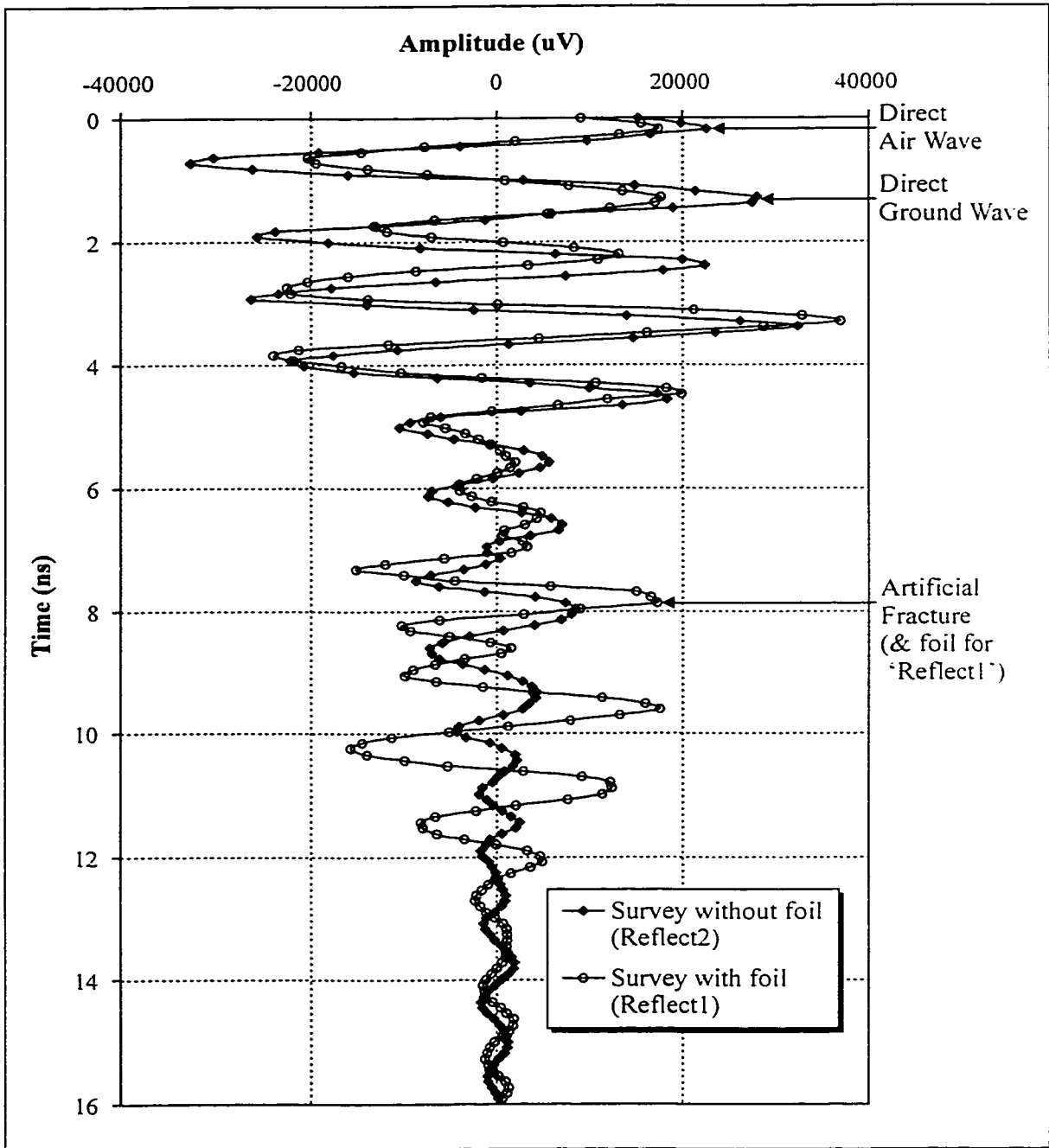
Figure 6-11 Comparison of an average trace from 'Reflect1 - with foil' to 'Reflect2 - without foil'.
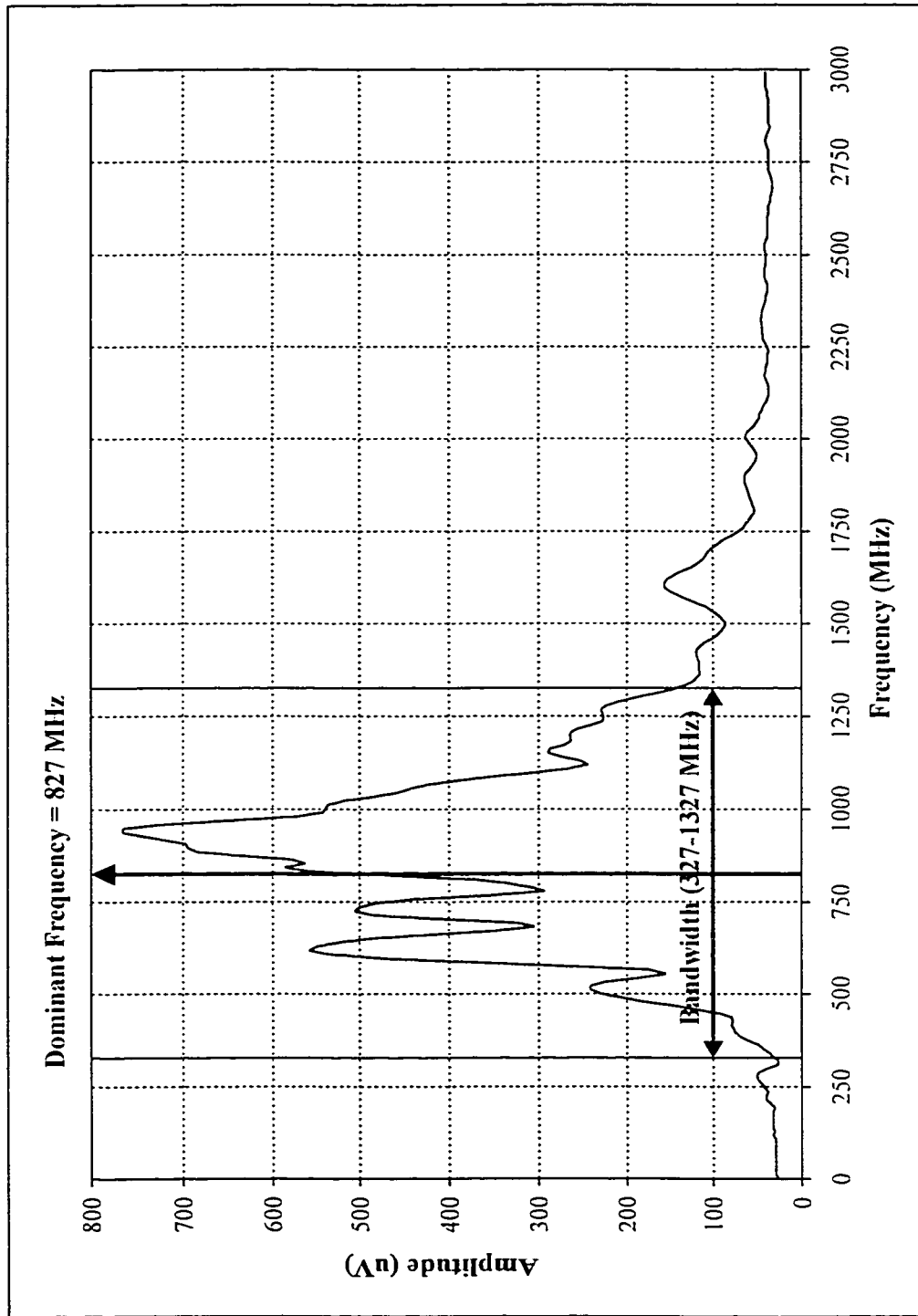
Figure 6-12 Representative amplitude spectrum for the high frequency surveys conducted on the gneiss blocks along the WGMC walkway.
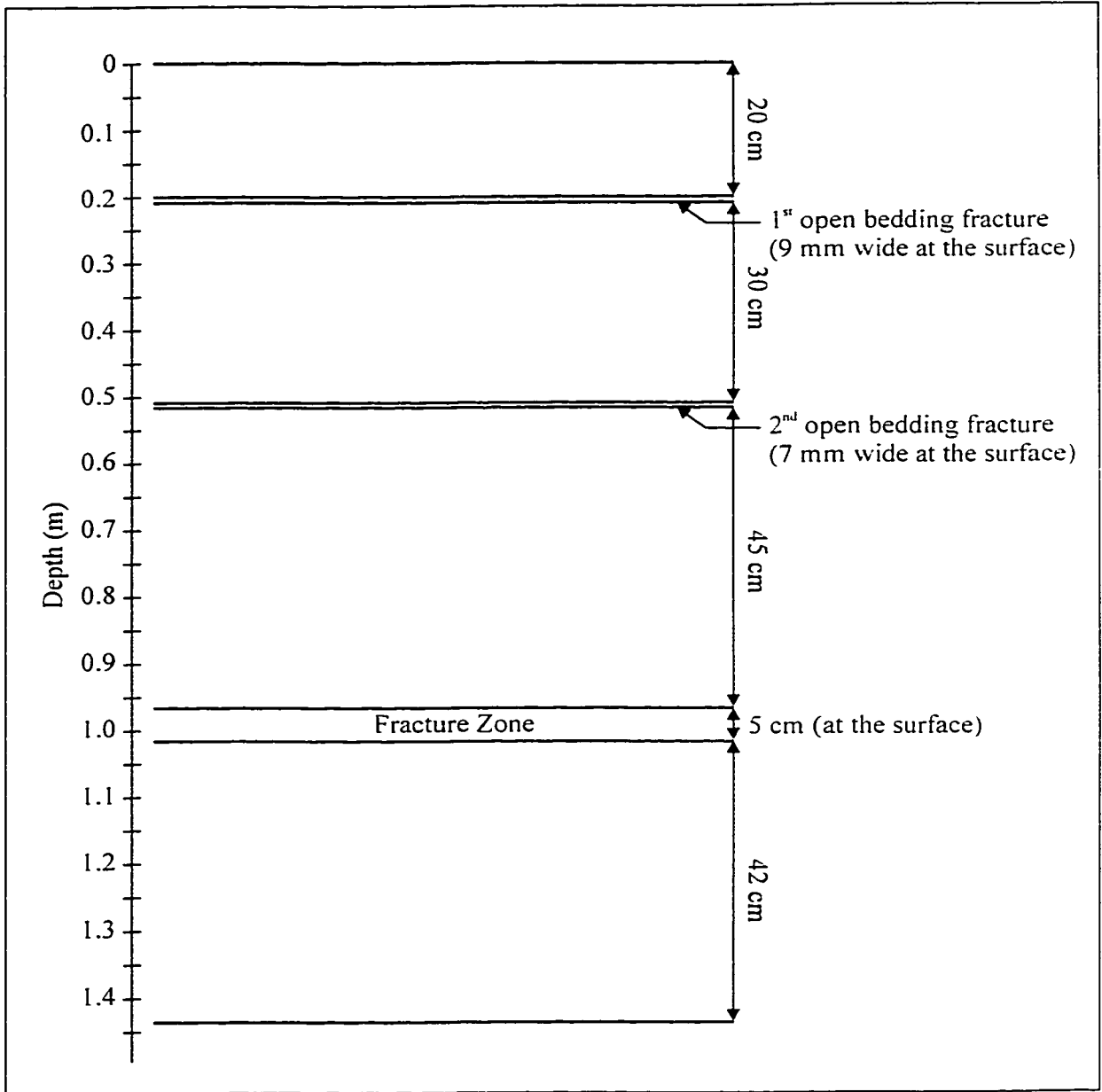
Figure 6-13 Geologic section for all Hwy 17 Bypass surveys.
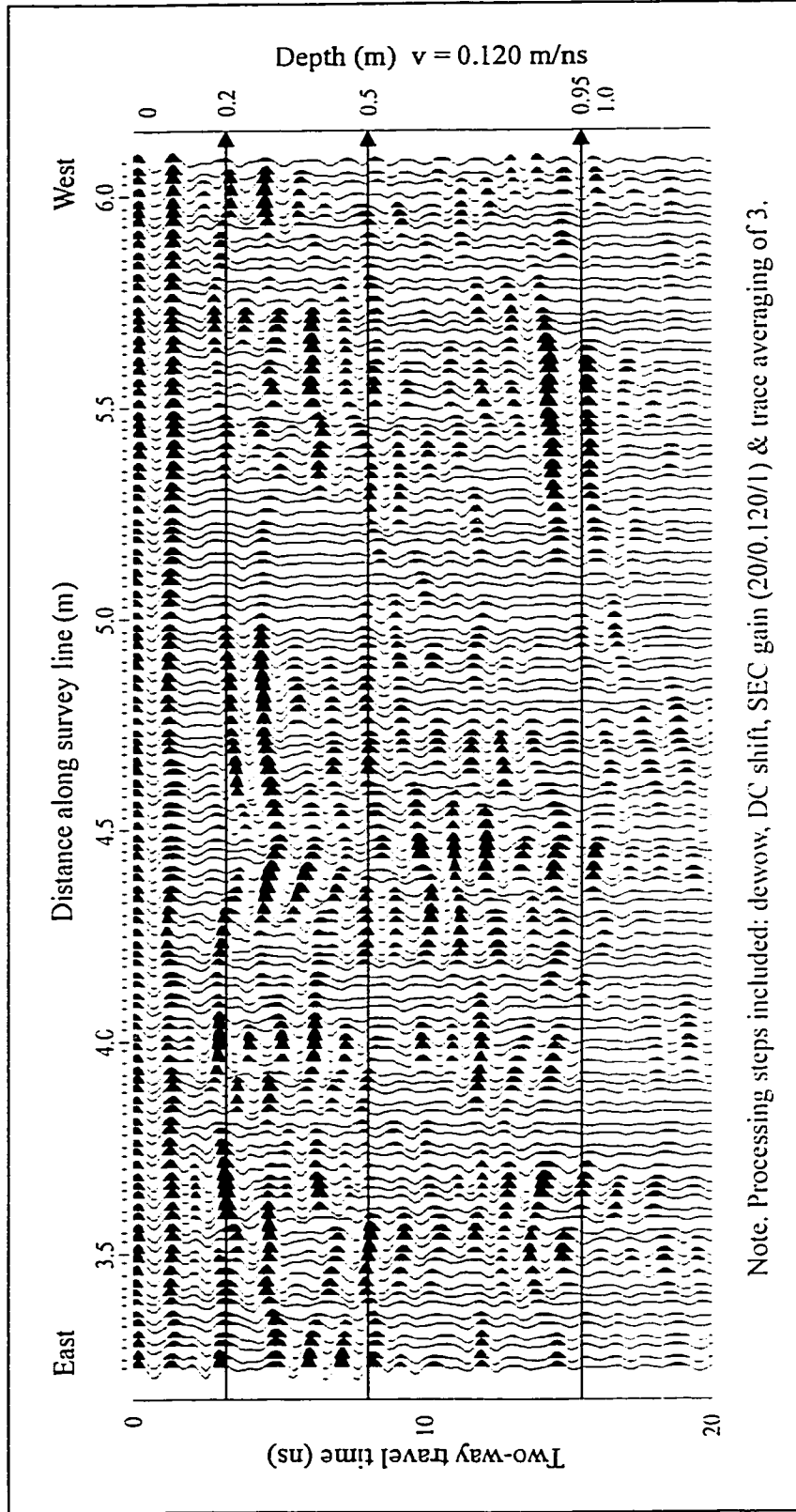
Figure 6-14 High frequency survey 'BY-1G-2a' with a trace-averaging filter; Hwy 17 Bypass. (Note: Surveyed with a sampling frequency of 6.6 GHz).

Note. Processing steps included: dewow, DC shift, SEC gain (20/0.120/1) & trace averaging of 3.
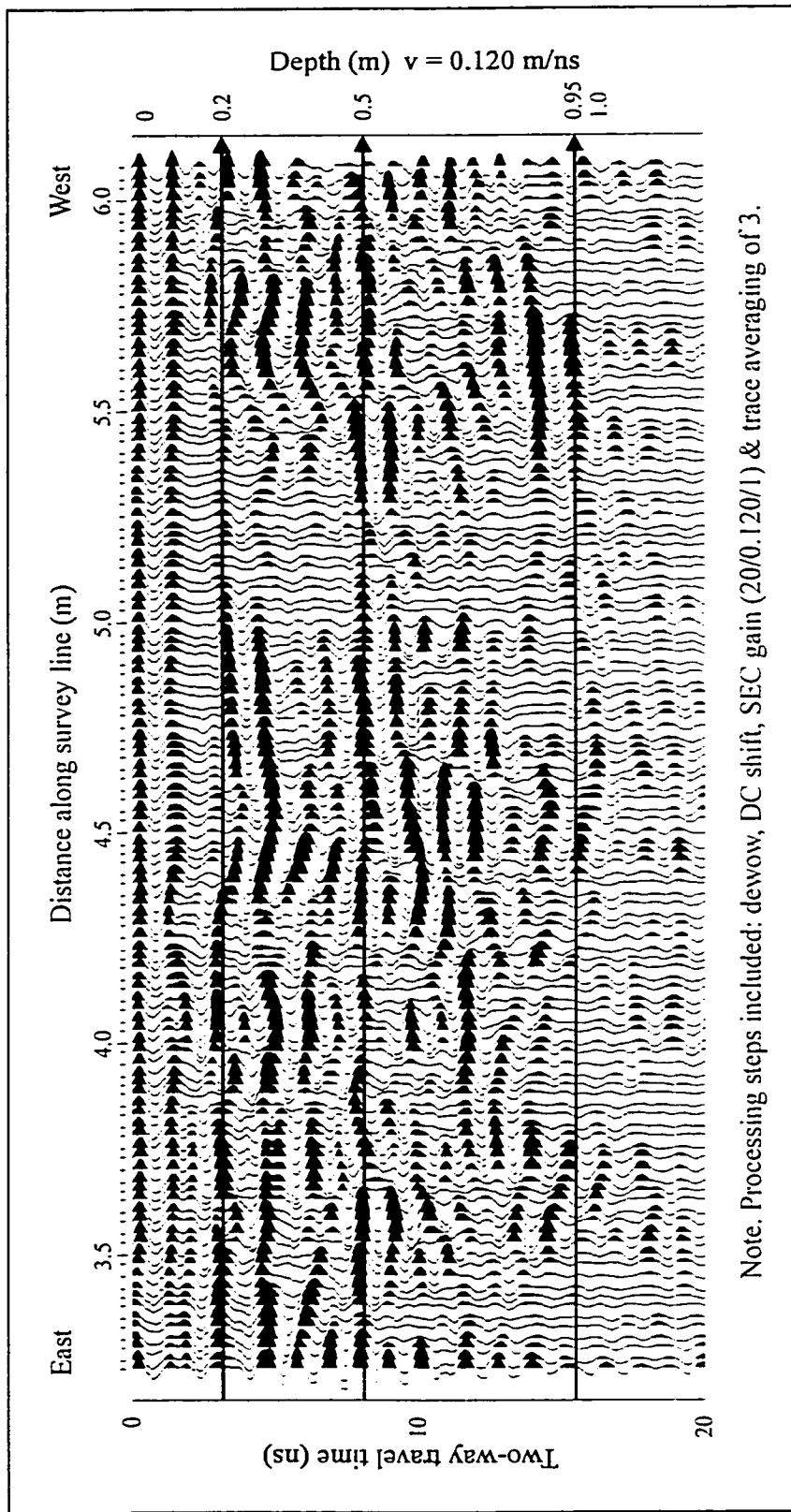
Figure 6-15 High frequency survey 'BY-1G-2c' with a trace-averaging filter; Hwy 17 Bypass Outcrop.
(Note: Surveyed with a sampling frequency of 10.8GHz).
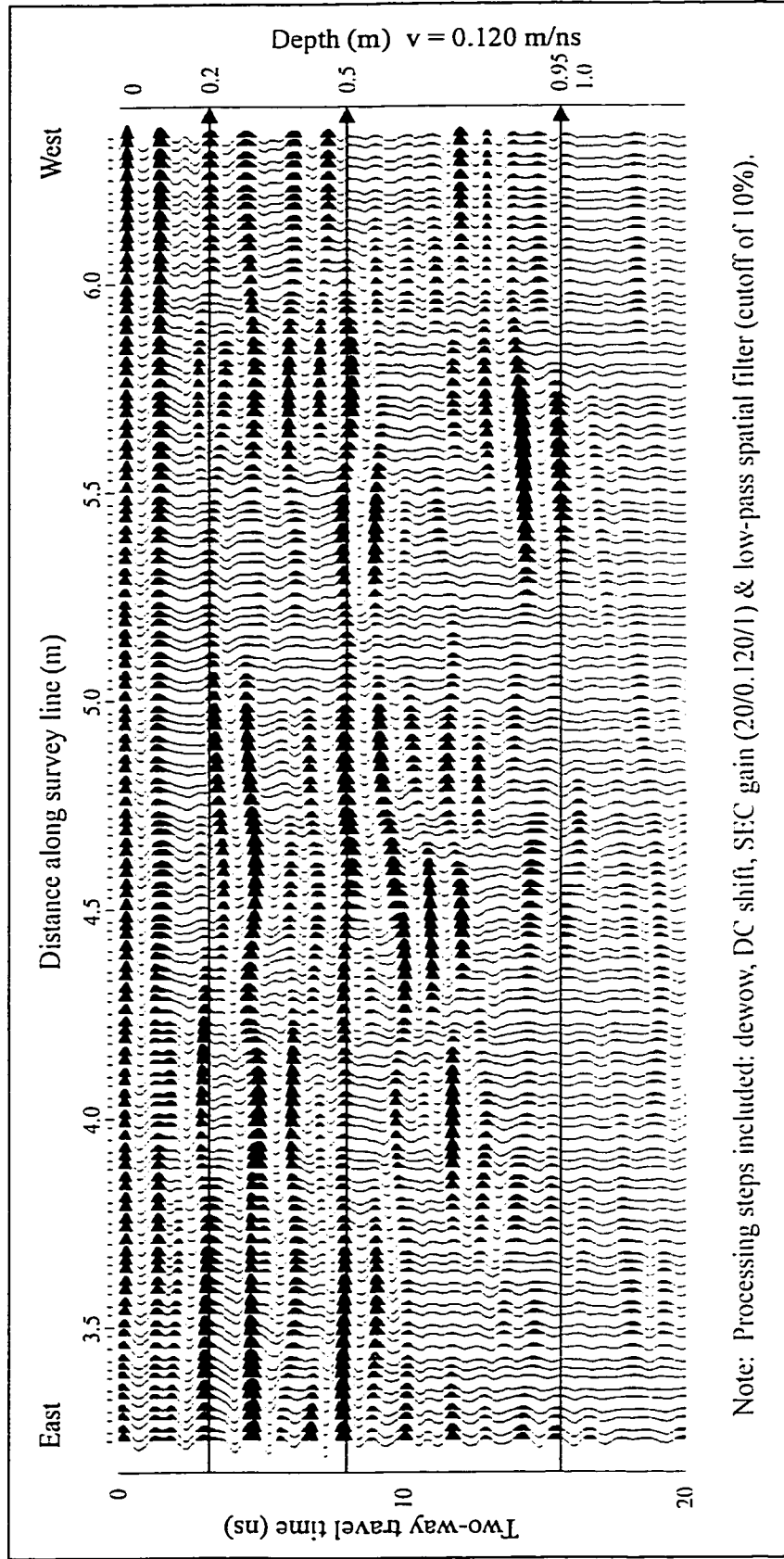
Note. Processing steps included: dewow, DC shift, SEC gain (20/0.120/1) & trace averaging of 3.

Figure 6-16 High frequency survey 'BY-1G-2c' with a low-pass spatial filter; Hwy 17 Bypass Outcrop. (Note: Surveyed with a station spacing of 2.5 cm).

Note: Processing steps included: dewow, DC shift, SEC gain (20/0.120/1) & low-pass spatial filter (cutoff of 10%).
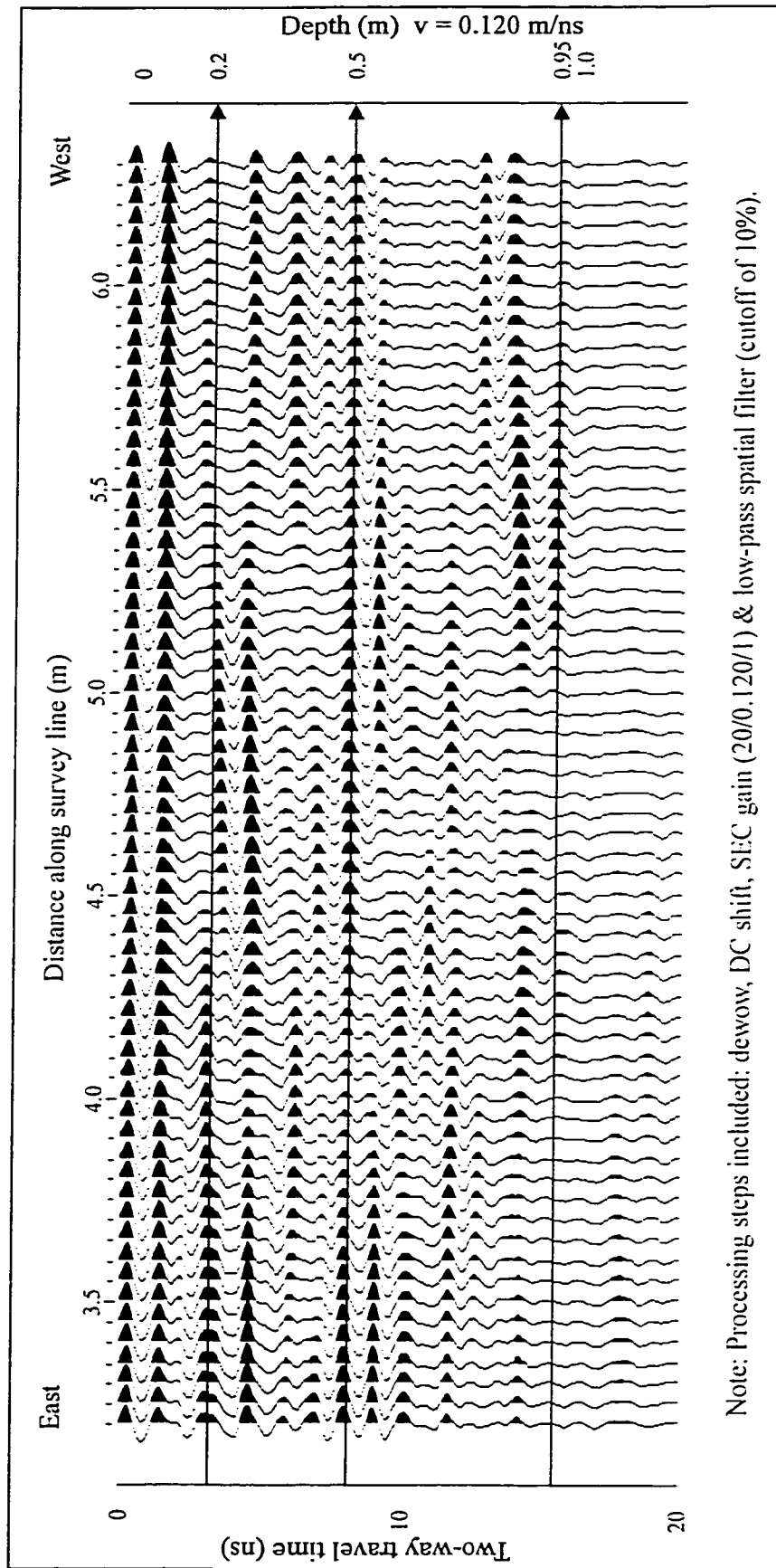
Figure 6-17 High frequency survey 'BY-1G-2d' with a low-pass spatial filter; Hwy 17 Bypass Outcrop. (Note: Surveyed with a station spacing of 5 cm).

Note: Processing steps included: dewow, DC shift, SEC gain (20/0.120/1) & low-pass spatial filter (cutoff of 10%).

215
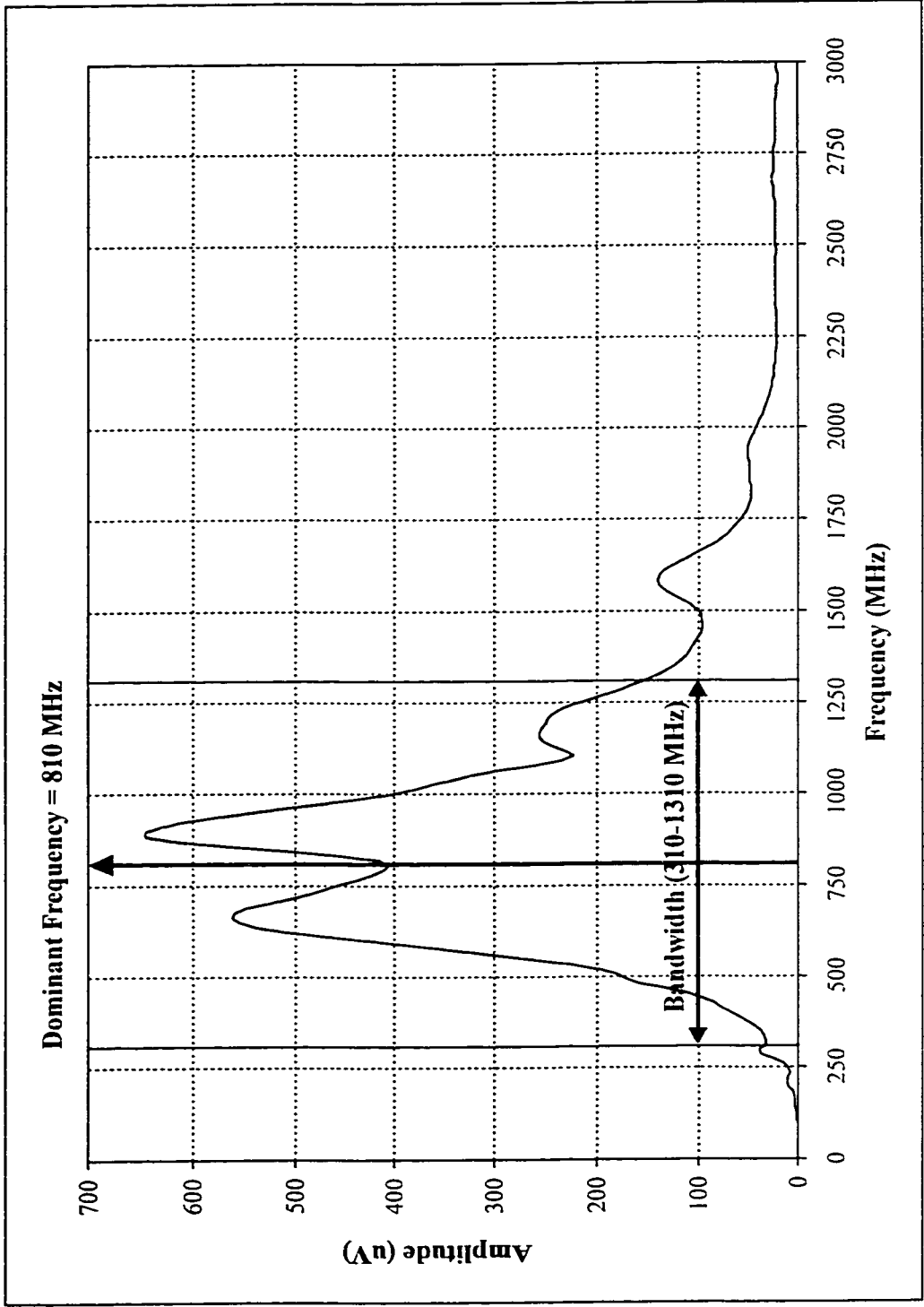
Figure 6-18 Representative amplitude spectrum for the high frequency surveys conducted at the Hwy 17 Bypass Outcrop.

Figure 6-19 Geologic section for the high frequency surveys at Vermilion River Outcrop.
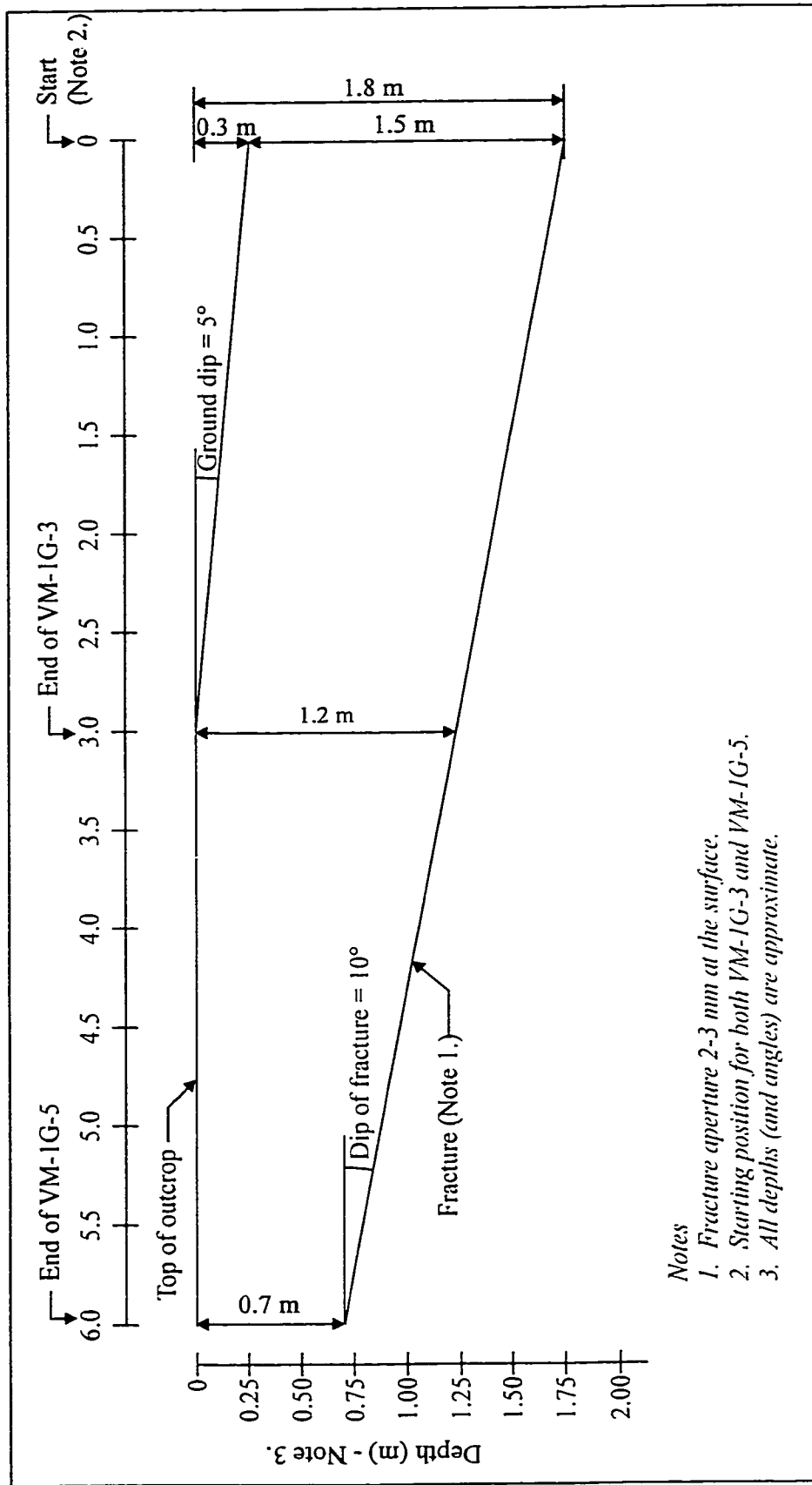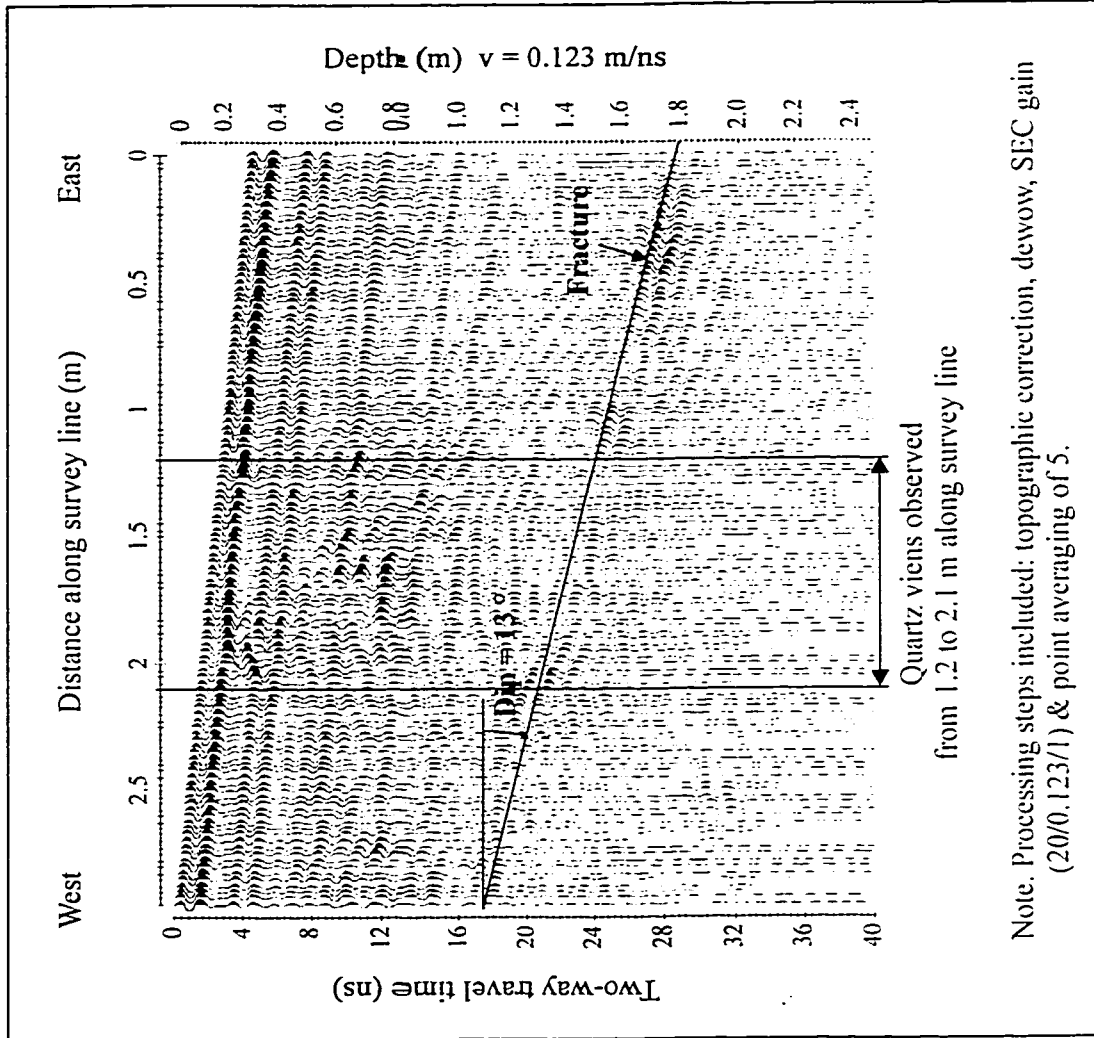
Notes
1. *Fracture aperture 2-3 mm at the surface.*
2. *Starting position for both VM-1G-3 and VM-1G-5.*
3. *All depths (and angles) are approximate.*

217

Figure 6-20 High frequency survey 'VM-1G-3' at Vermilion River Outcrop. (Note: Surveyed with a station spacing of 2.5 cm).
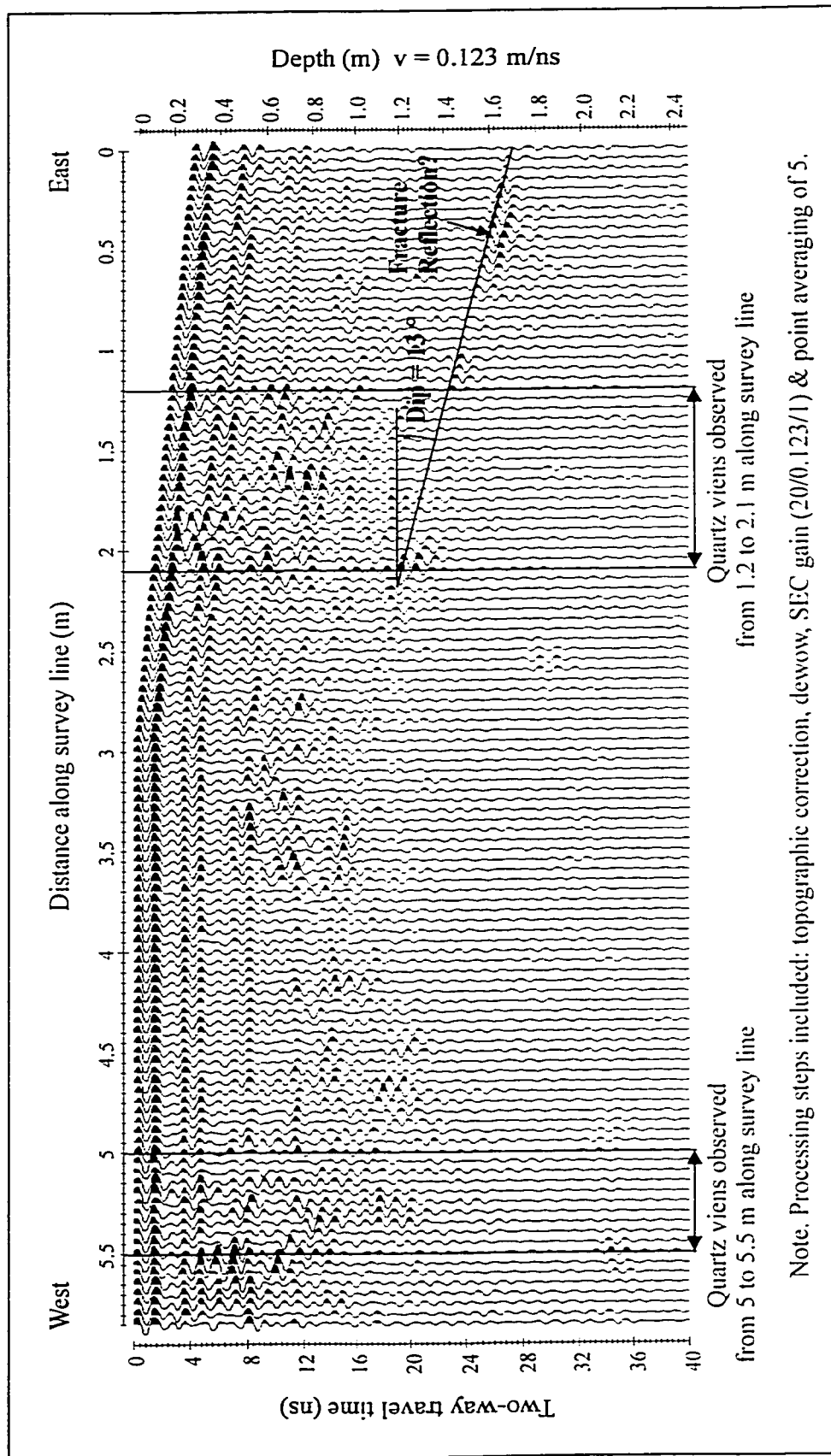
Note: Processing steps included: topographic correction, dewow, SEC gain (20/0.123/1) & point averaging of 5.

218

Figure 6-21 High frequency survey 'VM-1G-5' at Vermilion River Outcrop. (Note: Surveyed with a station spacing of 5 cm).

Note. Processing steps included: topographic correction, dewow, SEC gain (20/0.123/1) & point averaging of 5.
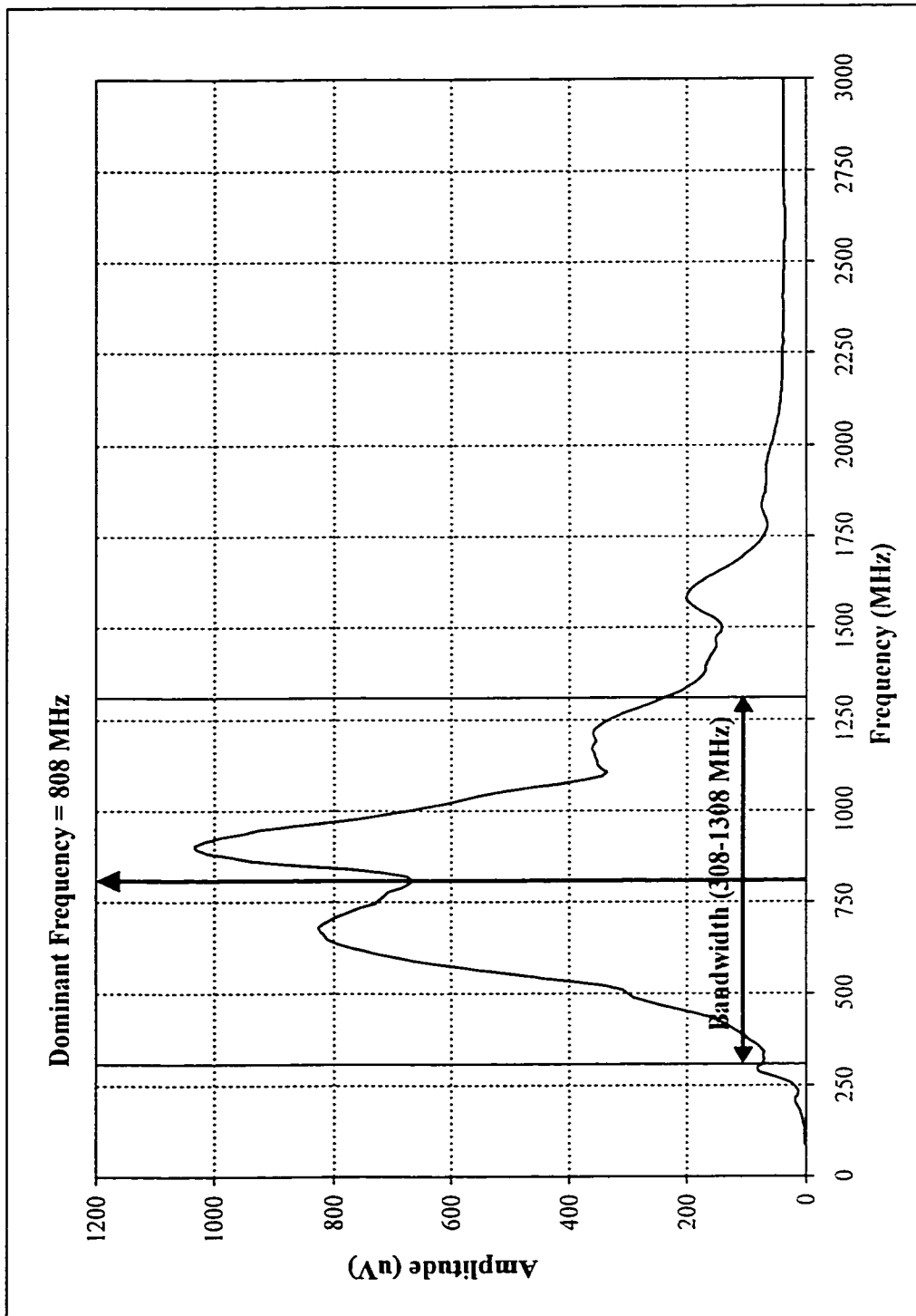
Figure 6-22 Representative amplitude spectrum for the high frequency surveys conducted at the Vermilion River Outcrop.

SE NW

Moss cover Soil veneer

sandstone sandstone sandstone siltstone??

Inferred bedding

40°

Horizontal Distance (m)

Approx. Depth (m)

b) Geologic section for the WGMC Outcrop 1.

Depth (m) v = 0.120 m/ns

NW Distance along survey line (m) SE

Dip ≈ 32°
(Note 1)

Two-way travel time (ns)

Note 1. Reflector has a radargram dip of 32° or actual dip of 39°.

a) Processed radar profile. Processing steps included: dewow,
DC shift, SEC gain (20/0.120/1) & point stacking of 5.

Figure 6-23 Low frequency survey 'WGMC1' at WGMC Outcrop 1: with accompanying geologic section.

Depth (m) Note 1.

Note 1. Depth scale based on signal velocity of 0.120 m/ns.

a) Processed radar profile. Processing steps included: dewow, DC shift, & SEC gain (20/0.120/1).

b) Geologic section for the WGMC Outcrop 1.
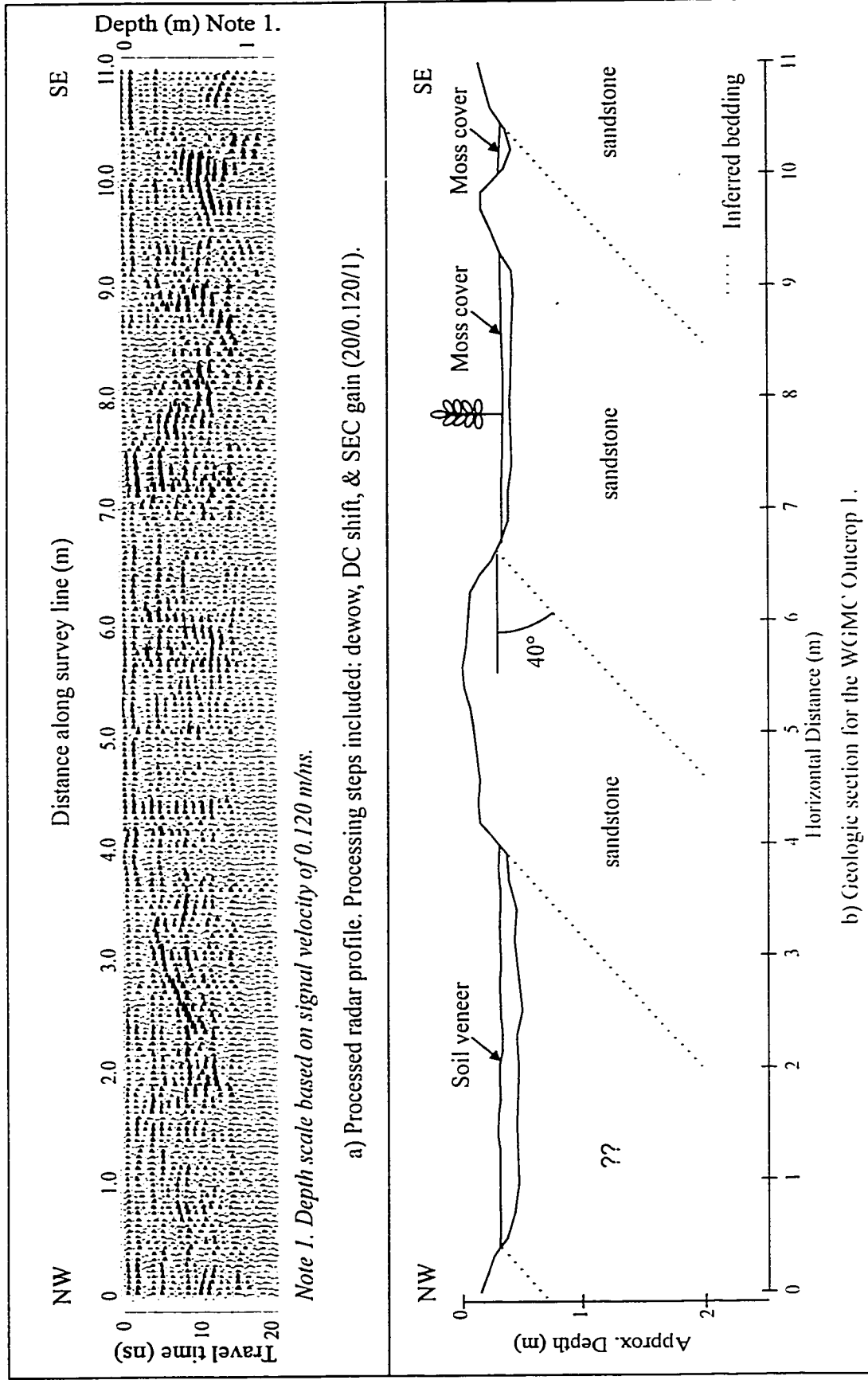
Figure 6-24 High frequency survey 'WGMC1G1' at WGMC Outcrop 1; with accompanying geologic section.

Figure 6-25 Average amplitude spectrum for the low frequency survey at WGMC Outcrop 1.
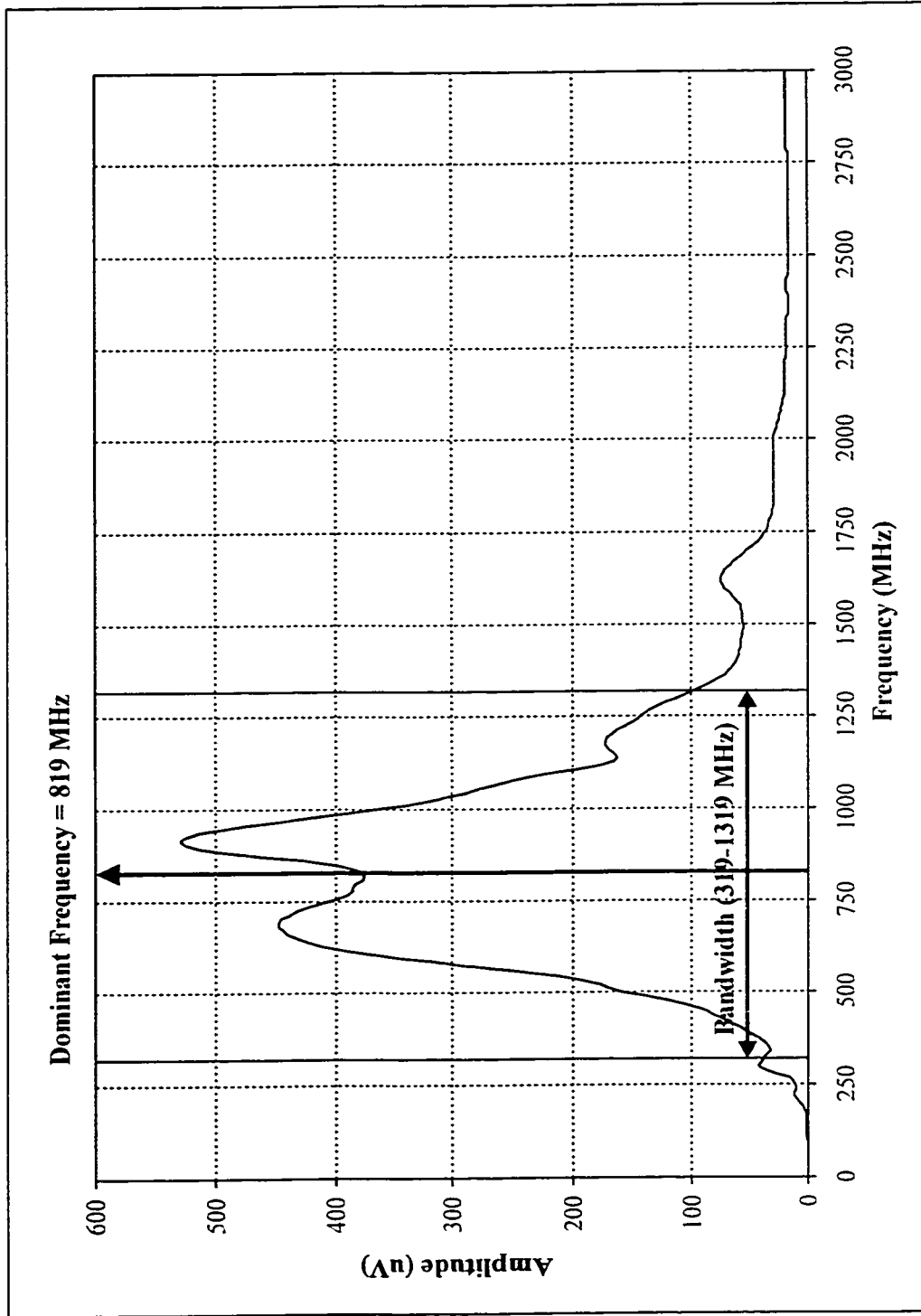
Figure 6-26 Average amplitude spectrum for the high frequency survey at WGMC Outcrop 1.

b) Geologic section for the WGMC Outcrop 2; with accompanying geologic section.

a) Processed radar profile. Processing steps included: topographic correction, dewow, DC shift, SEC gain (100/0.120/1) & point stacking of 7.
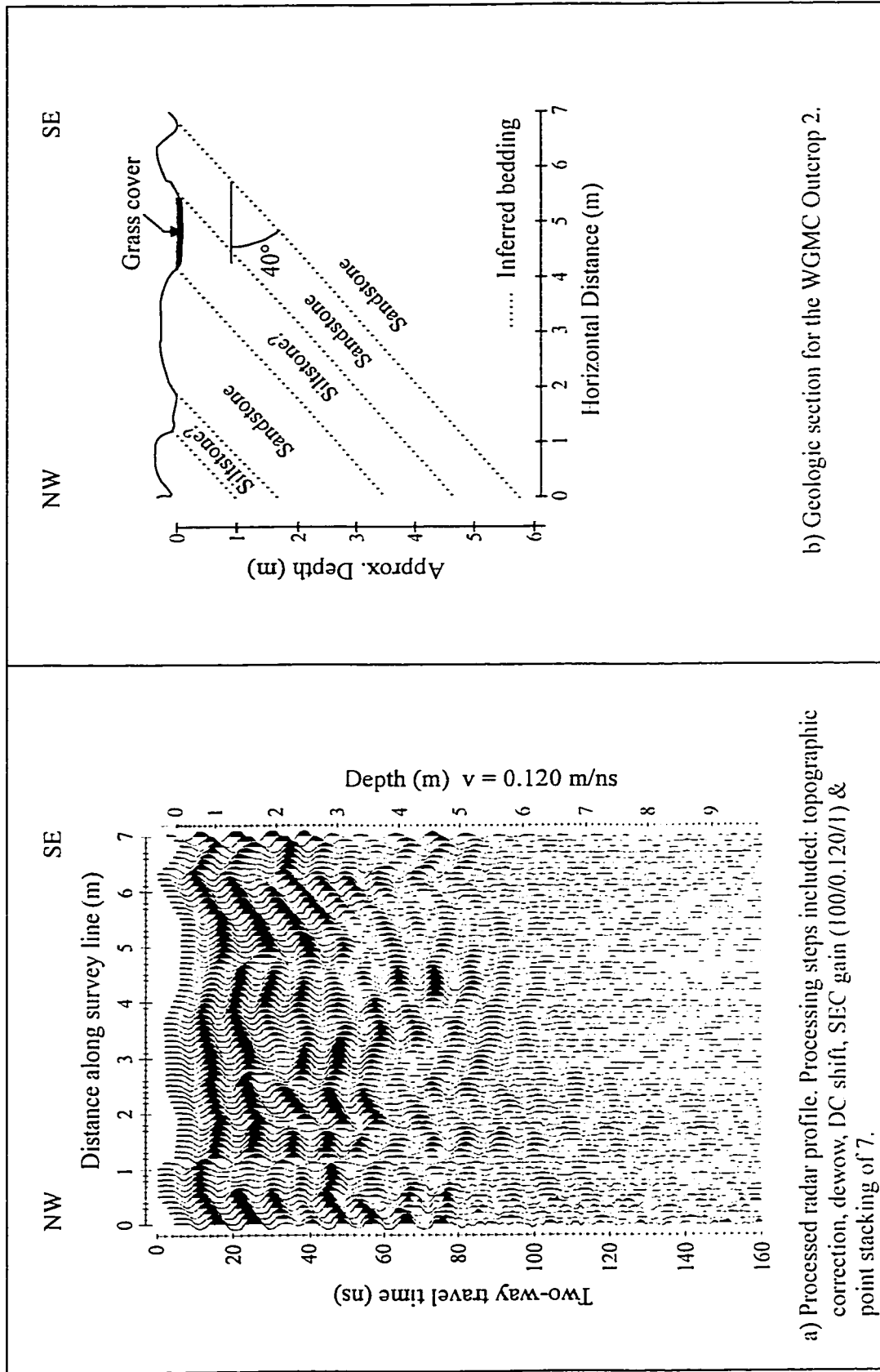
Figure 6-27 Low frequency survey 'WGMC2' at WGMC Outcrop 2; with accompanying geologic section.

Depth (m) Note 1.

0
0.2
0.4
0.6
0.8
1.0
1.2
1.4

NW 0   1   2   3   4   5   6   7 SE

Distance along survey line (m)

Travel time (ns)

0
4
8
12
16
20
24

Note 1. Depth scale based on signal velocity of 0.120 m/ns.

a) Processed radar profile. Processing steps included: topographic correction, dewow, DC shift, SEC gain (100/0.120/1) & point stacking of 5.

NW 0   1   2   3   4   5   6   7 SE

Horizontal Distance (m)

Approx. Depth (m)

0
0.5
1.0
1.5

Grass cover

Sandstone

Siltstone?

Sandstone

Siltstone?

Sandstone

Sandstone

········ Inferred bedding

b) Geologic section for the WGMC Outcrop 2.

Figure 6-28 High frequency survey 'WGMC1G3e' at WGMC Outcrop 2: with accompanying geologic section.
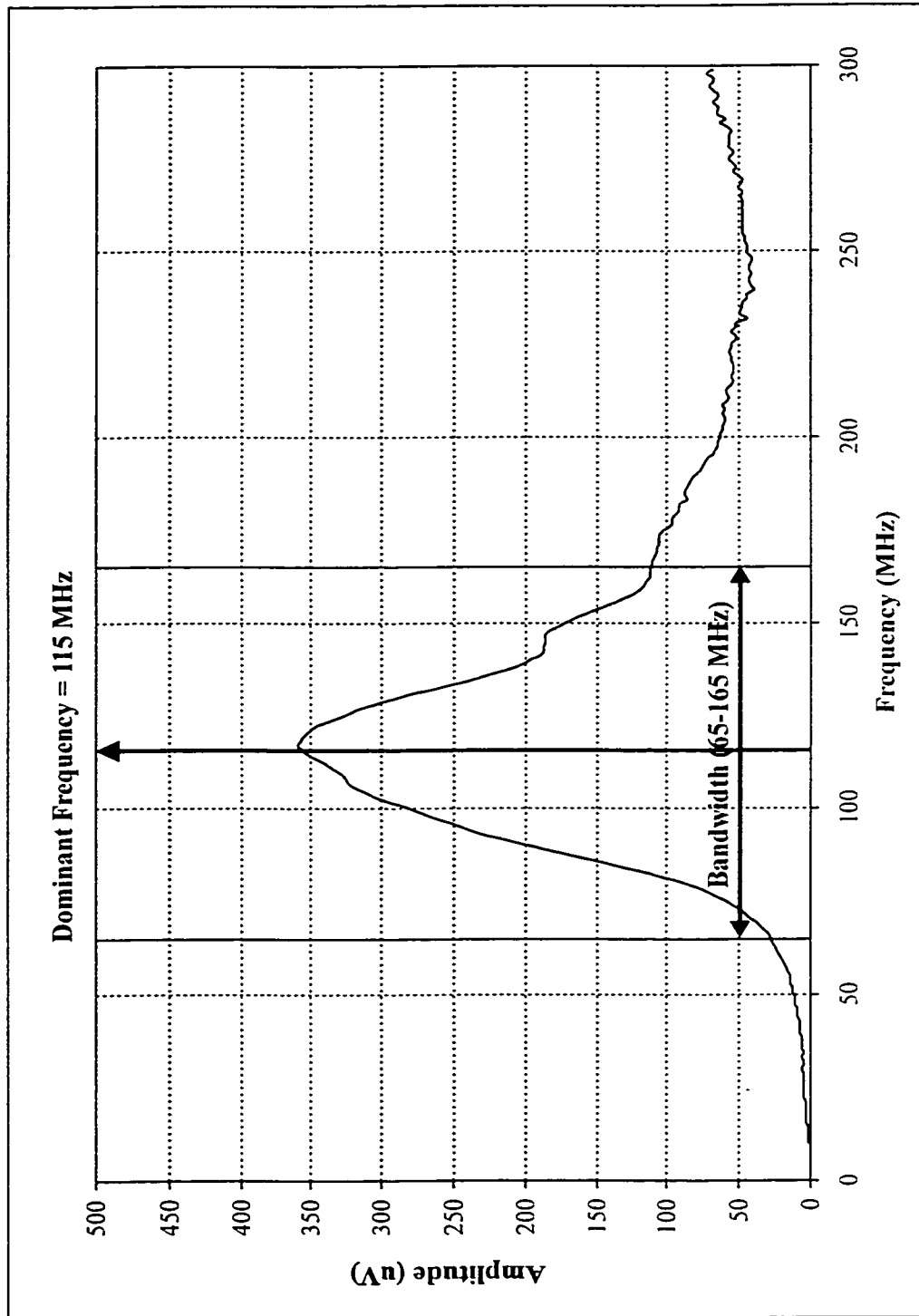
Figure 6-29 Average amplitude spectrum for the low frequency survey at WGMC Outcrop 2.

227
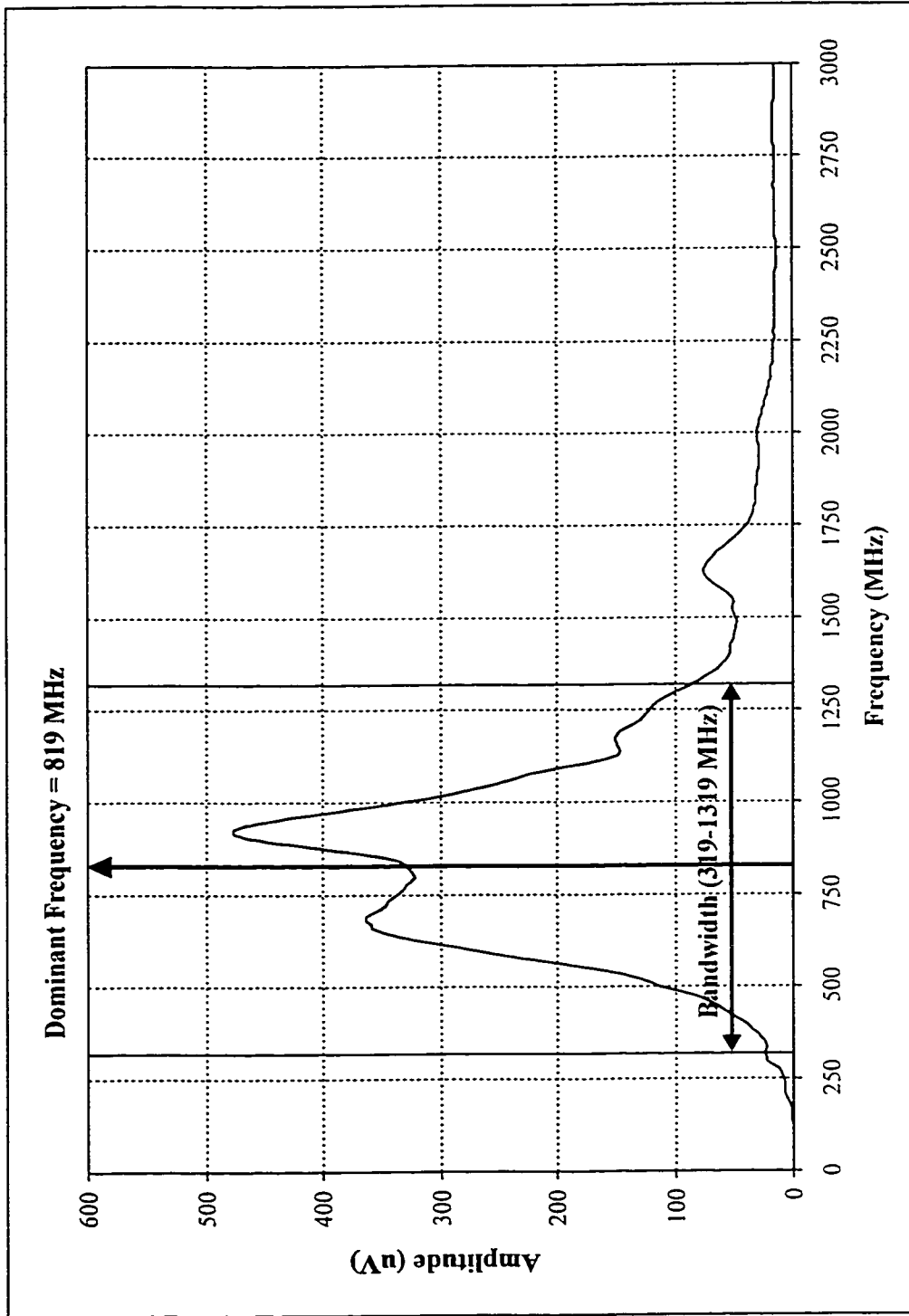
Figure 6-30 Average amplitude spectrum for the high frequency survey at WGMC Outcrop 2.

Figure 6-31 Low frequency Survey Line 1 (File Name: Killarney) at Hwy 637 - Killarney Outcrop.

Note: Processing steps included: polarity reversal, dewow, DC shift, constant gain of 10, & trace averaging of 5.

Fracture zone
@ approx. 3 m depth

Depth (m)   v = 0.120 m/ns

0 1 2 3 4 5 6 7 8 9

South
0 1 2 3 4 5 6 7 8 9 10 11 12 13 14 15 16 17 18 19 20
North

Horizontal distance along top of outcrop (m)

0 10 20 30 40 50 60 70 80 90 100 110 120 130 140 150 160

Two-way travel time (ns)
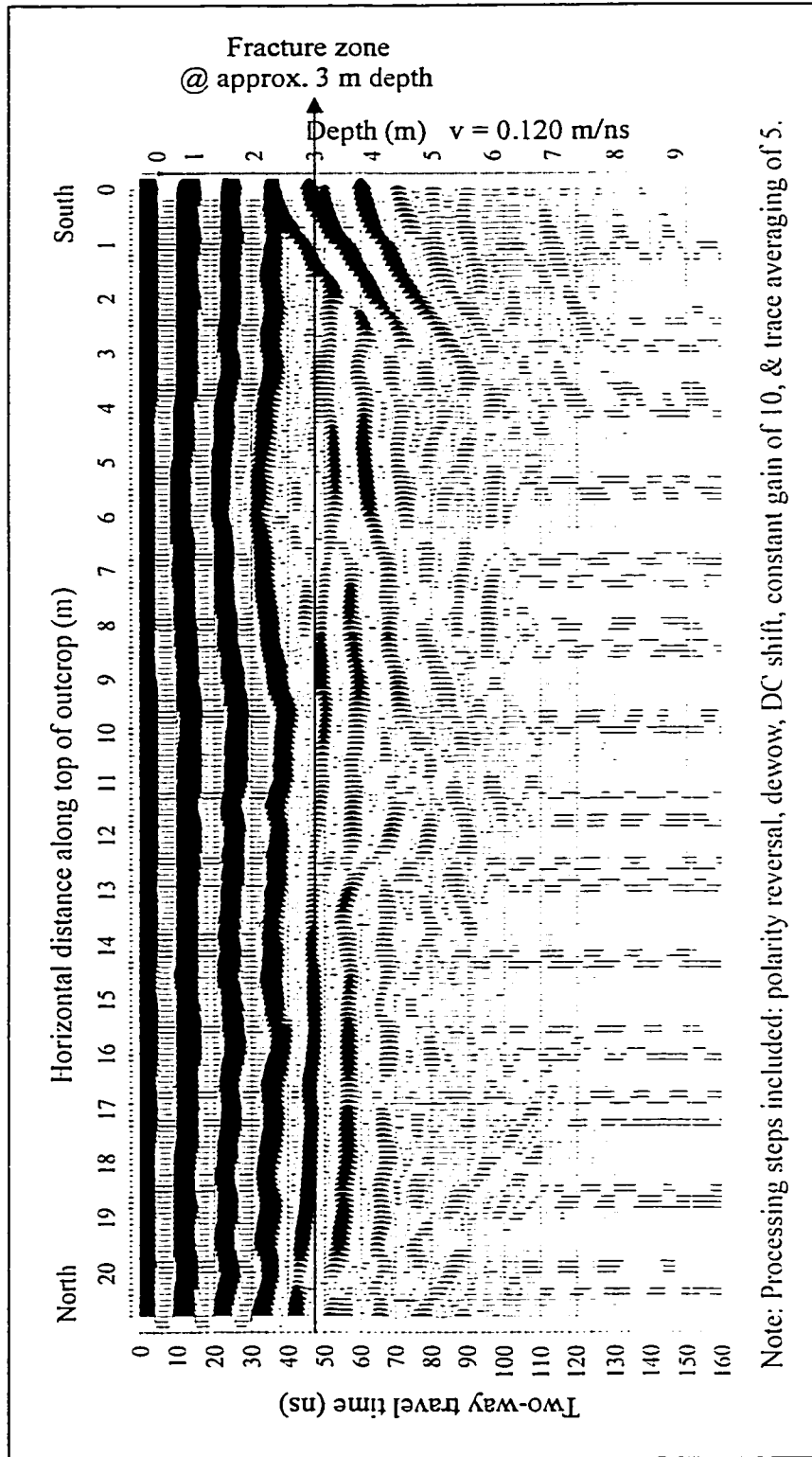
Figure 6-32 Low frequency Survey Line 2 (File Name: Kilar-2) at Hwy 637 - Killarney Outcrop.

Note: Processing steps included: polarity reversal, dewow, DC shift, constant gain of 10, & trace averaging of 5.
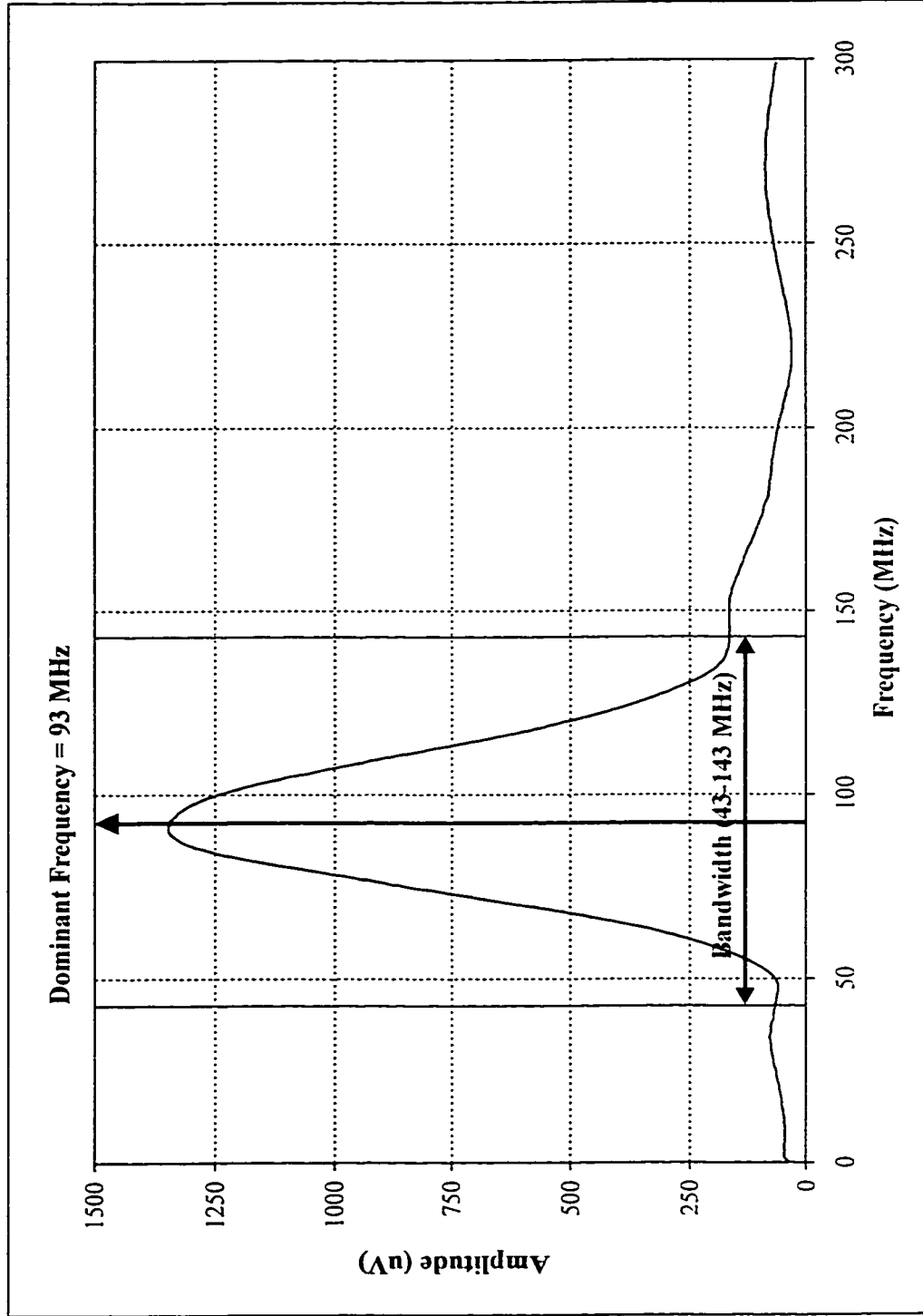
Figure 6-33 Representative amplitude spectrum for the low frequency surveys conducted at Hwy 637 - Killarney Outcrp.

Note 1. Dipping reflectors have apparent dips between 36°-38° or true dips between 47-51°.

Processing steps included: topographic correction, dewow, DC shift, SEC gain (150/0.120/1) & point stacking of 2.
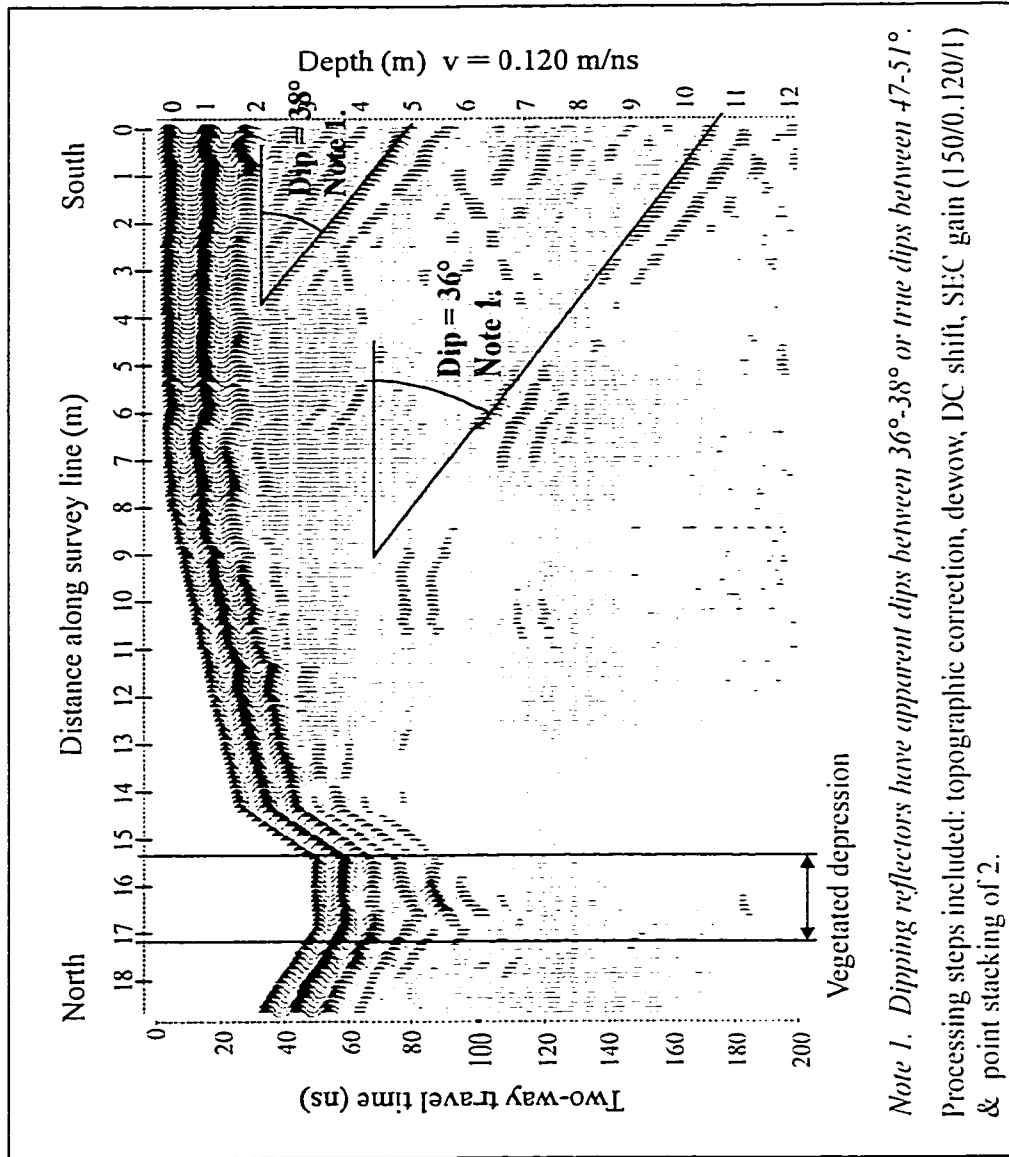
Figure 6-34 Low frequency survey 'Camp-1' at Elbow Lake Outcrop 1.
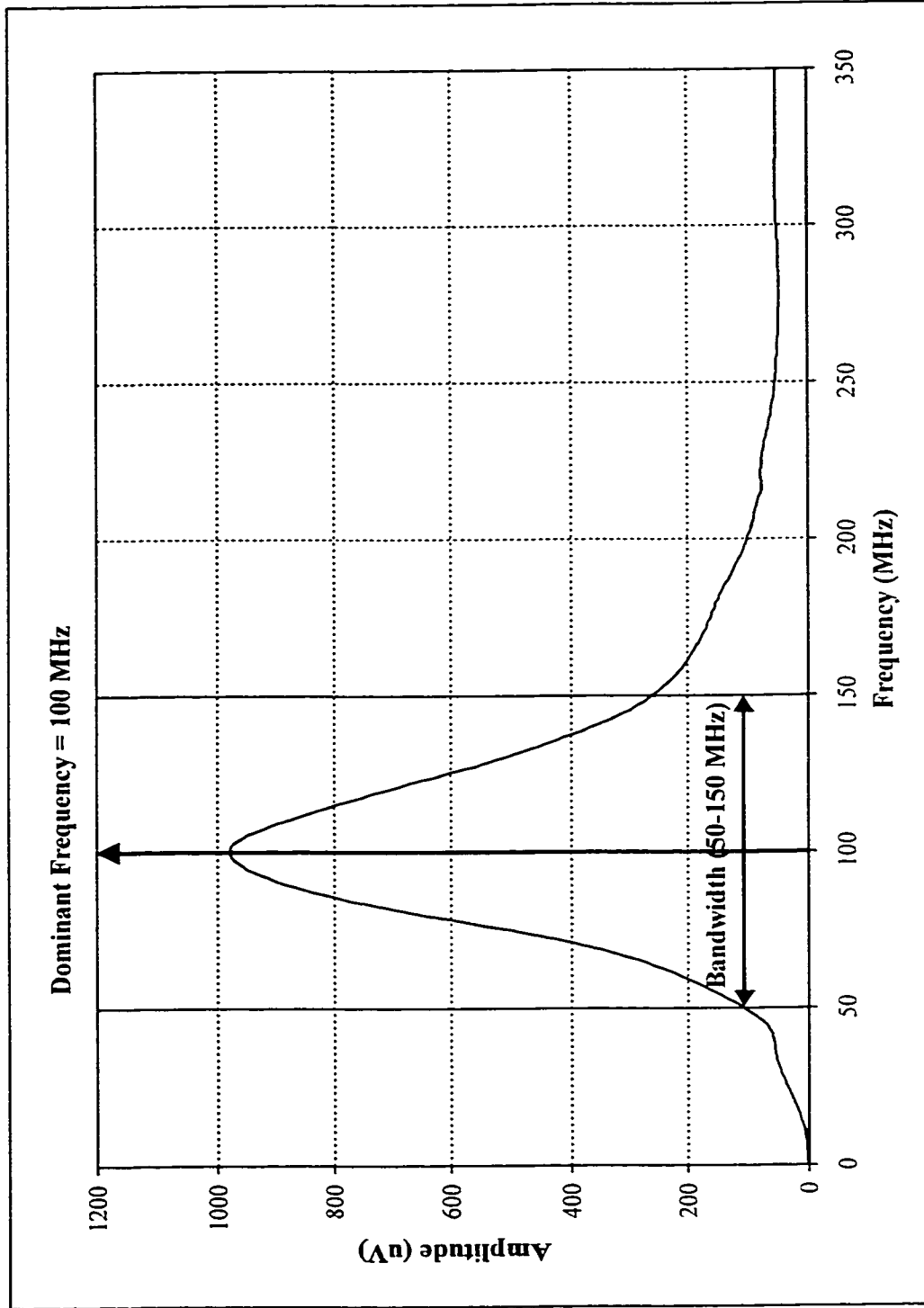
Figure 6-35 Average amplitude spectrum for the low frequency survey at Elbow Lake Outcrop 1.

233

a) Processed radar profile. Processing steps included: topographic correction, polarity reversal, dewow, DC shift, SEC gain (150/0.120/5) & point stacking of 5.

b) Geologic section for Outcrop 2 low frequency survey.
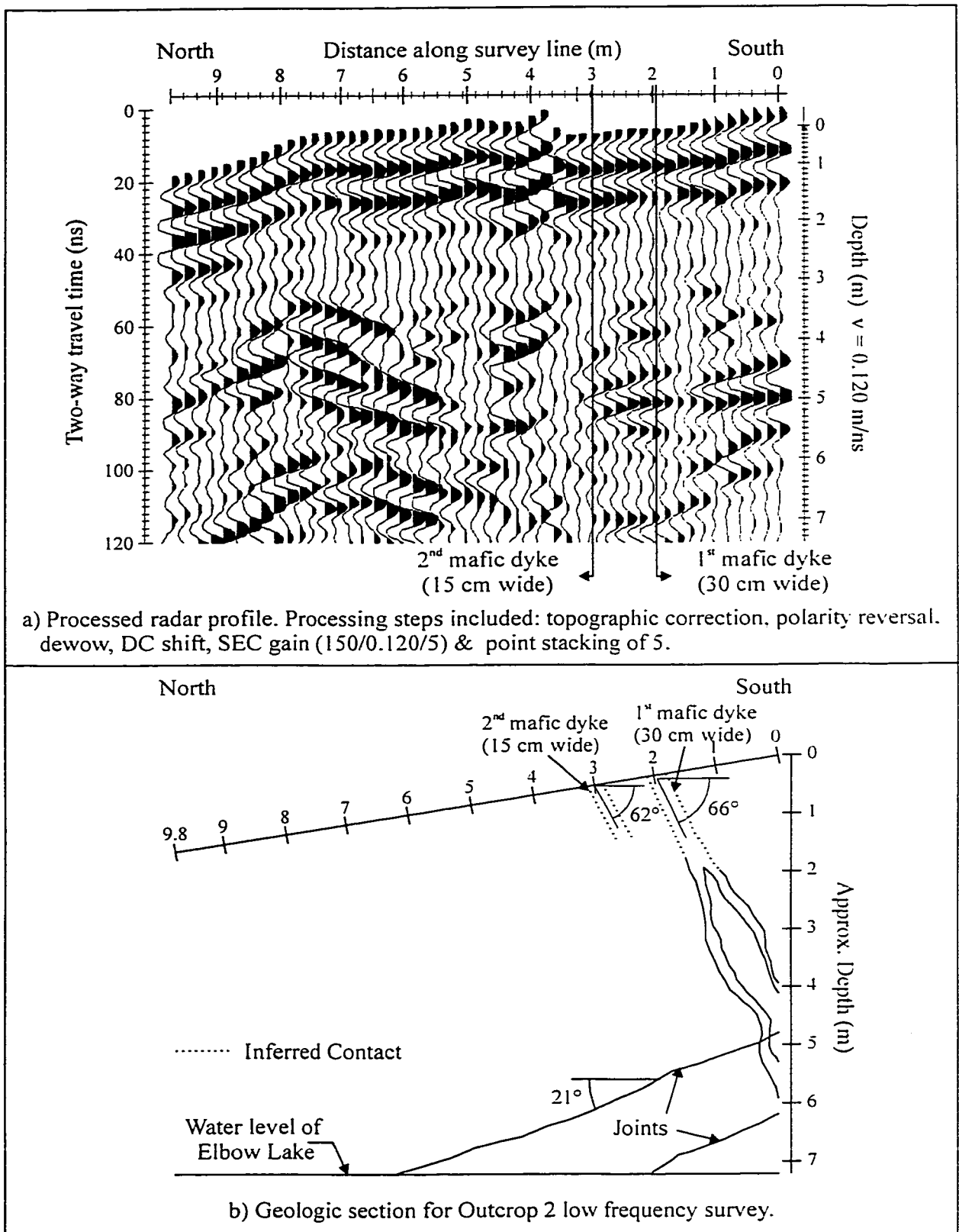
Figure 6-36 Low frequency survey 'Camp-2' at Elbow Lake Outcrop 2; with accompanying geologic section.

234

Figure 6-37 High frequency survey 'Camp-4' at Elbow Lake Outcrop 2.

Processing steps included: topographic correction, dewow, DC shift, SEC gain (50/0.120/2) & point stacking of 5.

235
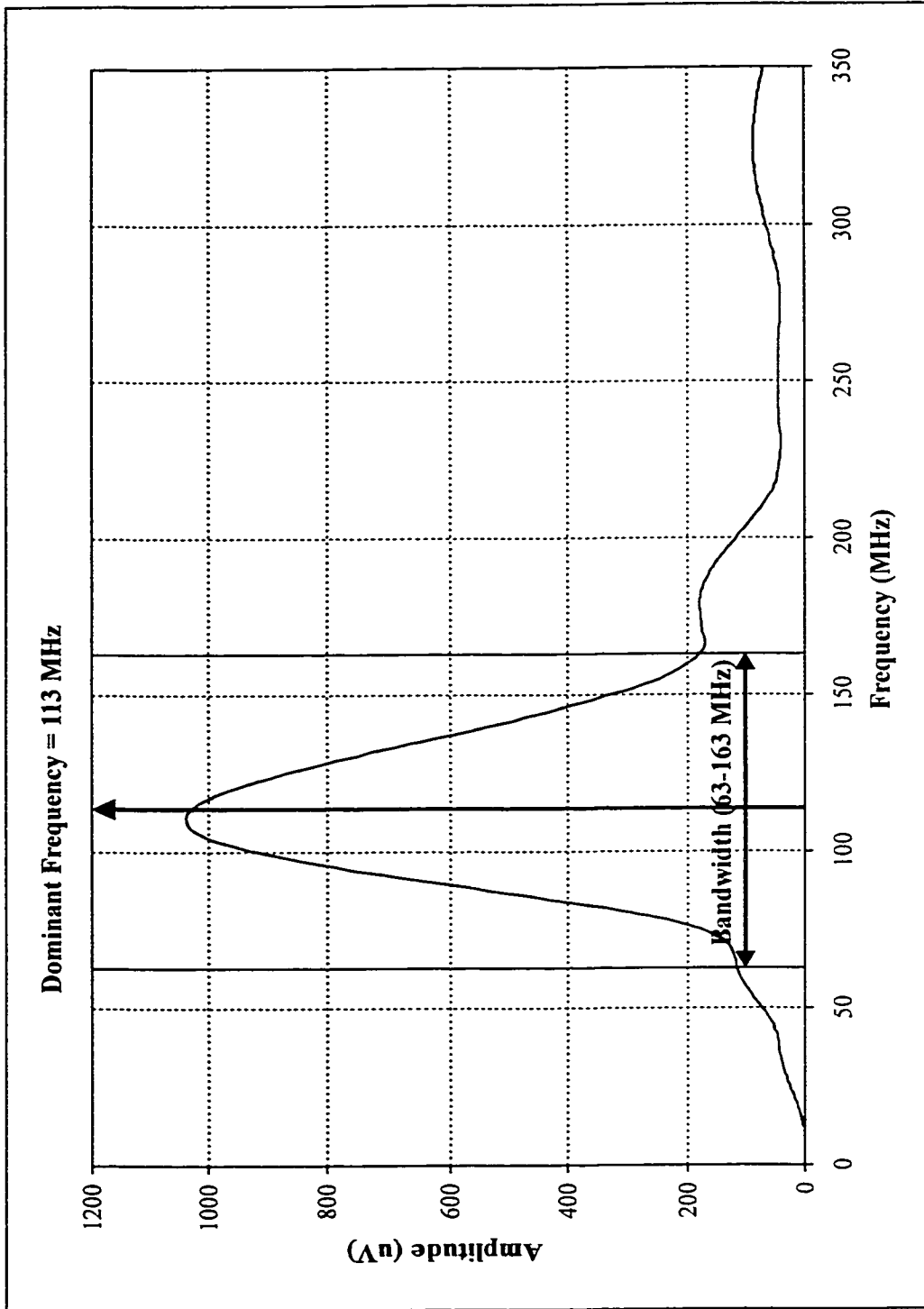
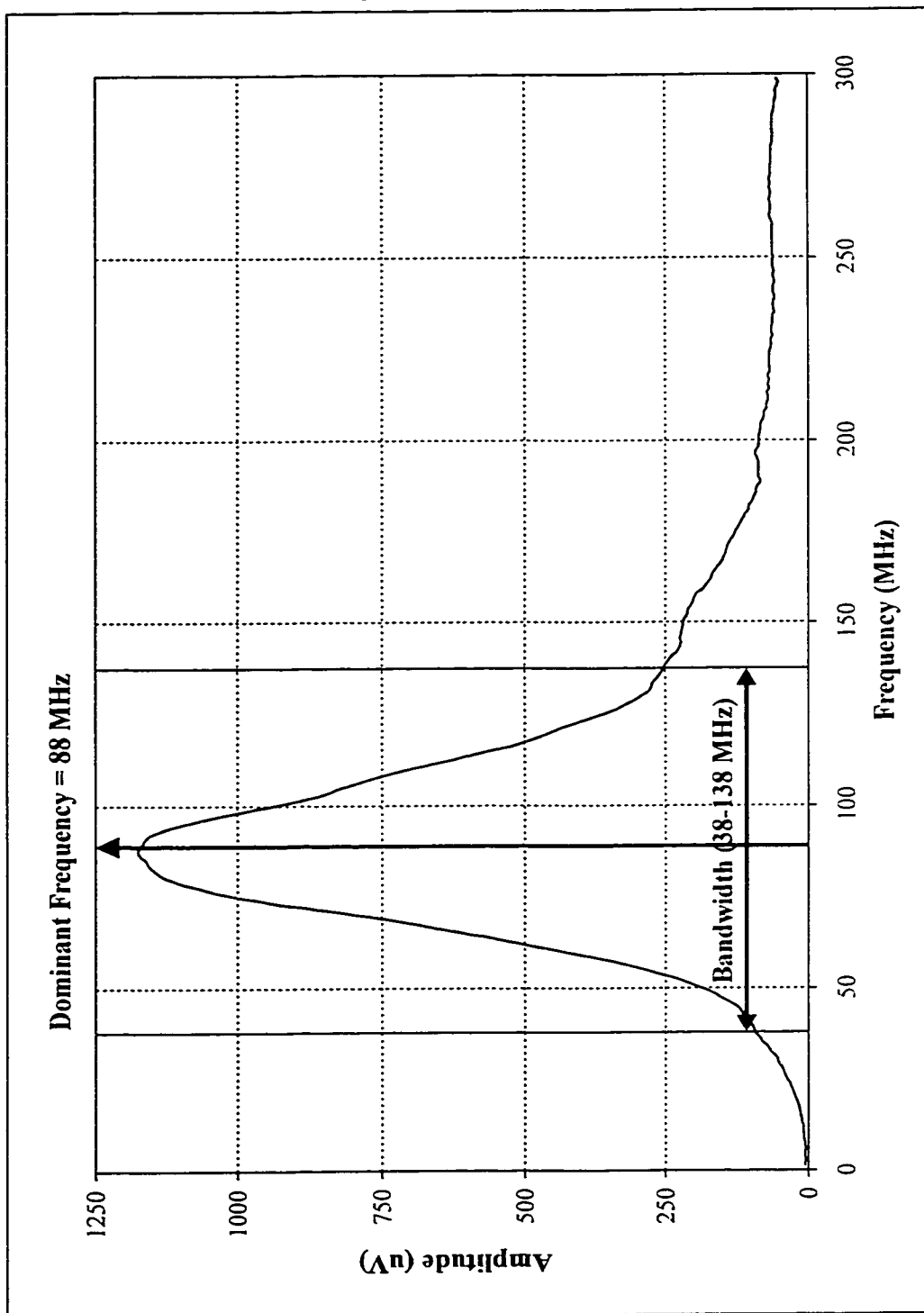Figure 6-38 Average amplitude spectrum for the low frequency survey at Elbow Lake Outcrop 2.
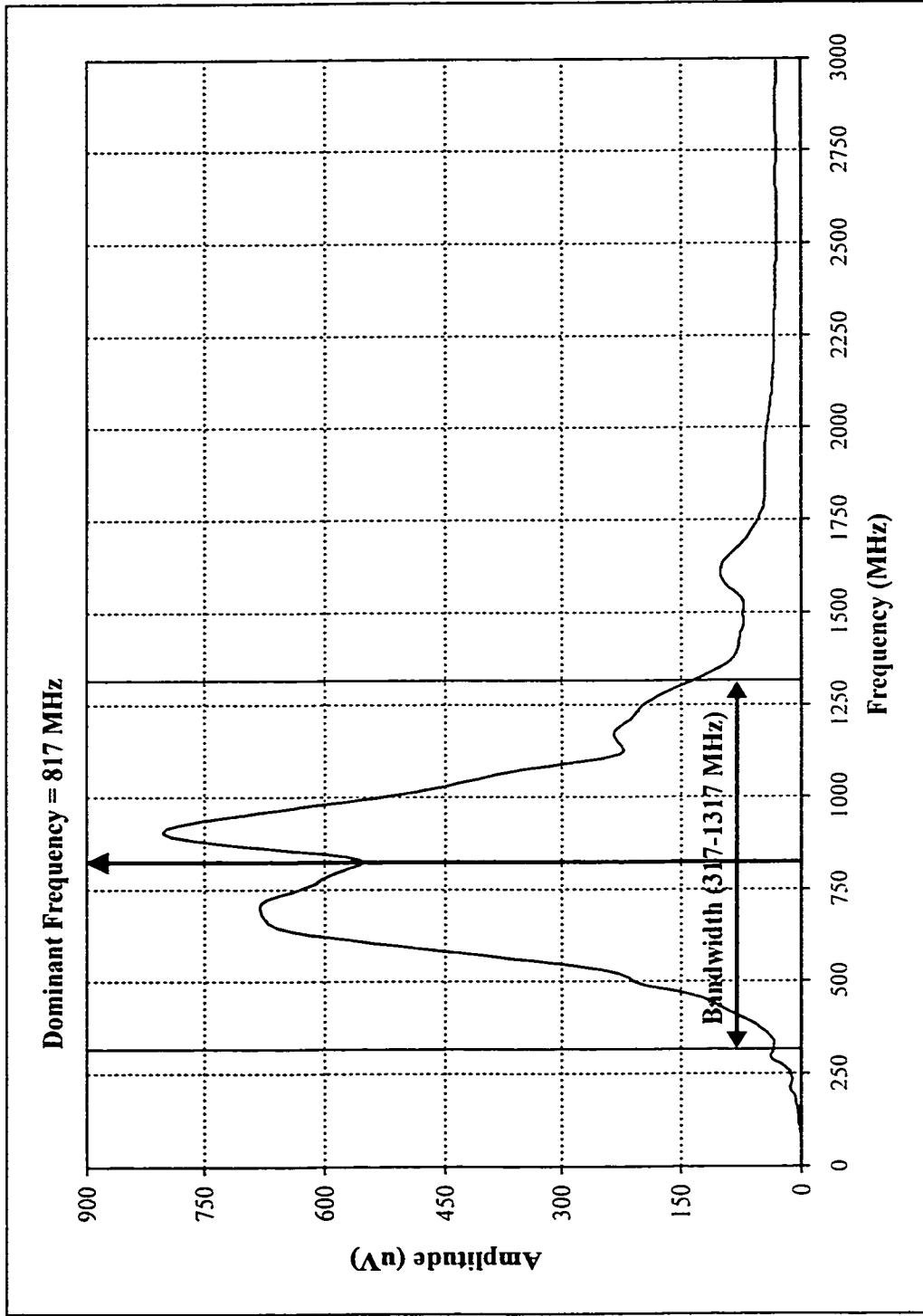
Figure 6-39 Average amplitude spectrum for the high frequency survey at Elbow Lake Outcrop 2.
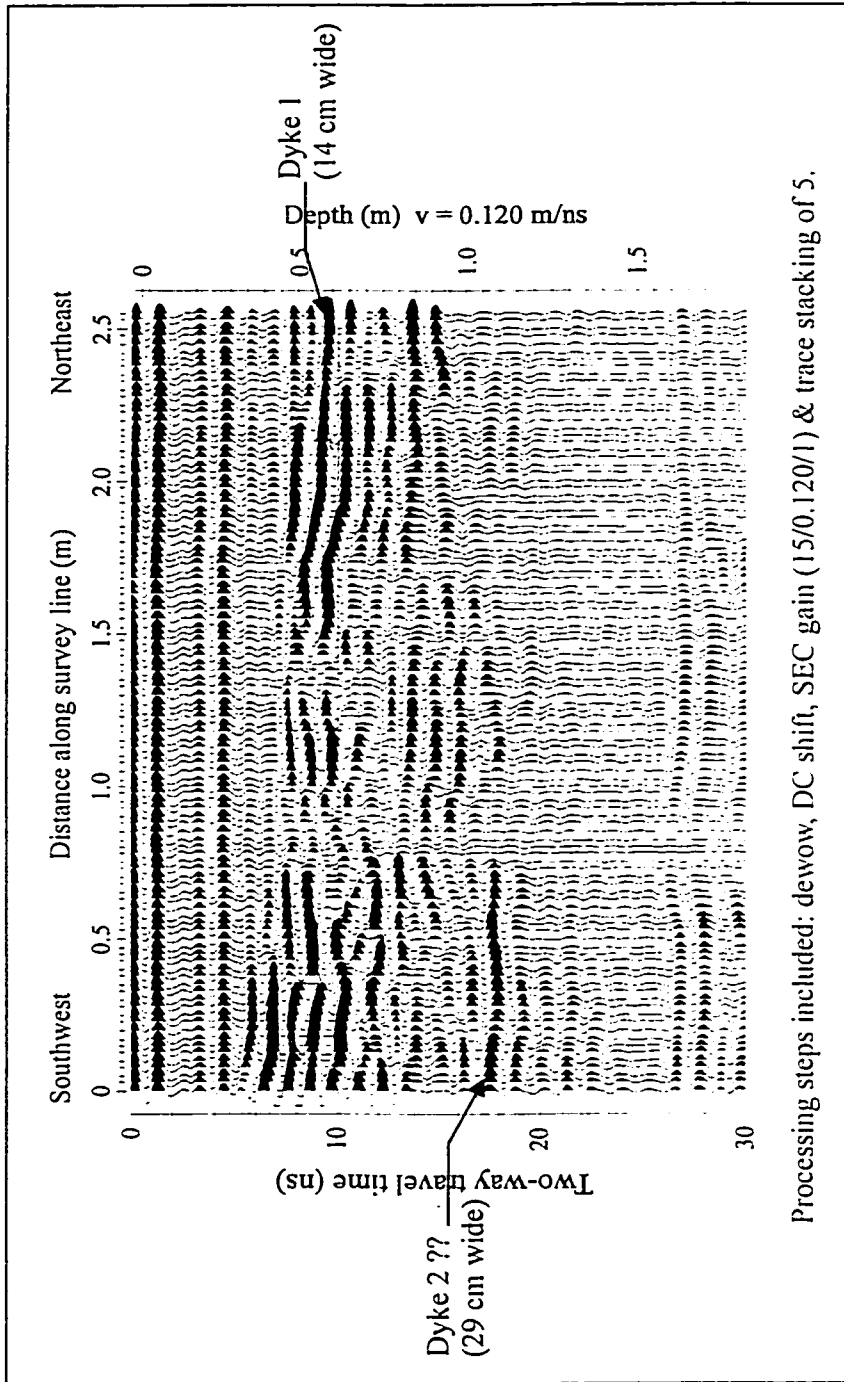
237

Figure 6-40 High frequency Upper Survey Line (File name: Camp-5d) at Elbow Lake Outcrop 3.
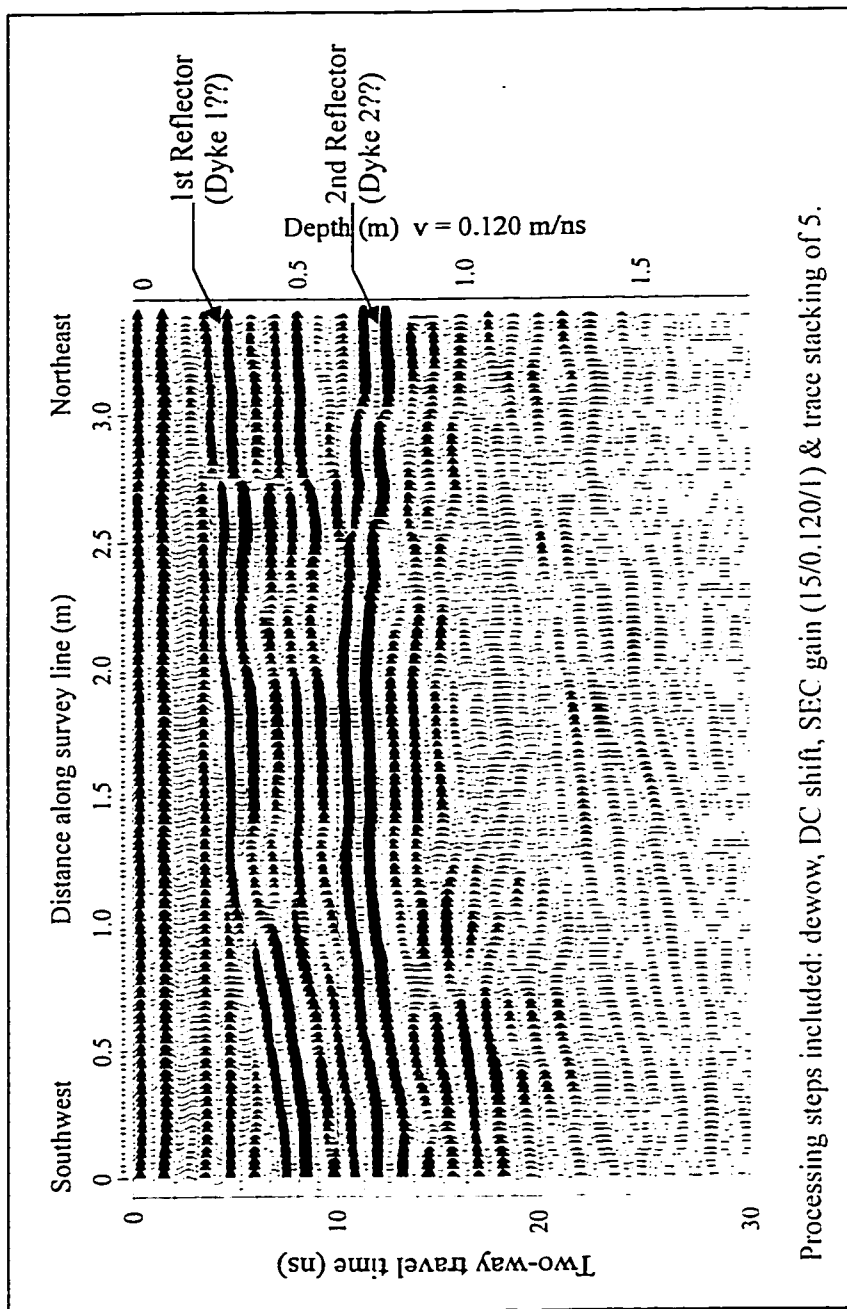
238

Figure 6-41 High frequency survey Lower Survey Line (File name: Camp-5c) at Elbow Lake Outcrop 3.

239
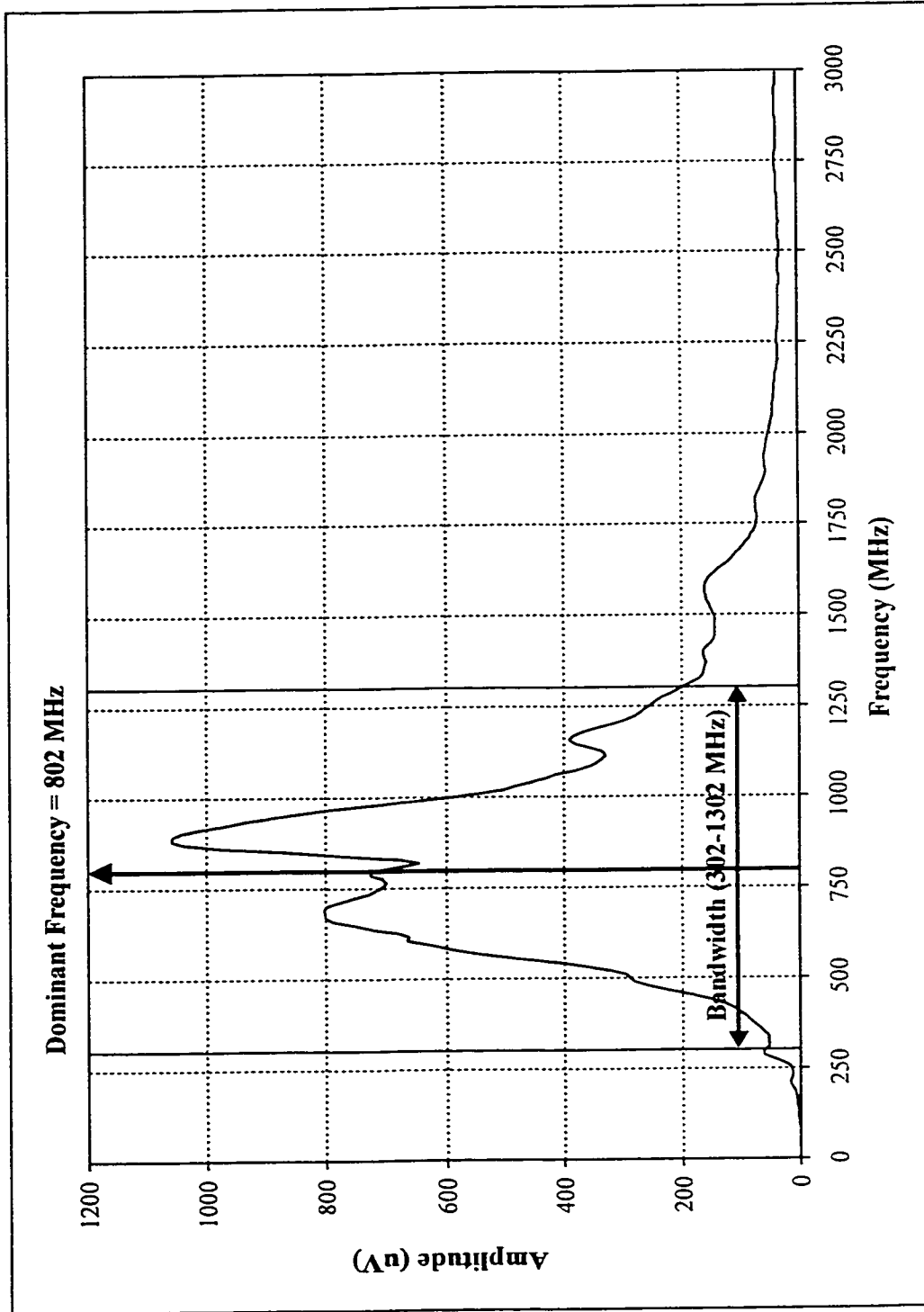
Figure 6-42 Representative amplitude spectrum for the high frequency surveys at Elbow Lake Outcrop 3.

240

b) Geologic section for the low frequency survey at the Hwy 17 Site (File name: Prof21).

Note 1. Fracture aperture and infilling unknown.

a) Processed radar profile. Processing steps included: dewow, DC shift, SEC gain (30/0.123/1), trace stacking of 5, & point stacking of 3.
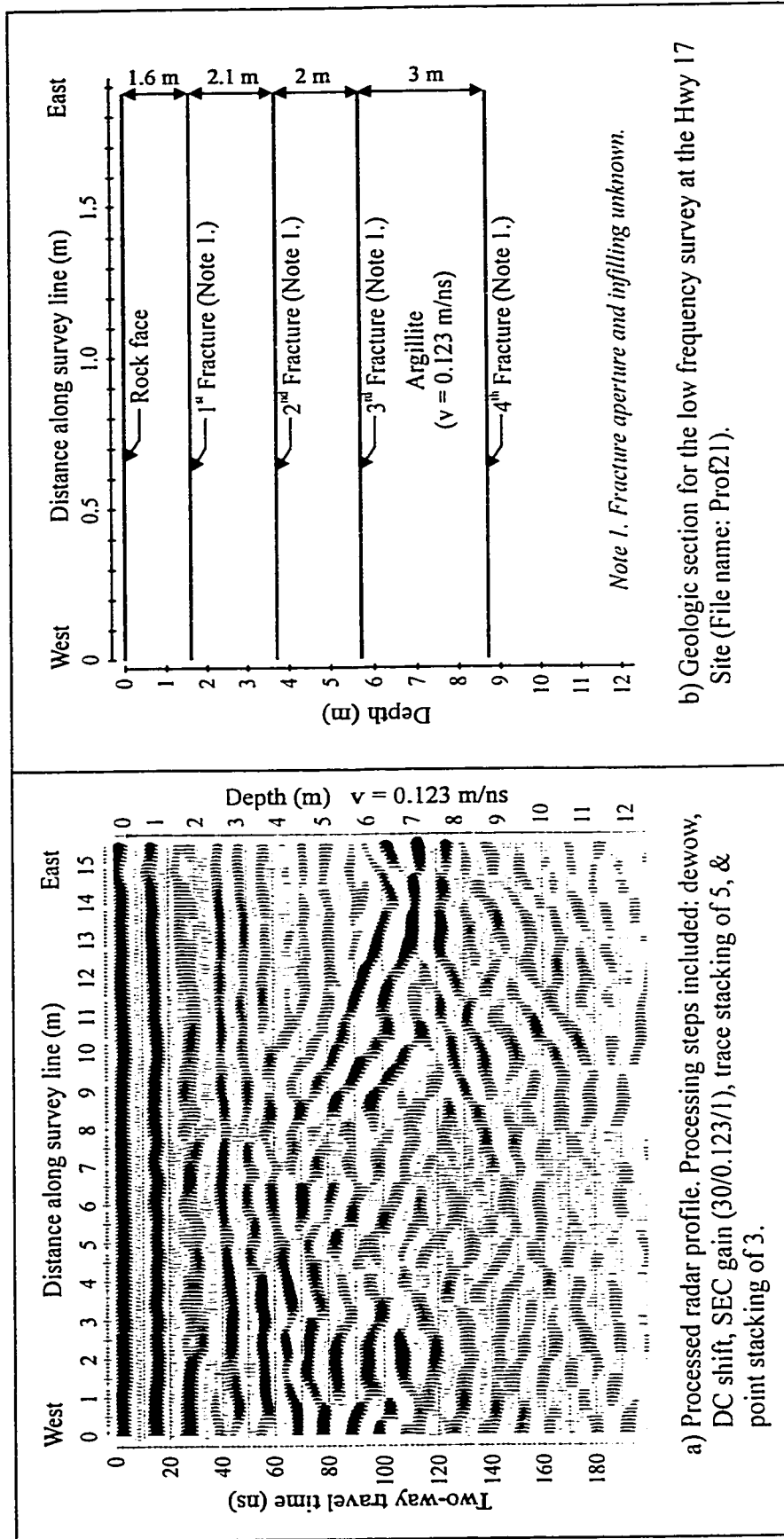
Figure 6-43 Low frequency survey 'Prof21' at Hwy 17 Outcrop; with accompanying geologic profile.

241
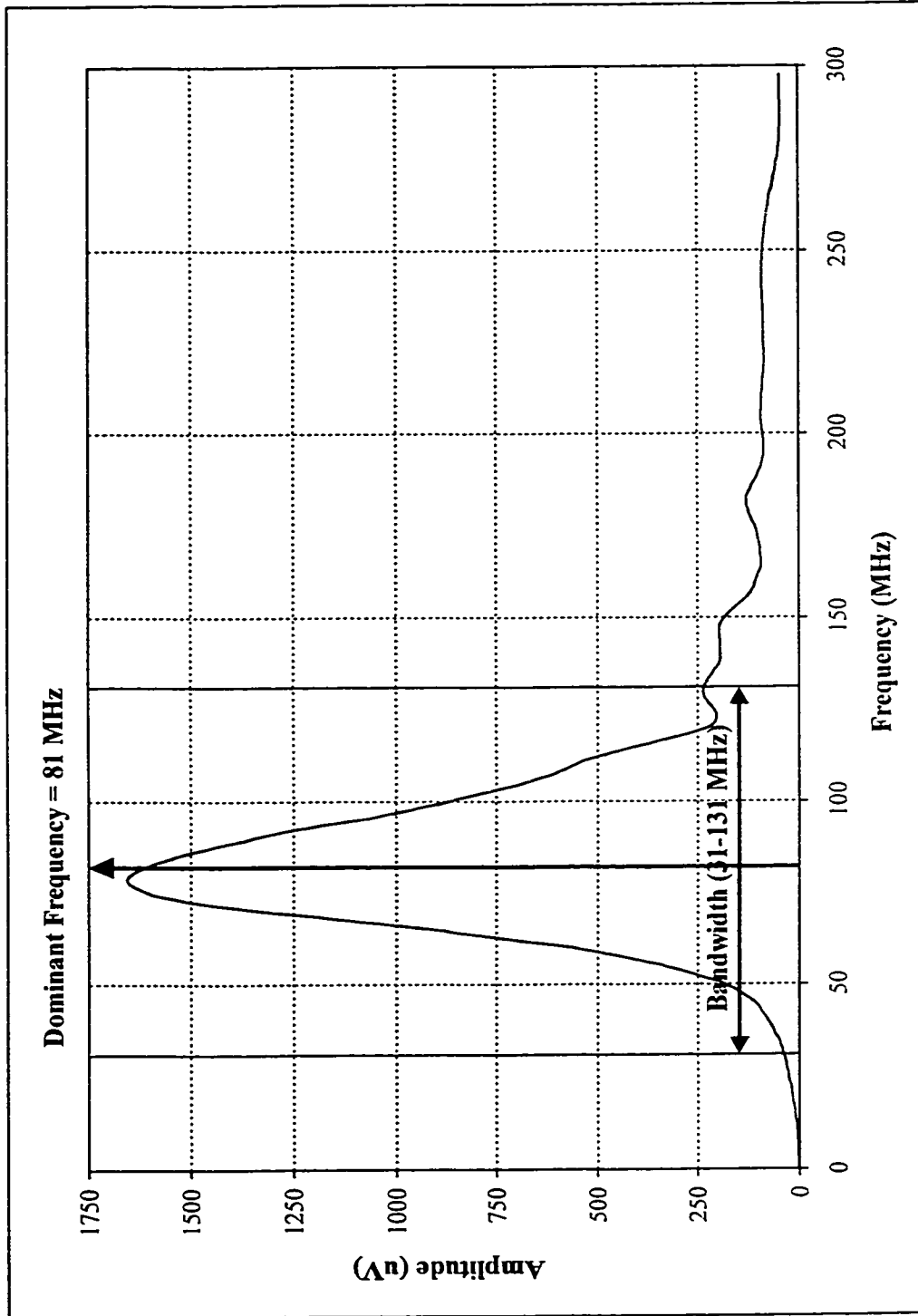
Figure 6-44 Average amplitude spectrum for the low frequency survey at the Hwy 17 Outcrop.

b) Geologic section for the high frequency survey at the Hwy 17
Site (File name: HWY171G2).

Note 1. Fracture aperture 3-4 cm at the surface.

a) Processed radar profile. Processing steps included: dewow,
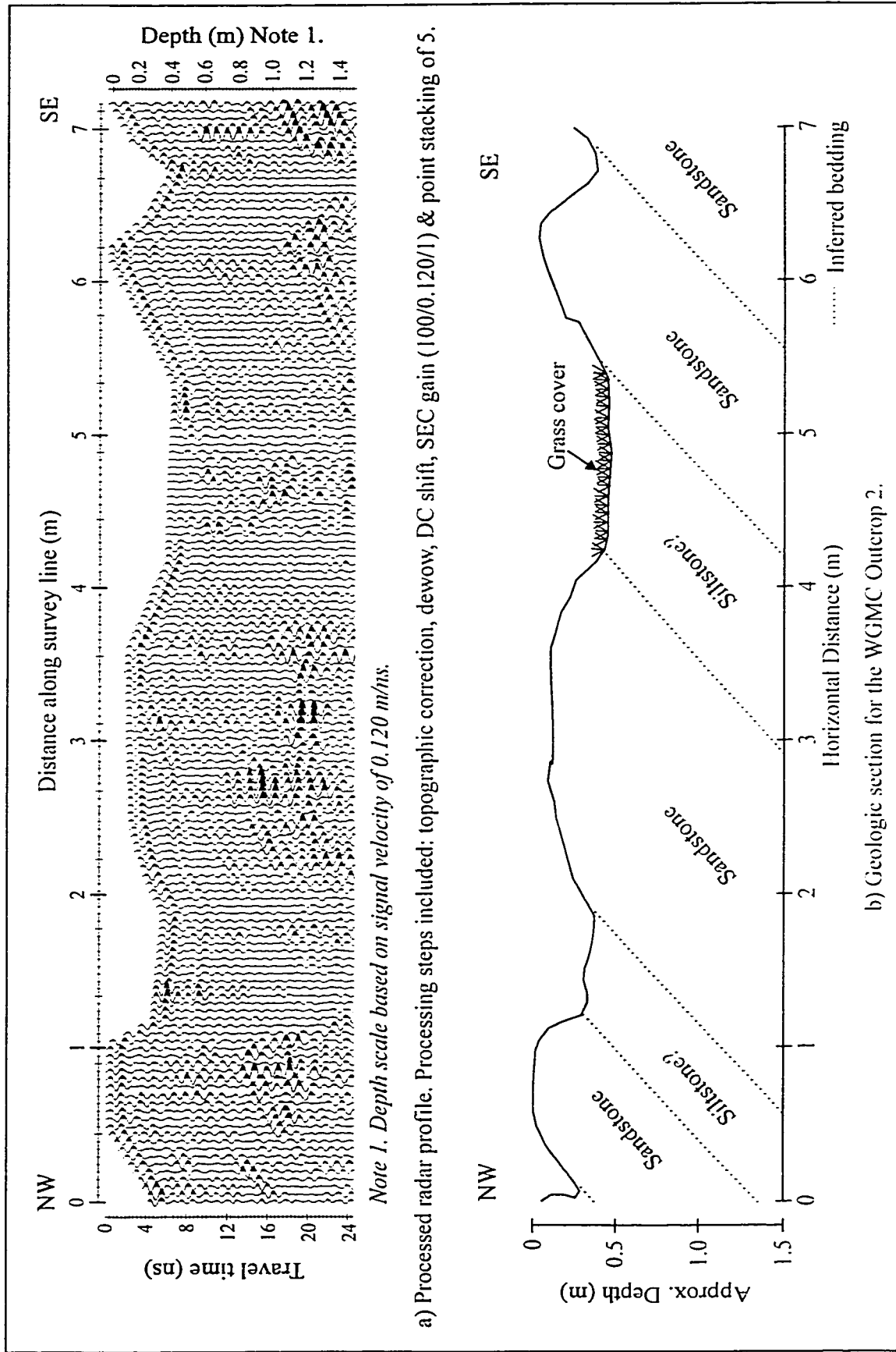DC shift, SEC gain (30/0.123/1), trace stacking of 2, &
point stacking of 7.
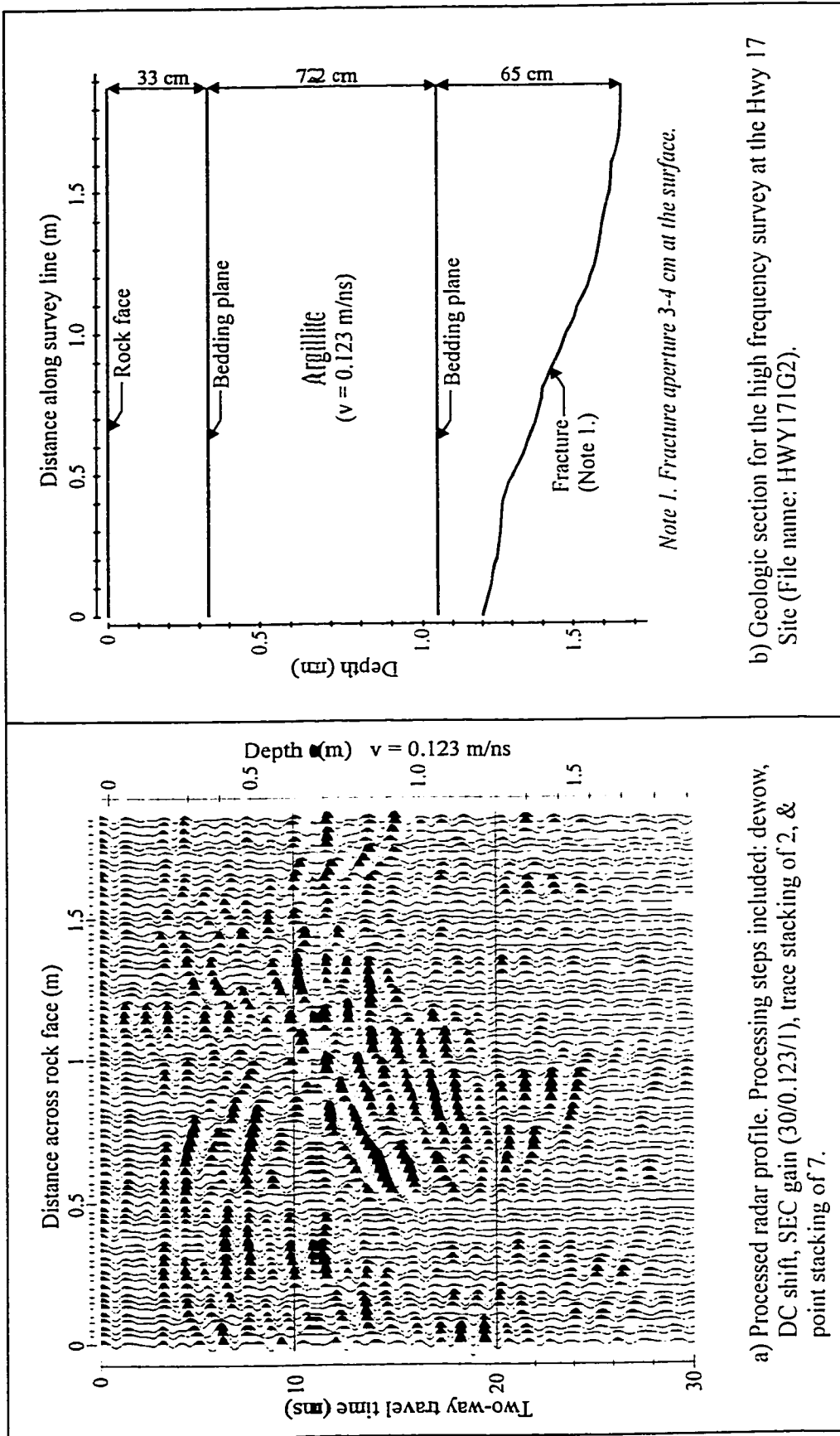
Figure 6-45 High frequency survey 'Hwy171G2' at Hwy 17 Outcrop; with accompanying geologic section.

243
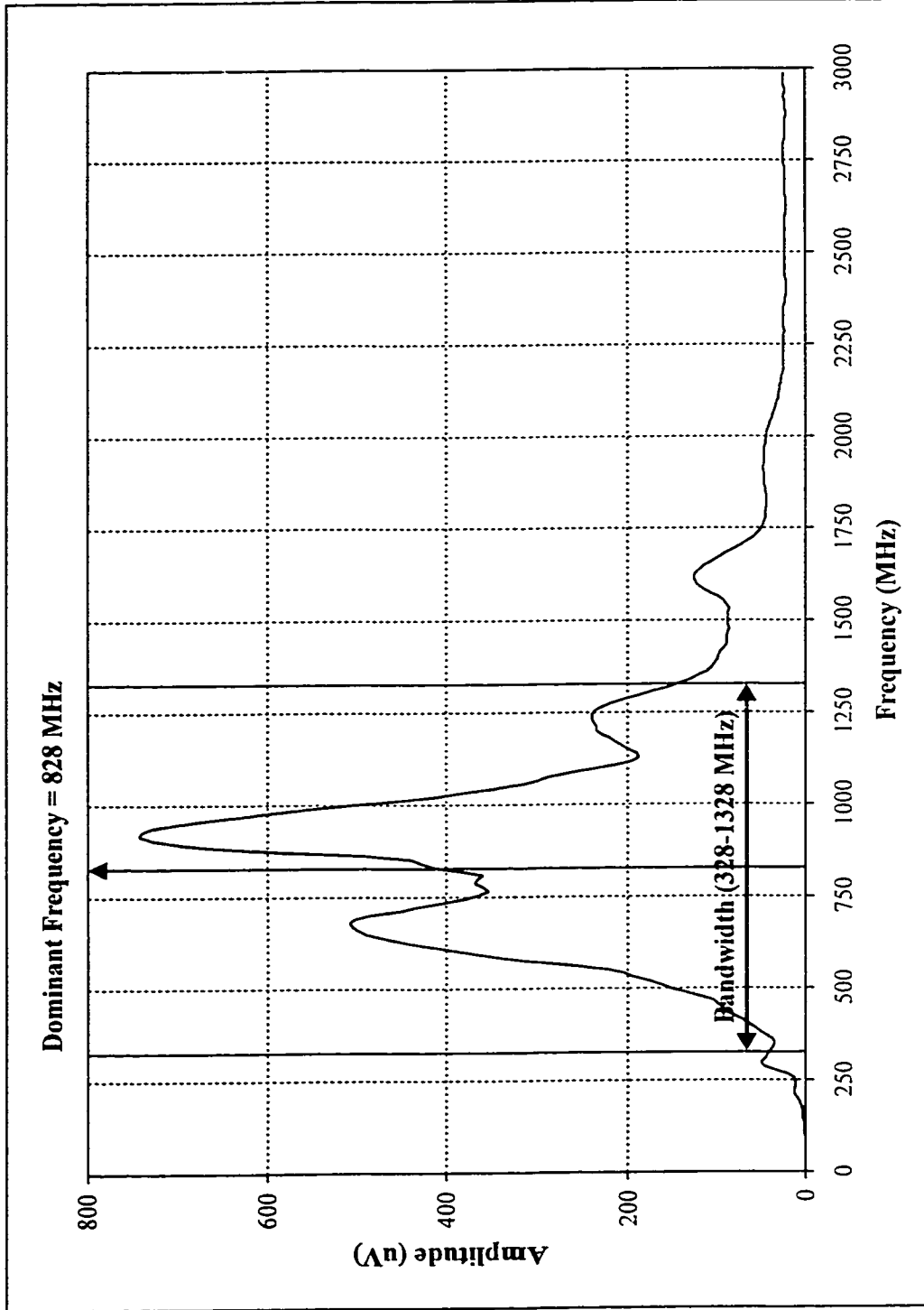
Figure 6-46 Average amplitude spectrum for the high frequency survey at the Hwy 17 Outcrop.

244
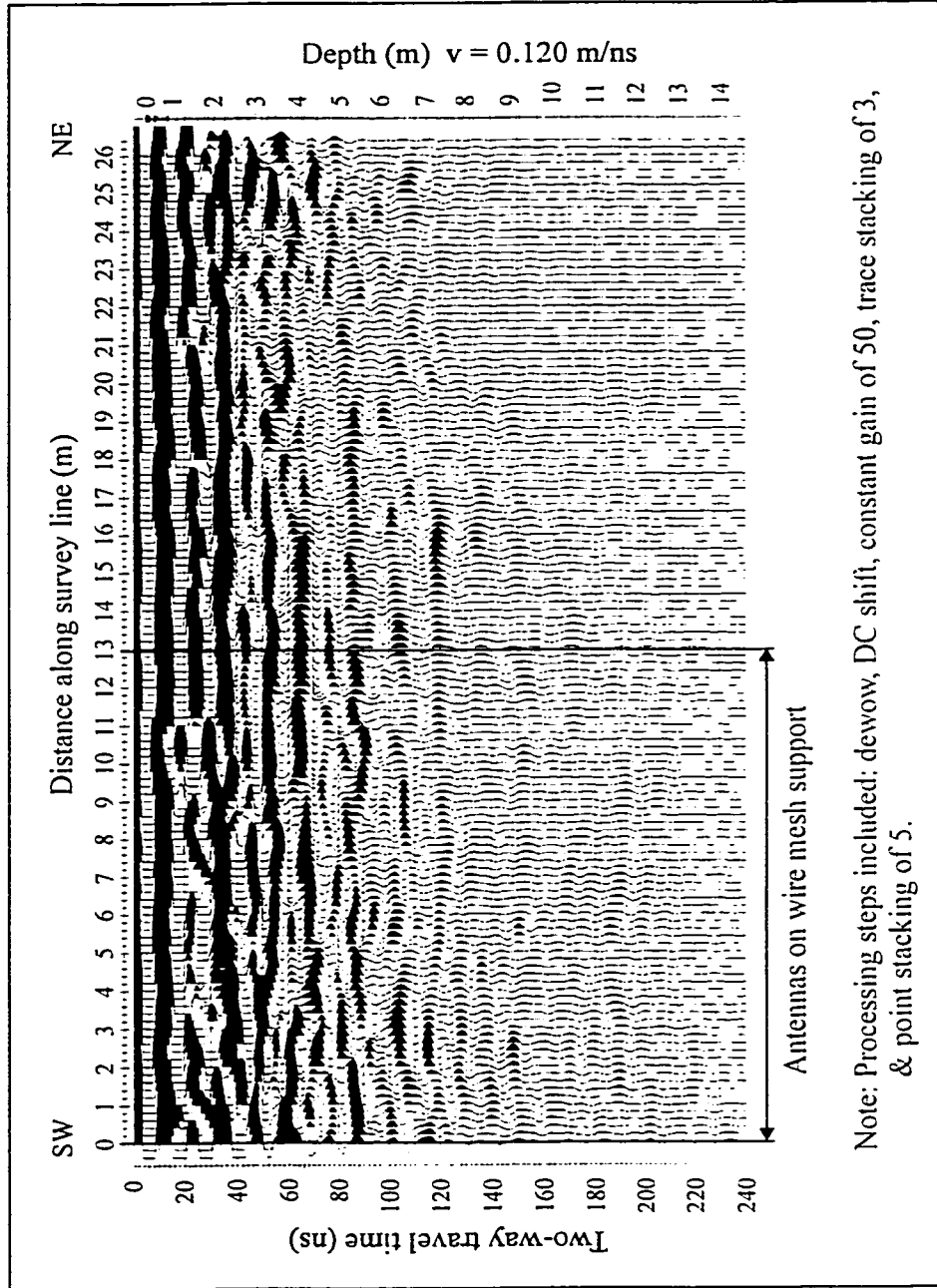
Figure 6-47 Low frequency survey '175-a' with a constant gain; NW sidewall in 7715 Drift; 175-Orebody.
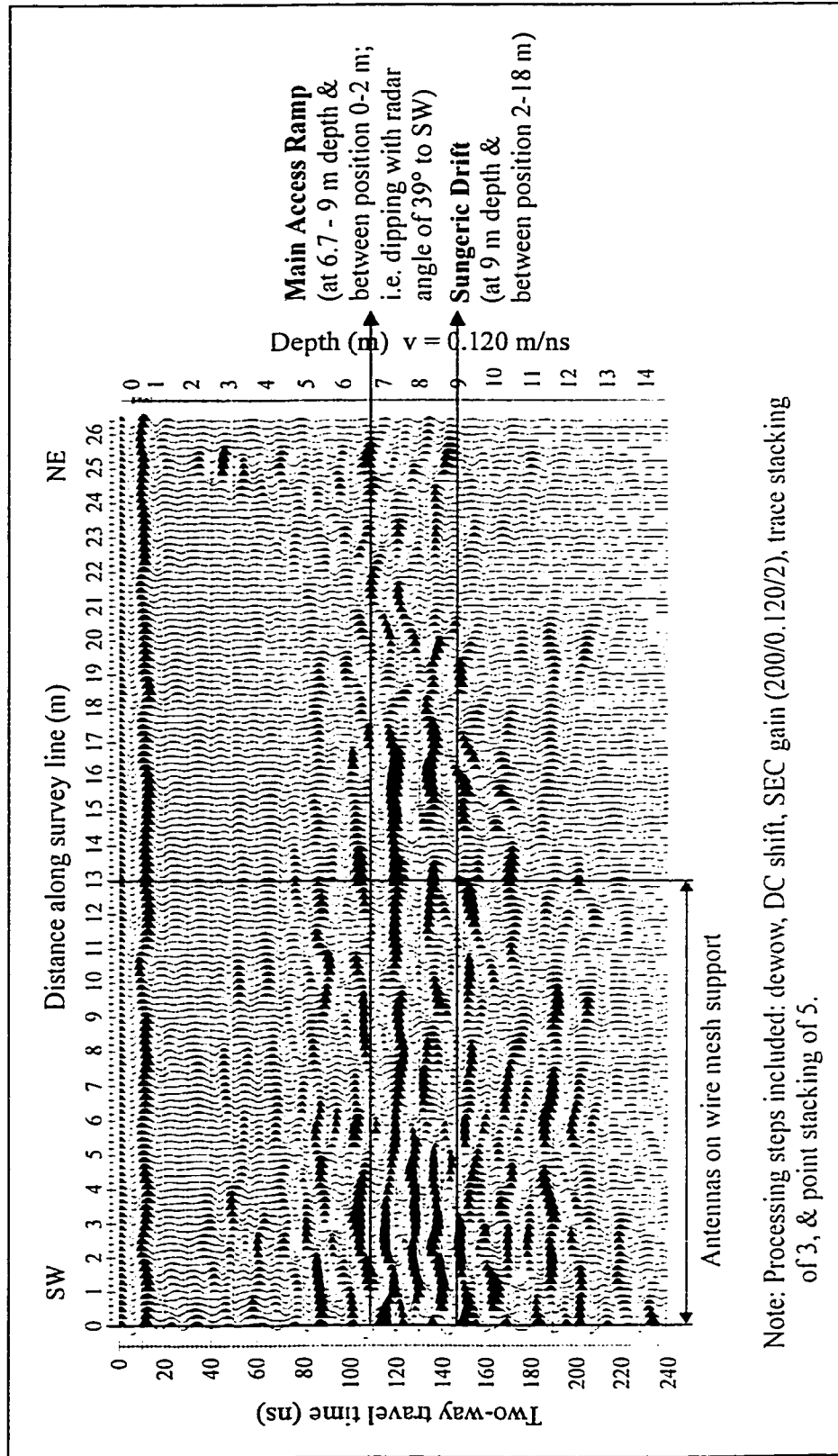
245

Figure 6-48 Low frequency survey '175-a' with a SEC gain; NW sidewall in 7715 Drift; 175-Orebody.

Note: Processing steps included: dewow, DC shift, SEC gain (200/0.120/2), trace stacking of 3, & point stacking of 5.

246

Figure 6-49 Low frequency survey '175-d2' with a constant gain; SE sidewall in 7715 Drift; 175-Orebody.
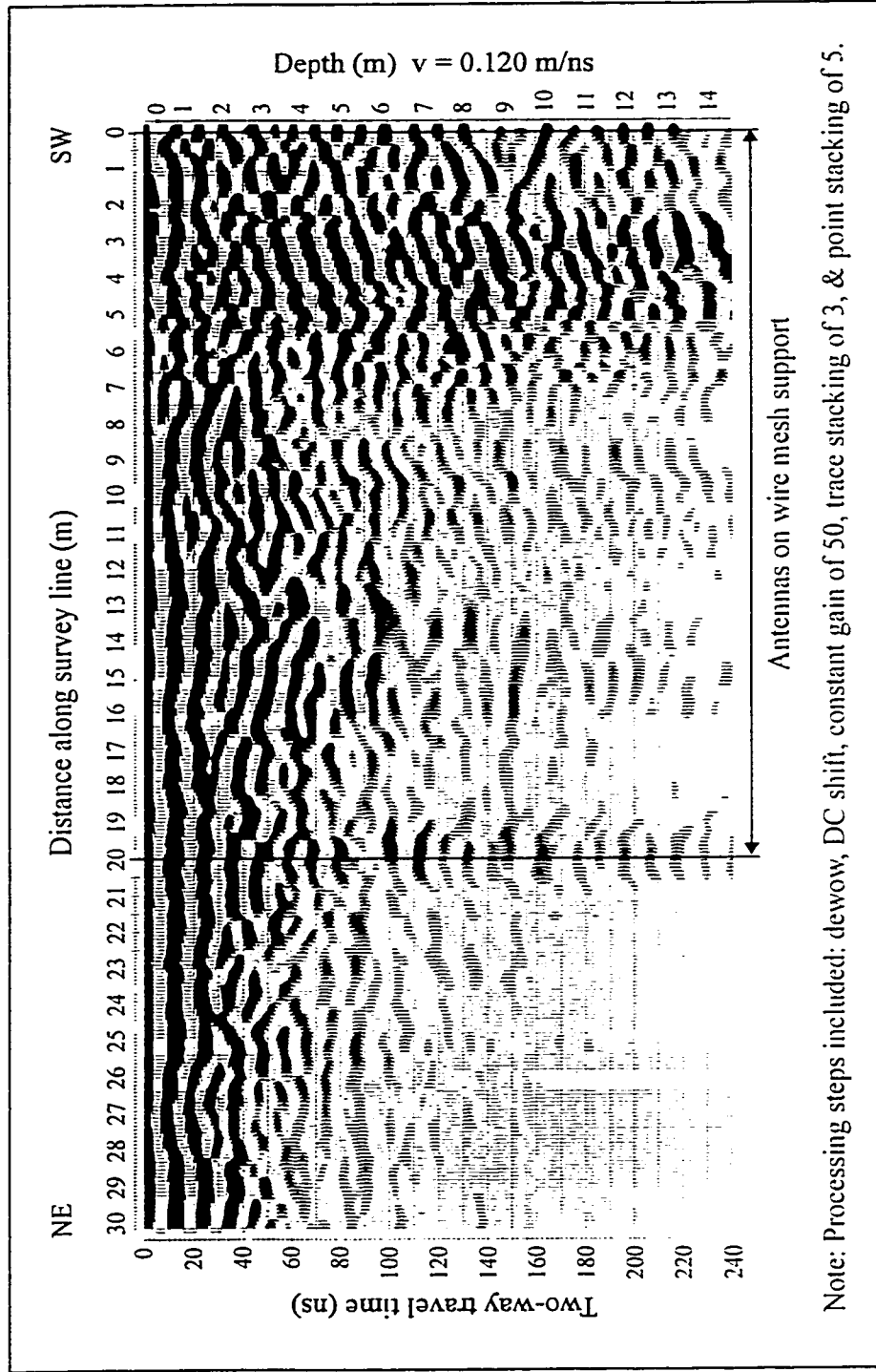
Note: Processing steps included: dewow, DC shift, constant gain; constant gain of 50, trace stacking of 3, & point stacking of 5.

247
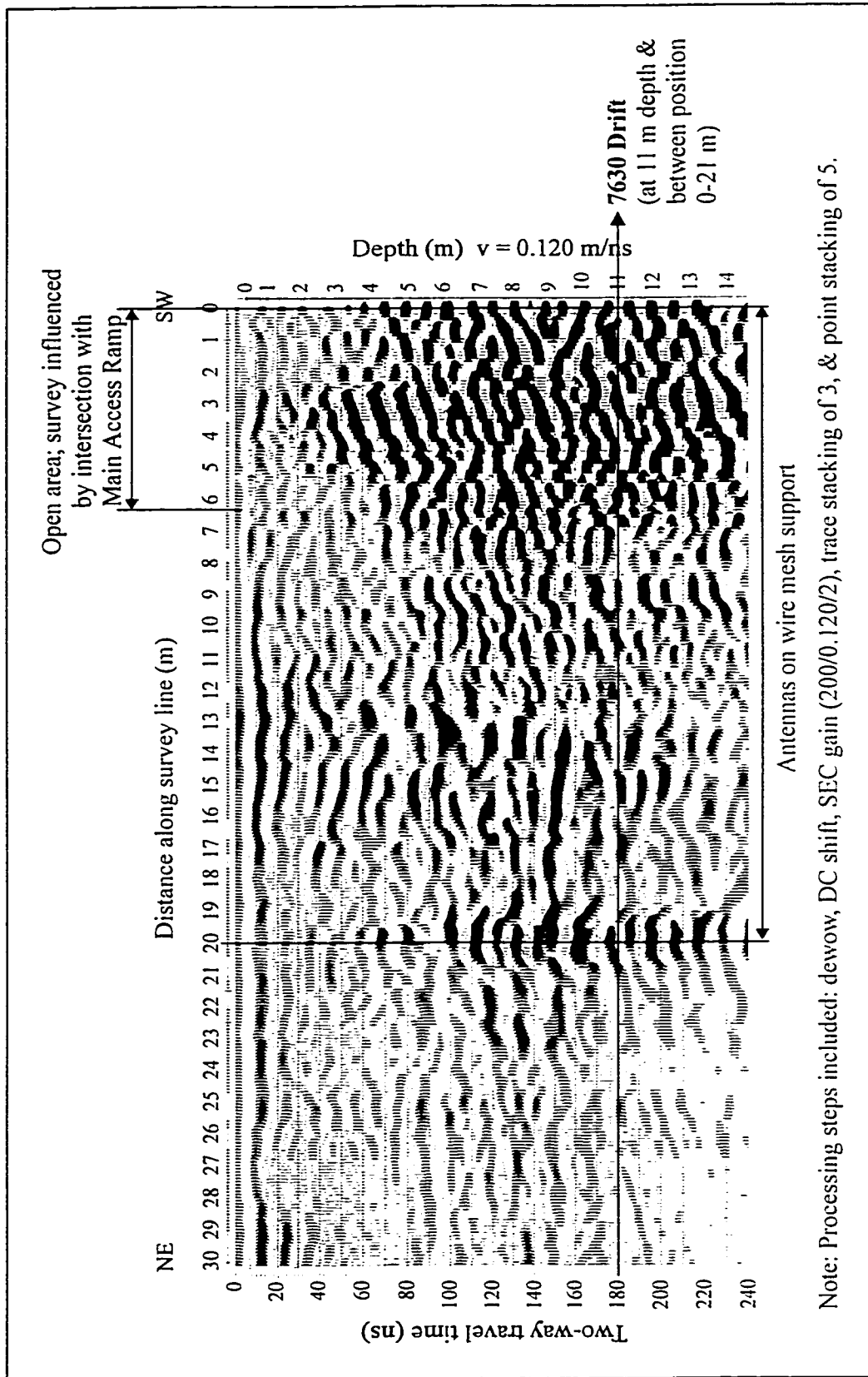
Figure 6-50 Low frequency survey '175-d2' with a SEC gain; SE sidewall in 7715 Drift; 175-Orebody.
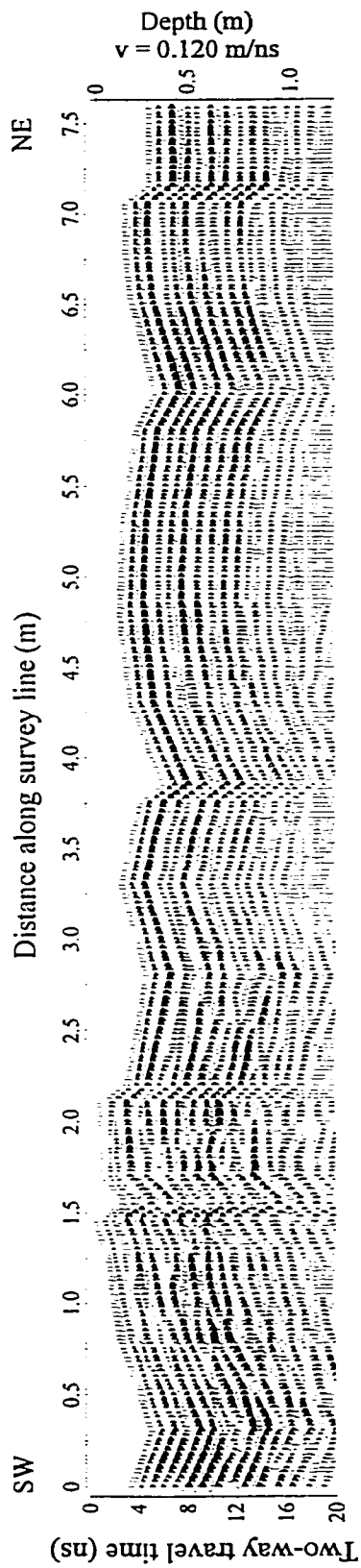
Note: Processing steps included: dewow, DC shift, SEC gain (200/0.120/2), trace stacking of 3, & point stacking of 5.

248
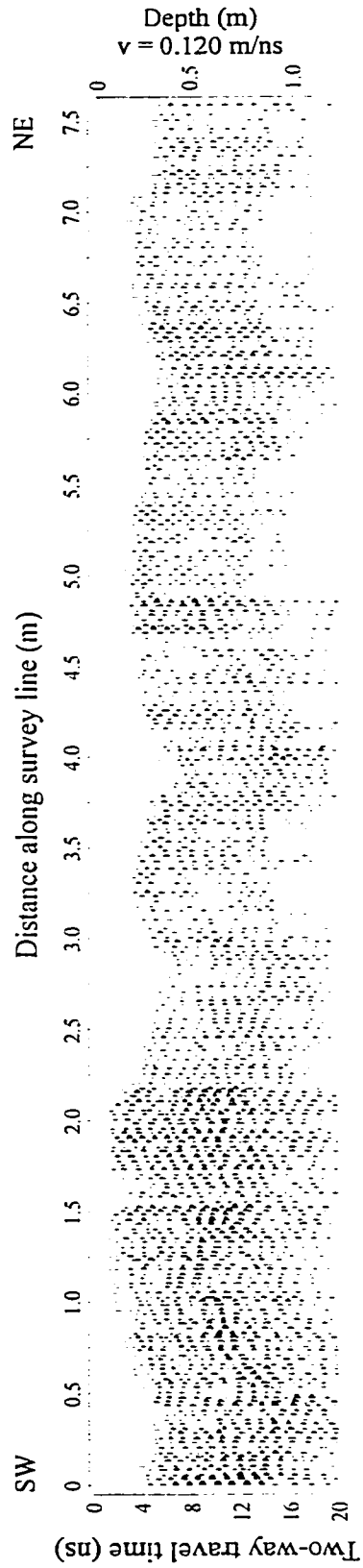
Figure 6-51 High frequency survey '175-1G-3' after various processing techniques: NW Sidewall in 7715 Drift; 175-Orebody.

249
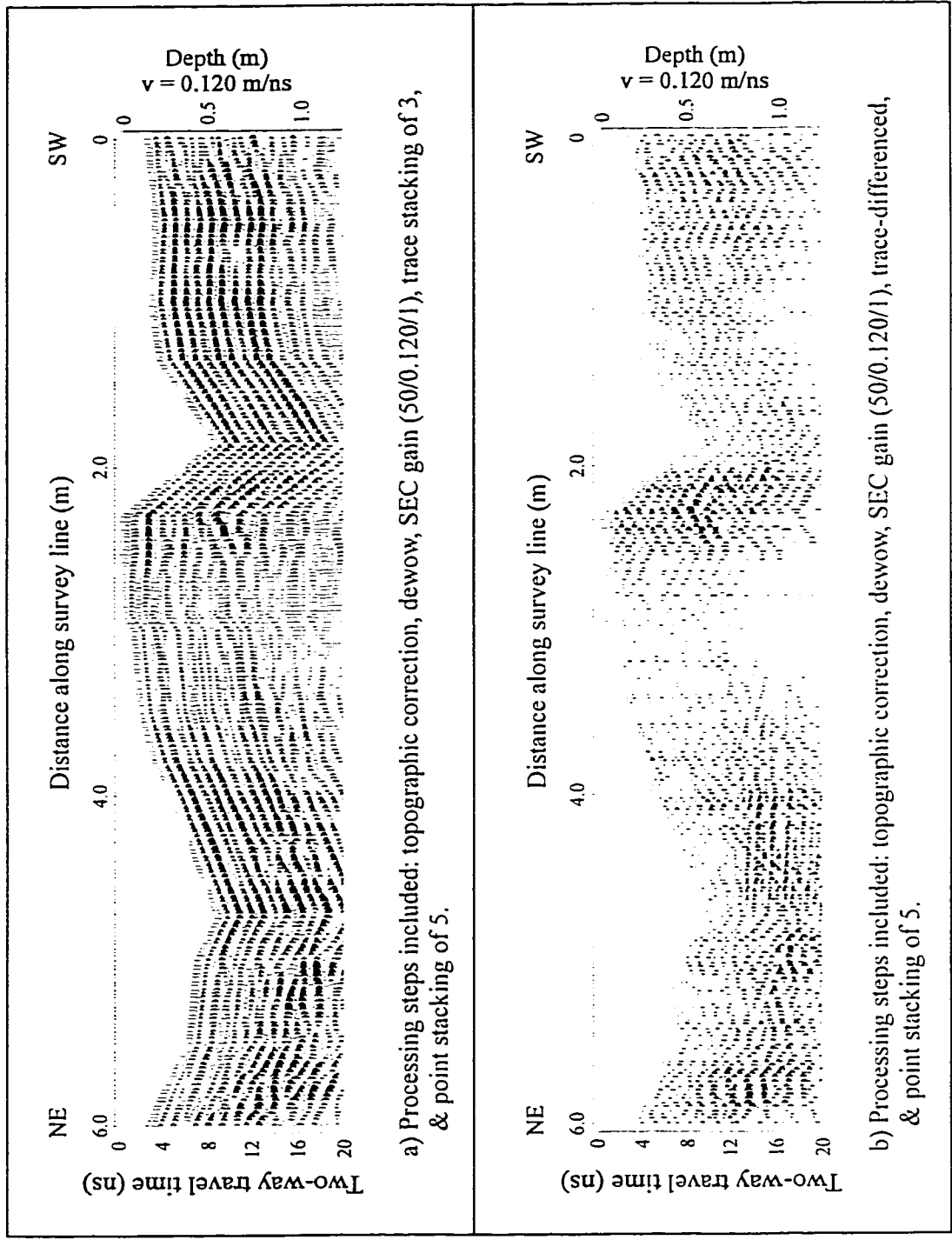
Figure 6-52 High frequency survey 175-1G-1 after various processing techniques; SE Sidewall in 7715 Drift; 175-Orebody.

250
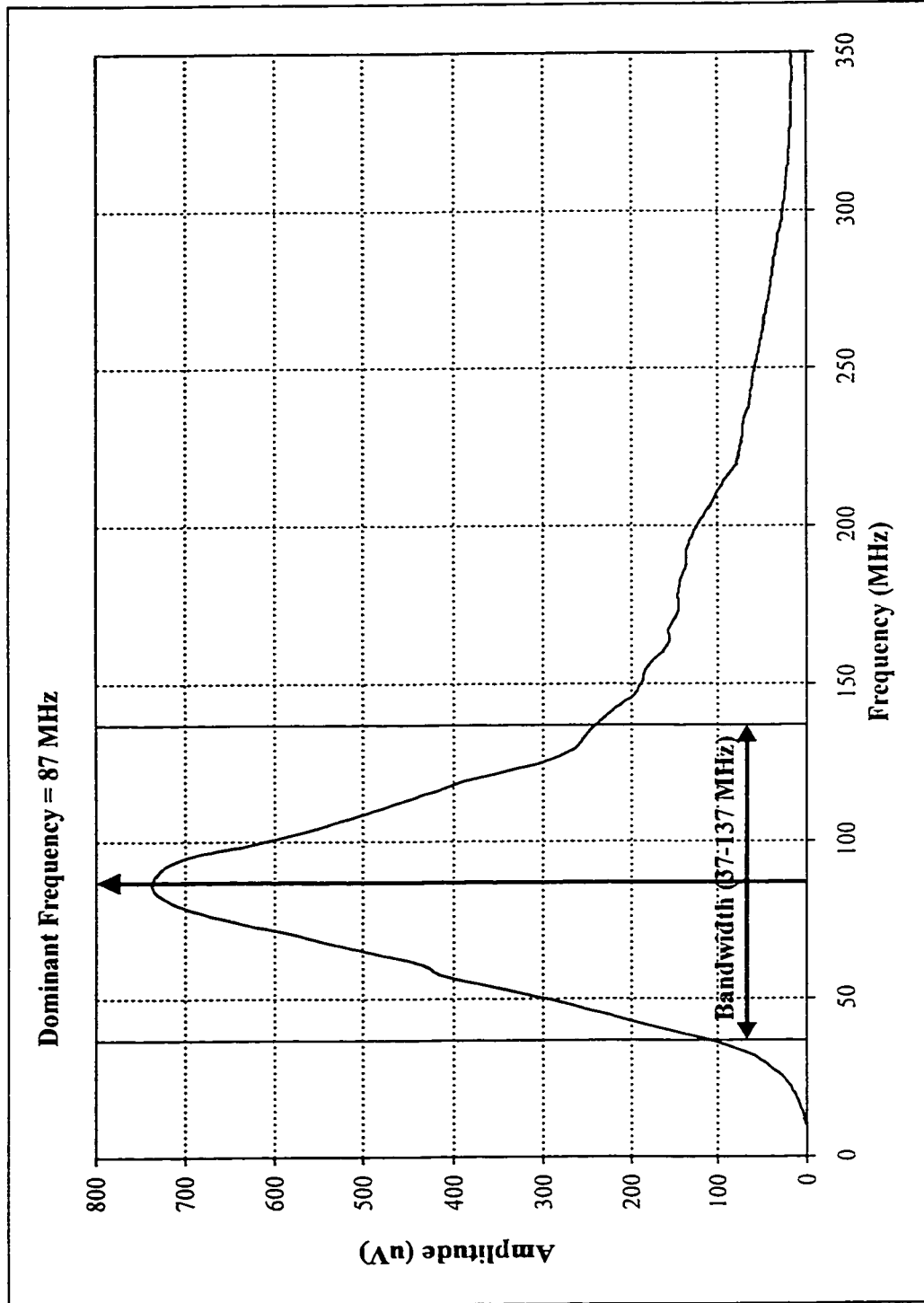
Figure 6-53 Representative amplitude spectrum for the low frequency surveys in 7715 Drift; 175-Orebody.

251
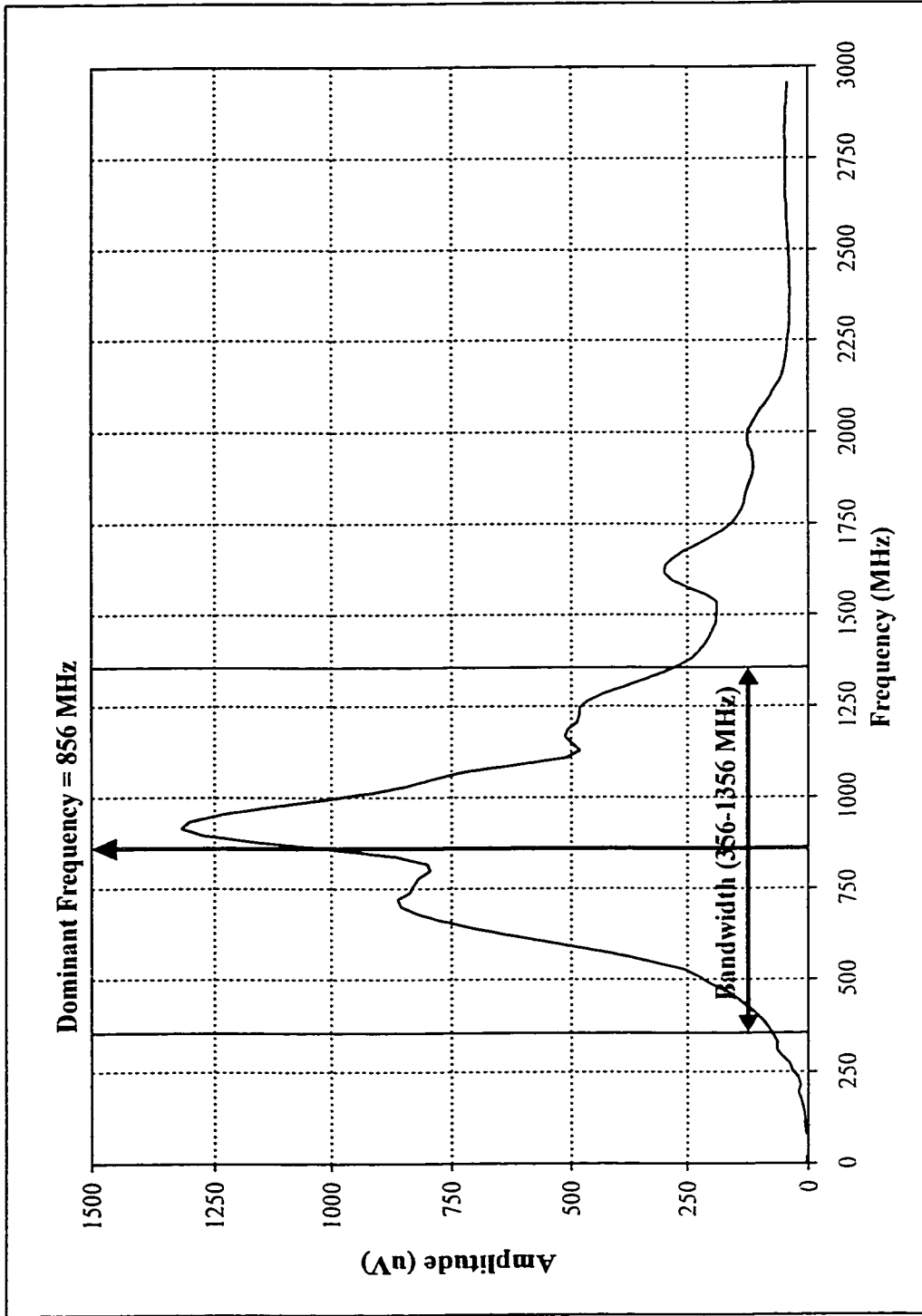
Figure 6-54 Representative amplitude spectrum for the hig frequency surveys in 7715 Drift; 175-Orebody.
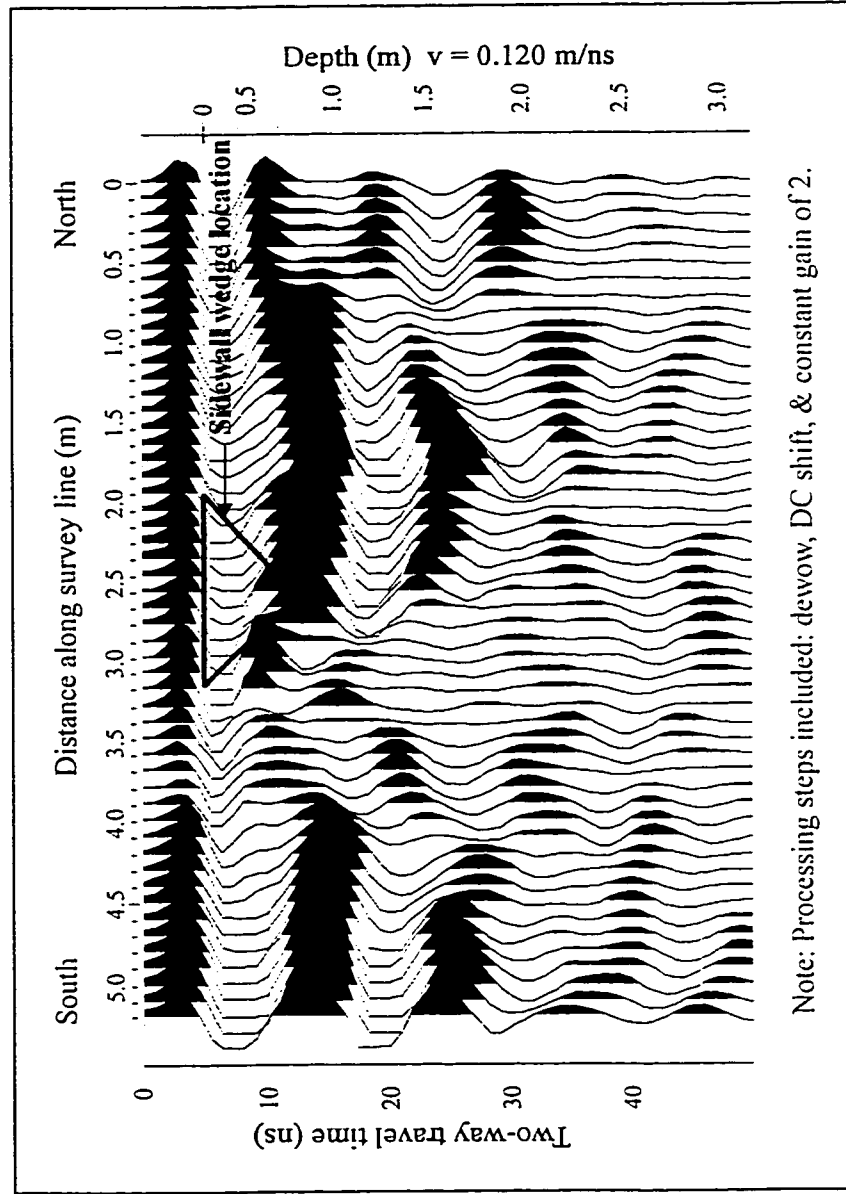
Figure 6-55 Low frequency survey '175-c' across SW sidewall of 7500 Main Access Ramp; 175-Orebody.

253
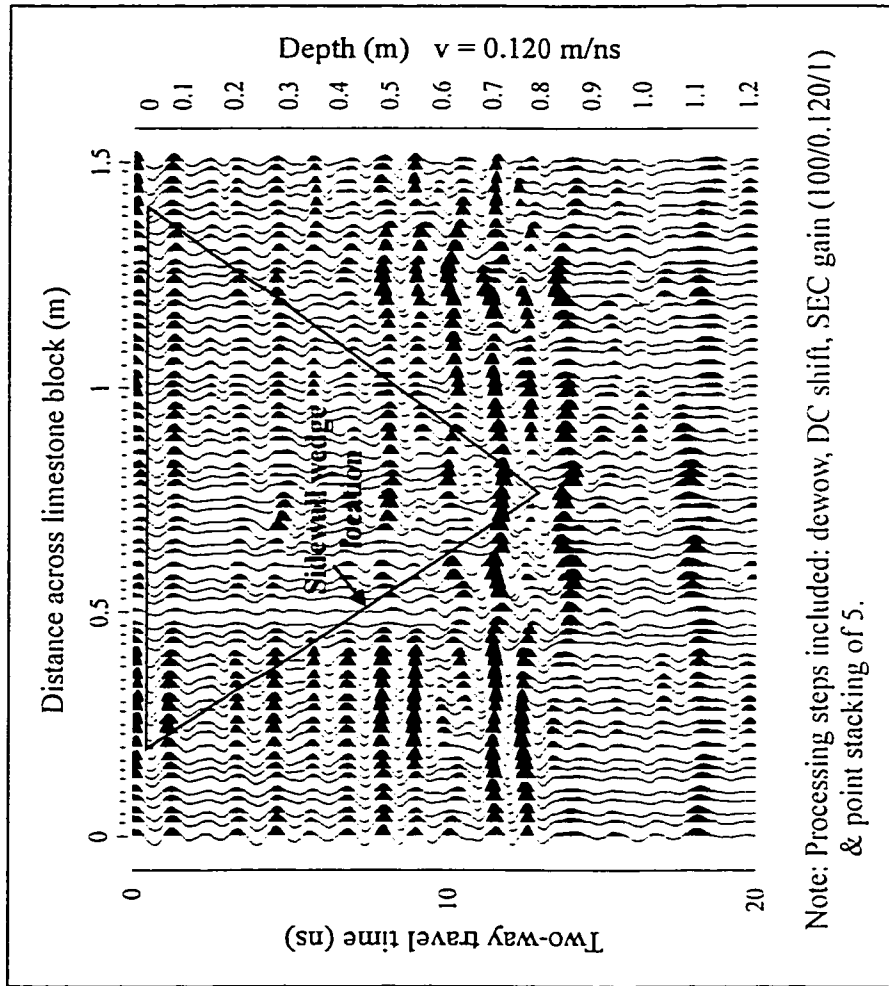
Figure 6-56 High frequency survey 'Wedge1G2' across SW sidewall of 7500 Main Access Ramp; 175-Orebody.

Note: Processing steps included: dewow, DC shift, SEC gain (100/0.120/1) & point stacking of 5.

254
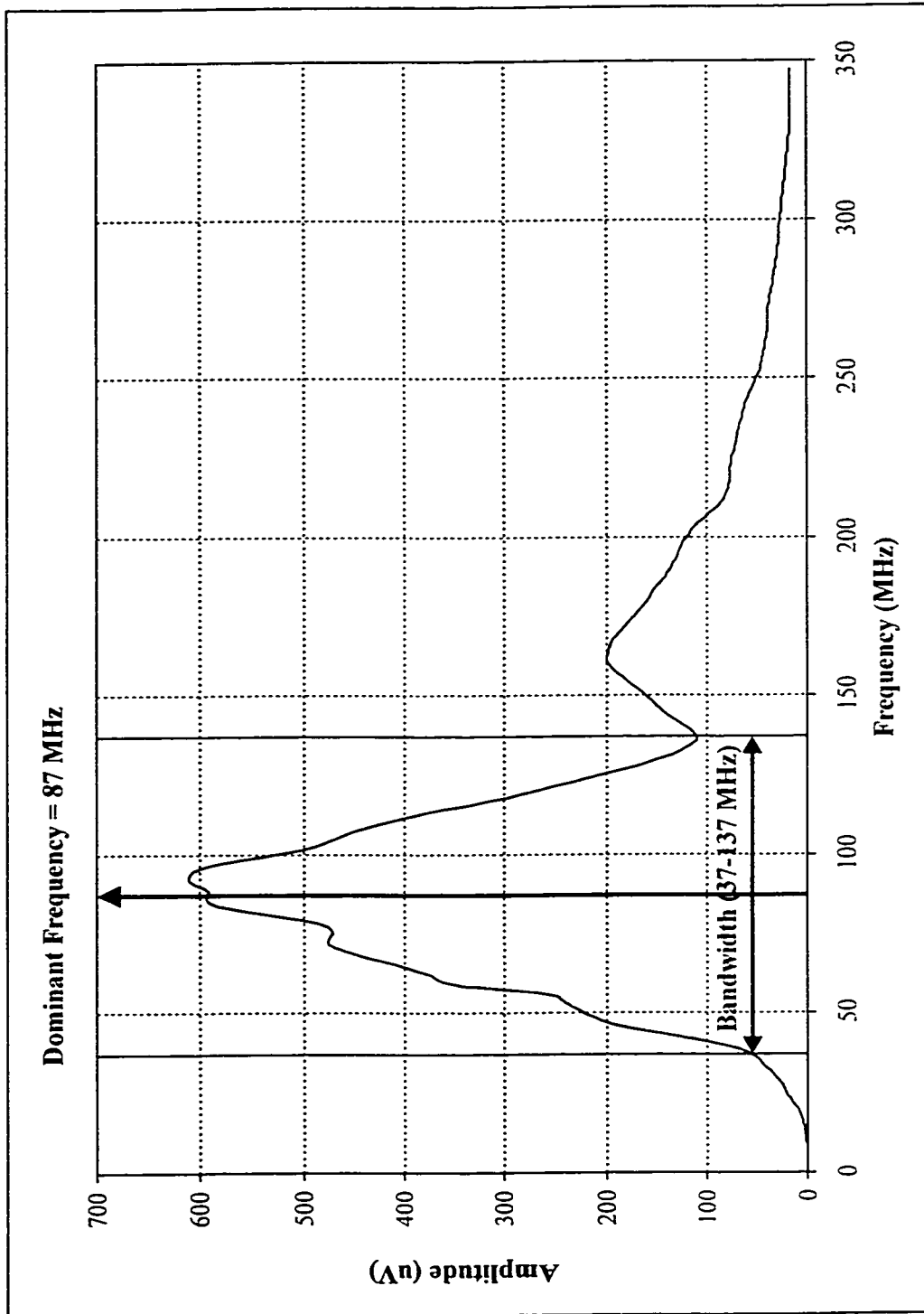
Figure 6-57 Average amplitude spectrum for the low frequency survey across the SW sidewall of the 7500 Main Access Ramp.
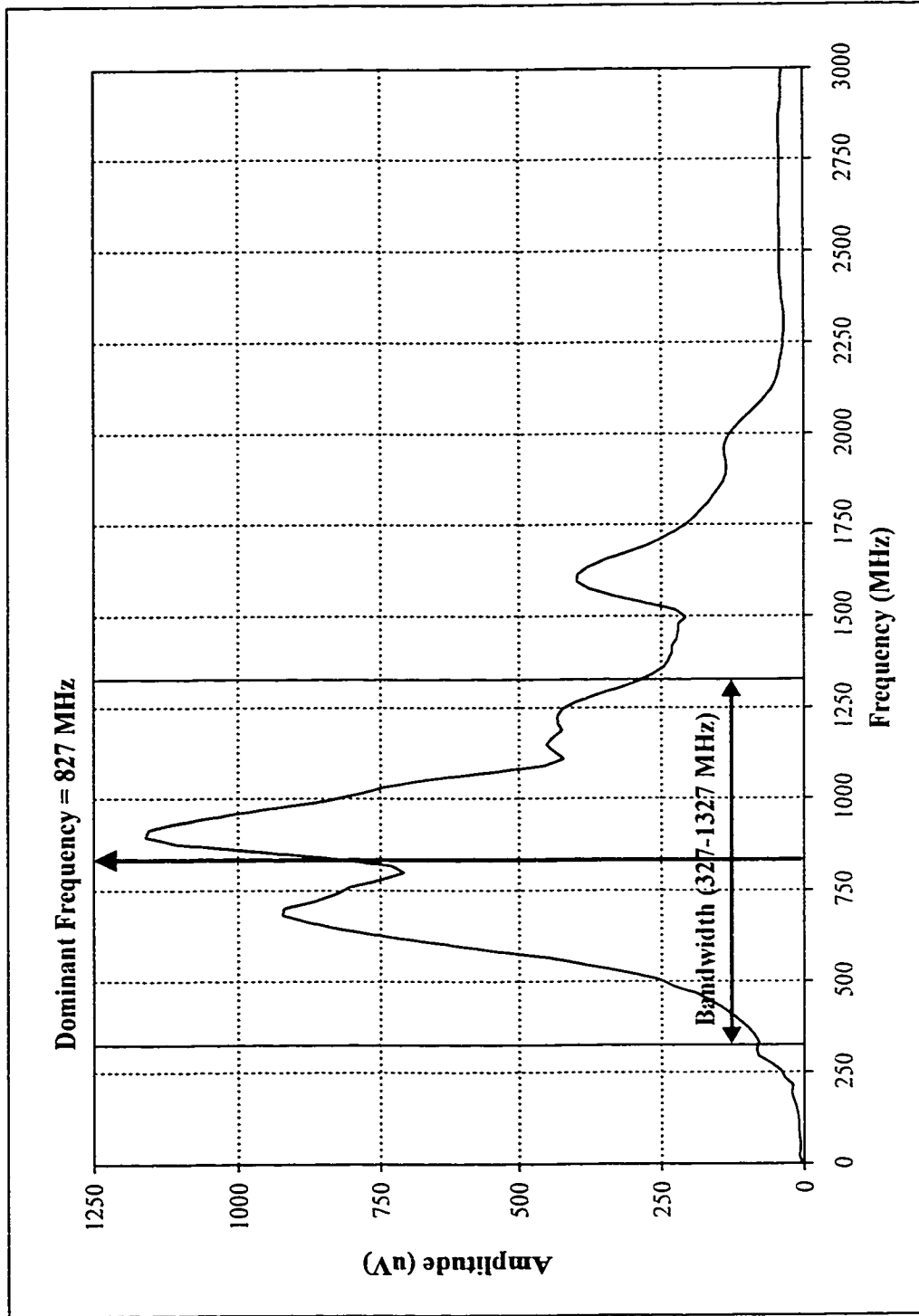
Figure 6-58 Average amplitude spectrum for the high frequency survey across the SW sidewall of the 7500 Main Access Ramp.

a) Plot for air-filled fractures.

b) Plot for water-filled fractures.
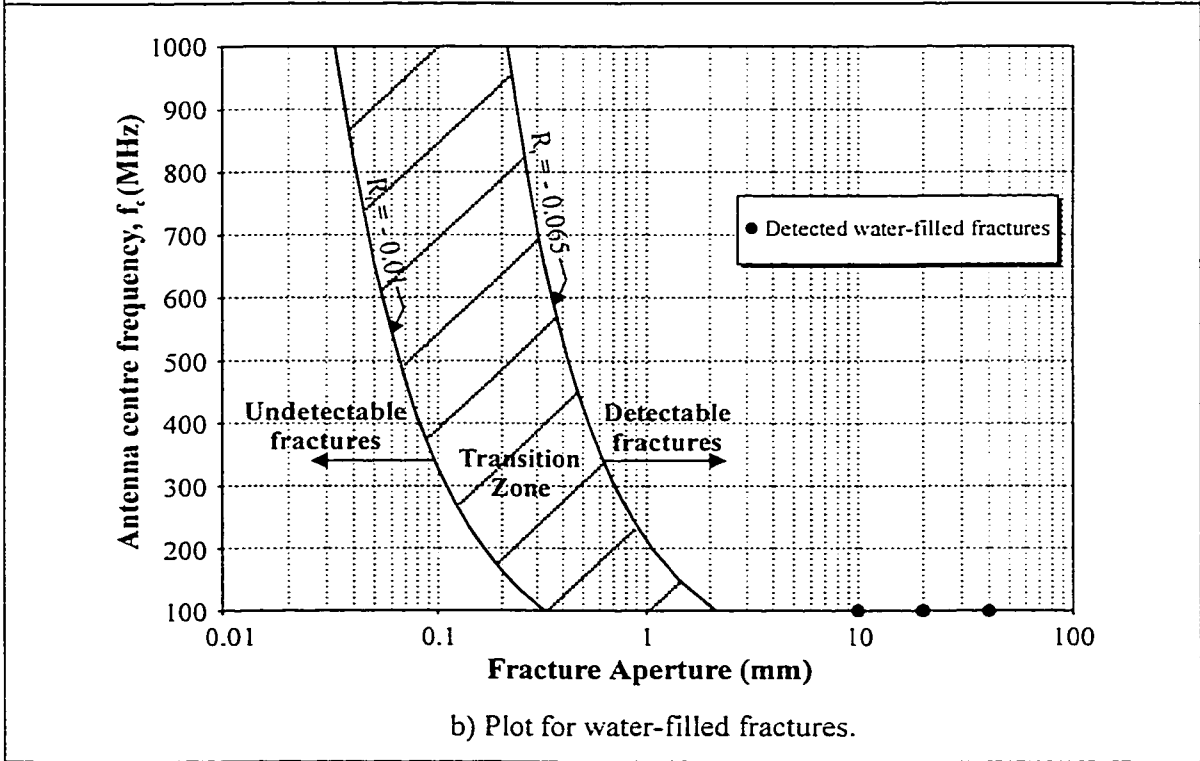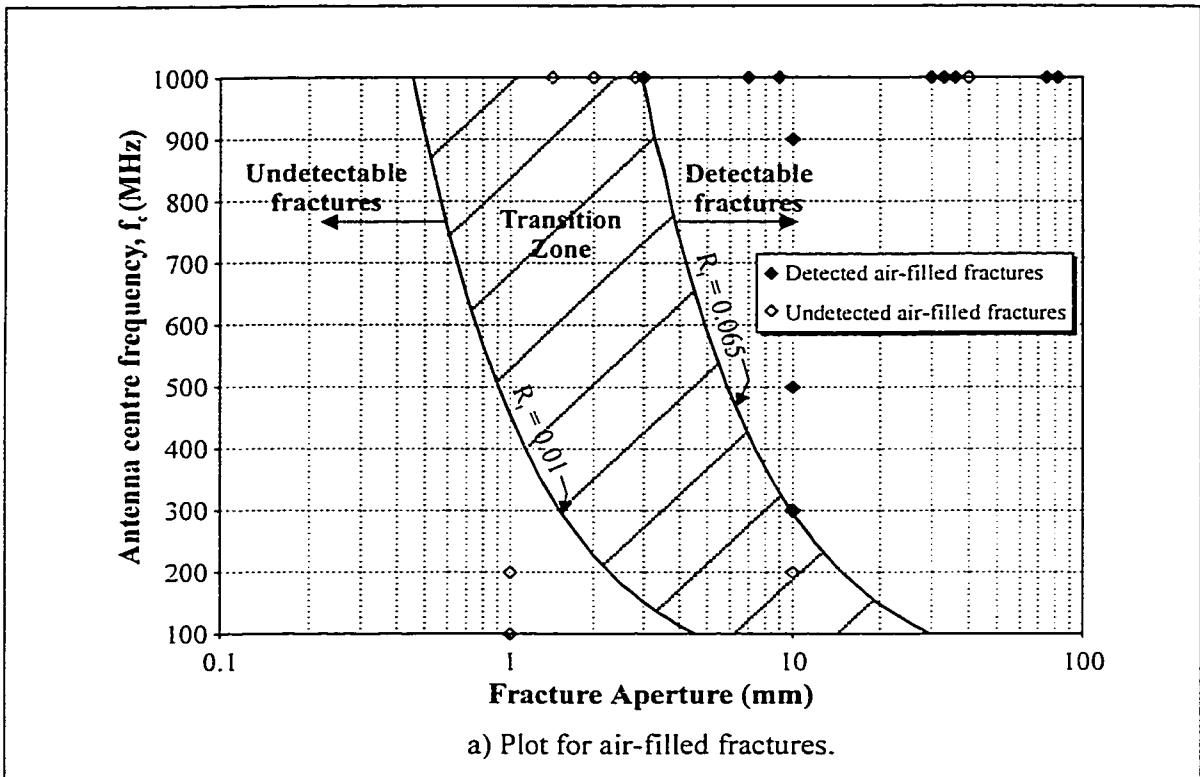
Figure 6-59 Antenna centre frequency (MHz) versus fracture aperture; including detected and undetected fractures from the thesis field surveys and Chapter 4 case studies (Note: For the theoretical reflectivity lines, assumed $\varepsilon_r = 6.25$ for rock, $\varepsilon_r = 1$ for air, & $\varepsilon_r = 80$ for water.)

257

CHAPTER 7: CONCLUSIONS AND RECOMMENDATIONS

7.1 CONCLUSIONS

The main purpose of this thesis was to evaluate whether ground penetrating radar can be used for detection of rock structure. Other researchers have considered this application, however the opinions regarding how well GPR works are conflicting. As such, the thesis began with four inter-related objectives:

1. to review the theory of this geophysical technique;
2. to evaluate whether ground penetrating radar can be used to detect rock structure with a focus on discontinuities with apertures less than 1 cm (i.e. small-scale structural features);
3. to determine the conditions required for successful detection of rock structure;
4. to determine the limitations of GPR for this application.

By reviewing the relevant theoretical geophysical principles, compiling past research conducted on this topic, and conducting GPR reflection surveys in various environments these four objectives have all been met.

Important Theoretical Concepts Behind GPR

Ground penetrating radar is a geophysical technique that is rapidly gaining popularity as an investigative tool within the geotechnical engineering community. The rapid, non-destructive, high-resolution, portable, and continuous profiling features are the principal advantages of GPR over conventional investigation techniques such as drilling and sampling.

Ground penetrating radar depends on the dielectric properties (i.e. dielectric constant and conductivity) of the ground and the radar target(s). The radar system emits pulses containing a broadband of frequencies into the subsurface using antennas, then energy is reflected from interfaces with different dielectric constants. Rock discontinuities such as joints are generally infilled with water, air, or gouge, so the contrast between the infilling material's dielectric properties and the surrounding host rock may act as a strong reflector.

Detection and resolution of sub-surface targets depends on the contrast in dielectric properties, the minimum target dimension, the amount of background noise, and available ground-truthing information. There are theoretical equations that can estimate whether or not a specific target can be detected and/or resolved under given site and survey conditions. However, in GPR, a distinction has to be made between large and small-scale targets because they may be governed by different equations. A target whose thickness is less than the dominant radar wavelength is classified as a 'thin layer'. The Fresnel Reflection Coefficient (R_t), which is dependent on the target thickness, governs the detection capability of small-scale targets (and sometimes large-scale targets). Unfortunately, GPR cannot resolve a thin layer. In other words, the aperture or width of a thin layer cannot be determined using radar.

Utility of GPR for Detection of Rock Structure

After understanding the theoretical basis of target detection and based on the results of field case studies, ground penetrating radar should be regarded as a reliable, rapid, and cost-effective tool for mapping rock structure in appropriate geological settings. The term appropriate refers to sites where there is a high contrast in dielectric constant between the host and target, reflector

geometry is simple, ground conductivity is low (< 10 mS/m), and the smallest target dimension is sufficiently large such that it can be detected. Without satisfying all these requirements, GPR will be ineffective.

For detection of large-scale structural features such as faults, the literature reports that GPR has been highly successful in unweathered, non-conductive, igneous or metamorphic shield rock. For example, in Canada, GPR was used to detect fracture zones within granite at the Underground Research Laboratory in Manitoba. Using low frequency antennas (i.e. 20 MHz to 120 MHz), fractures were located at depths between 30 to 110 m.

For small-scale structural features, the results are not as positive. Past case studies on small-scale fracture detection and the reflection surveys conducted in Sudbury show results that vary from no success to high success. There is a potential to detect discontinuities less than 1 cm in thickness (or aperture) but success is highly dependent on the antenna centre frequency, the infilling medium and aperture.

Conditions Required for Successful Detection of Rock Structure

Successful detection of rock structure is dependent on a number of factors. The site itself should not contain many sources of interference. For example, radio transmitters, power lines, and vehicles may preclude the use of GPR by either saturating the electronics or attenuating the signal so penetration is significantly reduced. Secondly, it is better to have a survey environment which has simple geologic conditions. For example the ground should be relatively homogeneous and have a conductivity, σ less than 10-15 mS/m for propagation of the radar. Simplicity is advantageous because data interpretation becomes more difficult as the ground conditions become more complex.

Successful detection is also heavily dependent on the GPR survey itself. Of utmost importance is using the correct antenna centre frequency for the given site and target conditions. As well, survey design requires proper selection of various survey parameters (e.g. station spacing, sampling frequency, and antenna separation) depending on the survey goals and local site conditions. An improper survey design can result in either unsuccessful detection of the particular target(s) or can make data interpretation more difficult.

Finally, the radar targets have a large influence on how successful detection is. Ideally, the radar target(s) should have a high contrast in dielectric properties from that of the surrounding geologic media. As well, the contrast should be sharp, not gradual. It is also better for the target to have smooth surfaces instead of rough because as the surface roughness increases, more energy is scattered. As for orientation, detection is more successful when the target is orientated parallel to the surveyed surface. Another advantage of flat-lying targets is that no dip correction is required.

Conditions for Successful Detection of Small-Scale Structural Features

Aside from the conditions mentioned above, detection of a small-scale target using GPR is highly dependent on the target's smallest dimension; for example, the aperture of an open joint. Case studies show that targets less than 1 cm in thickness are capable of being detected provided all other survey conditions are satisfied (e.g. proper antenna frequency, adequate depth of penetration, minimal sources of interference, etc.). Unfortunately, until this study was completed, there was little guidance on how small a fracture could be detected at various antenna frequencies. In other words, there was no guidance on the Fresnel Reflection Coefficient, R_t threshold - the R_t value that separates target detection from non-detection.

259

With this problem in mind, the results contained within this thesis were used to develop rough criteria as to what is detectable versus non-detectable. With compilation of all detected and undetected fracture apertures (with the associated antenna frequencies) from the literature as well as from results of the field surveys, the R_t threshold for fracture identification is estimated to be between 0.01 to 0.065. This means a target is detectable as long as at least 1 % to 6.5 % of the incident energy is reflected back to the receiver antenna.

It is important to recognize that this threshold range was selected based on limited data, but the concept of providing the engineer with better guidance on the minimum detectable fracture thickness was required. However, the upper threshold limit of 6.5% is likely a more realistic value because it best matches the field data results. With this said, dry fractures with apertures less than 1 cm may be detected using an antenna centre frequency greater than 300 MHz, but the minimum detectable aperture is approximately 3 mm using 1000 MHz antennas. Under saturated conditions, apertures less than 1 cm may be detected using frequencies greater than 100 MHz, but the minimum detectable aperture is approximately 0.2 mm using 1000 MHz antennas. Closed joints cannot be detected using GPR because the R_t value approaches zero.

Aside from thickness, the contrast in dielectric constant for detection of small-scale fractures is also very important. There is a significantly higher chance of detecting water-filled fractures in comparison to dry fractures because the higher contrast in dielectric constant yields a higher Fresnel Reflection Coefficient and a polarity change in the wavelet. Ultimately, this means the reflection amplitudes are higher, so identification of fracture reflections in the profile is easier.

Limitations of GPR

Although GPR has the potential to detect various types of rock structure, there are numerous limitations to be aware of. GPR does not work in all geologic environments. Radar propagation works for low loss, homogeneous, isotropic geologic media; however, most rock is heterogeneous, anisotropic, and can be highly conductive. It is therefore unusual that Buursink and Lane (1999) claim radar can detect rock fractures in more geologically complex environments using low frequency (100 MHz) antennas. Their success in heterogeneous conditions is also in contrast to the difficulties observed at some of the Sudbury project sites, specifically at the Hwy 17 Bypass Outcrop and the gneiss blocks along the WGMC walkway.

It also appears that GPR has little success in detecting rock structure in underground hard-rock mining environments. This conclusion is based on the results of past case studies conducted in such environments and on the unsuccessful detection of joints at the 175-Orebody using 100 MHz and 1 GHz antennas. The poor success at detection is primarily attributed to high radar signal attenuation from nearby metallic support and equipment. As well, there is limited room available to conduct GPR surveys and close contact between the antennas and the rock cannot be achieved due to the rough walls.

Another limitation is that people experienced in ground penetrating radar are required conduct data collection, processing and interpretation. The engineer has the background to learn how to properly use this tool, but it may takes months to do so. GPR surveying should therefore be left to geophysicists.

However even with experienced people, processing and interpretation can be both difficult and time-consuming, which can offset the cost-savings from reduced amounts of drilling. For example, with data interpretation there are always problems due to non-uniqueness. Non-

uniqueness can make it difficult to identify rock structure from a radar profile. In simple terms, this means reflections from a joint, foliation plane, or bedding surface can all look the same in a radar profile. The field surveys conducted at the Hwy 17 Bypass are examples showing the ambiguous nature of radargrams. At this site, some of the bedding joints were detected, however there was also significant signal scattering due to mineralogical changes. The response of the 1000 MHz to these heterogeneous rock conditions made the resulting profile complex. In fact, any interpreter of this data likely would have suggested more fractures existed than were actually observed.

The problem of nonuniqueness is therefore exacerbated with heterogeneous rock and the use of high frequency antennas, which will pick up small variations in ε_r. If the rock contains more than one type of small-scale rock structure (i.e. gneissic foliation and jointing), the high frequency antennas will pick up all sorts of rock features. The GPR system cannot be tweaked to identify joints from foliation planes. Because of this, it falls on the shoulders of the interpreter to distinguish reflections from foliation planes from those of joints, however this is a nearly impossible task without other ground-truthing information. The high frequency field surveys conducted across the gneiss blocks are yet another example showing the difficulty of heterogeneous rock. At this site, foliation reflections could not be distinguished from a fracture reflection.

There are also problems associated with detecting small-scale features such as joints. The engineering community is interested in finding investigative tools - such as GPR - that could detect fractures with apertures less than 0.5 mm. Assuming that detection of these small targets requires a R_t of 0.065, only water-filled fractures have a chance of being detected at antenna frequencies greater than 500 MHz. Air-filled fractures with apertures less than 0.5 mm cannot be detected with antenna frequencies currently available. This has important implications for the use of GPR in natural rock exposures because many joints are dry and have apertures between 0.1-0.3 mm.

Radar data can only be properly interpreted with information from boreholes or geologic field mapping else the radar profiles cannot confidently be calibrated or evaluated. With the majority of the field surveys discussed in this thesis, the characteristics of the primary targets could be measured or reasonably assumed. With the case studies, there were many claims of success using radar without any ground-truthing information. For these studies, the conclusions made are questionable.

Finding new techniques to detect structure is favorably looked upon but GPR is like most remote methods, as it will likely only provide information on the location and possibly orientation of the structural feature. Structure characteristics such as geometry, roughness, and infilling will not be determined. Because of this lack of resolution of rock structure and the limitations described in the above paragraphs, radar cannot presently replace geologic mapping, but may provide complementary information regarding rock structure.

7.2 RECOMMENDATIONS

On the basis of the above conclusions, more testing is required for detection of small-scale rock structure using ground penetrating radar with frequencies greater than 100 MHz. Based on the field studies conducted within the district of Sudbury, it would be beneficial to conduct additional reflection surveys on slabs of cut rock, on surface outcrops where well-defined discrete fractures exist, and at underground sites with simple geology.

Because it has already been confirmed that air-filled fractures approximately 3 mm thick can be detected using 1000 MHz antennas, it would advantageous to examine fractures between 0.1 to 0.5 mm – classified as tight to partly open. It would also be beneficial to test GPR capabilities under both dry and saturated conditions. Rock blocks (or slabs of cut rock) offer a good opportunity to seal off the fracture and then inject water to simulate saturated conditions. To reduce edge effects, rock blocks as large as possible should be used.

At present, the R_t threshold needed to distinguish between detectable and non-detectable fractures is a range of 0.01 to 0.065. There is some uncertainty with this range, however by conducting additional tests using smaller apertures these R_t values can be refined. Refining the limits would be beneficial because the R_t threshold provides the engineer with better guidance as to where this geophysical tool has a high chance for fracture detection.

With rock structure detection on surface outcrops, it would be beneficial to conduct additional testing at site where fractures are well-defined. Antenna frequencies greater than 100 MHz but less than 1000 MHz should be tested to determine their limitations. Sites that contain fractures with either water or clay infilling should be sought out because there is a higher chance of detection in comparison to dry sites.

Because of the strong desire to use GPR in underground environments, it is recommended that additional testing be conducted either at the 175-Orebody or within another hard-rock underground environment. Similar to the surface testing recommended above, additional underground GPR surveys should be conducted at frequencies greater than 100 MHz but less than 1 GHz. These are more difficult environments, so it is further recommended that future surveys be performed over non-metallic thin-membrane support and not across wire mesh and rock bolts. This will reduce the amount of signal attenuation and cause more radar energy to penetrate into the rock. As well, any additional testing should be done using either shielded antennas or with radio-frequency absorbing material placed around the antennas. Lastly, surfaces that are relatively planar should be sought out instead of rough and irregular surfaces.

The final recommendation is to conduct additional surveys in heterogeneous (or geologically complex) environments. This recommendation is based on the fact there is some dispute regarding whether radar can be successfully used to detect fractures in geologically complex environments. Buursink and Lane (1999) claimed they successfully used low frequency (100 MHz) antennas to detect joints at a site composed of a variety of igneous and metamorphic rocks. However, these authors failed to discuss variations in dielectric properties between the different rock types and merely use a single value for the dielectric constant. It is dangerous to assume that based on this single study that radar will be successful for fracture detection in other complex rock environments.

REFERENCES

Annan, A. P. 1989. Evaluation of ground penetrating radar for loose rock detection at the Denison Mine, Elliot Lake, Ontario. Proceedings, Mine Accident Prevention Association of Ontario Annual Meeting. Toronto, Ontario. PEMD # 48. May 24-26, 1989. pp. 1-6.

Annan, A. P. 1997. Engineering and environmental geophysics: the future. *In* Modern Geophysics in Engineering Geology. *Edited by* D. M. McCann, M. Eddleston, P. J. Fenning, and G. M. Reeves, Geological Society Engineering Geology Special Publication 12. pp. 419-426.

Annan, A. P. 1999. Ground penetrating radar workshop notes. Sensors & Software Inc., Mississauga, Ontario.

Annan, A. P., and Chua, L. T. 1992. Ground penetration radar performance predictions. *In* Ground penetrating radar. *Edited by* J. A. Pilon: Geological Survey of Canada, Paper 90-4. pp. 5-13.

Annan, A. P., and Davis, J. L. 1977. Radar range analysis for geological materials. *In* Current research, Part B. Geological Survey of Canada, Paper 77-1B. pp. 117-124.

Annan, A. P., and Davis, J. L. 1978. Methodology for radar transillumination experiments. *In* Report of Activities, Geological Survey of Canada, Paper 78-1B. pp. 107-110.

Annan, A. P., Cosway, S. W., and Redman, J. D. 1991. Water table detection with ground penetrating radar. *In* Expanded abstracts with biographies: 1991 Technical Program. 61st Annual International SEG Meeting, Tulsa, OK. pp. 494-496.

Annan, A. P., Davis, J. L., and Gendzwill, D. 1988. Radar sounding in potash mines, Saskatchewan, Canada. Geophysics, 53 (12): 1556-1564.

Anon. 1997. Code of Practice for Site Investigation. British Standards Institution, London.

Barton, N. 1978. Suggested methods for the quantitative description of discontinuities in rock masses. International Society for Rock Mechanics Commission on Standardization of Laboratory and Field Tests. International Journal of Rock Mechanics and Mining Sciences and Geomechanics Abstracts, 15: 319-368.

Bates, R. L., and Jackson, J. A. 1984. Dictionary of geological terms, Third Edition. American Geological Institute. Doubleday, New York. 571 pp.

Benson, A. K. 1995. Applications of ground penetrating radar in assessing some geological hazards: examples of groundwater contamination, faults, cavities. Journal of Applied Geophysics, 33: 177-193.

Brassington, R. 1998. Field Hydrogeology. John Wiley & Sons. Chichester, U.K. 248 pp.

Brewster, M.L. and Annan, A. P. 1994. Ground-penetrating radar monitoring of a controlled DNAPL release: 200 MHz radar. Geophysics, 59(8): 1211-1221.

Buursink, M.L., and Lane, J.W.Jr. 1999. Characterizing fractures in a bedrock outcrop using ground-penetrating radar at Mirror Lake, Grafton County, New Hampshire. *Presented at the* USGS Toxic Substances Hydrology Program Meeting, Charleston, SC. March 8-12, 1999. pp. 1-8.

Campbell, F. F. 1965. Fault criteria. Geophysics, 30(6): 976-997.

Card, K. D. 1979. Regional geological synthesis. Central Superior Province. *In* Current Research, Part A, Geological Survey of Canada, Paper 79-1A. pp. 87-90.

Card, K. D., Gupta, V.K., McGrath, P. H., and Grant, F. S. 1984. The Sudbury Structure: Its regional geological and geophysical setting. *In* The geology and ore deposits of the Sudbury Structure, Ontario Geological Survey, Special Volume 1. pp. 25-44.

Clayton, C.R.I., and Hope, V.S. 1996. Moderator's report on Session 5: Geophysical Testing. *In*: Advances in site investigation practice. Thomas Telford, London. pp. 774-788.

Coffeen, J. A. 1986. Seismic exploration fundamentals: Seismic techniques for finding oil. Second Edition. PennWell Publishing Company, Tulsa. 347 pp.

Collins English Dictionary. 1994. Third Edition. Harper Collins Publishers, Glasgow. 1791 pp.

Cook, J. C. 1975. Radar transparencies of mine and tunnel rocks. Geophysics, 40: 865-885.

Corin, L., Couchard, I., Dethy, B., Halleux, L., Monjoie, A., Richter, T., and Wauters, J. P. 1997. Radar tomography applied to foundation design in a karstic environment. *Edited by* D. M. McCann, M. Eddleston, P. J. Fenning, and G. M. Reeves, Geological Society Engineering Geology Special Publication 12. pp. 167-173.

Daniels, D. J. 1996. Surface-penetrating radar. The Institution of Electrical Engineers, London. 300 pp.

Daniels, J. J., Harris, D., Roberts, R., and Schilling, B. 1992. GPR measurements for locating underground mine workings at an active open-pit mine. *In* Proceedings of the Fourth International Conference on Ground Penetrating Radar. Rovaniemi, Finland. pp. 237-245.

Davis, J. L., and Annan, A. P. 1989. Ground-penetrating radar for high-resolution mapping of soil and rock stratigraphy. Geophysical Prospecting, 37: 531-551.

Davis, J. L., and Annan, A. P. 1992. Applications of ground penetrating radar to mining, groundwater, and geotechnical projects: selected case histories. *In* Ground penetrating radar. *Edited by* J. A. Pilon; Geological Survey of Canada, Paper 90-4. pp. 49-55.

Davis, S. N. 1969. Porosity & permeability in natural materials. *In* Flow through porous media. *Edited by* R. J. M. DeWiest. Academic Press, New York. pp. 53-89.

Dennen, R. S., and Stroud, W. P. 1991. Radar hazard detection in a coal structure. Mining Engineering, April. pp. 413-418.

Dowding, C. H., Goodman, R. E., Einstein, H. H., Friedman, M, Lytle, R. J., and Price. T. O. 1981. Mapping of natural and artificial fractures. *In* Rock-Mechanics Research Requirements

for Resource Recovery, Construction, and Earthquake-Hazard Reduction. *Edited by* the Panel on rock-mechanics research requirements, U.S. National Committee for Rock Mechanics. Assembly of Mathematical and Physical Sciences, and National Research Council. National Academy Press. Washington, D.C. pp. 67-85.

Dressler, B. O. 1984. General geology of the Sudbury area. *In* The geology and ore deposits of the Sudbury Structure, Ontario Geological Survey. Special Volume 1. pp. 57-82.

Dressler, B. O., Peredery, W. V., and Muir, T. L. 1992. Geology and mineral deposits of the Sudbury Structure. Ontario Geological Survey. Ministry of Northern Development and Mines. Guidebook 8. 33 pp.

Fenner, T. 1995. Ground penetrating radar for identification of mine tunnels and abandoned mine stopes. Mining Engineering. March. pp. 280-284.

Fetter, C.W. 1988. Applied hydrogeology. Macmillan Publishing Company. New York. 592 pp.

Fisher, E., McMechan, G. A., and Annan, A. P. 1992a. Acquisition and processing of wide-aperture ground-penetrating radar data. Geophysics, 57 (3): 495-504.

Fisher, E., McMechan, G. A., Annan, A. P., and Cosway, S. W. 1992b. Examples of reverse-time migration of single-channel, ground penetrating radar profiles. Geophysics. 57 (4): 577-586.

Fisher, S. C., Stewart, R. R., and Jol, H. M. 1994. Processing ground penetrating radar data. *In* Proceedings of the Fifth International Conference on Ground Penetrating Radar. Kitchener. Ontario. Vol.2. pp. 661-675.

Goodman, R. A. 1989. Introduction to Rock Mechanics. John Wiley & Sons. New York. 562 pp.

Grant, R. W., and Bite, A. 1984. Sudbury quartz diorite offset dikes. *In* The geology and ore deposits of the Sudbury Structure, Ontario Geological Survey, Special Volume 1. pp. 275-300.

Grasmueck, M. 1994. Application of seismic processing techniques to discontinuity mapping with ground-penetrating radar in crystalline rock of the Gotthard Massif. Switzerland. *In* Proceedings of the Fifth International Conference on Ground Penetrating Radar, Kitchener, Ontario. pp. 1135-1149.

Grasmueck, M. 1996. 3-D ground-penetrating radar applied to fracture imaging in gneiss. Geophysics, 61(4): 1050-1064.

Hogan, G. 1988. Migration of ground penetrating radar data: A technique for locating subsurface targets. *In* Proceedings of the symposium on the application of geophysics to engineering and environmental problems. *Edited by* D. Fitterman, R. Bell, J. Corbett, C. Davenport, S. Hulse, and C. Bierley. Society of Engineering and Mineral Exploration Geophysicists: United States Geological Survey. pp. 809-822.

Holloway, A. L. 1992. Fracture mapping in granite rock using ground probing radar. *In* Ground penetrating radar. *Edited by* J. A. Pilon; Geological Survey of Canada, Paper 90-4. pp. 85-100.

Holloway, A. L., and Mugford, J. C. 1990. Fracture characterization in granite using ground probing radar. CIM Bulletin, **83**(940):61-70.

Holloway, A. L., Soonawala, N.M., and Collett, L.S. 1986. Three-dimensional fracture mapping in granite excavations using ground-penetrating radar. CIM Bulletin, **79**(896): 54-59.

Horvath, C. L. 1998. An evaluation of ground penetrating radar for investigation of palsa evolution, Macmillan Pass, Northwest Territories. M.Sc. Thesis, University of Alberta, Edmonton, Alberta.

Hunt, R. E. 1984. Geotechnical engineering investigation manual. McGraw-Hill Book Company. New York. 983 pp.

Hyde, C., and Dyke, L. 1999. Chapter 2 - Electromagnetic techniques. *In* A handbook of geophysical techniques for geomorphic and environmental research. Geological Survey of Canada. Open File 3731. pp. 3-30.

Kearey, P., and Brooks, M. 1991. An introduction to geophysical exploration. Blackwell Scientific Publications, London. 254 pp.

Keller, G. V. 1989. Section V: Electrical Properties. *In* Practical handbook of physical properties of rocks and minerals. *Edited by* R. S. Carmichael. CRC Press, Inc., Florida.

Kulhawy, F., and Carter, J. P. 1992. Settlement and bearing capacity of foundations on rock masses. *In* Engineering in Rock Masses. *Edited by* F. G. Bell, Butterworth-Heinemann Ltd. Oxford. pp. 231-245.

LaFleche, P. T., Todoeschuck, J. P., Jensen, O. G., and Judge, A. S. 1991. Analysis of ground-probing radar data: predictive deconvolution. Canadian Geotechnical Journal, **28**: 134-139.

Li, Z. 1998. Applications of ground penetrating radar in Three Gorges Project. *In* Proceedings of the Seventh International Conference on Ground Penetrating Radar. Lawrence, Kansas, US. Vol. 1. pp. 209-213.

MacArthur, J. 1988. Real time Kirchhoff migration on ground penetrating radar data. *In* Second International Symposium on Geotechnical Applications of Ground Penetrating Radar. Gainesville, Florida. March 6-10, 1988. pp. 40-41.

Maijala, P. 1992. Application of some seismic data processing methods to ground penetrating radar data. *In* Proceedings of the Fourth International Conference on Ground Penetrating Radar. Rovaniemi, Finland. pp. 103-110.

MALA GeoScience. 1997. RAMAC/GPR software manual, version 2.28. August 1997. 66 pp.

MALA GeoScience. 1999. website: www.malags.se/ramac/hardware. September 28, 1999.

McCann, D.M., Culshaw, M.G., and Fenning, P.J. 1997. Setting the standard for geophysical surveys in site investigation. *In* Modern Geophysics in Engineering Geology. *Edited by* D. M. McCann, M. Eddleston, P. J. Fenning, and G. M. Reeves, Geological Society Engineering Geology Special Publication No. 12. pp. 3-34.

McMechan, G. A. 1981. Modeling of zero-offset reflection profiles with asymptotic ray theory. Canadian Journal of Earth Science, **18**: 551-560.

Milsom, J. 1996. Chapter 10 – Ground penetrating radar. *In* Field Geophysics. Second Edition. John Wiley & Sons Ltd, Chichester. pp. 131-140.

Momayez, M., Hassani, F. P., Hara, A., and Sadri, A. 1996. Application of GPR in Canadian mines. CIM Bulletin, **89**: 107-110.

Noon, D. A. 1996. Stepped-frequency radar design and signal processing enhances ground penetrating radar performance. Ph.D. thesis, University of Queensland. Brisbane, Queensland, Australia.

Olsson, O., and Falk, L. 1990. Borehole radar - A new technique for characterization of rock at great depth. *In* Proceedings of Rock at Great Depth. Vol. 3. *Edited by* V. Maury and D. Fourmaintraux. pp. 1229-1234.

Olsson, O., Anderson, P., Carlsten, S., Falk, L., Niva, B., and Sandberg, E. 1992. Fracture characterization in crystalline rock by borehole radar. *In* Ground penetrating radar. *Edited by* J. A. Pilon; Geological Survey of Canada, Paper 90-4. pp. 139-150.

Palacky, G. J. 1988. Resistivity characteristics of geological targets. *In* Electromagnetic methods in applied geophysics. Vol. 1. *Edited by* M. N. Nabighian; Society of Exploration Geophysicists, Tulsa, Oklahoma. pp. 53-129.

Parry, N. S. and Davis, J. L. 1992. GPR systems for roads and bridges. *In* Proceedings of the Fourth International Conference on Ground Penetrating Radar. Rovaniemi, Finland. pp. 247-257.

Peters, L.Jr., Daniels, J.J., and Young, J.D. 1994. Ground penetrating radar as a subsurface environmental sensing tool. *In* Proceedings of the Institute of Electrical and Electronics Engineers (IEEE). **82** (12): 1802-1822.

Piccolo, M. 1992. GPR applications for the definition of unconformities in a Carrara Marble Quarry (Massa Carrara – Italy). *In* Proceedings of the Fourth International Conference on Ground Penetrating Radar. Rovaniemi, Finland. pp. 223-228.

Pilon, J., Scaife, J., Gerabek, P., Timoshenko, E., and Kurfurst, P. 1996. Ground penetrating radar survey to define fractures in bedrock, Little French River, Ontario. *In* Current Research 1996-C; Geological Survey of Canada. pp. 169-176.

Robinson, S. D., and Michaud, Y. 1999. Chapter 5 - Ground penetrating radar. *In* A handbook of geophysical techniques for geomorphic and environmental research. Geological Survey of Canada. Open File 3731. pp. 69-102.

Sheriff, R. E. 1973. Encyclopedic dictionary of exploration geophysics. Society of Exploration Geophysicists. Tulsa, Oklahoma. 264 pp.

Stephansson, O. 1992. Underground chambers in hard rock masses. *In* Engineering in Rock Masses. *Edited by* F. G. Bell, Butterworth-Heinemann Ltd, Oxford. pp. 440-464.

Stevens, K. M., Everitt, R. A., Street, P. J., and Lodha, G. S. 1994. Litho-structural characterization in granitic rocks using single-hole and crosshole radar techniques. *In* Proceedings of the Fifth International Conference on Ground Penetrating Radar, Kitchener, Ontario. pp. 625-638.

Telford, W. M., Geldart, L. P., and Sheriff, R. E. 1990. Chapter 5 - Electrical properties of rocks and minerals. *In* Applied geophysics. Cambridge University Press. pp. 283-292.

Todd, D. K. 1964. Groundwater, handbook of applied hydrology. McGraw-Hill, New York.

Todoeschuck, J. P., LaFleche, P. T., Jensen, O. G., Judge, A. S., and Pilon, J. A. 1992. Deconvolution of ground penetrating radar data. *In* Ground penetrating radar. *Edited by* J. A. Pilon; Geological Survey of Canada, Paper 90-4. pp. 227-230.

Toshioka, T., Tsuchida, T., and Sasahara, K. 1995. Application of GPR to detecting and mapping cracks in rock slopes Journal of Applied Geophysics, 33: 119-124.

Turner, G. 1992. Propagation deconvolution. *In* Proceedings of the Fourth International Conference on Ground Penetrating Radar. Rovaniemi, Finland. pp. 85-93.

Unterberger, R. R. 1978. Radar propagation in rock salt. Geophysical Prospecting, 26: 312-328.

Unterberger, R. R. 1992. Ground penetrating radar finds disturbed earth over burials. *In* Proceedings of the Fourth International Conference on Ground Penetrating Radar. Rovaniemi, Finland. pp. 351-357.

Van Overmeeren, R. A. 1997. Imaging groundwater 'steps' in push moraines by georadar. *In* Modern Geophysics in Engineering Geology. *Edited by* D. M. McCann, M. Eddleston, P. J. Fenning, and G. M. Reeves, Geological Society Engineering Geology Special Publication No. 12. pp. 63-73.

White, H., Meyer, P., and Doorgapershad, A. 1996. Quantitative ground penetrating radar for rock mass characterization. Journal of the South African Institute of Mining and Metallurgy. 96(5): 197-200.

Wyatt, D. E. and Temples, T. J. 1996. Ground-penetrating radar detection of small-scale channels, joints, and faults in the unconsolidated sediments of the Atlantic Coastal Plain Environmental Geology, 27(3): 219-225.

Yilmaz, O. 1987. Seismic data processing: Investigations in geophysics, Vol. 2. Society of Exploration Geophysics, Tulsa. 526 pp.

APPENDIX : GPR SURVEY TABLES FOR EACH PROJECT SITE

Table A-1

Project Site: Jarvis Resources Ltd.
Location: Block Site 1
Host Rock: Limestone
Primary Radar Target(s):   Air-filled gap between limestone slabs and marble block
Total no. of surveys: 3

RAMAC File Name	High Frequency Surveys		
	Jarvis1h	Jarvis1e	Jarvis1f
System Parameters:			
Antenna centre frequency [1]	1 GHz	1 GHz	1 GHz
Antenna separation (m)	0.10	0.10	0.10
Sampling frequency (MHz)	10,826	10,826	10,826
Time window (ns)	47	47	47
Station spacing (m)	0.01	0.025	0.025
No. of traces	121	47	47
No. of points/trace	512	512	512
No. of stacks	16	16	16
Total survey length (m)	1.21	1.175	1.175
Sampling interval (ns)	0.092	0.092	0.092
Nyquist frequency (MHz)	5,413	5,413	5,413
Nyquist wavenumber (cycles/m)	50	20	20
Survey Details:			
Survey date	August 18, 1999	August 19, 1999	August 19, 1999
Trend of survey line	082°	082°	082°
Survey direction	east → west	west → east	west → east
Comments	no foil	no foil	foil reflector @ 17.6 cm depth
Processing Details:			
Radar velocity through host rock (m/ns) [2]	0.110	0.110	0.110
Time gain	none	none	none
Filter	trace stacking = 5	trace stacking = 2	trace stacking = 2
Actual antenna centre frequency (MHz) [3]	825	820	820

Notes:
1. This antenna centre frequency is a reference value for a signal propagating through air.
2. Signal propagation velocity back-calculated knowing distance to fracture.
3. The actual antenna centre frequency was determined from the corresponding plot of amplitude vs. frequency.

Table A-2

Project Site: Jarvis Resources Ltd.
Location: Block Site 2
Host Rock: Limestone
Primary Radar Target(s): Air-filled gap between limestone blocks
Total no. of surveys: 1

	High Frequency Survey
RAMAC File Name	Jarvis2
System Parameters:	
Antenna centre frequency [1]	1 GHz
Antenna separation (m)	0.10
Sampling frequency (MHz)	10,826
Time window (ns)	47
Station spacing (m)	0.01
No. of traces	202
No. of points/trace	512
No. of stacks	16
Total survey length (m)	2.0
Sampling interval (ns)	0.092
Nyquist frequency (MHz)	5,413
Nyquist wavenumber (cycles/m)	50
Survey Details:	
Survey date	August 18, 1999
Trend of survey line	152°
Survey direction	north → south
Comments	none
Processing Details:	
Radar velocity through host rock (m/ns) [2]	0.110
Time gain [3]	SEC (2/0.110/1)
Filter	trace stacking = 5
Actual antenna centre frequency (MHz) [4]	807

Notes:
1. This antenna centre frequency is a reference value for a signal propagating through air.
2. Signal propagation velocity back-calculated knowing distance to fracture.
3. For the SEC gain, the values in brackets correspond to maximum gain, radar velocity (in m/ns), and attenuation constant (in dB/m).
4. The actual antenna centre frequency was determined from the corresponding plot of amplitude vs. frequency.

Table A-3

Project Site: Jarvis Resources Ltd.
Location: Block Site 3
Host Rock: Limestone
Primary Radar Target(s): Air-filled gap between limestone blocks
Total no. of surveys: 2

RAMAC File Name	High Frequency Surveys	
	Jarvis4	Jarvis4f
System Parameters:		
Antenna centre frequency [1]	1 GHz	1 GHz
Antenna separation (m)	0.10	0.10
Sampling frequency (MHz)	10,826	10,826
Time window (ns)	47	47
Station spacing (m)	0.02	0.02
No. of traces	105	106
No. of points/trace	512	512
No. of stacks	16	16
Total survey length (m)	2.10	2.12
Sampling interval (ns)	0.092	0.092
Nyquist frequency (MHz)	5,413	5,413
Nyquist wavenumber (cycles/m)	25	25
Survey Details:		
Survey date	August 19, 1999	August 19, 1999
Trend of survey line	071°	071°
Survey direction	west → east	west → east
Comments	none	foil reflector @ 39.5 cm depth
Processing Details:		
Radar velocity through host rock (m/ns) [2]	0.110	0.110
Time gain	none	none
Filter	trace stacking = 5	trace stacking = 5
Actual antenna centre frequency (MHz) [3]	834	828

Notes:
1. This antenna centre frequency is a reference value for a signal propagating through air.
2. Signal propagation velocity back-calculated knowing distance to fracture.
3. The actual antenna centre frequency was determined from the corresponding plot of amplitude vs. frequency.

Table A-4

Project Site: WGMC Walkway
Location: -
Host Rock: Gneiss
Primary Radar Target(s): Air-filled gap between gneiss blocks
Total no. of surveys: 2

RAMAC File Name	High Frequency Surveys	
	Reflect1	Reflect2
System Parameters:		
Antenna centre frequency [1]	1 GHz	1 GHz
Antenna separation (m)	0.10	0.10
Sampling frequency (MHz)	10,826	10,826
Time window (ns)	47	47
Station spacing (m)	0.02	0.02
No. of traces	64	64
No. of points/trace	512	512
No. of stacks	8	8
Total survey length (m)	1.28	1.28
Sampling interval (ns)	0.092	0.092
Nyquist frequency (MHz)	5,413	5,413
Nyquist wavenumber (cycles/m)	25	25
Survey Details:		
Survey date	August 12, 1999	August 12, 1999
Trend of survey line	252°	252°
Survey direction	east → west	east → west
Comments	foil reflector @ ≈50 cm depth	none
Processing Details:		
Radar velocity through host rock (m/ns) [2]	0.120	0.120
Time gain [3]	SEC (2/0.120/1)	SEC (2/0.120/1)
Filter	trace stacking = 5	trace stacking = 5
Actual antenna centre frequency (MHz) [4]	827	836

Notes:
1. This antenna centre frequency is a reference value for a signal propagating through air.
2. Typical signal propagation velocity for gneissic rock - from the literature.
3. For the SEC gain, the values in brackets correspond to maximum gain, radar velocity (in m/ns), and attenuation constant (in dB/m).
4. The actual antenna centre frequency was determined from the corresponding plot of amplitude vs. frequency.

Table A-5

Project Site: Hwy 17 Bypass
Location: -
Host Rock: Subarkose
Primary Radar Target(s):   Bedding joints at 20 cm & 50 cm & fracture zone at 95-100 cm
Total no. of surveys: 3

RAMAC File Name	High Frequency Surveys		
	BY-1G-2a	BY-1G-2c	BY-1G-2d
System Parameters:			
Antenna centre frequency [1]	1 GHz	1 GHz	1 GHz
Antenna separation (m)	0.10	0.10	0.10
Sampling frequency (MHz)	6,616	10,826	10,826
Time window (ns)	73	44	44
Station spacing (m)	0.025	0.025	0.05
No. of traces	253	255	127
No. of points/trace	480	480	480
No. of stacks	16	16	16
Total survey length (m)	6.325	6.375	6.35
Sampling interval (ns)	0.151	0.092	0.092
Nyquist frequency (MHz)	3,308	5,413	5,413
Nyquist wavenumber (cycles/m)	20	20	10
Survey Details:			
Survey date	August 5, 1999	August 5, 1999	August 5, 1999
Trend of survey line	240°	240°	240°
Survey direction	east → west	east → west	east → west
Comments	none	none	none
Processing Details:			
Radar velocity through host rock (m/ns) [2]	0.120	0.120	0.120
Time gain [3]	SEC (20/0.120/1)	SEC (20/0.120/1)	SEC (20/0.120/1)
Filter	trace stacking = 3	trace stacking = 3; or low-pass spatial filter with cutoff of 10%	low-pass spatial filter with cutoff of 10%
Actual antenna centre frequency (MHz) [4]	799	818	810

Notes:
1. This antenna centre frequency is a reference value for a signal propagating through air.
2. Typical signal propagation velocity for rock - from the literature.
3. For the SEC gain, the values in brackets correspond to maximum gain, radar velocity (in m/ns), and attenuation constant (in dB/m).
4. The actual antenna centre frequency was determined from the corresponding plot of amplitude vs. frequency.

Table A-6

Project Site: Vermilion River
Location: -
Host Rock: Argillite
Primary Radar Target(s):   Joint at $\approx$ 0.7-1.8 m depth (dipping 10° to the east)
Total no. of surveys: 2

	High Frequency Surveys	
RAMAC File Name	VM-1G-3	VM-1G-5
System Parameters:		
Antenna centre frequency [1]	1 GHz	1 GHz
Antenna separation (m)	0.10	0.10
Sampling frequency (MHz)	10,826	10,826
Time window (ns)	44	47
Station spacing (m)	0.025	0.05
No. of traces	119	118
No. of points/trace	480	480
No. of stacks	16	8
Total survey length (m)	2.975	5.90
Sampling interval (ns)	0.092	0.092
Nyquist frequency (MHz)	5,413	5,413
Nyquist wavenumber (cycles/m)	20	10
Survey Details:		
Survey date	August 5, 1999	August 12, 1999
Trend of survey line	252°	253°
Survey direction	east → west	east → west
Comments	topographic correction required	topographic correction required
Processing Details:		
Radar velocity through host rock (m/ns) [2]	0.123	0.123
Time gain [3]	SEC (20/0.123/1)	SEC (20/0.123/1)
Filter	point averaging = 5	point averaging = 5
Actual antenna centre frequency (MHz) [4]	808	775

Notes:
1. This antenna centre frequency is a reference value for a signal propagating through air.
2. Signal propagation velocity back-calculated knowing distance to joint.
3. For the SEC gain, the values in brackets correspond to maximum gain, radar velocity (in m/ns), and attenuation constant (in dB/m).
4. The actual antenna centre frequency was determined from the corresponding plot of amplitude vs. frequency.

Table A-7

Project Site:	Willet Green Miller Centre
Location:	Outcrop 1
Host Rock:	Subarkose or feldspathic sandstone
Primary Radar Target(s):	Bedding planes (dipping 40° to the northwest)
Total no. of surveys:	2

	Low & High Frequency Surveys	
RAMAC File Name	WGMC1	WGMC1G1
System Parameters:		
Antenna centre frequency [1]	100 MHz	1 GHz
Antenna separation (m)	1.0	0.10
Sampling frequency (MHz)	1,133	10,826
Time window (ns)	424	44
Station spacing (m)	0.10	0.05
No. of traces	102	217
No. of points/trace	480	480
No. of stacks	8	16
Total survey length (m)	10.20	10.85
Sampling interval (ns)	0.883	0.092
Nyquist frequency (MHz)	566	5,413
Nyquist wavenumber (cycles/m)	5	10
Survey Details:		
Survey date	July 27, 1999	August 5, 1999
Trend of survey line	130°	130°
Survey direction	NW → SE	NW → SE
Comments	none	none
Processing Details:		
Radar velocity through host rock (m/ns) [2]	0.120	0.120
Time gain [3]	SEC (2/0.120/1)	SEC (2/0.120/1)
Filter	point averaging = 5	none
Actual antenna centre frequency (MHz) [4]	88	819

Notes:

1. This antenna centre frequency is a reference value for a signal propagating through air.
2. Typical signal propagation velocity for rock - from the literature.
3. For the SEC gain, the values in brackets correspond to maximum gain, radar velocity (in m/ns), and attenuation constant (in dB/m).
4. The actual antenna centre frequency was determined from the corresponding plot of amplitude vs. frequency.

Table A-8

Project Site: Willet Green Miller Centre
Location: Outcrop 2
Host Rock: Subarkose or feldspathic sandstone
Primary Radar Target(s): Bedding planes (dipping 40° to the northwest)
Total no. of surveys: 2

RAMAC File Name	Low & High Frequency Surveys	
	WGMC2	WGMC1G3c
System Parameters:		
Antenna centre frequency [1]	100 MHz	1 GHz
Antenna separation (m)	1.0	0.10
Sampling frequency (MHz)	1,133	10,826
Time window (ns)	424	44
Station spacing (m)	0.10	0.05
No. of traces	71	146
No. of points/trace	480	480
No. of stacks	8	16
Total survey length (m)	7.1	7.3
Sampling interval (ns)	0.883	0.092
Nyquist frequency (MHz)	566	5,413
Nyquist wavenumber (cycles/m)	5	10
Survey Details:		
Survey date	July 27, 1999	August 5, 1999
Trend of survey line	149°	149°
Survey direction	NW → SE	NW → SE
Comments	topographic correction required	topographic correction required
Processing Details:		
Radar velocity through host rock (m/ns) [2]	0.120	0.120
Time gain [3]	SEC (100/0.120/1)	SEC (100/0.120/1)
Filter	point averaging = 7	point averaging = 5
Actual antenna centre frequency (MHz) [4]	115	819

Notes:
1. This antenna centre frequency is a reference value for a signal propagating through air.
2. Typical signal propagation velocity for rock - from the literature.
3. For the SEC gain, the values in brackets correspond to maximum gain, radar velocity (in m/ns), and attenuation constant (in dB/m).
4. The actual antenna centre frequency was determined from the corresponding plot of amplitude vs. frequency.

277

Table A-9

RAMAC File Name	Low Frequency Surveys	
	Kilarney	**Kilar-2**
System Parameters:		
Antenna centre frequency [1]	100 MHz	100 MHz
Antenna separation (m)	1.0	1.0
Sampling frequency (MHz)	1,133	1,133
Time window (ns)	424	424
Station spacing (m)	0.10	0.10
No. of traces	240	208
No. of points/trace	480	480
No. of stacks	8	8
Total survey length (m)	24.0	20.8
Sampling interval (ns)	0.883	0.883
Nyquist frequency (MHz)	566	566
Nyquist wavenumber (cycles/m)	5	5
Survey Details:		
Survey date	July 28, 1999	July 28, 1999
Trend of survey line	149°	149°
Survey direction	NW → SE	NW → SE
Comments	topographic correction required	topographic correction required
Processing Details:		
Radar velocity through host rock (m/ns) [2]	0.120	0.120
Time gain	constant gain = 10	constant gain = 10
Filter	trace stacking = 5	trace stacking = 5
Actual antenna centre frequency (MHz) [3]	93	90

Notes:

1. This antenna centre frequency is a reference value for a signal propagating through air.
2. Typical signal propagation velocity for rock - from the literature.
3. The actual antenna centre frequency was determined from the corresponding plot of amplitude vs. frequency.

Table A-10

Project Site: Elbow Lake
Location: Outcrop 1
Host Rock: Migmatitic biotite gneiss
Primary Radar Target(s):   Gneissic foliation and/or mafic dykes
Total no. of surveys: 1

	Low Frequency Survey
RAMAC File Name	Camp1
System Parameters:	
Antenna centre frequency [1]	100 MHz
Antenna separation (m)	1.0
Sampling frequency (MHz)	1.133
Time window (ns)	424
Station spacing (m)	0.10
No. of traces	186
No. of points/trace	480
No. of stacks	8
Total survey length (m)	18.6
Sampling interval (ns)	0.883
Nyquist frequency (MHz)	566
Nyquist wavenumber (cycles/m)	5
Survey Details:	
Survey date	July 29, 1999
Trend of survey line	321°
Survey direction	south → north
Comments	topographic correction required
Processing Details:	
Radar velocity through host rock (m/ns) [2]	0.120
Time gain [3]	SEC (150/0.120/1)
Filter	point averaging = 2
Actual antenna centre frequency (MHz) [4]	100

Notes:
1. This antenna centre frequency is a reference value for a signal propagating through air.
2. Signal propagation velocity back-calculated knowing distance to fracture.
3. For the SEC gain, the values in brackets correspond to maximum gain, radar velocity (in m/ns), and attenuation constant (in dB/m).
4. The actual antenna centre frequency was determined from the corresponding plot of amplitude vs. frequency.

Table A-11

Project Site: Elbow Lake
Location: Outcrop 2
Host Rock: Migmatitic biotite gneiss
Primary Radar Target(s): Gneissic foliation and/or mafic dykes
Total no. of surveys: 2

| RAMAC File Name | Low & High Frequency Surveys | |
	Camp2	Camp4
System Parameters:		
Antenna centre frequency [1]	100 MHz	1 GHz
Antenna separation (m)	1.0	0.10
Sampling frequency (MHz)	1,133	10,826
Time window (ns)	424	47
Station spacing (m)	0.10	0.01
No. of traces	98	250
No. of points/trace	480	512
No. of stacks	8	8
Total survey length (m)	9.8	2.5
Sampling interval (ns)	0.883	0.092
Nyquist frequency (MHz)	566	5,413
Nyquist wavenumber (cycles/m)	5	50
Survey Details:		
Survey date	July 30, 1999	August 16, 1999
Trend of survey line	322°	314°
Survey direction	south → north	south → north
Comments	topographic correction required	topographic correction required
Processing Details:		
Radar velocity through host rock (m/ns) [2]	0.120	0.120
Time gain [3]	SEC (150/0.120/5)	SEC (50/0.120/2)
Filter	point averaging = 5	point averaging = 5
Actual antenna centre frequency (MHz) [4]	113	817

Notes:
1. This antenna centre frequency is a reference value for a signal propagating through air.
2. Typical signal propagation velocity for rock - from the literature.
3. For the SEC gain, the values in brackets correspond to maximum gain, radar velocity (in m/ns), and attenuation constant (in dB/m).
4. The actual antenna centre frequency was determined from the corresponding plot of amplitude vs. frequency.

Table A-12

Project Site: Elbow Lake
Location: Outcrop 3
Host Rock: Migmatitic biotite gneiss
Primary Radar Target(s): Mafic dykes
Total no. of surveys: 2

	High Frequency Surveys	
RAMAC File Name	Camp5c	Camp5d
System Parameters:		
Antenna centre frequency [1]	1 GHz	1 GHz
Antenna separation (m)	0.10	0.10
Sampling frequency (MHz)	10,826	10,826
Time window (ns)	47	47
Station spacing (m)	0.025	0.025
No. of traces	135	103
No. of points/trace	512	512
No. of stacks	16	16
Total survey length (m)	3.375	2.575
Sampling interval (ns)	0.092	0.092
Nyquist frequency (MHz)	5,413	5,413
Nyquist wavenumber (cycles/m)	20	20
Survey Details:		
Survey date	August 19, 1999	August 19, 1999
Trend of survey line	047°	044°
Survey direction	west → east	west → east
Comments	lower survey line	upper survey line
Processing Details:		
Radar velocity through host rock (m/ns) [2]	0.120	0.120
Time gain [3]	SEC (15/0.120/1)	SEC (15/0.120/1)
Filter	trace stacking = 5	trace stacking = 5
Actual antenna centre frequency (MHz) [4]	802	802

Notes:
1. This antenna centre frequency is a reference value for a signal propagating through air.
2. Typical signal propagation velocity for gneissic rock - from the literature.
3. For the SEC gain, the values in brackets correspond to maximum gain, radar velocity (in m/ns), and attenuation constant (in dB/m).
4. The actual antenna centre frequency was determined from the corresponding plot of amplitude vs. frequency.

Table A-13

Project Site: Hwy 17 Site
Location: -
Host Rock: Argillite
Primary Radar Target(s):   Joints parallel to surveyed surface
Total no. of surveys: 2

RAMAC File Name	Low & High Frequency Surveys	
	Prof21	Hwy171G2
System Parameters:		
Antenna centre frequency [1]	100 MHz	1 GHz
Antenna separation (m)	1.0	0.10
Sampling frequency (MHz)	1,235	10,826
Time window (ns)	389	44
Station spacing (m)	0.10	0.025
No. of traces	155	75
No. of points/trace	480	480
No. of stacks	16	16
Total survey length (m)	15.5	1.875
Sampling interval (ns)	0.810	0.092
Nyquist frequency (MHz)	618	5,413
Nyquist wavenumber (cycles/m)	5	20
Survey Details:		
Survey date	June 16, 1999	August 5, 1999
Trend of survey line	060°	-
Survey direction	west → east	top → bottom
Comments	horizontal survey line	vertical survey line
Processing Details:		
Radar velocity through host rock (m/ns) [2]	0.123	0.123
Time gain [3]	SEC (150/0.120/5)	SEC (50/0.120/2)
Filter	point averaging = 5	point averaging = 5
Actual antenna centre frequency (MHz) [4]	81	828

Notes:
1. This antenna centre frequency is a reference value for a signal propagating through air.
2. Used the same velocity as at the Vermilion River project site.
3. For the SEC gain, the values in brackets correspond to maximum gain, radar velocity (in m/ns), and attenuation constant (in dB/m).
4. The actual antenna centre frequency was determined from the corresponding plot of amplitude vs. frequency.

Table A-14

	Low & High Frequency Surveys	
RAMAC File Name	175-a	175-1G-3
System Parameters:		
Antenna centre frequency [1]	100 MHz	1 GHz
Antenna separation (m)	1.0	0.10
Sampling frequency (MHz)	1,133	19,848
Time window (ns)	424	24
Station spacing (m)	0.20	0.025
No. of traces	133	304
No. of points/trace	480	480
No. of stacks	8	16
Total survey length (m)	26.6	7.6
Sampling interval (ns)	0.883	0.050
Nyquist frequency (MHz)	566	9,924
Nyquist wavenumber (cycles/m)	2.5	20
Survey Details:		
Survey date	June 22, 1999	August 4, 1999
Trend of survey line	030°	030°
Survey direction	SW→ NE	SW→ NE
Comments	none	topographic correction required
Processing Details:		
Radar velocity through host rock (m/ns) [2]	0.120	0.120
Time gain [3]	constant gain = 50; or SEC (200/0.120/2)	SEC (50/0.120/1)
Filter	trace stacking = 3 & point averaging = 5	trace stacking = 3 & point averaging = 5; or trace-difference & point averaging of 5
Actual antenna centre frequency (MHz) [4]	87	856

Notes:

1. This antenna centre frequency is a reference value for a signal propagating through air.
2. Typical signal propagation velocity for diorite – Refer to Table 2-2.
3. For the SEC gain, the values in brackets correspond to maximum gain, radar velocity (in m/ns), and attenuation constant (in dB/m).
4. The actual antenna centre frequency was determined from the corresponding plot of amplitude vs. frequency.

Table A-15

Project Site: 175-Orebody
Location: 7715 Drift – SE Sidewall
Host Rock: Quartz-diorite to diorite
Primary Radar Target(s): Joints
Total no. of surveys: 2

	Low & High Frequency Surveys	
RAMAC File Name	175-d2	175-1G-1
System Parameters:		
Antenna centre frequency [1]	100 MHz	1 GHz
Antenna separation (m)	1.0	0.10
Sampling frequency (MHz)	1,133	19,848
Time window (ns)	424	24
Station spacing (m)	0.10	0.025
No. of traces	301	279
No. of points/trace	480	480
No. of stacks	8	16
Total survey length (m)	30.1	6.975
Sampling interval (ns)	0.883	0.050
Nyquist frequency (MHz)	566	9,924
Nyquist wavenumber (cycles/m)	5	20
Survey Details:		
Survey date	June 23, 1999	August 4, 1999
Trend of survey line	030°	030°
Survey direction	SW→ NE	SW→ NE
Comments	none	topographic correction required
Processing Details:		
Radar velocity through host rock (m/ns) [2]	0.120	0.120
Time gain [3]	constant gain = 50; or SEC (200/0.120/2)	SEC (50/0.120/1)
Filter	trace stacking = 3 & point averaging = 5	trace stacking = 3 & point averaging = 5; or trace-difference & point averaging of 5
Actual antenna centre frequency (MHz) [4]	96	848

Notes:
1. This antenna centre frequency is a reference value for a signal propagating through air.
2. Typical signal propagation velocity for diorite – Refer to Table 2-2.
3. For the SEC gain, the values in brackets correspond to maximum gain, radar velocity (in m/ns), and attenuation constant (in dB/m).
4. The actual antenna centre frequency was determined from the corresponding plot of amplitude vs. frequency.